



**Studies on the interaction between inhaled drug
molecules and mucin**

by

Melania Giorgetti

A thesis submitted in partial fulfilment for the
degree of Doctor of Philosophy

in the

Faculty of Science

School of Pharmacy

2016

This copy of the thesis has been supplied on condition that anyone who consults it is understood to recognise that its copyright rests with the author and that use of any information derived there from must be in accordance with current UK Copyright Law. In addition, any quotation or extract must include full attribution.

Declaration of authorship

I declare that the work in this thesis submitted by me for the degree of Doctor of Philosophy is my work, except where due reference is made to other authors, and has not been previously submitted by me for a degree at this or any other university.

Melania Giorgetti

Abstract

Mucus is a dynamic gel network primarily composed of water. The principal “non-water” component of mucus is mucin, a macromolecular glycoprotein largely responsible for the viscoelastic gel nature of mucus. Recent evidence indicates that some inhaled antibiotics are bound by mucus components and their biological activity reduced.

This thesis focussed upon the mucin binding of a panel of epithelial sodium channel (ENaC) blockers that have been studied as experimental therapeutic agents for cystic fibrosis (CF). Using porcine gastric mucin (PGM) as a model system the directional transport of FL-Na, FITC dextran probes (4-70 kDa) and two ENaC blockers was determined using Franz diffusion cells. Size-dependent restriction of dextran transport was accompanied by a large disparity in the passage of two structurally similar ENaC blockers with differing lipophilic character. A 96-well ultrafiltration assay was developed to study mucin-binding of 12 related ENaC blockers of two main structural groups: quaternary amine compounds (QQA) and non-quaternary amine (NQQA) analogues. The extent of binding was variable within sub-groups and correlated well with $\log P_{o/w}$. Other physical parameters (e.g. rotatable bond number, PSA) served as good correlates only for QQA structures. In contrast, the apical-basolateral transport of ENaC blockers across restrictive Calu-3 monolayers was not clearly predicated by solute hydrophobicity. Saturation Transfer Difference (STD)-NMR spectroscopy was used to gather structural details of mucin-drug interactions. These studies provide the first evidence that STD-NMR can be used to identify discrete molecular regions that participate in interactions with mucin.

In conclusion, these data indicate that some inhaled drugs undergo reversible interactions with mucus. This finding could have wide implications for the design of new inhaled therapies for lung diseases where binding to supraphysiological amounts of airway mucus may modulate drug disposition and clinical response.

Acknowledgement

I would like to deeply express my sincere to my primary supervisor, Dr Chris Morris for working hard with me with understanding, patience and continuous support throughout the whole period of my PhD. My gratefulness also goes to Dr David Sandham and Professor Brian Cox for their enthusiasm and encouragement. I would like to take this opportunity to express my gratitude to Dr Jesus Angulo for supervision and assistance throughout the STD-NMR work.

I would like to thank all friends I have made during my stay in Norwich; Simona, Alessandro, Paolo, Cristina, Kenzi, Matthew, Teresa, Alessia, Maria Giovanna, Valeria, Giulia, Marco and Doroty. You made this journey in Norwich unforgettable!

Thank you also to my office mates, Desire', Kate, Matteo, Mohammed and Carl for all the laughs, coffees and great company. Thank you Carl to always cheer me up in the darkest time of my PhD ...with a burger, a pizza or a kebab (or even all at once!).

I special thanks goes to all my colleagues at University of East Anglia especially to Karol, Susanna, Hui and Elise who with a glass of wine, beer and a ginger beer made the PhD funnier and sweeter.

Moreover, I would love to thank the little Elisa who with her 7 teeth smile swept away all of my worries during my stay in Chessa-Nevola's house.

Lastly and the most important, I would like to thank my family who have encouraged and supported me since I started my PhD journey. Thank you all very much.

Contents

Declaration	II
Abstract	III
Acknowledgements	IV
Table contents	V
Figure List	X
Table list	XIII
Abbreviation List	XIV
Chapter 1: General Introduction	1
1.1 Pulmonary Delivery	2
1.1.1 Anatomy of the pulmonary tract	3
1.2 Barriers of the pulmonary route	6
1.2.1 Formulation challenges	6
1.2.2 Biological barriers	8
1.3 Lung models for the investigation of lung permeability (in vivo, in vitro and ex vivo)	13
1.3.1 Permeability principles	15
1.3.2 Transport pathways across the pulmonary epithelium	16
1.4 Mucus layer	20
1.4.1 Airway of patients with respiratory diseases	26
1.4.2 Mucus as a barrier for drug delivery	28
1.4.3 Serum protein binding and its effect on drug disposition	31
1.4.4 Mucus models to evaluate drug diffusion	33
1.4.5 Method to study drug binding to biomacromolecules	34
1.5 Cystic fibrosis	41
1.5.1 ENaC blockers	46
1.6 Thesis Aims and objectives	54
1.7 References	56
Chapter 2: Materials and Methods	70
2.1 Normal Human Bronchial Epithelial	71
2.1.1 NHBE cells culture reagents and media preparation	71
2.1.2 NHBE Cell Culture	71
2.1.3 Cell counting and viability	73
2.1.4 Cytokine Treatment	74

2.1.5 Electrical Measurements	74
2.1.6 Immunochemistry assay for MUC5AC identification	75
2.1.7 Human mucus harvesting from NHBE cells	75
2.1.8 Identification of mucin structure by AFM	76
2.2 Ex vivo system using porcine respiratory tract mucus	76
2.2.1 Materials for porcine lung mucus extraction	77
2.2.2 Tracheal and lung dissection and mucus harvest	77
2.2.3 Alcian Blue Staining	78
2.2.4 Determination percentage dry weight of sample harvest from porcine trachea and bronchi and purified gut porcine mucin	79
2.3 Solute transport assays using purified PGM	80
2.3.1 Franz-cell chamber	80
2.3.2 High-performance liquid chromatography (HPLC)	81
2.3.3 Materials	84
2.3.4 Descriptions of samples preparations	84
2.3.5 Analysis of solute transport across PGM solutions	85
2.3.5.1 Quantification of FL-Na and FITC-dex probes in diffusion assay	86
2.3.5.2 Quantification of amiloride and benzamil in diffusion assay	87
2.3.5.3 Apparent permeability coefficient	87
2.4 Biochemical Analysis of ex vivo PLM and PJM	88
2.4.1 Materials details	88
2.4.2 Respiratory porcine mucus pH determination	89
2.4.3 Determination of mucin concentration	89
2.4.4 Determination of DNA concentration	89
2.4.5 Investigation of the amiloride and benzamil interaction with mucin	90
2.4.6 Fluorescence spectroscopy	90
2.4.7 Ultraviolet-Visible Spectrophotometer (UV-VIS)	91
2.4.8 Materials	92
2.4.9 Sample preparation	92
2.4.10 Fluorescence spectroscopy	92
2.4.10.1 Effect of solvent polarity on amiloride and benzamil fluorescence	93
2.4.11 UV spectroscopic approach	93
2.5 Development of ultrafiltration binding assay	94
2.5.1 96-well ultrafiltration assay	94
2.5.2 Materials	94
2.5.3 Sample preparation	95

2.5.4 Sample preparation for ultrafiltration assay	98
2.5.5 Analyses of interaction between 552-02 and benzamil with reduced mucin	99
2.5.6 Mucin precipitation	99
2.5.7 Solute analysis	99
2.5.8 Determination of Mass Balance	99
2.5.9 Determination of % binding	101
2.5.10 Determination of non-specific binding (%NSB)	101
2.5.11 Isothermal binding curve	101
2.5.12 Ultrafiltration binding assay using DNA and Alginate	102
2.6 Calu-3 cell culture	103
2.6.1 Calu-3 cell culture reagents and media preparation	103
2.6.2 Calu-3 cell culture	103
2.6.3 Sample preparation for transportation assay through Calu-3	104
2.6.4 Transportation assay	104
2.6.5 Permeation assay through Calu-3 using 552-02 in mucin solution	105
2.6.6 HPLC analysis	105
2.6.7 P_{app} calculation	106
2.7 Purification of porcine jejunal mucin	106
2.7.1 Materials	106
2.7.2 PJM collection	106
2.7.3 Mucus preparation	107
2.8 Application of STD-NMR for ligand characterization	110
2.8.1 Nuclear magnetic resonance (NMR)	110
2.8.1.1 Theoretical background	110
2.8.2 Saturation Transfer Difference -NMR	112
2.8.3 Material	113
2.8.4 A Application of STD-NMR to Salbutamol and Tobramycin using fresh PLM and PGM	114
2.8.5 Application of STD-NMR to OF-80-NS22 and 552-02 in PGM solution and PJM	115
2.8.5.1 Elimination of glycerol contamination from mucin	115
2.8.5.2 STD-NMR Analyses of OF-80-NS22 and 552-02 in PGM solution	116
2.8.5.3 Competition STD-NMR for the detection of high-affinity ligands	116
2.8.5.4 Analyses of OF-80-NS22 and 552-02 in PJM solution	116
2.9 References	118
Chapter 3: Identification and characterisation of mucus model for drug permeation studies	119

3.1 Introduction	120
3.2 Materials and Methods	123
3.3 Results	125
3.3.1 Growth and differentiation of NHBE monolayers on Transwell culture inserts	125
3.3.2 Investigation of porcine lung tissue as a source of respiratory mucus	132
3.3.2.1 Biochemical and physical analysis of porcine mucus	134
3.3.3 Application of Sigma PGM model to mucin permeability studies	136
3.3.3.1 Validation of fluorescence-based analytical methods	136
3.3.3.2 Permeability of reconstituted PGM gels to a molecular weight range of fluorescent probes	137
3.2.4 Transport of amiloride and benzamil across PGM gels	142
3.4 Discussion	146
3.5 Reference	156
Chapter 4: Understanding of physical-chemical relationship between mucin-ENaC blockers interactions	160
4.1 Introduction	161
4.2 Material and methods	166
4.3 Results	169
4.3.1 Identification of amiloride and benzamil binding to mucin study by florescence and UV-visible spectrophotometry	169
4.3.2 Development of fluorescence-based analytical methods for amiloride and analogues	176
4.3.2.1 Validation of ultrafiltration binding assay using a multiscreen 96-wells Plate	176
4.3.3 Isotherm binding and physical-chemical correlation between mucin and amiloride analogues	178
4.3.4 Influence of Alginate and DNA in ENaC blocker disposition	190
4.3.5 Effect of TCEP on Benzamil and 552-02 mucin binding	199
4.3.6 Permeability characteristic of calu-3 monolayer: in-vitro correlation to predict amiloride and analogue absorption in the lung	200
4.3.6.1 Relationship between drug physicochemical properties and transport across Calu-3 cell	204
4.3.6.2 Statistical analysis of mucin binding and Papp across Calu-3 with SPSS	206
4.3.7 Influence of porcine purified mucin on 552-02 apparent permeability across Calu-3 monolayer	209
4.4 Discussion	211
4.5 Reference	231

Chapter 5: Investigation of drug-mucin interaction by STD-NMR	237
5.1 Introduction	238
5.2 Material and methods	242
5.3 Results	244
5.3.1 Tobramycin binding to mucin study by STD-NMR	244
5.3.2 Salbutamol binding to mucin study by STD-NMR	248
5.3.3 Analysis of OF-80-NS22 and 552-02 binding to mucin by STD-NMR	250
5.3.4 PJM purification and biochemical analysis	254
5.3.5 STD-NMR studies of OF-80-NS22 and 552-02 binding to PJM	258
5.4 Discussion	264
5.5 Reference	277
Chapter 6: General Discussion, Conclusions and Future Work	282

Figures List

		Page
Figure 1.1	Trachea anatomy	4
Figure 1.2	The Weibel model of lung anatomy	5
Figure 1.3	Example of particles interaction	7
Figure 1.4	Airway Epithelium	9
Figure 1.5	Conventional epithelia transport paradigm	18
Figure 1.6	Representation of “gel-on-liquid” model (A) and “gel-on-brush” model (B)	21
Figure 1.7	Mucin structure	22
Figure 1.8	Secreted and membrane bound mucin	26
Figure 1.9	Airway in CF	27
Figure 1.10	Effect of IL-13 on Goblet cells density (GCD)	28
Figure 1.11	Mechanisms that may stop particles from readily diffusing through mucus gel	30
Figure 1.12	Protein-Ligand classic hyperbolic binding curve	35
Figure 1.13	Separation of bound and free compound by non-spectroscopy technique	36
Figure 1.14	CFTR structure and gating conformation	42
Figure 1.15	CFTR gene mutations are categorised into five classes	43
Figure 1.16	Model depicting ion transport mechanisms regulating ASL volume in normal (A) and CF airway epithelia (B)	44
Figure 1.17	The epithelial sodium channel	47
Figure 1.18	Amiloride structure	48
Figure 1.19	Benzamil (A) and phenamil (B) structure	49
Figure 1.20	Compound 552-02 structure	50
Figure 1.21	Example of non-pyrazinoyl guanidine ENaC blocker	51
Figure 1.22	Example of quaternary amines (A) and α -branched quaternary amines ENaC Blockers (B)	52
Figure 1.23	NVP-QBE-170 structure	53
Figure 2.1	NHBE cells ALI culture	73
Figure 2.2	Porcine lung dissection	78
Figure 2.3	Franz-cell system	80
Figure 2.4	HPLC system	82
Figure 2.5	Multiscreen plate	94
Figure 2.6	Structure of amiloride and its analogues used in this project	96
Figure 2.7	Porcine Small intestine used for mucin extraction	107
Figure 2.8	Sealing of centrifuge tube	108
Figure 2.9	A representations of nucleus orientation	111
Figure 2.10	Schematic representation of STD-NMR	113
Figure 3.1	Transepithelial resistance of NHBE cells	126

Figure 3.2	NHBE at day 3 of Air Lift (10x)	127
Figure 3.3	Alcian Blue Staining of NHBE cell +/- IL13 mucus	128
Figure 3.4	Immunofluorescence images of IL-13 treated NHBE cells (10X)	129
Figure 3.5	Confocal images from NHBE cell IL-13 treated	130
Figure 3.6	AFM images of mucus harvested from NHBE cells	131
Figure 3.7	Tissue kept in aseptic (A) and non-aseptic (B) condition	132
Figure 3.8	Alcian blue staining of mucus harvested from fresh porcine lung tissue	134
Figure 3.9	Cumulative transport of FL-Na and FITC-dextran probes across 1% PGM gels using Franz cell diffusion cells	138
Figure 3.10	Influence of the molecular weight of probes on the Papp	142
Figure 3.11	Example cumulative mass transport of amiloride and benzamil across 1% PGM	143
Figure 4.1	Fluorescent emission of amiloride and benzamil upon titration into mucin	170
Figure 4.2	The linear relationship between Δ fluorescence intensity and drugs concentration	171
Figure 4.3	Fluorescence intensity of amiloride and benzamil in different proportions of EtOH	171
Figure 4.4	UV-Vis absorption spectra of the mixture mucin-drug in the presence of different concentration (a-l) of amiloride (A) or benzamil (B)	173
Figure 4.5	UV-Vis absorption UV-vis spectra of the mixture mucin-drug mixture (solid line) and summed absorbance of mucin and drug alone (control dotted line)	175
Figure 4.6	Drug-mucin binding isotherm (1)	181
Figure 4.7	Drug-mucin binding isotherm (2)	182
Figure 4.8	Mucin- binding at 20 μ M correlated with amiloride and analogues physical parameters	185
Figure 4.9	Mucin- binding at 20 μ M correlated with amiloride and analogues physical parameters (1)	187
Figure 4.10	Mucin- binding at 20 μ M correlated with amiloride and analogues physical parameters (2)	188
Figure 4.11	Retention time of amiloride and analogues correlated with $\log P_{o/w}$	189
Figure 4.12	Non Specific Binding at 20 μ M correlated with amiloride and analogues physical parameters	190
Figure 4.13	Alginate binding (gray bar) and non-specific binding (black bar) at 20 μ M of NQQA and QQA after ultrafiltration assay	192
Figure 4.14	Alginate-binding at 20 μ M correlated with amiloride and analogues physical parameters (1)	193
Figure 4.15	Alginate-binding at 20 μ M correlated with amiloride and analogues physical parameters (2)	194
Figure 4.16	DNA binding (gray bar) and non-specific binding (black bar) at 20 μ M of NQQA and QQA after ultrafiltration assay	196

Figure 4.17	DNA- binding at 20 μ M correlated with amiloride and analogues physical parameters (1)	197
Figure 4.18	DNA- binding at 20 μ M correlated with amiloride and analogues physical parameters (2)	198
Figure 4.19	Mucin binding of benzamil and 552-02 at 20 μ M with (gray bar) or without (black bar) 50mM TCPE treatment	199
Figure 4.20	Transepithelial resistance of calu-3 cells	201
Figure 4.21	Cumulative transport of amiloride and analogues across Calu-3 monolayer (A) NQQA and (B) QQA	202
Figure 4.22	Apparent permeability of amiloride and analogues at 100 μ M correlated vs physical parameters	205
Figure 4.23	Apparent permeability of amiloride and analogues at 100 μ M across cell-free Transwell inserts correlated vs physical parameters	206
Figure 4.24	Transport of 552-02 across Calu-3 cell monolayers in the presence and absence of purified mucin	210
Figure 4.25	Theoretical representation of monolayer binding fitted by Langmuir model and multilayer binding fitted by GAB model	218
Figure 5.1	STD-NMR spectroscopy for the study of tobramycin-porcine respiratory mucus binding	245
Figure 5.2	STD-NMR spectroscopy for the study of tobramycin-PGM mucin binding	247
Figure 5.3	STD-NMR spectroscopy for the study of salbutamol-PGM mucin binding	249
Figure 5.4	STD-NMR spectroscopy for the study of drug-mucin binding	252
Figure 5.5	STD-NMR spectroscopy for the competitive study of ligands-mucin binding	253
Figure 5.6	1 ^o Schematic of the mucin product from CsCl gradient centrifugation	254
Figure 5.7	1 ^o CsCl gradient centrifugation	255
Figure 5.8	2 nd CsCl density-gradient ultracentrifugation	256
Figure 5.9	2 nd CsCl density-gradient ultracentrifugation	257
Figure 5.10	Glycerol contamination of PJM	259
Figure 5.11	STD-NMR spectroscopy for the study OF-80-NS22 and purified mucin binding.	260
Figure 5.12	STD-NMR spectroscopy for the study 552-02 and purified mucin binding	262
Figure 5.13	Saturation curve of 552-02 and percentage of magnetisation transfer	263
Figure 5.14	Theoretical saturation curve of 552-02	275
Figure 6.1	552-02 “Interacting” and “non-interacting” protons	

Tables List

Table 1.1	Type and tissue expression of human mucins	24
Table 2.1	Summary of calibration curve range and analytical method used to analyse probes and drug molecules used for the permeation assay	87
Table 2.2	Summary of dilution used for Mucin and DNA assay for different mucus/mucin model: <i>ex vivo</i> porcine respiratory mucus, PGM 1,3,5%, purified gut mucin	90
Table 2.3	Summary of Amiloride and analogues calibration range, EM/EX, Analytical method, LOD/LOQ, analyte retention time (RT) and internal standard used for the development of the multiscreen binding assay	97
Table 2.4	Concentration of drug molecules (analyte) used to study the interaction with mucin (1 μ M) and concentration of internal standard used for each analyte	98
Table 2.5	Representation of gradient method used to analyse Amiloride and Analogues after transport assay through Calu-3	105
Table 2.6	Buffers needed for gut mucin preparation	107
Table 3.1	Condition tested for respiratory porcine mucus production	133
Table 3.2	Determination of % dry solids for porcine lung mucus	134
Table 3.3	Determination of mucin and DNA %	135
Table 3.4	Nominal molecular weight and Stokes diameter of all fluorescent probes applied to PGM gels	136
Table 3.5	Linearity and sensitivity of the method	137
Table 3.6	Influence of mucin concentration on FL-Na and FITC probes diffusion 30-120 min	140
Table 3.7	Influence of mucin concentration on Amiloride and Benzamil compared with FL-Na	145
Table 4.1	Compounds, FL-Na and FD4 mass balance in solution +/- mucin, %NSB and % mucin binding determined after ultrafiltration assay	178
Table 4.2	Physical properties of amiloride and analogues	184
Table 4.3	Permeability of Calu-3 monolayers or bare Transwell inserts to amiloride and analogues	203
Table 4.4	Statistical analysis of mucin binding and P_{app} across calu-3 with SPSS	208
Table 5.1	Determination of % dry solids	258

Abbreviations list

A→B	apical to basolateral
AB	alcian blue
AFM	Atomic Force Microscopy
ALI	Air Liquid Interface
ASL	airway surface liquid
B-ALI TM	Bronchial Air Liquid Interface media
BCRP	breast cancer resistance protein
BSA	bovine serum albumin
Caco-2	colorectal carcinoma cell line
Calu-3	human bronchial adenocarcinoma cell line
CF	cystic fibrosis
CFTR	Cystic Fibrosis Transmembrane conductance Regulator
CNA	cianoacetamide
COPD	Chronic Obstructive Pulmonary Disease
CsCl	caesium chloride
D ₂ O	Deuterium oxide
DABA	3,5 diaminobenzoic acid
DMEM	Dulbecco's Modified Eagles Medium
DNA	deoxyribonucleic acid
ENaC	Epithelia Sodium Channel
EtOH	ethanol
FBS	fetal bovine serum
FL-Na	sodium fluorescein
FDx	FITC-labelled dextran of x kDa molecular weight
g	gram
GdnCl	guanidinium chloride
h	hour
HPLC	High-Performance Liquid Chromatography
H ₂ O	water
I _{sc}	short-circuit current
IL	interleukin
ITC	isothermal titration microcalometry
kDa	kiloDalton
L	litre
LOD	limit of detection
LOQ	limit of quantification
M	molar
m	metre
MC	mucociliary clearance
min	minute(s)
µm	micrometre
mL	millilitre
µL	microliter
mM	millimolar

μM	micromolar
MW	molecular weight
NaCl	sodium chloride
NaOH	sodium hydroxide
NaPO ₄	sodium phosphate buffer (Na ₂ HPO ₄ and NaH ₂ PO ₄)
NHBE	normal human bronchial epithelial
nm	nanometre
NMR	Nuclear magnetic resonance
nmole	nanomole
NP	Nanoparticles
NQQA	non-quaternary amine
NSB	non-specific binding
Papp	apparent permeability coefficient
PAH	polycyclic aromatic hydrocarbons
PBS	phosphate buffered saline
PCL	periciliary liquid layer
PEG	poly(ethylene glycol)
PGM	porcine gastric mucin
PJM	porcine jejunal mucin
PLM	porcine lung mucus
pMDI	pressurised metered dose inhaler
PSA	polar surface area
QQA	quaternary amine
RPMI	Roswell Park Memorial Institute medium
RNA	ribonucleic acid
RT	room temperature
s	seconds
scFv	short chain fragment variable antibody fragment
SEM	scanning electron microscope
SLC	solute carrier transport family
STD-NMR	Saturation-Transfer Difference NRM
TCEP	Tris (2-carboxyethyl) phosphine hydrochloride
TER	transepithelial electrical resistance
TJ	tight junction
UV/Vis	Ultra-violet/visible
VIF	Variance inflation factor
WGA	wheat germ agglutinin
w/v	weight/volume

Chapter 1

Chapter 1 : General Introduction

1.1 Pulmonary Delivery

Pulmonary delivery of drugs has become an attractive target of scientific and biomedical interest in the health care and research area thanks to capability of lung of absorbing pharmaceuticals either for local transport or for systemic delivery. The lungs provide a huge surface area of alveoli, of approximately 70-140 m² in adult humans, ⁽¹⁾ with a rich capillary network which acts as an excellent absorbing surface for administration of drugs.

The first to demonstrate that the lungs were naturally permeable to peptides was in 1925 when Gansslen ⁽²⁾ discovered the possibility to lower blood glucose in diabetic subject following inhalation of insulin, 51-amino-acid peptide (5.7 kDa). Later in 1989, Patton, McCabe ⁽³⁾ showed that human growth hormone (hGH), 192-amino-acid protein (22 kDa), following instillation into the rats' lungs was absorbed into the systemic circulation.

Initially, pulmonary delivery seemed to be complicated and unreliable due to its unknown long-term safety. Things changed in 1990 when a startup company (Nektar) started the development of inhaled insulin, and is now being continued by a variety of companies ⁽⁴⁾. Particularly for drugs with poor oral absorption such as peptides and proteins ⁽⁵⁾, the pulmonary route promises a progressive alternative way of reaching the systemic circulation (thereby avoiding painful injections). Compared to the gastrointestinal tract and liver, in the lungs drug-metabolizing enzymes are in much lower concentrations ⁽⁶⁾ ⁽⁷⁾ and the inhaled drug are less likely to be degraded than if they had been delivered orally. This huge advances in aerosol technology allows to

control deposition, to deliver aerosols at the correct part of the inspirational cycle and increase reliability of deposition pattern. Thanks to advancement in application, nowadays pulmonary drug delivery is useful to treat several disease diabetes ⁽⁸⁾, bone disorders ⁽⁹⁾, tuberculosis ⁽¹⁰⁾, migraine acute lung injury and others.

Currently, inhalation therapy is the best option for lung diseases like asthma, cystic fibrosis, and COPD. The most commonly used aerosols, designed for local drug delivery in the therapy of lung diseases contain bronchodilators used to improve mucociliary clearance in COPD ⁽¹¹⁾, or glucocorticoids that are applied directly to the lung for therapy of obstructive airway and inflammatory diseases. Pulmonary delivery is also used for local delivery of aerosolized aminoglycosides such as tobramycin, for the treatment of pulmonary infection by *P. aeruginosa* ⁽¹²⁾.

1.1.1 Anatomy of the pulmonary tract

The pulmonary tract includes tracheo-bronchial tree, which resembles an inverted tree, bronchus, bronchiole and alveolus. The trachea has an inner diameter of about 25 millimetres and a length of about 10 to 16 centimetres, is made of about 20 rings of tough cartilage rings with a membrane in between. The trachea is nearly but not quite cylindrical, being flattened posteriorly, in fact the back part of each ring is made of smooth muscle and connective tissue. The point where trachea branches in bronchus is called carina (Figure 1.1).

Chapter 1

The lung anatomy can be described with the Weibel model, which is the simplest model of human lung developed in 1963. Weibel represented the lung anatomy as a system of 23-fold bifurcating tubes, called generations, based on the dimension of the airways. Weibel divided the lung into two zones: conducting zone and respiratory zone. The only function for the conductive zone is to direct air into the lung. Gas exchange occurs only at the respiratory zone inside alveoli.

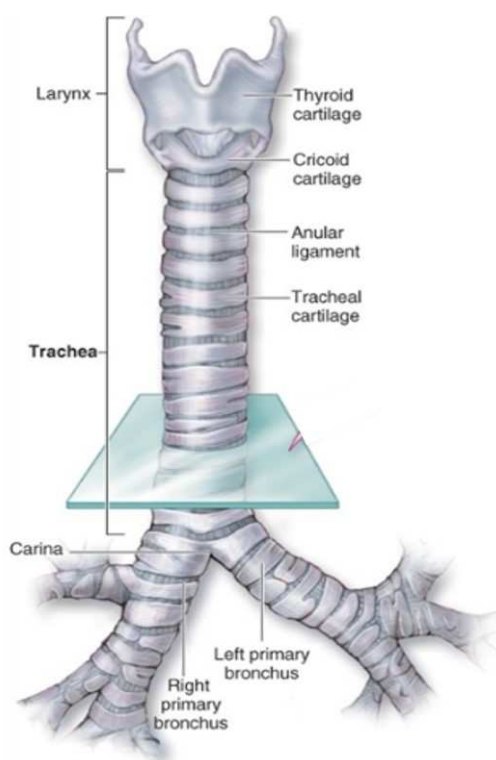


Figure 1.1 Trachea anatomy

The trachea begins immediately below the larynx. Around the trachea wall there is a series of 16 to 20 C-shape cartilage rings. Rings encircle the front part of the trachea but are open where the trachea lies next to the esophagus. The tracheal rings are joined together by anular ligaments. The trachea bifurcates into the primary bronchi and the cartilaginous ridge at the site of the tracheal bifurcation is called Carina. *Taken from Healthy lifestyle, 2013. Human Anatomy Trachea.*

In the Weibel model, the trachea is indicated as generation 0 ($G=0$), this is a straight duct and at its end is divided in right and left mainstem bronchus that serve the right and left

Chapter 1

lung respectively. Bronchi successively branch into increasingly narrow and short bronchioles until G=16. At this point the respiratory tract is still surrounded by cartilage. After G=16 bronchioles no longer have cartilage around. After a total of about 23 divisions, the bronchioles end at alveolar ducts. At the end of each alveolar duct, there are clusters of alveoli (air sacs), which is the site where gas exchange occurs (Figure 1.2 (13)).

	Anatomy	Structure	Generation (Z)
Conducting zone		Larynx	N/A
		Trachea	0
		Primary bronchi	1
		Secondary bronchi	2
		Tertiary bronchi	3
		Small bronchi	4
		Bronchioles	5
		Terminal bronchioles	6-16
Respiratory zone		Respiratory bronchioles	17-19
		Alveolar sacs	23

Figure 1.2 The Weibel model of lung anatomy

The airway structures of Weibel's model branches in 23 generations with the trachea representing the G=0. The lung is divided into two zones: the conducting zone comprising covering G=0 to 16 (including trachea, bronchi and bronchioles) and the transitory and respiratory zone from G=17 to 23 (including respiratory bronchioles, alveolar ducts and alveolar sacs). Taken from ⁽¹³⁾.

1.2 Barriers of the pulmonary route

1.2.1 Formulation challenges

A very controlled aerosol creation process is required to achieve highly controlled drug doses in fine droplets or particle clouds. The complexity of pulmonary delivery derives from the need to quickly convert formulations into fixed-dose aerosol clouds and to deliver these in a minimum number of inspirations. Particles of the aerosol clouds should be neither too large (to avoid deposit primarily in the upper airways, mouth and throat), nor too small (exhalation risk).

One of the most important design variables for an aerosol formulation is the particle size. Aerosol sizes, expressed as aerodynamic diameters, depends on the area of distribution and should preferably be 3-7 μm for tracheobronchial deposition, or 1-3 μm for deposition in the lower pulmonary regions ⁽¹⁴⁾. The design of the particles should be so accurate to make sure it will reach a specific region of the respiratory tract.

The deposition of a particles depends on the flow velocity, particle size, density and rate of breathing so mainly occurs near the bifurcations of large conducting airways where air velocities are high. Gravitation sedimentation occurs for the deposition in the small conducting airway of particles with diameter of 1-5 μm , while with diameter of 0.5 μm or less, acquire a random Brownian motion which can result in particle deposition in small airways and alveoli where air velocities are very low.

Another barrier for particle deposition in aerosol therapy is the physical interactions of particles such as van der Waals (due to electromagnetic nature of particles), or mechanical interlocking, depending of the roughness surface, ⁽¹⁵⁾ (Figure 1.3).

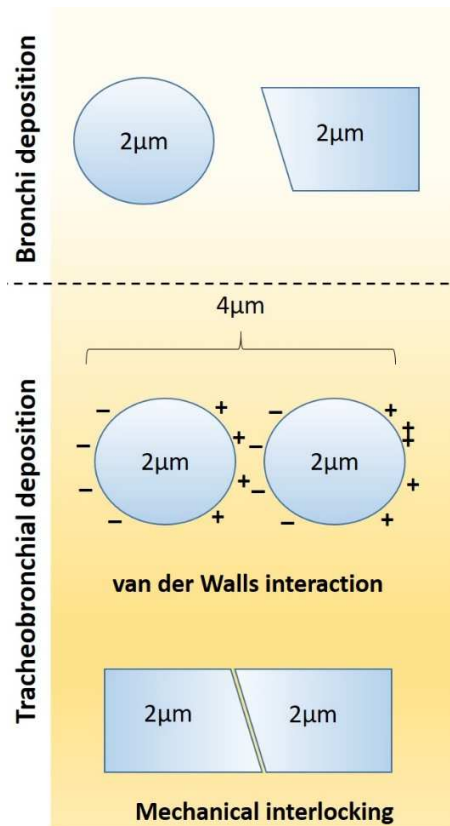


Figure 1.3 Example of particles interaction. Particles 2µm in diameter will deposit in bronchi. Particles may undergo to van der Wall interaction or particles of a certain shape can mechanically interlock forming a larger particle with consequent deposition in a different site.

The physical-chemical stability and pharmaceutical properties (e.g. dissolution) of the active pharmaceutical ingredient may be enhanced with the use excipients which act to improve formulation efficacy but are not intended to have therapeutic effects (e.g. sugar, cholesterol). Despite the efficiency of advanced dosage form designs, certain barriers, such as cells of the airway or alveolar epithelium, and mucus, still compromise the absorption of drug, peptides and proteins by the lung.

1.2.2 Biological barriers

The air we breathe is full of chemicals and harmful substances, including dust, bacteria, fungi, viruses and pollutants. The respiratory system is equipped with a number of defence barriers to clean and protect itself: bronchial and trachea epithelium, alveolar epithelium, macrophages and mucus

Bronchial and Tracheal Epithelium

The epithelium lining the upper airways is classified as ciliated pseudostratified columnar epithelium. At least eight morphologically distinct epithelial cell types are present in human respiratory epithelium, although based on ultrastructural, functional and biochemical criteria these may be classified into three: ciliated cells, secretory cells and basal cells (Figure 1.4). The ciliated cells (Figure 1.4) are columnar epithelial cells with specialized ciliary modifications. They are the predominant cell type within the conducting airways, accounting for over 50% of all epithelial cells ⁽¹⁶⁾. Up to 300 cilia/cell are usually present on a cell's surface and beat in a coordinated manner from the lung to the throat ⁽¹⁷⁾. *Basal cells* are small, nearly cuboidal cells thought to have some ability to differentiate into other cells types found within the epithelium (Figure 1.4) ⁽¹⁸⁾. Within the epithelium, basal cells are the only cell that are firmly attached via hemidesmosomal complexes to the basement membrane and as such, play a role in the attachment of more superficial cells to the basement membrane ⁽¹⁹⁾. Secretory cells (Figure 1.4) are columnar epithelial cells that contain membrane-bound mucous granules and secrete mucus to trap foreign objects in the airway lumen ⁽²⁰⁾. Production of the correct amount

of mucus and the viscoelasticity of mucus are important for efficient mucociliary clearance (MC) which is a mechanism that protects the lungs from deleterious effects of irritants and pathogens. The foreign matter is trapped by the mucus and moved up to the mouth thanks to the beating of cilia where it is swallowed or coughed up.

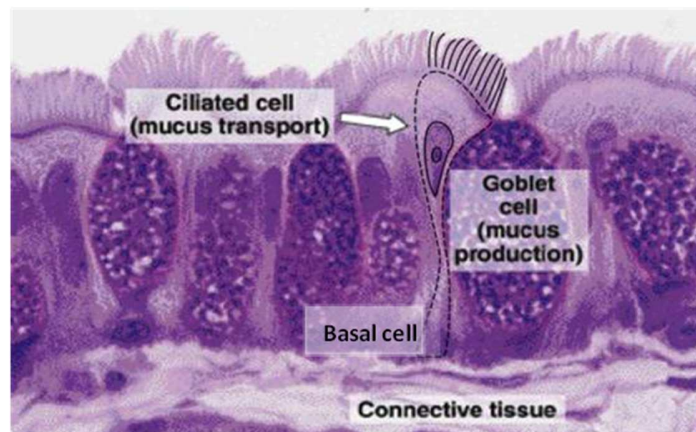


Figure 1.4 Airway Epithelium. Micrograph depicting the main components of the tracheobronchial epithelium, ciliated and goblet cells. The nuclei of basal cells are present also. Taken from *Junqueira and Carneiro, Basic Histology, a text and atlas*, p. 350, Figure 17-2.

In normal human trachea, it is estimated that there are up to 6800 mucus-secreting cells/mm² of surface epithelium, although in chronic airway inflammatory diseases such as chronic bronchitis and asthma, mucous cell hyperplasia (increase in the number of cells) and metaplasia (replacement of one differentiated cell type with another mature differentiated cell type) is a common pathological finding and is thought to contribute to the productive cough associated with these diseases ⁽²¹⁾. These cells are thought to be capable of self-renewal and may also differentiate into ciliated epithelial cells ⁽¹⁹⁾. Secretory cells have been further divided into subtypes based on their microscopic appearance, Club, goblet, and serous cells which are three types of non-ciliated epithelial cells.

Chapter 1

- Goblet cells, so named because of their 'wine goblet' shape, are the predominant secretory cell of adult human tracheobronchial surface epithelium, are glandular simple columnar epithelial cells whose function is to secrete mucin. In the respiratory tract they are found inside the trachea, bronchus, and larger bronchioles. The nuclei tend to be displaced toward the basal end of the cell body, leading to intense basophilic staining. Goblet cells are the secretory cell generated in larger numbers in response to infection ⁽²²⁾ and chronic irritation ⁽²³⁾ of the airways.
- Club cells are the predominant secretory cell in the bronchioles, are smaller and less numerous of the other secretory cells and with an irregular shape. Club cells (formerly known as Clara cells) are dome-shaped cells with short microvilli and are found in the bronchioles. They can be distinguished from goblet and serous cells by low cuboidal shape. Moreover, they act as a stem cell being progenitor cells of goblet and ciliated cells ⁽²⁴⁾. Secreting a small variety of products, such as Club Cell Secretory Protein (CCSP) and 10 a solution similar to the lung surfactant, Club cells protect the bronchiolar epithelium.
- Serous cells, with goblet cells, are considered to be progenitors of the secretory cells of the trachea. They are present in the tracheobronchial tree. Serous cells exist in the human epithelium before birth but not after ⁽²⁵⁾. After birth it is possible to find serous cells only at submucosal glands. They protect the airway surface from the destructive effects of bacterial producing one or more protease inhibitors ⁽²⁶⁾. For this reason, serous cell resembles an immobilized neutrophil.

The Alveolar Epithelium

There are three major cell types in the alveolar wall: *Type I pneumocytes* (squamous alveolar) cells that form the structure of an alveolar wall. These cells that make up 90% of the alveolar surfaces area ⁽²⁷⁾. They are specialized in gas exchanges, in fact serve as very thin (often only 25 nm deep) gas-permeable components of the blood-air barrier. *Type II pneumocyte* (great alveolar) constitute 15% of the lung and 10% of the total alveolar cells ⁽²⁷⁾. They are interspersed among the type I cells, to which they attach by desmosomes and occluding junctions. Type II cells pneumocytes are secretory cells. Their secretory product, pulmonary surfactant, is assembled and stored in the lamellar bodies. Surfactant is continuously released by exocytosis. Alveolar macrophages, known also as dust cells, destroy foreign material that escapes the mucus and cilia in the conducting portion of the system. Alveolar macrophages are important regulators of immune system activity through secretion of pro/anti-inflammatory cytokines (IL-1, IL-6, IL-8, TGF- β), but are also involved in the phagocytosis of cells in the normal lung that have undergone cell-death (apoptotic or necrotic cells) for cell turnover, repair of injured epithelium ⁽²⁸⁾.

Lung surface lining (mucus and surfactant)

Mucus is a complex aqueous mixture of water (95%) and solids glycoproteins (mucins) (1-5%), mineral salts (0.5%), lipids (0.5-1%), free proteins (1%) and cellular debris ⁽²⁹⁾. The higher levels of the respiratory tract, trachea and bronchi, are covered by a mucus gel layer, which in the case of the mammalian trachea and large bronchi was observed to

Chapter 1

average 1-10 μm in thickness and is situated at the level of the tip of the cilia. Specialized epithelial cells called secretory cells secrete mucus, which adheres to the epithelial surface and forms a protective diffusion barrier between the lumen and the cell surface. The respiratory mucus gel performs a number of essential functions that collectively lead to the protection of the airways. Mucus secretions have important protective and lubricative properties, primarily owing to their ability to form a gel layer adherent to the underlying epithelium. In the airway, the major functional role of mucus is to entrap foreign particles and pathogens facilitating their clearance from the lung by means of ciliary transport or cough ⁽³⁰⁾. In fact, mucus is adhesive and this helps to trap dust particles, bacteria and other inhaled debris. Thus, mucus is not only vital for human health, but it also significantly limits the potential for localized and sustained drug and gene delivery to mucosal surfaces ⁽³¹⁾.

While the mucus blanket covering the airways is a hydrogel formed by glycoproteins (mucins), the alveolar epithelium is covered by a thin lining fluid, the so-called surfactant secreted by type II pneumocytes. Its major function is to facilitate the “wetting” of the alveolar epithelium by the respiratory gases. It is a very thin layer of fluid that averages about 50-80 nm, but may be several microns thick in pooled areas and as thin as 15-20 nm in others ⁽³²⁾. Pulmonary surfactant lowers the surface tension of water and allows the membrane to separate, therefore increasing its capability to exchange gases. It forms an underlying aqueous protein-containing hypophase and an overlying phospholipid film composed primarily of dipalmitoyl phosphatidylcholine.

1.3 Lung models for the investigation of lung permeability (*in vivo*, *in vitro* and *ex vivo*)

Experimental protocols for the conduct of *in-vivo* drug absorption studies have been developed in early 1970s by Schanker and co-workers^{(33) (34) (35)} who primarily used small rodents as experimental species for *in vivo* studies of drug molecules administered by intra-tracheal instillation or by aerosol. *In vivo* approaches in laboratory rats continue to be the most important improvements have been made with the use of more sophisticated lung-dosing methods (such as forced instillation, nebulization and aerosol puff) which afford reproducible dosing and control of lung-regional distribution. Whole body pharmacokinetic and dispositional processes complicate greatly the interpretation of *in vivo* data and this is a major drawback of *in vivo* lung PK studies.

A variety of *in vitro* lung epithelial cell lines and primary cultured lung epithelial cell monolayers offer opportunity to investigate the more detailed kinetics and mechanisms of transepithelial drug transport. Cell culture models include primary cell model from human or rodent or cell lines derived from malignant tissue or, alternatively, normal cells transformed by viruses e.g. SV40. While primary cells are relatively expensive (NHBE cells) and / or time-consuming (primary rat epithelia), continuous cell lines (A549, Calu-3, 16HBE14o-) can be maintained and propagated following standard media and protocols to give reproducible results.

The high permeability of the A549 human alveolar cell line make them unsuitable for use in drug permeability experiments. NHBE cells, differentiated normal human bronchial

Chapter 1

epithelial cells, are considered a good system to mimic the bronchial epithelium thanks to mucociliary differentiation when grown at air-liquid interface⁽³⁶⁾ and the expression of multiple integrin subunits that bind to collagen and laminin and mediate adhesion to fibronectin which closely mimics by bronchial epithelial cells *in vivo*⁽³⁷⁾. However, this cell system is difficult to culture, requires specialist defined media that has a short shelf-life, expensive and time and labour-intensive. There is also significant batch-to-batch and inter-donor variability. An alternate approach for a suitable airway epithelium model is to use cancerous lung epithelial cell lines e.g. Calu-3.

Calu-3 cells, derive from a human bronchial adenocarcinoma and are widely used because of their lower cost, reproducibility and ease of use. Calu-3 are cuboidal cells and subapical granules that resembled goblet cell of NHBE cells have been identified by electron microscopic analysis⁽³⁸⁾. They express desmosomes but mucus production and ciliogenesis is reduced under submerged culture conditions⁽³⁹⁾. They are well established system for conducting broncho-epithelial permeability studies *in vitro*⁽⁴⁰⁾⁽⁴¹⁾ expressing the cystic fibrosis transmembrane conductance regulator (CFTR) protein⁽⁴²⁾⁽⁴³⁾ and form a restrictive monolayers resembling well the *in vivo* lung epithelial barrier⁽⁴⁴⁾⁽⁴⁵⁾ thanks to the formation of tight junction *in vitro*. Thanks to this, Calu-3 cells display low paracellular permeability and high electrical resistance. Nevertheless, the using a cell culture model to represent the complex disposition of intact lung may still be debatable. The deficiencies of *in vivo* and *in vitro* models appeared to be resolved with the use of the isolated perfused lung (IPL) as an *ex vivo* model. Despite this *ex vivo* model showed

limitations concerning short viable periods (2-3h), resulted to be kinetically predictive of *in-vivo*.

1.3.1 Permeability principles

Studies on the disappearance of radiolabelled molecules from the lungs of animals, shown that the pulmonary bioavailability of many small molecules is about 100%⁽³³⁾⁽³⁴⁾, probably due to the rapid, extensive absorption and low concentration of enzymes in the lung compared the oral route⁽⁶⁾. The absorption half-life can be roughly estimated using a log octanol–water partition coefficients ($\text{Log } P_{o/w}$). Small hydrophobic inhaled molecules with $\text{Log } p > 1$ appear to be absorbed very rapidly (seconds-minutes) from the lung epithelium, such as nicotine⁽⁴⁶⁾, morphine⁽⁴⁷⁾. Neutral or negatively charged hydrophilic small molecules can be absorbed rapidly (minutes)⁽³⁴⁾ and have a half-life of about 60 minutes⁽⁴⁸⁾.

Although the rapid absorption may have many medical uses, there are situations where is necessary to slow the absorption of an inhaled particles, to regulate its absorption into the body or keep it acting over enough time locally in the lung. There are at least two instances in which small molecules are much more slowly absorbed: high hydrophobicity or positively charged molecules. Molecules with very high hydrophobicity may become too insoluble for rapid absorption and can persist in the lungs for hours, days⁽⁴⁸⁾, such as amphotericin B⁽⁴⁹⁾ and all-trans retinoic acid⁽⁵⁰⁾. Specific interactions (e.g., hydrogen bonds) caused by electron density distribution may also help the mechanism of retention

(e.g., amphotericin B with endogenous sterols). Strongly cationic drugs such as pentamidine and tobramycin are absorbed over a period of hours following inhalation in humans. The long retention has been attributed to the positive charges on the molecules⁽⁵¹⁾ ⁽⁵²⁾ which may bind to the ubiquitous negative charges of the mucin glycoprotein on the epithelia⁽⁵³⁾.

1.3.2 Transport pathways across the pulmonary epithelium

In the context of our understanding of the molecular basis of transepithelial transport it appears that lipophilic molecules are rapidly absorbed presumably because they can integrate into the lipid bilayer surrounding the cells. This translocation constitutes the “transcellular pathway” in which molecules pass by a cell through a cell by diffusing through the cellular membrane, whereas hydrophilic molecules can be absorbed by the epithelium via a “paracellular route” passing through aqueous pores in the intercellular tight junctions⁽⁵⁴⁾ (Figure 1.5). Tight junctions are complexes of proteins that act as a barrier to fluid flow, important for ion selectivity and conductance controlling the passage of ions and neutral species through the intercellular. It has been noticed that the degree of solute ionization correlates inversely with absorption rate. This is thought to be due to interactions with the proteins (occludin, claudin family, junctional adhesion molecule) and lipids within lipid bilayers that line the pore. Macromolecular drug absorption from the lungs can be regulated by vesicular transport where a membrane protein regulates/facilitates the molecular movement⁽⁵⁵⁾.

Chapter 1

Another mechanism of transportation of small molecule through the epithelium is the “active transport” where molecules are transported into the cell (carriers) or out the cell (efflux) by binding to specific carrier proteins on the cell surface and using energy exchange to drive against a concentration gradient. The active transporters in the lung are can influence the residence time of drug in the lung and affect the drug absorption profile. The current knowledge of expression, localization, functionality of drug transporters in the lung is poorly understood.

The transporters most likely to affect the disposition of inhaled compounds are;

- The ATP-binding cassette (ABC) superfamily. ABC transporter are family of transmembrane protein which function as ATP-dependent efflux pumps for wide range of structurally diverse molecules from the cell cytoplasm to external environment to which belong P-glycoprotein (P-gp), the multidrug resistance protein (MRPs), breast cancer resistance protein (BCRP).
- The solute-linked carrier (SLC and SLCO) superfamily which includes the peptide transporters (PEPT1/PEPT2), the family of organic cation transporters (OCTs) and organic cation/carnitine transporters (OCTNs), organic anion transporters (OATs) and organic anion polypeptides transporters (OATPs).

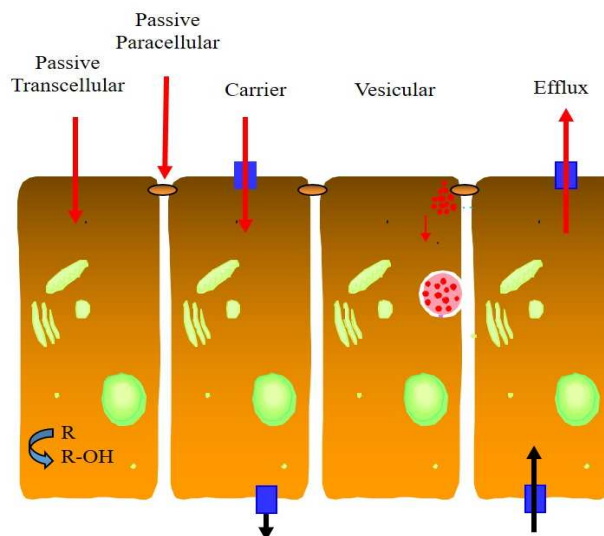


Figure 1.5 Conventional epithelia transport paradigm. Passive transcellular; transportation of solutes by a cell through a cell. Passive paracellular; diffusion between cell junctions. Carrier; molecules movement occurs via special transport proteins. Vesicular; molecular movement is regulates or facilitates by membrane protein. Efflux; molecules are moved out the cell via transporters.

P-glycoprotein

P-gp is 170 kDa transporter encoded by the multi drug resistance (MDR1) gene in humans and contains electronegative groups and weak positive charge. Probably due to the polyspecific nature of the P-gp binding pocket, the substrate specificity of this efflux transporter comprises a broad range of chemically diverse molecules. As a result, lipophilic and amphiphilic molecules can both serve as substrates for P-gp ⁽⁵⁶⁾ ⁽⁵⁷⁾. Expression of P-gp was observed in human lung ⁽⁵⁸⁾, on the apical of bronchial epithelial cells ⁽⁵⁹⁾ ⁽⁶⁰⁾.

Organic cation transporters (OCTs) and organic cation/carnitine transporters (OCTNs).

OCTs transporter have the capacity to translocate neutral and positively charged endogenous and exogenous molecules across the plasma membrane in both directions. The majority of OCT/OCTN substrates are positively charged at physiological pH and include hormones, neurotransmitters, and drugs⁽⁶¹⁾. The expression of OCTs and OCTNs in the lung has been poorly studied but evidence of the expression on the human airway epithelia cells are available for both OCTs^{(62) (63)} and OCTNs⁽⁶⁴⁾. Lips, Volk⁽⁶³⁾ reported the expression of OCT1-3 on the luminal membrane in ciliated epithelial cells with also evidence of OCT3 in basal cells. OCTN1 have been observed in the apical side of airway epithelial cells, whereas there are observations of OCTN2 on both lung epithelium and alveolar type I epithelium⁽⁶⁵⁾.

Organic anion transporters (OATs) and organic anion polypeptides transporters (OATPs)

OATs are members of the solute carrier family 22 (SLC22), and OATPs belong to the solute carrier family SLC21/SLC0 and mediate the absorption and elimination of endogenous and exogenous organic anions. For these transporter there is a lack of expression within the lung tissue.

1.4 Mucus layer

Mucus is a slippery secretion containing DNA, lipids, immunoglobulins, inorganic salts, antimicrobial enzymes (such as lysozyme), proteins (such as lactoferrin) ⁽⁶⁶⁾, and glycoproteins (mucins) that are produced by goblet cells in the mucous membranes and submucosal glands. The thickness of this mucus layer varies on different mucosal surfaces, from 50 to 450 μm in the stomach ⁽⁶⁷⁾, to less than 1 μm in the oral cavity. Mucus is a gel with properties of both a soft (deformable), elastic solid and a viscous fluid ⁽⁶⁸⁾ ⁽⁶⁹⁾ that has evolved into a dynamic semi-permeable barrier, impermeable to most pathogens and nanoparticles (NP) while enable exchange of water, hormones, nutrients. In the lung is conveyed upwards by epithelial cilia, an essential clearance mechanism that removes foreign material from the tracheobronchial tree, and as well, maintains the patency of small bronchi and bronchioles.

The lung mucus blanket is not a continuous sheet but comprises two layers of differing physical properties: an upper gel layer consisting of mucus with a high viscosity that traps inhaled particles and facilitates their transport and a lower layer called periciliary liquid layer (PCL) that contacts surface epithelial cells where cilia beat and cell-surface is lubricated. This lower PCL layer was thought to be thin and watery with a low viscosity ⁽³⁰⁾ (Figure 1.6) and formed the basis for the gel-on liquid model (Figure 1.6 A) of lung mucus. However, this model did not explain why components of the upper gel layer do not penetrate into the lower layer. Recently, Button *et al* proposed a gel-on-brush model (Figure 1.6 B) in which the watery layer (PCL) of the airway epithelial surface, contains

tethered macromolecules, such as membrane-bound mucins, forming a brush-like structure of the PCL that stabilizes the two layers and prevents the penetration of MUC5AC and MUC5B mucins in the mucus layer and inhaled particles into the intercellular space ⁽⁷⁰⁾.

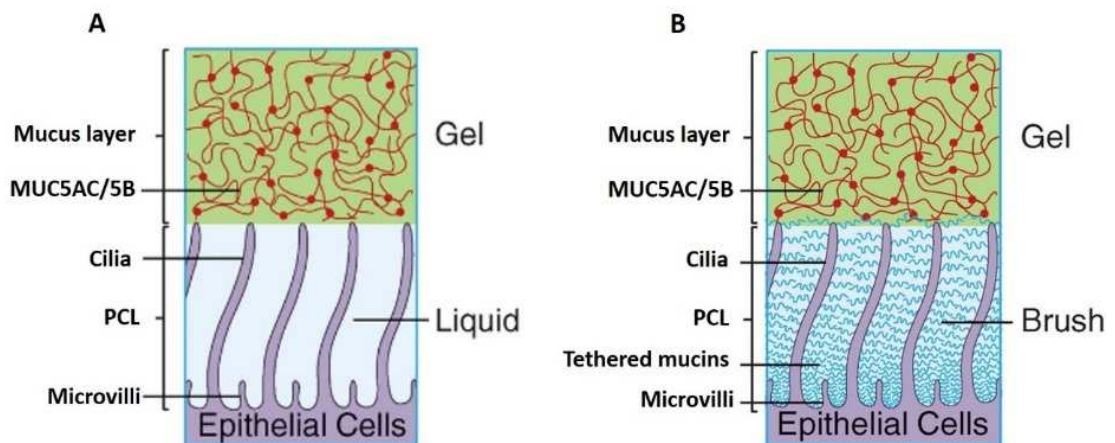


Figure 1.6 Representation of “gel-on-liquid” model (A) and “gel-on-brush” model (B). A Mucus layer comprised of MUC5AC and MUC5B and the PCL. B Mucus layer comprised of MUC5AC and MUC5B and a brush-like structure of the PCL with tethered mucins ⁽⁷⁰⁾.

Mucins, the principal “non-water” component of mucus, are long flexible strings coated with glycans, most of which show a negative charge (sulfate and carboxy group) and can be defined as a glycoproteins of high molecular weight produced by epithelial tissues.

The MUC gene family

The human MUC gene family codes up to 20 known proteins and it is possible to distinguish two main forms of mucin; soluble secretory mucin and membrane bound-mucin ⁽⁷¹⁾. Bound mucins differ from the secretory mucin most sharply by the presence of a hydrophobic domain anchoring the molecules in the membrane and lack

intermolecular interaction through disulfide bridges. Mucins are composed of approximately 75% carbohydrate and 25% amino acids linked via O-glycosidic bonds between N-acetylgalactosamine ⁽⁷²⁾. These macromolecules result to be polydisperse in terms of oligosaccharide composition, chain length and even when isolated from the same organ show an heterogeneous molecular weight ⁽⁷³⁾. The carbohydrate chains can have branched structures and every carbohydrate chains can have 2-15 sugars in length and the most commune sugar residue found in mucin are; fucose, N-acetylgalactosamine, N-acetylglucosamine, galactose and sialic acid ⁽⁷⁴⁾. These glycosylated and highly hydrophilic regions are separated by “naked” central region formed by serine, threonine-rich tandem repeat domains and low amount of aromatic amino acid ⁽⁷⁵⁾. All mucins contain a flexible domains made of proline, threonine and serine named “PTS domain” highly glycosylated with glycan O-linked to serine and threonine.

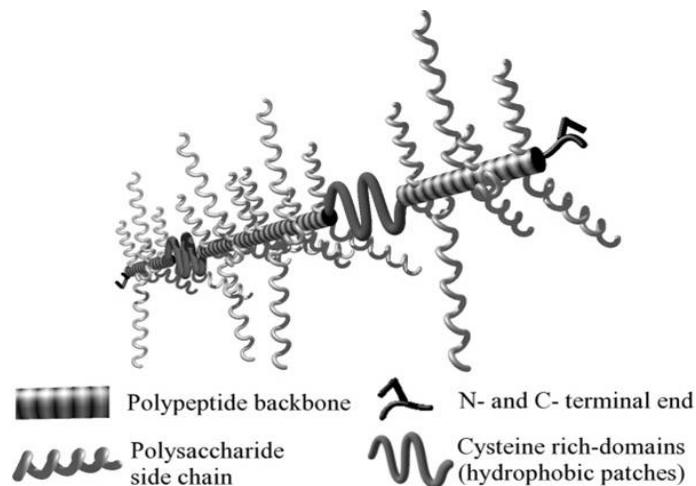


Figure 1.7 Mucin structure. Mature mucins are composed of two distinct regions: The amino- and carboxy-terminal regions are very lightly glycosylated, but rich in cysteines. A large central region formed of multiple tandem repeats of 10 to 80 residue sequences ⁽⁷⁶⁾.

Chapter 1

The N- and C-terminal regions of secretory mucin are rich in cysteines which establish disulfide linkages within and among mucin monomers ⁽⁷⁶⁾ (Figure 1.7).

In past decades mucins have been challenging to study because of their large size and enrichment in glycosidic modification which masks a large portion of the central protein core. Thanks to a number of MUC-specific antibodies, investigators have identified and localised the mucin glycoproteins in a number of human epithelial tissues (Table 1.1) ⁽⁷⁷⁾. Tethered or membrane-bound mucin includes; MUC1, MUC3A/B, MUC4, MUC12, MUC13, MUC15, MUC16, MUC17, MUC20. The role of these non-gel forming mucin includes the activation of intracellular signal transduction pathways, cell differentiation, proliferation and regulation of the immune response ⁽⁷⁸⁾. Secreted mucin can be divided in two groups; gel-forming mucin cysteine rich including MUC2, MUC5AC, MUC5B, MUC6, MUC19 and non-cysteine rich including MUC7, MUC8, MUC9 ⁽⁷⁹⁾ (Figure 1.8).

Table 1.1 Type and tissue expression of human mucins.Adapted from ⁽⁷⁷⁾.

<i>Mucin</i>	<i>Tissue expression</i>	<i>Reference</i>
Secreted mucins		
Gel forming		
<i>MUC2</i>	Jejunum, ileum, colon, endometrium, tear fluid	(80)
<i>MUC5AC</i>	Trachea, bronchi, stomach, conjunctiva, endocervix, endometrium	(81, 82)
<i>MUC5B</i>	Trachea, bronchi, submandibular glands, endocervix	(81, 82)
<i>MUC6</i>	Stomach, ileum, endocervix, endometrium	(81, 83)
<i>MUC19</i>	Lacrimal gland, ocular surface, trachea, middle ear, salivary gland	(84-87)
Secreted mucins		
Non-gel forming		
<i>MUC7</i>	Sublingual, submandibular glands, bronchi, lacrimal gland, conjunctiva	(88) (89)
<i>MUC8</i>	Nasal epithelial, uterus, endocervix, endometrium	(90, 91)
<i>MUC9</i>	Fallopian tubes, lacrimal gland, conjunctiva	(92, 93)
Membrane-associated		
<i>MUC1</i>	Trachea, bronchi, breast, pancreas, duodenum, ileum, colon, cornea, conjunctiva, fallopian tubes, uterus, endometrium, endocervix, ectocervix, vagina	(81, 94) (95)
<i>MUC3A/B</i>	Small intestine, colon	(96)
<i>MUC4</i>	Bronchi, breast, respiratory tract, small intestine, colon, conjunctiva, cornea, endocervix, ectocervix, vagina, endometrium	(81, 97) (98)
<i>MUC12</i>	Colon, stomach	(99)
<i>MUC13</i>	Colon, trachea, kidney, small intestine, conjunctiva	(99, 100)
<i>MUC15</i>	Colon, small intestine, prostate, conjunctiva	(99, 101)
<i>MUC16</i>	Ovary, cornea, conjunctiva, trachea, endometrium	(99, 102)
<i>MUC17</i>	Stomach, duodenum, colon, conjunctiva	(99, 100)
<i>MUC20</i>	Colon, kidney, liver, lung, prostate, endometrial	(103, 104)

Chapter 1

MUC1 and MUC4 are the major membrane-associated mucins of the airway that may function as cellular receptors and are present at the apical surface of ciliated cells. While MUC1 is more enriched in cells that express microvilli, MUC4 appears more strongly associated with cilia⁽¹⁰⁵⁾. The secreted non-gel forming mucin, MUC7⁽⁸⁸⁾ is expressed in serous cells of the submucosal glands, while the main secreted gel-forming mucin expressed in the airways are MUC5AC and MUC5B. These are the most important structure-forming component of the mucus gel, resulting in its characteristic gel-like, cohesive and adhesive properties. MUC5AC is mainly produced and secreted by goblet cells instead MUC5B is secreted by submucosal glands⁽¹⁰⁶⁾.

Once the N-glycosylated polypeptide chain of mucin has been synthesized and translocated into the endoplasmic reticulum, dimers are formed by disulfide-bonded through its COOH-terminal and cystine knot (CK) -domains. The dimers are then transported to the Golgi apparatus where glycan chains are added to the protein through successive addition of simple sugars by glycosyltransferase and assembled into disulfide-bonded multimers. Once mucins glycoproteins are produced they are packaged into secretory granules and expelled to protect the surface epithelium⁽¹⁰⁷⁾. This secretion occurs by conventional exocytosis with fusion of a mucous granule membrane and the apical plasma membrane⁽¹⁰⁸⁾.

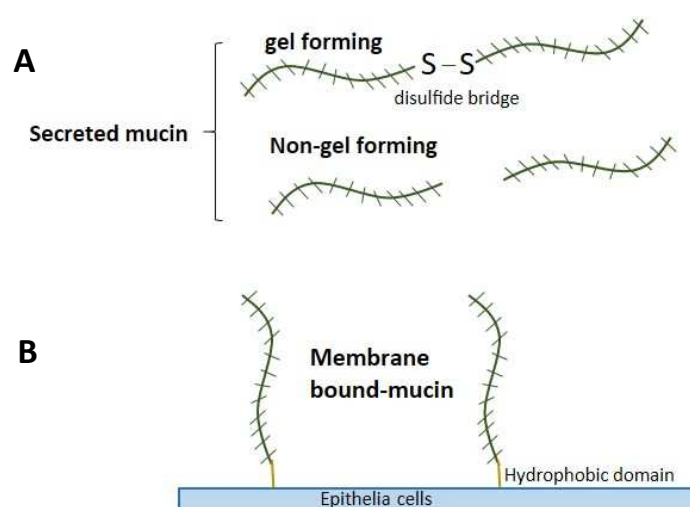


Figure 1.8. Secreted and membrane bound mucin. **A** Secreted mucin can be divided in gel-forming and non-gel forming mucin. Mucin with cysteine and C and N-terminal, form disulphide bridge with other mucin (gel forming mucin). **B** membrane-bound mucins are attached to the epithelium by hydrophobic domain.

1.4.1 Airway of patients with respiratory diseases

Although mucus provides a physical and biological barrier to airway surface, impaired clearance or excessive mucus contributes to the pathogenesis of all the common airway diseases ⁽¹⁰⁹⁾. Mucus hypersecretion plays a significant role in severe/terminal COPD and may contribute to chronic airway infection and obstruction, lung failure and death in patients with CF ⁽¹¹⁰⁾. In asthma, smooth muscle hyperplasia cause airway thickening and narrowing ⁽¹¹¹⁾ which causes breathing difficulty and can be worsened by airway obstruction that results from mucus hypersecretion ⁽¹¹²⁾.

Following the exposure of the airway epithelium to environmental irritants (allergens, infectious pathogens or toxins), inflammatory or immune response mediators are activated with the generation of a secretory cascade of mucin glycoprotein from the goblet cells granules or submucosal glands onto the epithelium. Moreover

inflammatory/immune response mediators upregulate MUC genes to replenish the secretory granules due to mucin hypersecretion ^{(69) (113)} with a consequent increase in production and secretion of stored mucin. In chronic inflammatory airway diseases, MUC2, MUC5AC and MUC5B expression appear increased ^{(113) (88) (114)} compared with non-diseased airways. In CF lung disease the host is unable to clear the initial colonization and infection of the airways. This is followed by an influx of neutrophils, macrophages that initiate and coordinate the innate defence system with release of proteases, oxidants, and α -defensins that contribute to tissue destruction and consequent release of extracellular DNA from lysed neutrophils, epithelial cells, and bacteria which can make mucus more thick and vulnerable to infection and inflammation (Figure 1.9) ⁽¹¹⁵⁾.

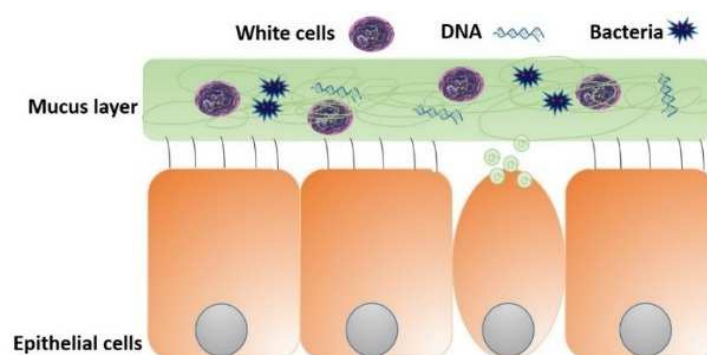


Figure 1.9. Airway in CF. The thick mucus secreted by goblet cells obstructs airways and allows bacterial infection and inflammation to occur. DNA left from neutrophil after fight bacteria lead to increased adhesive characteristic of mucus.

As a consequence of bacterial infection Th2 lymphocytes produce anti-inflammatory cytokines, including IL-4, IL-5, IL-9 and IL-13. In fact, the complex network of cytokines balances pro-inflammatory and anti-inflammatory effects. Although each of these

cytokines are implicated respiratory diseases, IL-13 is thought to be critical. IL-13 induces many features of allergic lung disease, including airway goblet cell metaplasia ⁽¹¹⁶⁾ (Figure 1.10) and mucin (mainly MUC5AC) hypersecretion, which all contribute to airway obstruction. IL-4 contributes to these physiologic changes, but is less important than IL-13 which induces secretion of chemokines that are required for recruitment of allergic effector cells to the lung ⁽¹¹⁷⁾.

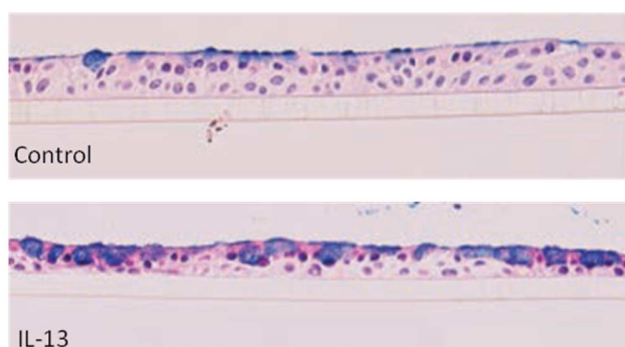


Figure 1.10. Effect of IL-13 on Goblet cells density (GCD)
Treatment of human bronchial epithelial cells (HBEs) with IL-13 (1ng/ml) induced an increase in GCD as assessed by manual counting of Alcian blue-stained cells ⁽¹¹⁶⁾.

1.4.2 Mucus as a barrier for drug delivery

Once secreted, mucus forms a barrier to protect against infection and injury but it can potentially trap and affect the absorption or action of orally inhaled drugs. The influence of mucus layer on drug absorption has been widely investigated in intestinal perfusion studies ⁽¹¹⁸⁾ and diffusion studies which confirmed that gastrointestinal mucus is a barrier

Chapter 1

to absorption and diffusion of drug molecules ⁽¹¹⁹⁾. Furthermore, *in vitro* studies have suggested that intestinal mucus layer produced by HT29-H goblet cells is a significant barrier for the absorption of high hydrophobic drugs such as testosterone but not to hydrophilic molecules such as mannitol ⁽¹²⁰⁾ ⁽¹²¹⁾ ⁽¹¹⁹⁾. This was also confirmed later by Behrens, Stenberg ⁽¹²²⁾ who analysed six molecules having 128-288 g/ml and Log P in the range of -1.4 to 3.3 and noticed a significant decrease in the rate of drug diffusion for molecules with a Log P >1.

The ability of a drug or drug delivery system to diffuse through the mucus depends on the mesh spacing of the mucus and the relative size of the drug molecule. Furthermore, the physicochemical properties of the drug and mucins can influence the barrier function of mucus ⁽¹²³⁾. In fact, it is thought that particles and solutes may be stopped from their diffusion through mucus gel by two main mechanisms: size filtering and interaction filtering (Figure 1.11) ⁽¹²⁴⁾. In the size filtering mechanism drug molecules smaller than the cut-off size of the mesh will pass through the mucus gel, whereas larger molecules will be hindered by mucin fibres or other mucus components. In the interaction filtering mechanism physicochemical properties such as electrostatic, hydrophobic forces, hydrogen bonds or specific binding interaction are involved. Particles can strongly interact with the polymer matrix of the hydrogel and be trapped by the mucus. Opposite to this, some molecules can show only weak interactions and be allowed to pass.

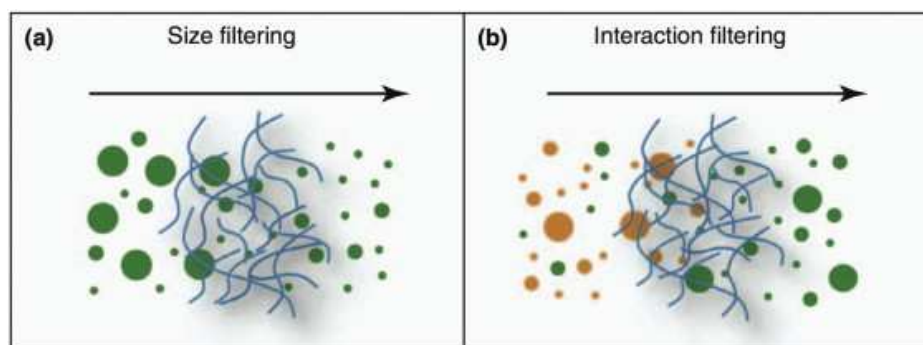


Figure 1.11. Mechanisms that may stop particles from readily diffusing through mucus gel. (A) Size filtering mechanism allows particles that are smaller than the mesh of the mucus to pass. **(B)** In the interaction filtering mechanism, particles are distinguished according to their surface properties: same particles (orange) can interact strongly with mucus components and are trapped, whereas other particles (green) show only weak interactions and are not hindered to pass. Taken from ⁽¹²⁴⁾.

Physical characteristic of lung mucus.

The mucins in airways mucus consisted is a heterogeneous mixture of extremely large glycoproteins. The molecular weight has been estimated to be in the range of 2-50 MDa measured by light-scattering ^(125, 126). Monomers or subunits of mucin are linearly assembled and held together by disulfide bonds and the estimate length appears polydisperse, from 0.5 to 10 μm in length. Whole mucins purified from healthy human tracheobronchial secretion in 4-6 M-guanidinium chloride was studied with electron microscopy and showed length of 0.5-1 μm ^(125, 126). The mesh pores of mucus isolated from NHBE was studied by Matsui, Verghese ⁽¹²⁷⁾ from the images acquired with confocal microscopy and pores were estimated to be 1-8 μm . Kirch, Schneider ⁽¹²⁸⁾ using a cryo-scanning electron microscope (SEM) showed that the mesh size of native respiratory mucus is 100 nm to 10 μm in diameter and a thickness of ~ 500 nm. Moreover, the mesh spacing of PCL in sample of respiratory mucus from NHBE cells reported by Button, Cai

⁽⁷⁰⁾ was on the order of ~20- 40µm estimated using rapid freezing techniques coupled with electron microscopy.

Mucus-penetrating particles

Nanoparticles are defined as particles with sizes between 1 and 100 nm. Mucus penetrating particles can potentially improve drug delivery by shielding the drug molecules and overcoming the MC mechanism. Several types of nanoparticles have been developed for mucus penetration by most of them are efficiently trapped in and rapidly removed by mucus, making controlled release difficult. Mucus penetrating particles can potentially improve drug delivery by shielding the drug molecules and overcoming the MC mechanism. A promising approach for improved mucus penetration has been described in several papers from Hanes and co-workers. They have demonstrated that controlled coating of nanoparticles (up to 200 nm) with the hydrophilic and uncharged polymer, polyethylene glycol (PEG), were able to rapidly penetrate fresh, undiluted human mucus ⁽¹²⁹⁾. This possibility to reduce particles affinity to mucus may be promising in improving drug delivery to mucosal tissues. The challenge remains to develop a mucus-penetrating nanoparticle that can efficiently deliver its loaded drug cargo to the epithelial surface before triggered drug release.

1.4.3 Serum protein binding and its effect on drug disposition

Serum proteins and plasma proteins serve many different functions, including transport of hormones, lipids, vitamins in the circulatory system. The ability of plasma proteins to

Chapter 1

interact with drugs is well established and the plasma protein binding (PPB) of drugs may have a significant effect on pharmacokinetics and pharmacodynamics ^{(130) (131) (132)}. Binding experiments of PPB-drug interaction are widely used in drug discovery to guide the design of new drug model and optimize *in vivo* efficacy.

Although the plasma contains many other proteins, serum albumin (55%) is the most abundant protein in plasma and with α 1-acid glycoprotein (AGP) can play a dominant role in drug disposition and efficacy. Serum albumin has multiple hydrophobic binding sites and has been shown to bind to a wide set of aromatic ligands such as thyroxine ⁽¹³³⁾ and a wide range of drugs e.g. warfarin, diazepam, ibuprofen⁽¹³⁴⁾. In the context of inhaled drugs the inhaled corticosteroid, ciclesonide displays extensive PPB of 98% in human serum ⁽¹³⁵⁾. Serum Albumin binding is capable of altering drug pharmacokinetics. It has a central role in drug distribution as most drug reach the target tissue bound to serum albumin and its prevents drug from being metabolized with consequent increases their biological lifetime. Moreover, serum protein helps hydrophobic compounds solubilisation and drug distribution through the body ^{(136) (137)}.

Kratochwil, Huber ⁽¹³⁸⁾ suggested that the interaction of drugs with plasma protein is not only based on hydrophobic interaction but different forces are involved, such as charge interactions, hydrogen bonds, and space-filling of binding pockets. It is assumed that in plasma, acidic drugs manly bound to human serum albumin whereas AGP has the ability

to bind mainly basic drugs like such as propranolol⁽¹³⁹⁾ but AGP interaction to acidic drugs has also been demonstrated, such as phenobarbital⁽¹⁴⁰⁾ and endogenous steroids⁽¹⁴¹⁾.

The administration of therapeutics by pulmonary route represents a significant opportunity for several classes of drugs (small molecules/macromolecules). PPB is an important factor and a subject of concern for the systemic delivery of various drugs through aerosol administration and with evidence of drug-mucus binding for a number of drugs it is key that more is learned about the extent and nature of these interactions and whether they can affect the PK/PD of inhaled drugs.

1.4.4 Mucus models to evaluate drug diffusion

Various mucus models are described in the literature, including *in vivo*, *ex vivo* and *in vitro* models, from the crude (natural) to the simplest methods only represented by mucin solution. Natural mucus from airway is probably the most ideal to study drug diffusion through lung but has some drawback; in a healthy person the mucus layer is very thin, strongly attached to the epithelium and difficult to access. Cervical mucus may be used as a more voluminous mucus model⁽¹⁴²⁾ and a relatively larger amount of mucus can be obtained from porcine gastrointestinal mucus⁽¹⁴³⁾⁽¹⁴⁴⁾ but *in vivo* and *ex vivo* assays may be time consuming and a number of animals are required. Pig and human mucus, as showed by Kararli⁽¹⁴⁵⁾, displayed similarity in structure and molecular weight but for both human and pig mucus the physical-chemical properties and composition are subjected to inter-individual variability⁽¹⁴⁶⁾⁽¹⁴⁷⁾ so that mucus properties may vary

between batches. To overcome this problem mucus from different batches can be pooled together and frozen at -20 °C until needed without significant effect on viscoelasticity ⁽¹⁴⁶⁾ and the diffusion coefficient of drugs ⁽¹⁴³⁾.

PGM has a more stable composition and has been used to prepare mucin solution or to reproduce a mucus “substitute” by adding buffer, bovine serum albumin (BSA) and dipalmitoylphosphatidylcholine (DPPC) ⁽¹⁴⁸⁾ or buffer, BSA, lecithin ⁽¹⁴⁹⁾, but as showed by McGill and Smyth ⁽¹⁵⁰⁾ the heterogeneity observed for natural mucus was not overcome with the mucus “substitute” used for *in vitro* assays.

1.4.5 Method to study drug binding to biomacromolecules

The classical ligand protein interaction depends on the following assumptions:

- The interaction is reversible
- All the receptor molecules are equivalent and independent
- The biological response depends on the number of occupied receptor sites
- The interaction and response are measured at equilibrium.

At equilibrium ligand (L) binding to a protein (P) gives a stabilized complex (PL) represented as follows:



The equilibrium constant for association K_a for this reaction is given by:

$$K_a = \frac{[PL]}{[P][L]}$$

The equilibrium constant for dissociation K_d is:

$$K_d = \frac{[P][L]}{[PL]}$$

Plotting $\frac{[PL]}{[P_t]}$ versus $[L]$ the graph in Figure 1.12 will be obtained. Increasing the ligand concentration, the PL increases until binding sites are saturated. For the total amount of protein $[P_t]$ the maximum fraction PL is 1. K_d is L concentration at which half P is half saturated.

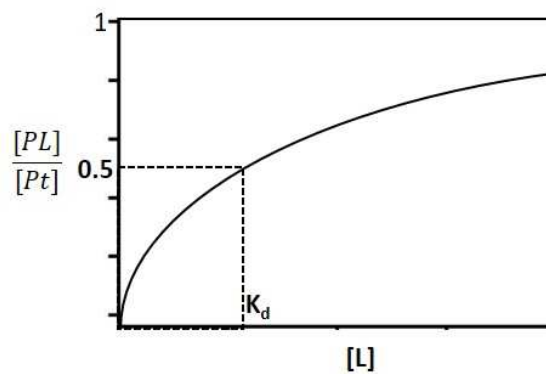


Figure 1.12 Protein-Ligand classic hyperbolic binding curve. As L concentration increases the PL increases reaching a plateau. K_d is the L concentration at $\frac{PL}{P_t} = 0.5$

The methods used for the investigation of drug binding to macromolecules can be broadly divided into spectroscopic and non-spectroscopy techniques.

- *Non-spectroscopic techniques*

Non-spectroscopic techniques (Figure 1.13) involve the separation of the free drug from the complex drug-macromolecule and allow the monitoring of the free drug levels.

The most widely used methods are equilibrium dialysis and ultrafiltration ⁽¹⁵¹⁾ ⁽¹⁵²⁾ as these methods can be applied to measure solutions with high protein concentrations.

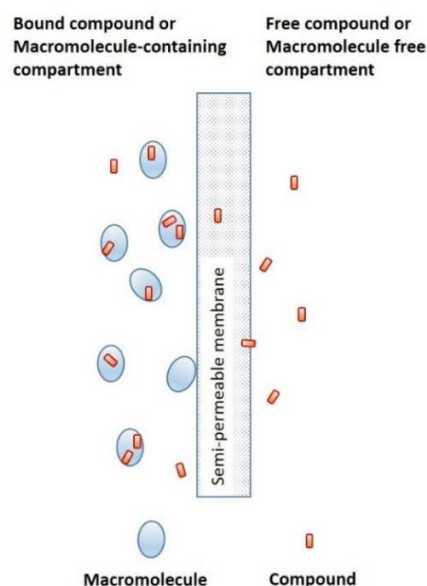


Figure 1.13 Separation of bound and free compound by non-spectroscopy technique. A semi-permeable membrane allows the passage of free compound retaining the compound bound to the macromolecules.

Equilibrium Dialysis

Equilibrium dialysis is considered the reference method although the long test period (hours or days) is inconvenient for routine testing. The development of rapid equilibrium dialysis offers the advantages of miniaturisation and a greatly reduced experimental duration (1-2 h) ⁽¹⁵³⁾. Drawbacks of the equilibrium dialysis approach include the potential for non-specific drug binding to the dialysis membrane. Moreover, analyte instability may compromise studies using conventional equilibrium dialysis techniques ^{(151) (152)}.

Ultrafiltration binding

Compared to equilibrium dialysis, ultrafiltration binding experiments are less labour-intensive, rapid, and able to accommodate the simultaneous testing of many drug and

protein mixtures on when presented in the multiwell plate format. The ultrafiltration assay combines the centrifugation speed with the separation of bound and unbound ligand by a membrane. Yet, ultrafiltration can be used for sample with small amount of protein to overcome the problem of oncotic pressure. The major difficulty for ultrafiltration is related to the membrane devices, which may induce additional binding effects ⁽¹⁵¹⁾ ⁽¹⁵⁴⁾ and membrane pores has to be chosen accurately to avoid the “sieve effect”. In fact, one drawback of ultrafiltration binding assay is the Non-specific binding (NSB) effect which refers to the binding of the ligand to something other than its “receptor” which seems correlated to the lipophilic character of molecules ⁽¹⁵⁵⁾. Another concern regarding the 96-well ultrafiltration plates is the “edge effect” which refers to the variation in filtrate volumes observed across the plate and has been considered is a major concern regarding the determination of free drug in PPB ⁽¹⁵⁶⁾. In short, more methods need to be developed and ideally the best method has to have a more convenient approaches for the analysis of the interacting amount of drug and be faster.

Chromatographic techniques

An alternative to dialysis and ultrafiltration is the use of chromatographic methods where is possible to distinguish two different approaches.

In the first approach both drug and protein may be mixed in the mobile phase. The mixture drug and protein can be injected through the column of the liquid chromatography which may be able to separate the free ligand from the complex ligand-macromolecule. The application of this system depends on the interaction kinetics, as it

requires no or little dissociation of the complex drug-protein ⁽¹⁵⁷⁾. Another approach using chromatography technique is the affinity chromatography, where one of the interacting species (macromolecules, drug) can be used as immobilised ligand ⁽¹⁵⁷⁾. This technique is usually applied for studying weak reversible equilibria typical of drug-protein interaction and relies on the chemical equilibrium between the molecules immobilized and those in solution. Thanks to Larsson ⁽¹⁵⁸⁾ this method assembled with HPLC has gained in precision and speed and the development of affinity chromatography with commercial serum albumin columns to evaluate PPB has widespread for drug screening in industry ⁽¹⁵⁹⁾.

Diffusion cells

Another method used to separate the free drug from the bounded form is the Franz-cell diffusion chamber. This system is commonly employed for the measurement of permeation kinetics of drugs across skin, synthetic (cellulose) membrane or biological membranes / tissues ⁽¹⁶⁰⁾. It was also used for studying drug diffusion through polymers ⁽¹⁶¹⁾. The system consists of two chambers, the donor and receiver chamber separated by a membrane impermeable to the system of interest. For the study of mucus permeation the mucus and drug are added onto the support membrane (or mucus layer) in the donor chamber and drug transport into the receiver chamber is determined by serial sampling from the receiver chamber. Franz-cell system is widely used for studying formulation but its open donor compartment design does not permit the use of any

stirring setup, as in the receptor compartment, so it is not suitable for the evaluation of solution or suspension-formulations or volatile drugs.

- *Spectroscopic technique*

Spectroscopic techniques are able to identify and characterize the drug-macromolecule binding by monitoring either the ligand or the target protein. Techniques include ultraviolet, fluorescent and visible spectroscopy, circular dichroism, Nuclear magnetic resonance (NMR) spectroscopies. To date each of these techniques has been used to study drug-mucin interactions.

UV–vis absorption is probably the simplest and most commonly employed instrumental technique for studying drug-macromolecules interactions by monitoring the changes in the absorption properties of the drug or macromolecule.

This technique relies on the fact that the small molecule shows an absorbing band in the UV/visible region. As attenuation of the beam increases, the absorbance of a solution increases and is directly proportional to the path length and the concentration of the matter.

Comparing the absorbing band when the ligand is free in solution to when is mixed with a macromolecule, the shifting of the position of the maximum value is an easy way to determine whether there is any interaction of the drug with other molecules. The strength of the interaction may be interpreted from the magnitude of this peak shifting or absorbance intensity increases ⁽¹⁶²⁾ ⁽¹⁶³⁾ ⁽¹⁶⁴⁾. The disadvantage of this technique is that

weak interactions cause minor changes in spectral profiles that may not be easily identifiable ⁽¹⁶⁵⁾. Moreover, the technique relies on the presence of an appropriate chromophore that does not significantly overlap with that of the macromolecule.

Fluorescence spectroscopy is electromagnetic spectroscopy used to analyse the fluorescence from a sample. It is a simple and fast method to determine the concentration of an analyte in solution based on its fluorescent properties. It is one of the techniques most commonly used to study interactions between small ligand molecules and macromolecules thanks to its high sensitivity, large linear concentration range and selectivity. Fluorescence emission may be very sensitive to the environment and the binding may cause spectral shifts in the excitation and emission spectra of drugs ⁽¹⁶⁶⁾. The interaction of a ligand to a molecule may lead to a significant enhancement or a reduction of the fluorescence intensity. For instance, the rotation of free molecules favours the radiation deactivation of the excited states, but when a drug molecule intercalates with a macromolecule, the small molecules are well protected from the aqueous solvent leading to a significant increasing in the fluorescence emission ⁽¹⁶⁷⁾. In contrast, in case of electrostatic, hydrogen bonding or hydrophobic interactions are involved and the molecules may not be protected from water-bound anionic fluorescence quenchers and it is possible to observe a decrease in the fluorescence intensity ⁽¹⁶⁷⁾.

1.5 Cystic fibrosis

Cystic fibrosis (CF) is a recessive autosomal genetic disease caused by mutations in the gene encoding cystic fibrosis transmembrane conductance regulator (CFTR). The CFTR protein is responsible for chloride and bicarbonate transportation across epithelial cell membranes. The most common mutation is a deletion of three nucleotides with a loss of a single phenylalanine amino acid at the 508th position on the protein, ($\Delta F508$). This mutation accounts for 70% of CF cases ⁽¹⁶⁸⁾ although over 1000 known mutations have been associated with CF. The CFTR protein is an ATP-binding cassette transporter and is made up of five domains: two transmembrane domains (TMD1/TMD2), two cytoplasmic nucleotide binding domains (NBD1 and NBD2) and a regulatory (RD) domain ⁽¹⁶⁹⁾ ⁽¹⁷⁰⁾ (Figure 1.14). The process of channel opening and closing is called “gating” and each domain is important for the correct function of the gating and for chloride transportation through the cell membrane. Channel opening is regulated by phosphorylation of the R domain by protein kinase A and recruitment of ATP to NBD1 and NBD2. To open the channel pore these domains dimerise (NBD1:NBD2) and dissociate to close the channel following ATP hydrolysis ⁽¹⁶⁹⁾ ⁽¹⁷¹⁾ (Figure 1.14).

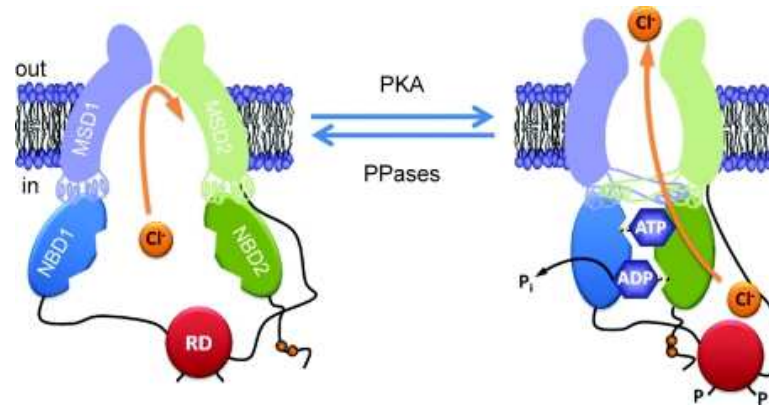


Figure 1.14 CFTR structure and gating conformation. CFTR is composed of two transmembrane domain MSD1-2 and three cytoplasmic domains; NBD1-2 and RD. CFTR channel closed (left) and open (right). Phosphorylation of the R Domain by the cAMP-dependent protein kinase (PKA) leads to the dimerization of NBD1 and NBD2 and consequent release of Cl⁻. Taken from ⁽¹⁷⁰⁾.

Five functional classes of CF mutations can be identified according to the nature of the gene mutation and its functional consequence on CFTR function ^{(172) (173)} (Figure 1.15):

- Class 1. Mutations produce few or no functioning CFTR chloride channels due to premature termination of CFTR protein production.
- Class 2. Defective trafficking. CFTR does not reach the apical surface membrane. This includes $\Delta F508$.
- Class 3. Limited channel gating. This includes G551D.
- Class 4. CFTR reaches the apical surface and able to open and close but conduction (passage of chloride ions through the channel) is defective.
- Class 5. Limited transcription regulation Reduced synthesis of functional CFTR

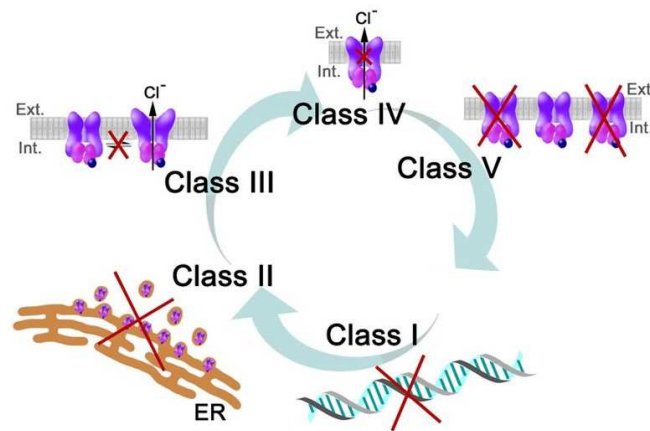


Figure 1.15 CFTR gene mutations are categorised into five classes. Class I mutations results from nonsense and frame-shift mutations or mRNA splicing defects. Class II mutations, results in folding or maturation defects, which consequent premature CFTR degradation. Class III mutations result in defective regulation (opening and closing). Class IV conductance defect of Cl⁻. Class V reduced quantity of the protein. Taken from ⁽¹⁷³⁾.

CFTR has a diffuse epithelial distribution in lung, pancreas, liver, kidneys and intestine ⁽¹⁷⁴⁾. As a consequence, CF patients experience a multiorgan disease involvement with variable degrees of severity. The inactive or inefficient function of CFTR leads to impaired Cl⁻ transport and the main signs of CF is a characteristically salty sweat. The Cl⁻ imbalance on internal organs leads to a build-up a dehydrated mucus in ducts of the pancreas, in male sex ducts and in lungs with consequent poor weight gain, infertility, shortness of breath, accumulation of thick and dehydrated mucus. The dehydrated mucus is due to the increased salt absorption which is believed to result by the involvement of another salt regulator functionally coupled with CFTR. The epithelial sodium channel (ENaC) with CFTR, is a major regulator of salt and water reabsorption in a number of epithelial tissues

(colon, the salivary duct, the cortical collecting duct of the kidney, lung) ⁽¹⁷⁵⁾ and is functionally related and influenced by intact CFTR ⁽¹⁷⁶⁾.

In a normal airway (Figure 1.16 A) CFTR regulates the movement of Cl⁻ across epithelial cell membranes which downregulate ENaC inhibiting an excessive absorption of Na⁺ and water, although the mechanism by which CFTR modulates the function of ENaC proteins is still not clear ⁽¹⁷⁷⁾ ⁽¹⁷⁸⁾. A defective inhibitory regulation of ENaC in CF (Figure 1.16 B) leads to enhanced Na⁺ absorption and, consequently, an increase of water volume absorbed across the CF airway epithelial cells ⁽¹⁷⁹⁾ ⁽¹⁸⁰⁾. Therefore, the water absorbed leads to a reduction in airway surface liquid and increased mucus viscosity that slows MC. Defective MC can predispose airways to bacterial infection leading to lung infections and pulmonary complication which is the primary cause of mortality in CF.

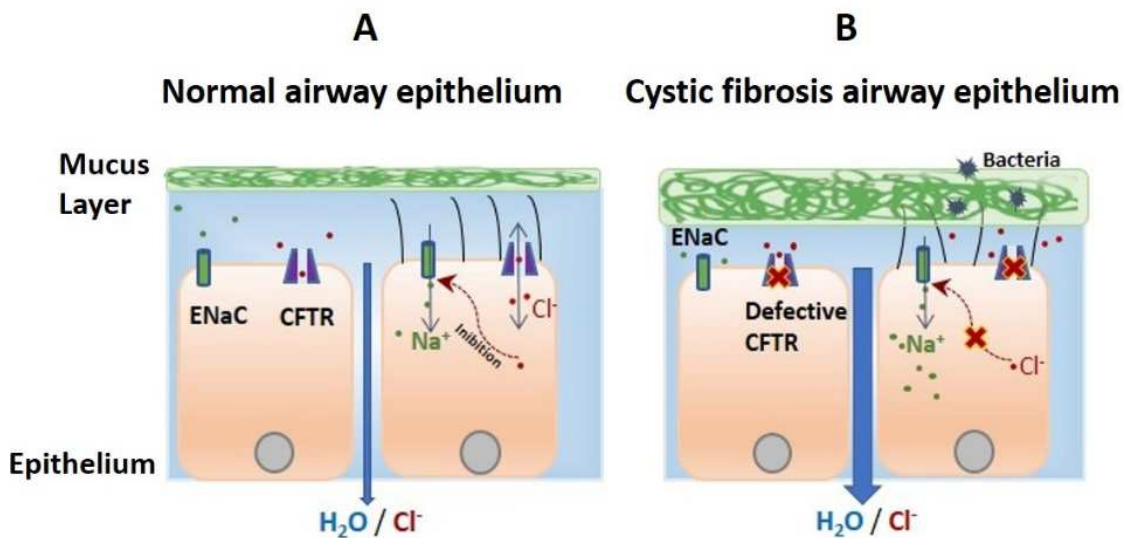


Figure 1.16 Model depicting ion transport mechanisms regulating ASL volume in normal (A) and CF airway epithelia (B). (A) CFTR pumps Cl⁻ in the cell which inhibits Na absorption through ENaC. (B) Defective CFTR leads to decrement of Cl⁻ with enhanced Na⁺ absorption through ENaC leading to a thicker mucus layer favorable to bacterial infection.

Chapter 1

No cure for cystic fibrosis is known. Nowadays the life expectancy is 42-50 years and failed lung compliance is responsible for about 80% of death ⁽¹⁸¹⁾. This improvement is due to the rationalisation of antibiotic therapy. Correction of the CF disease by gene therapy has been explored as a potential cure for CF has been widely tried. Several approaches have been tested to successfully deliver genetic material encoding for CFTR to the lung epithelium using liposomes ⁽¹⁸²⁾, recombinant viruses ⁽¹⁸³⁾, PEG-coated DNA nanoparticle ⁽¹⁸⁴⁾. Non-viral delivery systems penetrate the mucus layer inefficiently and immunogenicity, safety concerns have precluded successful viral approaches reaching the clinic to date ⁽¹⁸⁵⁾.

Novel oral therapeutics for CF are ataluren, lumacafton and ivacaftor. In particular, ataluren allows the ribosome to overcome premature stop mutations of CFTR. For mutation $\Delta F508$ a novel therapy consists in the use of lumacafton. In this class of mutation, the CFTR is only partially glycosylated and subject to degradation. Lumacaftor restores the post-translational modification at the endoplasmic reticulum avoiding degradation ⁽¹⁸⁶⁾. Improvement for gating mutations due to G551D mutation or other gating mutations have been made with ivacaftor which works as a CFTR potentiator ⁽¹⁸⁶⁾ ⁽¹⁸⁷⁾. Although the improvement led from these novel therapeutics, antibiotics and bronchodilators is still administered alongside and are essential in CF patients.

The development of new therapeutic options is essential for increasing survival. Therapies that increase the volume of airway surface liquid (ASL), and hence MC, should improve

life-quality of CF patients. Inhaled hypertonic saline has been shown to stimulate of MC⁽¹⁸⁸⁾ but the effects were transient and, therefore, with limited therapeutic benefit⁽¹⁸⁹⁾. ENaC inhibitors may be used in blocking the hyper absorption of sodium ions and water absorption across airway epithelia, so that the hydration of the ASL is likely to be reduced and MC enhanced.

1.5.1 ENaC blockers

The ENaC channel is a heteromeric membrane protein consisting of at least three similar subunits in α , β , and γ subunits with two transmembrane domains each^(190, 191) (Figure 1.17). All these subunits are essential to form a functional and highly Na⁺ selective channel^{(191) (192)}.

ENaC is involved in the transepithelial Na⁺-ion transport, which it accomplishes together with the Na⁺/K⁺-ATPase and is typically located at the apical membrane of epithelial tissues throughout the body. This indicates that ENaC functions as a regulator of osmolarity. Its presence has also been demonstrated on arterial endothelial cells where may act as a vascular mechanosensor^{(193) (194)}.

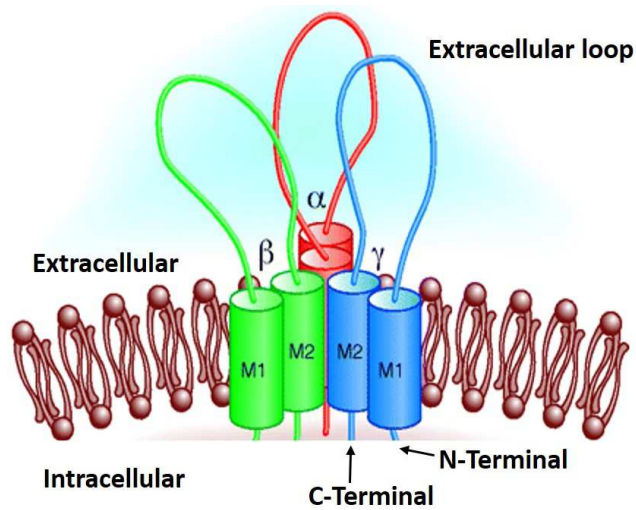


Figure 1.17. The epithelial sodium channel. ENaC consists of three related subunits, termed α , β , and γ . Each subunit (M) consists of two transmembrane helices, a cytoplasmic C-terminal and an N-terminal domain and a large extracellular loop.

Picture taken from jasn.asnjournals.org/content/19/10/1845

ENaCs are also known as amiloride-sensitive sodium channel as are characterized by their high affinity to the diuretic blocker amiloride ⁽¹⁹⁵⁾ ⁽¹⁹⁶⁾. Amiloride (Figure 1.18) is a selective ENaC blocker ⁽¹⁹²⁾ that was developed by Cragoe and his colleagues at Merck Pharmaceuticals in the early 1960s. It was initially designed to be delivered orally and act primarily as a “potassium-sparing diuretic” ⁽¹⁹⁷⁾ by directly blocking the ENaC thereby inhibiting sodium reabsorption at the lumen of distal cortical collecting duct in the kidneys ⁽¹⁹⁸⁾ and has been widely used for treating hypertension and congestive heart failure ⁽¹⁹⁹⁾.

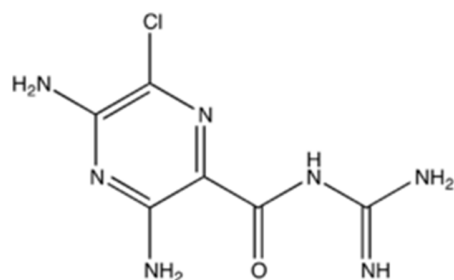


Figure 1.18 Amiloride structure

Decades later the effects of nebulized amiloride on pulmonary function were studied⁽²⁰⁰⁾⁽¹⁹⁷⁾. Studies showed that aerosol administration of amiloride to patients with COPD, cystic fibrosis, blocked entry of sodium into respiratory epithelial cells, thus reducing the potential difference of the airway epithelium⁽²⁰¹⁾ and improved the rheological properties of mucus⁽²⁰²⁾. Although there are *in vitro* data to support short-term improvements in MC and lung function following amiloride therapy^(200, 202, 203), early clinical trials (using a delivery dose of 0.2mg/ml) failed to demonstrate any clinically significant changes in both thickness and volume of ASL and pulmonary function of cystic fibrosis patients was not improved with amiloride⁽²⁰⁴⁾. The lack of therapeutic benefit was attributed to its low potency, and its short half-life (about 20 minutes) on airway surfaces^{(205) (206)} due to rapid absorption by the airway epithelium^{(207) (205, 208)}. Amiloride's limitations in enhancing MC for long periods can be due to a weak affinity of the ENaC blocker to its receptor so that complete block is not achieved^{(206) (204)} or its limited solubility may restrict the mass that could be delivered⁽²⁰⁹⁾. The clinical utility of amiloride is also limited by its rapid reversal form of ENaC block⁽²⁰⁸⁾. These limitations

led to the development of more potent, long-acting amiloride analogues as alternatives to amiloride for CF pharmacotherapy^{(206) (210) (211)}.

A chemical modification of ENaC blocker amiloride may result in the development of more efficiently ENaC inhibitor that may achieve more favorable pharmacodynamic properties than amiloride. Cragoe demonstrated that the 3,5-diamino-6-chloropyrazinoyl guanidine is a privileged structure for ENaC blockade and the most potent ENaC blockers must contain the same pyrazinoyl guanidine chemotype of amiloride^(212, 213). Benzamil (Figure 1.19 A) and phenamil (Figure 1.19 B) are two second generation amiloride analogues with benzyl and phenyl substitutions onto the guanidinium.

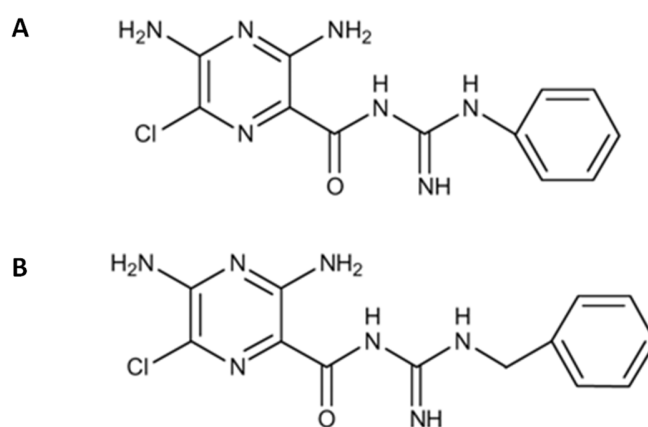


Figure 1.19 Benzamil (A) and phenamil (B) structure.

The guanidine moiety in amiloride imparts a cationic charge at physiologic pH (pKa 8.8 in H₂O). It exists primarily as a monovalent cation and interacts with sodium channel in its protonated form⁽²¹⁴⁾. The pKa values reported for its analogues are 8.1 for benzamil

and 7.8 for phenamil⁽²⁰⁹⁾. These results indicate that benzamil and phenamil are less protonated and more lipophilic than amiloride leading to an increased affinity to the ENaC⁽²⁰⁹⁾. The observation of increase ENaC affinity and potency for hydrophobic analogues supported the hypothesis that the binding site in ENaC has a hydrophobic binding pocket^{(215) (216) and (217)}. Although benzamil and phenamil are more potent than amiloride, they are predicted to be absorbed more rapidly and this could potentially increase their systemic absorption and toxicity. The whole body toxicity results from a reduction in Na⁺ absorption which alters the Na⁺/K⁺-ATPase with consequent hyperkalemia⁽²⁰⁶⁾.

To identify a selective blocker of airway ENaC a series of novel analogues were tested for potency, reversibility of ENaC block, epithelial absorption and biotransformation. Parion compounds 552-02 (Figure 1.20) and GS9411 (undisclosed structure) have been specifically designed for aerosol delivery to the pulmonary system and selected as potential lead compounds for CF⁽²¹⁸⁾.

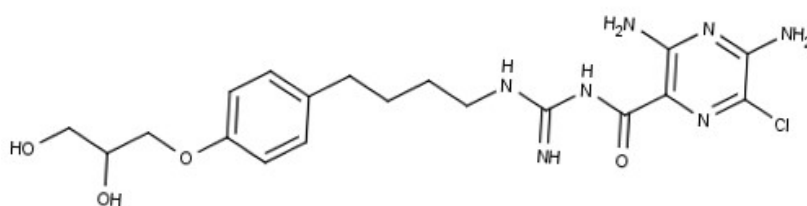


Figure 1.20 Compound 552-02 structure.

Both *in vitro* and *in vivo* testing showed that 552-02 crossed the epithelium more slowly, was 100-fold more potent and 5-fold less reversible than amiloride and displayed the

lowest IC_{50} value (7 nM) ever reported for an ENaC blocker ⁽²¹⁸⁾. Preclinical data support the clinical utility of 552-02 to promote an expansion in ASL volume, with or without hypertonic saline for lung disease and completed Phase II trials as a nebulized therapy for CF ⁽²¹⁹⁾ but when O'Riordan, Donn ⁽²²⁰⁾ reported GS9411-induced hyperkalemia the development of these compounds was halted. In contrast to most of the earlier investigations, Russ, Ried ⁽²²¹⁾ showed that a guanidine or amidine side chain in the 2-position of amiloride is not necessarily required to have a diuretic and natriuretic effect. The substitution of guanidine or amidine side with an amino group of similar basicity (Figure 1.21), protonated at physiological pH, was showed to retain diuretic, natriuretic and anti-kaliuretic effects and displayed an increase of potency up to 40 folds when compared to amiloride ⁽²²²⁾.

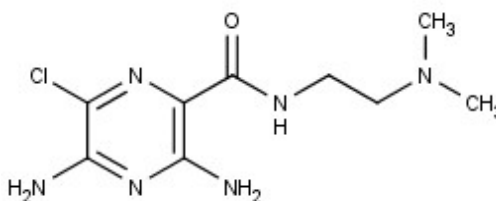


Figure 1.21 Example of non-pyrazinoyl guanidine ENaC blocker

Further, Novartis has reported the synthesis and biological evaluation of a novel series of human ENaC blockers that are structurally distinct from the pyrazinoyl guanidine chemotype found in amiloride analogues previously cited. As an amine should be significantly basic at physiological pH although less protonated than an acylguanidine, Hunt et al explored the use of amines as bioisosteres for the acyl guanidine present in

amiloride. These novel ENaC blocker, characterized by a permanent cation via quaternization of the amine (Figure 1.22 A) improves ENaC potency and increase solubility. Quaternary amines deliver compounds equipotent with compound 552-02⁽²²³⁾ which was hitherto the best examples of a promising new class of human ENaC blockers that showed improved potency at ENaC in HBEC cells, efficacy and duration of action in a sheep model when compared to amiloride⁽²¹⁹⁾. Following the hypothesis that a hydrophobic tail group is able to increase potency, a series of novel α -branched pyrazinoyl quaternary, exemplified by Figure 1.22 B were synthesised and it was demonstrated that these analogues provide up to a 20-fold improvement in potency⁽²²³⁾.

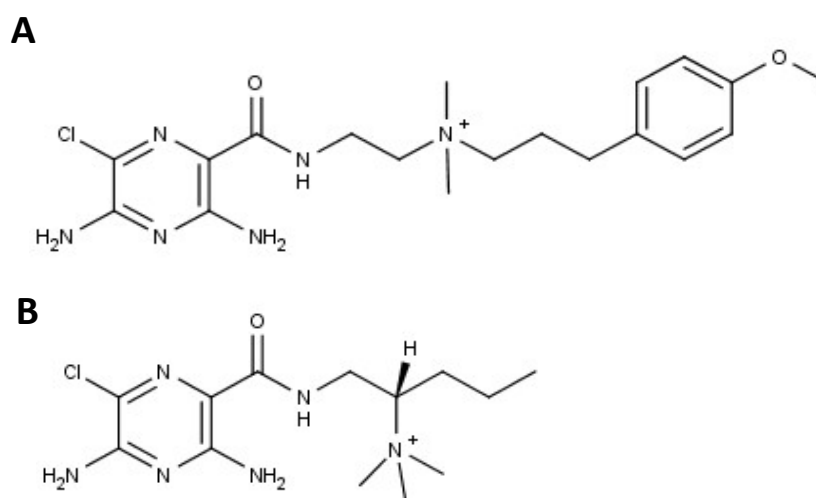


Figure 1.22 Example of quaternary amines (A) and α -branched quaternary amines ENaC Blockers (B)

A new ENaC inhibitor with molecular weight > 600 Da and decreased hyperkalaemic effect has been recently disclosed from Novartis. NVP-QBE-170 (Figure 1.23) is a dimeric amiloride-derivate which professed to improve mucus hydration and enhance

mucociliary clearance in CF people. The intra-tracheal installation of NVPQBE-170 in guinea pig airway showed the higher potency of this compound to inhibit ENaC and superior duration of action *in vitro* (NHBE cells) compared to amiloride. In particular, the recovery of short-circuit current (I_{sc}) was of around 100% for amiloride and 14% for NVPQBE-170 after 300 s.

NVP-QBE-170 also showed an improvement of MC in sheep airway after inhalation with a duration of action superior to hypertonic saline but long-term safety studies showed a hyperkalaemia effect after 28-days inhalation and studies have been halted. The development of a new class of inhaled ENaC blockers may represent a promising target for the improvement of MC in diseases such as cystic fibrosis.

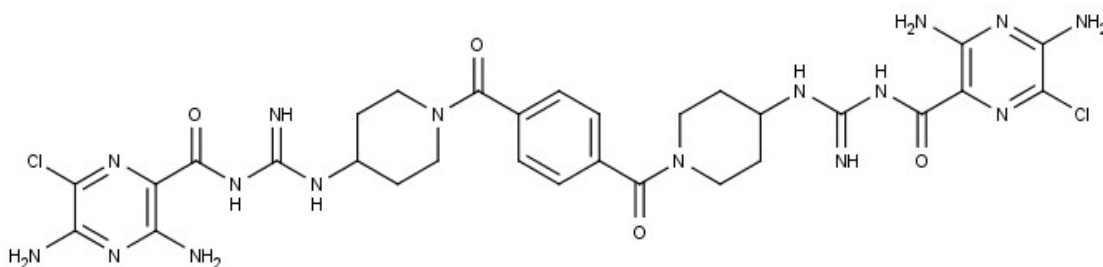


Figure 1.23 NVP-QBE-170 structure

The literature reported the interaction of mucin to inhaled drugs molecules and in this work we sought to determine if secreted mucin may represent a barrier for the disposition of ENaC blockers.

1.6 Thesis Aims and objectives

The overall aim of this thesis was to evaluate whether mucin may represent a dispositional barrier for the absorption of ENaC blockers after inhalation. General information of the source of material, sample preparation procedures and methodologies used throughout this PhD project are presented in Chapter 2 and the experimental work for this thesis is presented in three separate chapters (Chapters 3-5).

The work in chapter 3 was focused on the establishment and validation of mucin gel model for studying drug transportation through a 3D mucus model. Towards this aim, different sources of mucus were considered; human mucus from *in vitro* culture of human epithelial cells (NHBE cells), *ex-vivo* mucus from porcine lung and a commercial available porcine gastric mucin (PGM). PGM was chosen as mucus model to study the diffusion of FITC dextran probes at different molecular weight using the Franz-cell system. The diffusion studies were then extended on two ENaC blockers (amiloride and benzamil).

In Chapter 4, the amiloride and benzamil interaction to mucin was firstly studied using fluorescence and UV-spectroscopy techniques. The absence of a standard method for specifically study drug-mucin interactions lead us to the development of 96-well ultrafiltration assay which was used to screen a range of 12 ENaC blockers and correlate the extent of binding with the physical properties of the drug molecules. The 96-well ultrafiltration assay was also applied to study the extent of binding of drug molecules to

Chapter 1

other two macromolecules found in CF mucus, DNA and alginate. Chapter 4 ends with studies on the permeability characteristic of Calu-3 monolayer to predict amiloride and analogues absorption in lung.

The aim of Chapter 5 was to gain molecular level information of the drug-mucin interaction using the Saturation Transfer Difference-NMR spectroscopy (STD-NMR). In the same chapter, the purification and biochemical analysis of jejunal porcine mucin (PJM) is described. Early STD-NMR studies were focused on the interaction of salbutamol and tobramycin to PGM. STD-NMR was then used to identify “interacting” and “non-interacting” domains within two ENaC blockers, 552-02 and OF-80-NS22, and results obtained using PGM and PJM were comparable and confirmed the ultrafiltration binding assay results.

1.7 References

1. Groneberg DA, Witt C, Wagner U, Chung KF, Fischer A. Fundamentals of pulmonary drug delivery. *Respiratory medicine*. 2003;97(4):382-7.
2. Gänsslen. Uber inhalation von insulin. *Klin Wochenschr*. 1925;4:71.
3. Patton JS, McCabe JG, Hansen SE, Daugherty AL. Absorption of human growth hormone from the rat lung. *Biotechnology therapeutics*. 1989;1(3):213-28.
4. Patton JS, Bukar JG, Eldon MA. Clinical pharmacokinetics and pharmacodynamics of inhaled insulin. *Clinical pharmacokinetics*. 2004;43(12):781-801.
5. Steimer A, Haltner E, Lehr CM. Cell culture models of the respiratory tract relevant to pulmonary drug delivery. *Journal of aerosol medicine : the official journal of the International Society for Aerosols in Medicine*. 2005;18(2):137-82.
6. Tronde A, Norden B, Marchner H, Wendel AK, Lennernas H, Bengtsson UH. Pulmonary absorption rate and bioavailability of drugs in vivo in rats: structure-absorption relationships and physicochemical profiling of inhaled drugs. *J Pharm Sci*. 2003;92(6):1216-33.
7. Ji CM, Cardoso WV, Gebremichael A, Philpot RM, Buckpitt AR, Plopper CG, et al. Pulmonary cytochrome P-450 monooxygenase system and Clara cell differentiation in rats. *Am J Physiol*. 1995;269(3 Pt 1):L394-402.
8. Phung OJ. Technosphere insulin: An inhaled mealtime insulin for the treatment of type 1 and type 2 diabetes mellitus. *Formulary* 2011;46(1): 14-7.
9. Patton JS. Pulmonary delivery of drugs for bone disorders. *Advanced drug delivery reviews*. 2000;42(3):239-48.
10. Chow AH, Tong HH, Chattopadhyay P, Shekunov BY. Particle engineering for pulmonary drug delivery. *Pharmaceutical research*. 2007;24(3):411-37.
11. Fazio F, Lafortuna C. Effect of inhaled salbutamol on mucociliary clearance in patients with chronic bronchitis. *Chest*. 1981;80(6 Suppl):827-30.
12. Rosenfeld M, Cohen M, Ramsey B. Aerosolized antibiotics for bacterial lower airway infections: Principles, efficacy, and pitfalls. *Infect Dis Clin Prac*. 1998;7(2):66-79.
13. Berube K, Prytherch Z, Job C, Hughes T. Human primary bronchial lung cell constructs: the new respiratory models. *Toxicology*. 2010;278(3):311-8.
14. Byron PR. Prediction of Drug Residence Times in Regions of the Human Respiratory-Tract Following Aerosol Inhalation. *J Pharm Sci*. 1986;75(5):433-8.
15. Telko MJ, Hickey AJ. Dry powder inhaler formulation. *Respiratory care*. 2005;50(9):1209-27.
16. Spina D. Epithelium smooth muscle regulation and interactions. *American journal of respiratory and critical care medicine*. 1998;158(5 Pt 3):S141-5.
17. Knight DA, Holgate ST. The airway epithelium: structural and functional properties in health and disease. *Respirology*. 2003;8(4):432-46.

Chapter 1

18. Inayama Y, Hook GE, Brody AR, Cameron GS, Jetten AM, Gilmore LB, et al. The differentiation potential of tracheal basal cells. *Laboratory investigation; a journal of technical methods and pathology*. 1988;58(6):706-17.
19. Evans MJ, Plopper CG. The role of basal cells in adhesion of columnar epithelium to airway basement membrane. *The American review of respiratory disease*. 1988;138(2):481-3.
20. Jeffery PK. Morphology of the airway wall in asthma and in chronic obstructive pulmonary disease. *The American review of respiratory disease*. 1991;143(5 Pt 1):1152-8; discussion 61.
21. Lumsden AB, McLean A, Lamb D. Goblet and Clara cells of human distal airways: evidence for smoking induced changes in their numbers. *Thorax*. 1984;39(11):844-9.
22. Jones R, Baskerville A, Reid L. Histochemical identification of glycoproteins in pig bronchial epithelium: (a) normal and (b) hypertrophied from enzootic pneumonia. *The Journal of pathology*. 1975;116(1):1-11.
23. Jeffery PK, Reid LM. The effect of tobacco smoke, with or without phenylmethyloxadiazole (PMO), on rat bronchial epithelium: a light and electron microscopic study. *The Journal of pathology*. 1981;133(4):341-59.
24. Kotton DN, Morrissey EE. Lung regeneration: mechanisms, applications and emerging stem cell populations. *Nature medicine*. 2014;20(8):822-32.
25. McDowell EM, Barrett LA, Glavin F, Harris CC, Trump BF. The respiratory epithelium. I. Human bronchus. *Journal of the National Cancer Institute*. 1978;61(2):539-49.
26. Mooren HW, Meyer CJ, Kramps JA, Franken C, Dijkman JH. Ultrastructural localization of the low molecular weight protease inhibitor in human bronchial glands. *The journal of histochemistry and cytochemistry : official journal of the Histochemistry Society*. 1982;30(11):1130-4.
27. Crapo JD, Barry BE, Gehr P, Bachofen M, Weibel ER. Cell number and cell characteristics of the normal human lung. *Am Rev Respir Dis*. 1982;126(2):332-7.
28. Benoit A, Huang Y, Proctor J, Rowden G, Anderson R. Effects of alveolar macrophage depletion on liposomal vaccine protection against respiratory syncytial virus (RSV). *Clinical and experimental immunology*. 2006;145(1):147-54.
29. Rathbone MJ, Hadgraft J. Absorption of Drugs from the Human Oral Cavity. *Int J Pharm*. 1991;74(1):9-24.
30. Knowles MR, Boucher RC. Mucus clearance as a primary innate defense mechanism for mammalian airways. *J Clin Invest*. 2002;109(5):571-7.
31. Lai SK, Wang YY, Hanes J. Mucus-penetrating nanoparticles for drug and gene delivery to mucosal tissues. *Adv Drug Deliver Rev*. 2009;61(2):158-71.
32. Miller DS, Nobmann SN, Gutmann H, Toeroek M, Drewe J, Fricker G. Xenobiotic transport across isolated brain microvessels studied by confocal microscopy. *Mol Pharmacol*. 2000;58(6):1357-67.
33. Schanker LS, Mitchell EW, Brown RA, Jr. Species comparison of drug absorption from the lung after aerosol inhalation or intratracheal injection. *Drug metabolism and disposition: the biological fate of chemicals*. 1986;14(1):79-88.
34. Brown RA, Jr., Schanker LS. Absorption of aerosolized drugs from the rat lung. *Drug metabolism and disposition: the biological fate of chemicals*. 1983;11(4):355-60.

Chapter 1

35. Lin YJ, Schanker LS. Pulmonary absorption of amino acids in the rat: evidence of carrier transport. *The American journal of physiology*. 1981;240(5):C215-21.
36. Holmen JM, Karlsson NG, Abdullah LH, Randell SH, Sheehan JK, Hansson GC, et al. Mucins and their O-Glycans from human bronchial epithelial cell cultures. *Am J Physiol-Lung C*. 2004;287(4):L824-L34.
37. Mette SA, Pilewski J, Buck CA, Albelda SM. Distribution of integrin cell adhesion receptors on normal bronchial epithelial cells and lung cancer cells in vitro and in vivo. *American journal of respiratory cell and molecular biology*. 1993;8(5):562-72.
38. Kreda SM, Okada SF, van Heusden CA, O'Neal W, Gabriel S, Abdullah L, et al. Coordinated release of nucleotides and mucin from human airway epithelial Calu-3 cells. *The Journal of physiology*. 2007;584(Pt 1):245-59.
39. Fiegel J, Ehrhardt C, Schaefer UF, Lehr CM, Hanes J. Large porous particle impingement on lung epithelial cell monolayers--toward improved particle characterization in the lung. *Pharmaceutical research*. 2003;20(5):788-96.
40. Forbes B, Ehrhardt C. Human respiratory epithelial cell culture for drug delivery applications. *European journal of pharmaceutics and biopharmaceutics : official journal of Arbeitsgemeinschaft fur Pharmazeutische Verfahrenstechnik eV*. 2005;60(2):193-205.
41. Rothen-Rutishauser B, Blank F, Muhlfeld C, Gehr P. In vitro models of the human epithelial airway barrier to study the toxic potential of particulate matter. *Expert opinion on drug metabolism & toxicology*. 2008;4(8):1075-89.
42. Lee MC, Penland CM, Widdicombe JH, Wine JJ. Evidence that Calu-3 human airway cells secrete bicarbonate. *The American journal of physiology*. 1998;274(3 Pt 1):L450-3.
43. Shen BQ, Finkbeiner WE, Wine JJ, Mrsny RJ, Widdicombe JH. Calu-3: a human airway epithelial cell line that shows cAMP-dependent Cl⁻ secretion. *The American journal of physiology*. 1994;266(5 Pt 1):L493-501.
44. Borchard G. Calu-3 cells, a valid model for the airway epithelium? *Stp Pharma Sci*. 2002;12(4):205-11.
45. Foster KA, Avery ML, Yazdanian M, Audus KL. Characterization of the Calu-3 cell line as a tool to screen pulmonary drug delivery. *Int J Pharm*. 2000;208(1-2):1-11.
46. Burch SG, Erbland ML, Gann LP, Hiller FC. Plasma nicotine levels after inhalation of aerosolized nicotine. *The American review of respiratory disease*. 1989;140(4):955-7.
47. Dershwitz M, Walsh JL, Morishige RJ, Connors PM, Rubsamen RM, Shafer SL, et al. Pharmacokinetics and pharmacodynamics of inhaled versus intravenous morphine in healthy volunteers. *Anesthesiology*. 2000;93(3):619-28.
48. Patton. The lungs as a portal of entry for systemic drug delivery. *Proc Am Thorac Soc* 2004;1:338-44.
49. Beyer J, Schwartz S, Barzen G, Risse G, Dullenkopf K, Weyer C, et al. Use of Amphotericin-B Aerosols for the Prevention of Pulmonary Aspergillosis. *Infection*. 1994;22(2):143-8.
50. Brooks AD, Tong W, Benedetti F, Kaneda Y, Miller V, Warrell RP, Jr. Inhaled aerosolization of all-trans-retinoic acid for targeted pulmonary delivery. *Cancer chemotherapy and pharmacology*. 2000;46(4):313-8.

Chapter 1

51. Monk JP, Benfield P. Inhaled pentamidine. An overview of its pharmacological properties and a review of its therapeutic use in *Pneumocystis carinii* pneumonia. *Drugs*. 1990;39(5):741-56.
52. Newhouse MT, Hirst PH, Duddu SP, Walter YH, Tarara TE, Clark AR, et al. Inhalation of a dry powder tobramycin PulmoSphere formulation in healthy volunteers. *Chest*. 2003;124(1):360-6.
53. Sakagami M, Byron PR. Respirable microspheres for inhalation: the potential of manipulating pulmonary disposition for improved therapeutic efficacy. *Clinical pharmacokinetics*. 2005;44(3):263-77.
54. Saha P, Kim KJ, Yamahara H, Crandall ED, Lee VHL. Influence of Lipophilicity on Beta-Blocker Permeation across Rat Alveolar Epithelial-Cell Monolayers. *J Control Release*. 1994;32(2):191-200.
55. Gumbleton M. Caveolae as potential macromolecule trafficking compartments within alveolar epithelium. *Advanced drug delivery reviews*. 2001;49(3):281-300.
56. Raub TJ. P-glycoprotein recognition of substrates and circumvention through rational drug design. *Molecular pharmaceutics*. 2006;3(1):3-25.
57. Pajeva IK, Wiese M. Pharmacophore model of drugs involved in P-glycoprotein multidrug resistance: explanation of structural variety (hypothesis). *Journal of medicinal chemistry*. 2002;45(26):5671-86.
58. Jain V, Das SN, Luthra K, Shukla NK, Ralhan R. Differential expression of multidrug resistance gene product, P-glycoprotein, in normal, dysplastic and malignant oral mucosa in India. *International journal of cancer*. 1997;74(1):128-33.
59. Cordon-Cardo C, O'Brien JP, Boccia J, Casals D, Bertino JR, Melamed MR. Expression of the multidrug resistance gene product (P-glycoprotein) in human normal and tumor tissues. *The journal of histochemistry and cytochemistry : official journal of the Histochemistry Society*. 1990;38(9):1277-87.
60. Campbell L, Abulrob AN, Kandalaft LE, Plummer S, Hollins AJ, Gibbs A, et al. Constitutive expression of p-glycoprotein in normal lung alveolar epithelium and functionality in primary alveolar epithelial cultures. *The Journal of pharmacology and experimental therapeutics*. 2003;304(1):441-52.
61. Koepsell H, Lips K, Volk C. Polyspecific organic cation transporters: structure, function, physiological roles, and biopharmaceutical implications. *Pharmaceutical research*. 2007;24(7):1227-51.
62. Lips KS, Luhrmann A, Tschernig T, Stoeger T, Alessandrini F, Grau V, et al. Down-regulation of the non-neuronal acetylcholine synthesis and release machinery in acute allergic airway inflammation of rat and mouse. *Life sciences*. 2007;80(24-25):2263-9.
63. Lips KS, Volk C, Schmitt BM, Pfeil U, Arndt P, Miska D, et al. Polyspecific cation transporters mediate luminal release of acetylcholine from bronchial epithelium. *American journal of respiratory cell and molecular biology*. 2005;33(1):79-88.
64. Bleasby K, Castle JC, Roberts CJ, Cheng C, Bailey WJ, Sina JF, et al. Expression profiles of 50 xenobiotic transporter genes in humans and pre-clinical species: a resource for investigations into drug disposition. *Xenobiotica; the fate of foreign compounds in biological systems*. 2006;36(10-11):963-88.

Chapter 1

65. Horvath G, Schmid N, Fragoso MA, Schmid A, Conner GE, Salathe M, et al. Epithelial organic cation transporters ensure pH-dependent drug absorption in the airway. *American journal of respiratory cell and molecular biology*. 2007;36(1):53-60.
66. Singh PK, Parsek MR, Greenberg EP, Welsh MJ. A component of innate immunity prevents bacterial biofilm development. *Nature*. 2002;417(6888):552-5.
67. Keress S, Allen A, Garner A. A simple method for measuring thickness of the mucus gel layer adherent to rat, frog and human gastric mucosa: influence of feeding, prostaglandin, N-acetylcysteine and other agents. *Clin Sci (Lond)*. 1982;63(2):187-95.
68. Thornton DJ, Sheehan JK. From mucins to mucus: toward a more coherent understanding of this essential barrier. *Proceedings of the American Thoracic Society*. 2004;1(1):54-61.
69. Rose MC, Voynow JA. Respiratory tract mucin genes and mucin glycoproteins in health and disease. *Physiological reviews*. 2006;86(1):245-78.
70. Button B, Cai LH, Ehre C, Kesimer M, Hill DB, Sheehan JK, et al. A Periciliary Brush Promotes the Lung Health by Separating the Mucus Layer from Airway Epithelia. *Science*. 2012;337(6097):937-41.
71. Roussel P, Lamblin G, Lhermitte M, Houdret N, Lafitte JJ, Perini JM, et al. The Complexity of Mucins. *Biochimie*. 1988;70(11):1471-82.
72. Kornfeld R, Kornfeld S. Comparative aspects of glycoprotein structure. *Annual review of biochemistry*. 1976;45:217-37.
73. Spiro RG. Glycoproteins. *Annual review of biochemistry*. 1970;39:599-&.
74. Carlson DM. Structures and Immunochemical Properties of Oligosaccharides Isolated from Pig Submaxillary Mucins. *Journal of Biological Chemistry*. 1968;243(3):616-+.
75. Gibson RL, Emerson J, McNamara S, Burns JL, Rosenfeld M, Yunker A, et al. Significant microbiological effect of inhaled tobramycin in young children with cystic fibrosis. *American journal of respiratory and critical care medicine*. 2003;167(6):841-9.
76. Evans CM, Koo JS. Airway mucus: the good, the bad, the sticky. *Pharmacol Ther*. 2009;121(3):332-48.
77. Ablamowicz AF, Nichols JJ. Ocular Surface Membrane-Associated Mucins. *The ocular surface*. 2016;14(3):331-41.
78. Lillehoj EP, Kato K, Lu W, Kim KC. Cellular and molecular biology of airway mucins. *International review of cell and molecular biology*. 2013;303:139-202.
79. Rose MC, Voynow JA. Respiratory tract mucin genes and mucin glycoproteins in health and disease. *Physiol Rev*. 2006;86(1):245-78.
80. Gum JR, Jr., Hicks JW, Toribara NW, Siddiki B, Kim YS. Molecular cloning of human intestinal mucin (MUC2) cDNA. Identification of the amino terminus and overall sequence similarity to prepro-von Willebrand factor. *The Journal of biological chemistry*. 1994;269(4):2440-6.
81. Gipson IK, Ho SB, Spurr-Michaud SJ, Tisdale AS, Zhan Q, Torlakovic E, et al. Mucin genes expressed by human female reproductive tract epithelia. *Biology of reproduction*. 1997;56(4):999-1011.
82. Thornton DJ, Rousseau K, McGuckin MA. Structure and function of the polymeric mucins in airways mucus. *Annual review of physiology*. 2008;70:459-86.

Chapter 1

83. Owens SR, Chiosea SI, Kuan SF. Selective expression of gastric mucin MUC6 in colonic sessile serrated adenoma but not in hyperplastic polyp aids in morphological diagnosis of serrated polyps. *Modern pathology : an official journal of the United States and Canadian Academy of Pathology, Inc.* 2008;21(6):660-9.
84. Yu DF, Chen Y, Han JM, Zhang H, Chen XP, Zou WJ, et al. MUC19 expression in human ocular surface and lacrimal gland and its alteration in Sjogren syndrome patients. *Exp Eye Res.* 2008;86(2):403-11.
85. Chen Y, Zhu L, Widdicombe J. Complete Cloning Of Human MUC19 And A New In Vitro Model For The Study Of Glandular Mucins. *American journal of respiratory and critical care medicine.* 2011;183.
86. Kerschner JE, Khampang P, Erbe CB, Kolker A, Cioffi JA. Mucin gene 19 (MUC19) expression and response to inflammatory cytokines in middle ear epithelium. *Glycoconjugate J.* 2009;26(9):1275-84.
87. Chen Y, Zhao YH, Kalaslavadi TB, Halmati E, Nehrke K, Le AD, et al. Genome-wide search and identification of a novel gel-forming mucin MUC19/Muc19 in glandular tissues. *American journal of respiratory cell and molecular biology.* 2004;30(2):155-65.
88. Sharma P, Dudus L, Nielsen PA, Clausen H, Yankaskas JR, Hollingsworth MA, et al. MUC5B and MUC7 are differentially expressed in mucous and serous cells of submucosal glands in human bronchial airways. *American journal of respiratory cell and molecular biology.* 1998;19(1):30-7.
89. Jumblatt MM, McKenzie RW, Steele PS, Emberts CG, Jumblatt JE. MUC7 expression in the human lacrimal gland and conjunctiva. *Cornea.* 2003;22(1):41-5.
90. Cho KN, Choi JY, Kim CH, Baek SJ, Chung KC, Moon UY, et al. Prostaglandin E2 induces MUC8 gene expression via a mechanism involving ERK MAPK/RSK1/cAMP response element binding protein activation in human airway epithelial cells. *The Journal of biological chemistry.* 2005;280(8):6676-81.
91. Lagow E, DeSouza MM, Carson DG. Mammalian reproductive tract mucins. *Hum Reprod Update.* 1999;5(4):280-92.
92. Lapensee L, Paquette Y, Bleau G. Allelic polymorphism and chromosomal localization of the human oviductin gene (MUC9). *Fertil Steril.* 1997;68(4):702-8.
93. Gipson IK. Distribution of mucins at the ocular surface. *Exp Eye Res.* 2004;78(3):379-88.
94. Chang JF, Zhao HL, Phillips J, Greenburg G. The epithelial mucin, MUC1, is expressed on resting T lymphocytes and can function as a negative regulator of T cell activation. *Cellular immunology.* 2000;201(2):83-8.
95. Buisine MP, Devisme L, Copin MC, Durand-Reville M, Gosselin B, Aubert JP, et al. Developmental mucin gene expression in the human respiratory tract. *American journal of respiratory cell and molecular biology.* 1999;20(2):209-18.
96. Rakha EA, Boyce RW, Abd El-Rehim D, Kurien T, Green AR, Paish EC, et al. Expression of mucins (MUC1, MUC2, MUC3, MUC4, MUC5AC and MUC6) and their prognostic significance in human breast cancer. *Modern pathology : an official journal of the United States and Canadian Academy of Pathology, Inc.* 2005;18(10):1295-304.

Chapter 1

97. Cai H, Palitzsch B, Hartmann S, Stergiou N, Kunz H, Schmitt E, et al. Antibody induction directed against the tumor-associated MUC4 glycoprotein. *Chembiochem : a European journal of chemical biology*. 2015;16(6):959-67.
98. Bernacki SH, Nelson AL, Abdullah L, Sheehan JK, Harris A, Davis CW, et al. Mucin gene expression during differentiation of human airway epithelia in vitro. Muc4 and muc5b are strongly induced. *American journal of respiratory cell and molecular biology*. 1999;20(4):595-604.
99. Corrales RM, Galarreta DJ, Herreras JM, Calonge M, Chaves FJ. [Normal human conjunctival epithelium expresses MUC13, MUC15, MUC16 and MUC17 mucin genes]. *Archivos de la Sociedad Espanola de Oftalmologia*. 2003;78(7):375-81.
100. Hattrup CL, Gendler SJ. Structure and function of the cell surface (tethered) mucins. *Annual review of physiology*. 2008;70:431-57.
101. Nam KH, Noh TW, Chung SH, Lee SH, Lee MK, Hong SW, et al. Expression of the Membrane Mucins MUC4 and MUC15, Potential Markers of Malignancy and Prognosis, in Papillary Thyroid Carcinoma. *Thyroid*. 2011;21(7):745-50.
102. Davies JR, Hovenberg HW, Linden CJ, Howard R, Richardson PS, Sheehan JK, et al. Mucins in airway secretions from healthy and chronic bronchitic subjects. *The Biochemical journal*. 1996;313 (Pt 2):431-9.
103. Xiao XY, Wang LS, Wei P, Chi YY, Li DL, Wang QF, et al. Role of MUC20 overexpression as a predictor of recurrence and poor outcome in colorectal cancer. *J Transl Med*. 2013;11.
104. Wood JM, Hussey DJ, Woods CM, Watson DI, Carney AS. Biomarkers and laryngopharyngeal reflux. *The Journal of laryngology and otology*. 2011;125(12):1218-24.
105. Sheehan JK, Kesimer M, Pickles R. Innate immunity and mucus structure and function. *Novartis Foundation symposium*. 2006;279:155-66; discussion 67-9, 216-9.
106. Hovenberg HW, Davies JR, Carlstedt I. Different mucins are produced by the surface epithelium and the submucosa in human trachea: identification of MUC5AC as a major mucin from the goblet cells. *The Biochemical journal*. 1996;318 (Pt 1):319-24.
107. Rogers DF. Airway goblet cells: responsive and adaptable front-line defenders. *Eur Respir J*. 1994;7(9):1690-706.
108. Gill DJ, Chia J, Senewiratne J, Bard F. Regulation of O-glycosylation through Golgi-to-ER relocation of initiation enzymes. *The Journal of cell biology*. 2010;189(5):843-58.
109. Ross GF, Ikegami M, Steinhilber W, Jobe AH. Surfactant protein C in fetal and ventilated preterm rabbit lungs. *Am J Physiol*. 1999;277(6 Pt 1):L1104-8.
110. Kaliner M, Shelhamer JH, Borson B, Nadel J, Patow C, Marom Z. Human respiratory mucus. *Am Rev Respir Dis*. 1986;134(3):612-21.
111. Agrawal DK, Shao Z. Pathogenesis of allergic airway inflammation. *Current allergy and asthma reports*. 2010;10(1):39-48.
112. Kim YM, Kim YS, Jeon SG, Kim YK. Immunopathogenesis of allergic asthma: more than the th2 hypothesis. *Allergy, asthma & immunology research*. 2013;5(4):189-96.
113. Thai P, Loukoianov A, Wachi S, Wu R. Regulation of airway mucin gene expression. *Annual review of physiology*. 2008;70:405-29.

Chapter 1

114. Li. Transcriptional activation of mucin by *Pseudomonas aeruginosa* lipopolysaccharide in the pathogenesis of cystic fibrosis lung disease. *Proc Natl Acad Sci U S A*. 1997;94:967-72.
115. Bals R, Weiner DJ, Wilson JM. The innate immune system in cystic fibrosis lung disease. *The Journal of clinical investigation*. 1999;103(3):303-7.
116. Atherton HC, Jones G, Danahay H. IL-13-induced changes in the goblet cell density of human bronchial epithelial cell cultures: MAP kinase and phosphatidylinositol 3-kinase regulation. *American journal of physiology Lung cellular and molecular physiology*. 2003;285(3):L730-9.
117. Grunig G, Warnock M, Wakil AE, Venkayya R, Brombacher F, Rennick DM, et al. Requirement for IL-13 independently of IL-4 in experimental asthma. *Science*. 1998;282(5397):2261-3.
118. Cepinskas G, Specian RD, Kvietys PR. Adaptive cytoprotection in the small intestine: role of mucus. *The American journal of physiology*. 1993;264(5 Pt 1):G921-7.
119. Matthes I, Nimmerfall F, Sucker H. [Mucus models for investigation of intestinal absorption mechanisms. 2. Mechanisms of drug interactions with intestinal mucus]. *Die Pharmazie*. 1992;47(8):609-13.
120. Karlsson J, Wikman A, Artursson P. The Mucus Layer as a Barrier to Drug Absorption in Monolayers of Human Intestinal Epithelial HT29-H Goblet Cells. *Int J Pharm*. 1993;99(2-3):209-18.
121. Wikman A, Karlsson J, Carlstedt I, Artursson P. A drug absorption model based on the mucus layer producing human intestinal goblet cell line HT29-H. *Pharmaceutical research*. 1993;10(6):843-52.
122. Behrens I, Stenberg P, Artursson P, Kissel T. Transport of lipophilic drug molecules in a new mucus-secreting cell culture model based on HT29-MTX cells. *Pharmaceutical research*. 2001;18(8):1138-45.
123. Khanvilkar K, Donovan MD, Flanagan DR. Drug transfer through mucus. *Adv Drug Deliver Rev*. 2001;48(2-3):173-93.
124. Lieleg O, Ribbeck K. Biological hydrogels as selective diffusion barriers. *Trends in cell biology*. 2011;21(9):543-51.
125. Thornton DJ, Sheehan JK, Lindgren H, Carlstedt I. Mucus glycoproteins from cystic fibrotic sputum. Macromolecular properties and structural 'architecture'. *The Biochemical journal*. 1991;276 (Pt 3):667-75.
126. Thornton DJ, Davies JR, Kraayenbrink M, Richardson PS, Sheehan JK, Carlstedt I. Mucus glycoproteins from 'normal' human tracheobronchial secretion. *The Biochemical journal*. 1990;265(1):179-86.
127. Matsui H, Verghese MW, Kesimer M, Schwab UE, Randell SH, Sheehan JK, et al. Reduced three-dimensional motility in dehydrated airway mucus prevents neutrophil capture and killing bacteria on airway epithelial surfaces. *Journal of immunology*. 2005;175(2):1090-9.
128. Kirch J, Schneider A, Abou B, Hopf A, Schaefer UF, Schneider M, et al. Optical tweezers reveal relationship between microstructure and nanoparticle penetration of pulmonary mucus. *Proceedings of the National Academy of Sciences of the United States of America*. 2012;109(45):18355-60.

Chapter 1

129. Lai SK, O'Hanlon DE, Harrold S, Man ST, Wang YY, Cone R, et al. Rapid transport of large polymeric nanoparticles in fresh undiluted human mucus. *Proceedings of the National Academy of Sciences of the United States of America*. 2007;104(5):1482-7.
130. Banker MJ, Clark TH, Williams JA. Development and validation of a 96-well equilibrium dialysis apparatus for measuring plasma protein binding. *Journal of pharmaceutical sciences*. 2003;92(5):967-74.
131. Kariv I, Cao H, Oldenburg KR. Development of a high throughput equilibrium dialysis method. *Journal of pharmaceutical sciences*. 2001;90(5):580-7.
132. Sarre S, Vanbelle K, Smolders I, Krieken G, Michotte Y. The Use of Microdialysis for the Determination of Plasma-Protein Binding of Drugs. *J Pharmaceut Biomed*. 1992;10(10-12):735-9.
133. Carter DC, Ho JX. Structure of serum albumin. *Advances in protein chemistry*. 1994;45:153-203.
134. He XM, Carter DC. Atomic structure and chemistry of human serum albumin. *Nature*. 1992;358(6383):209-15.
135. Rohatagi S, Luo Y, Shen L, Guo Z, Schemm C, Huang Y, et al. Protein binding and its potential for eliciting minimal systemic side effects with a novel inhaled corticosteroid, ciclesonide. *American journal of therapeutics*. 2005;12(3):201-9.
136. Herve F. Drug binding in plasma. A summary of recent trends in the study of drug and hormone binding. *Clinical pharmacokinetics*. 1994;26(1):44-58.
137. Vorum H. Reversible ligand binding to human serum albumin. Theoretical and clinical aspects. *Danish medical bulletin*. 1999;46(5):379-99.
138. Kratochwil NA, Huber W, Muller F, Kansy M, Gerber PR. Predicting plasma protein binding of drugs: a new approach. *Biochem Pharmacol*. 2002;64(9):1355-74.
139. Albani F, Riva R, Contin M, Baruzzi A. Stereoselective Binding of Propranolol Enantiomers to Human Alpha-1-Acid Glycoprotein and Human-Plasma. *Brit J Clin Pharmacol*. 1984;18(2):244-6.
140. Schley J, Mulleroerlinghausen B. The Binding of Chemically Different Psychotropic-Drugs to Alpha-1-Acid Glycoprotein. *Pharmacopsychiatria*. 1983;16(3):82-5.
141. Grimaldi B, Hamberger C, Tremblay D, Barre J, Tillement JP. In vitro study of the binding of RU 486 and RU 42 633 to human serum proteins. *Progress in clinical and biological research*. 1989;300:445-8.
142. Lai SK, Wang YY, Hanes J. Mucus-penetrating nanoparticles for drug and gene delivery to mucosal tissues. *Adv Drug Deliv Rev*. 2009;61(2):158-71.
143. Larhed AW, Artursson P, Grasjo J, Bjork E. Diffusion of drugs in native and purified gastrointestinal mucus. *J Pharm Sci*. 1997;86(6):660-5.
144. Desai MA, Mutlu M, Vadgama P. A study of macromolecular diffusion through native porcine mucus. *Experientia*. 1992;48(1):22-6.
145. Kararli TT. Comparison of the gastrointestinal anatomy, physiology, and biochemistry of humans and commonly used laboratory animals. *Biopharmaceutics & drug disposition*. 1995;16(5):351-80.

Chapter 1

146. Sanders NN, De Smedt SC, Van Rompaey E, Simoens P, De Baets F, Demeester J. Cystic fibrosis sputum: a barrier to the transport of nanospheres. *American journal of respiratory and critical care medicine*. 2000;162(5):1905-11.
147. Groo AC, Saulnier P, Gimel JC, Gravier J, Ailhas C, Benoit JP, et al. Fate of paclitaxel lipid nanocapsules in intestinal mucus in view of their oral delivery. *International journal of nanomedicine*. 2013;8:4291-302.
148. Dawson M, Krauland E, Wirtz D, Hanes J. Transport of polymeric nanoparticle gene carriers in gastric mucus. *Biotechnology progress*. 2004;20(3):851-7.
149. Larhed AW, Artursson P, Bjork E. The influence of intestinal mucus components on the diffusion of drugs. *Pharmaceutical research*. 1998;15(1):66-71.
150. McGill SL, Smyth HD. Disruption of the mucus barrier by topically applied exogenous particles. *Molecular pharmaceutics*. 2010;7(6):2280-8.
151. Kwong TC. Free drug measurements: methodology and clinical significance. *Clinica chimica acta; international journal of clinical chemistry*. 1985;151(3):193-216.
152. Barre J. Problems in therapeutic drug monitoring: free drug level monitoring. *Therapeutic drug monitoring*. 1988;10(2):133-43.
153. Waters NJ, Jones R, Williams G, Sohal B. Validation of a rapid equilibrium dialysis approach for the measurement of plasma protein binding. *Journal of pharmaceutical sciences*. 2008;97(10):4586-95.
154. Hage DS, Tweed SA. Recent advances in chromatographic and electrophoretic methods for the study of drug-protein interactions. *Journal of chromatography B, Biomedical sciences and applications*. 1997;699(1-2):499-525.
155. Wang Y, Mathis CA, Huang GF, Debnath ML, Holt DP, Shao L, et al. Effects of lipophilicity on the affinity and nonspecific binding of iodinated benzothiazole derivatives. *Journal of molecular neuroscience : MN*. 2003;20(3):255-60.
156. Bowers WF, Fulton S, Thompson J. Ultrafiltration vs equilibrium dialysis for determination of free fraction. *Clinical pharmacokinetics*. 1984;9 Suppl 1:49-60.
157. Sebillé B, Zini R, Madjar CV, Thuaud N, Tillement JP. Separation procedures used to reveal and follow drug-protein binding. *Journal of chromatography*. 1990;531:51-77.
158. Larsson PO. High-performance liquid affinity chromatography. *Methods in enzymology*. 1984;104:212-23.
159. Vuignier K. High performance affinity chromatography (HPAC) as a high-throughput screening tool in drug discovery to study drug-plasma protein interactions. *Journal of pharmaceutical and biomedical analysis*. 2013;74:205-12.
160. Franz TJ. The finite dose technique as a valid in vitro model for the study of percutaneous absorption in man. *Current problems in dermatology*. 1978;7:58-68.
161. Bonferoni MC, Rossi S, Ferrari F, Caramella C. A modified Franz diffusion cell for simultaneous assessment of drug release and washability of mucoadhesive gels. *Pharmaceutical development and technology*. 1999;4(1):45-53.
162. Wei C, Wang J, Zhang M. Spectroscopic study on the binding of porphyrins to (G(4)T(4)G(4))₄ parallel G-quadruplex. *Biophysical chemistry*. 2010;148(1-3):51-5.

163. Bhadra K, Kumar GS. Interaction of berberine, palmatine, coralyne, and sanguinarine to quadruplex DNA: a comparative spectroscopic and calorimetric study. *Biochimica et biophysica acta*. 2011;1810(4):485-96.
164. Sun H, Xiang J, Liu Y, Li L, Li Q, Xu G, et al. A stabilizing and denaturing dual-effect for natural polyamines interacting with G-quadruplexes depending on concentration. *Biochimie*. 2011;93(8):1351-6.
165. Reddy KL, Reddy YH, Kumar KA, Vidhisha S, Satyanarayana S. Synthesis, characterization, DNA-binding, and DNA-photocleavage properties of [Co(bpy)₂(7-NO₂-dppz)]³⁺, and their toxicity on different microorganisms. *Nucleosides, nucleotides & nucleic acids*. 2009;28(3):204-19.
166. Suh D, Chaires JB. Criteria for the mode of binding of DNA binding agents. *Bioorganic & medicinal chemistry*. 1995;3(6):723-8.
167. Sirajuddin. Drug-DNA interactions and their study by UV-Visible, fluorescence spectroscopies and cyclic voltametry. *J Photochem Photobiol*. 2013; 124:1-19.
168. Kerem B, Rommens JM, Buchanan JA, Markiewicz D, Cox TK, Chakravarti A, et al. Identification of the cystic fibrosis gene: genetic analysis. *Science*. 1989;245(4922):1073-80.
169. Kirk KL, Wang W. A unified view of cystic fibrosis transmembrane conductance regulator (CFTR) gating: combining the allosterism of a ligand-gated channel with the enzymatic activity of an ATP-binding cassette (ABC) transporter. *The Journal of biological chemistry*. 2011;286(15):12813-9.
170. Hwang TC, Sheppard DN. Gating of the CFTR Cl⁻ channel by ATP-driven nucleotide-binding domain dimerisation. *The Journal of physiology*. 2009;587(Pt 10):2151-61.
171. Rogan MP, Stoltz DA, Hornick DB. Cystic fibrosis transmembrane conductance regulator intracellular processing, trafficking, and opportunities for mutation-specific treatment. *Chest*. 2011;139(6):1480-90.
172. Zielenski J, Tsui LC. Cystic fibrosis: genotypic and phenotypic variations. *Annual review of genetics*. 1995;29:777-807.
173. Bose SJ, Scott-Ward TS, Cai Z, Sheppard DN. Exploiting species differences to understand the CFTR Cl⁻ channel. *Biochemical Society transactions*. 2015;43(5):975-82.
174. Gruber AD, Gandhi R, Pauli BU. The murine calcium-sensitive chloride channel (mCaCC) is widely expressed in secretory epithelia and in other select tissues. *Histochemistry and cell biology*. 1998;110(1):43-9.
175. Enuka Y, Hanukoglu I, Edelheit O, Vaknine H, Hanukoglu A. Epithelial sodium channels (ENaC) are uniformly distributed on motile cilia in the oviduct and the respiratory airways. *Histochemistry and cell biology*. 2012;137(3):339-53.
176. Kunzelmann K, Schreiber R, Nitschke R, Mall M. Control of epithelial Na⁺ conductance by the cystic fibrosis transmembrane conductance regulator. *Pflugers Archiv : European journal of physiology*. 2000;440(2):193-201.
177. Kunzelmann K. ENaC is inhibited by an increase in the intracellular Cl⁻ concentration mediated through activation of Cl⁻ channels. *Pflugers Archiv : European journal of physiology*. 2003;445(4):504-12.
178. Berdiev BK, Qadri YJ, Benos DJ. Assessment of the CFTR and ENaC association. *Molecular bioSystems*. 2009;5(2):123-7.

Chapter 1

179. Boucher RC. Airway surface dehydration in cystic fibrosis: pathogenesis and therapy. *Annual review of medicine*. 2007;58:157-70.
180. Donaldson SH, Boucher RC. Sodium channels and cystic fibrosis. *Chest*. 2007;132(5):1631-6.
181. O'Sullivan BP, Freedman SD. Cystic fibrosis. *Lancet*. 2009;373(9678):1891-904.
182. McLachlan G, Davidson DJ, Stevenson BJ, Dickinson P, Davidson-Smith H, Dorin JR, et al. Evaluation in vitro and in vivo of cationic liposome-expression construct complexes for cystic fibrosis gene therapy. *Gene therapy*. 1995;2(9):614-22.
183. Sinn PL, Burnight ER, McCray PB. Progress and Prospects: prospects of repeated pulmonary administration of viral vectors. *Gene therapy*. 2009;16(9):1059-65.
184. Suk JS, Kim AJ, Trehan K, Schneider CS, Cebotaru L, Woodward OM, et al. Lung gene therapy with highly compacted DNA nanoparticles that overcome the mucus barrier. *Journal of controlled release : official journal of the Controlled Release Society*. 2014;178:8-17.
185. Griesenbach U, Alton EW, Consortium UKCFGT. Gene transfer to the lung: lessons learned from more than 2 decades of CF gene therapy. *Advanced drug delivery reviews*. 2009;61(2):128-39.
186. Boyle MP, Bell SC, Konstan MW, McColley SA, Rowe SM, Rietschel E, et al. A CFTR corrector (lumacaftor) and a CFTR potentiator (ivacaftor) for treatment of patients with cystic fibrosis who have a phe508del CFTR mutation: a phase 2 randomised controlled trial. *The Lancet Respiratory medicine*. 2014;2(7):527-38.
187. Ramsey BW, Davies J, McElvaney NG, Tullis E, Bell SC, Drevinek P, et al. A CFTR potentiator in patients with cystic fibrosis and the G551D mutation. *The New England journal of medicine*. 2011;365(18):1663-72.
188. Robinson M, Regnis JA, Bailey DL, King M, Bautovich GJ, Bye PT. Effect of hypertonic saline, amiloride, and cough on mucociliary clearance in patients with cystic fibrosis. *American journal of respiratory and critical care medicine*. 1996;153(5):1503-9.
189. Tarran R, Grubb BR, Parsons D, Picher M, Hirsh AJ, Davis CW, et al. The CF salt controversy: in vivo observations and therapeutic approaches. *Molecular cell*. 2001;8(1):149-58.
190. Gamper N, Shapiro MS. Regulation of ion transport proteins by membrane phosphoinositides. *Nature reviews Neuroscience*. 2007;8(12):921-34.
191. Canessa CM, Schild L, Buell G, Thorens B, Gautschi I, Horisberger JD, et al. Amiloride-sensitive epithelial Na⁺ channel is made of three homologous subunits. *Nature*. 1994;367(6462):463-7.
192. Horisberger JD. Amiloride-sensitive Na channels. *Current opinion in cell biology*. 1998;10(4):443-9.
193. Golestaneh N, Klein C, Valamanesh F, Suarez G, Agarwal MK, Mirshahi M. Mineralocorticoid receptor-mediated signaling regulates the ion gated sodium channel in vascular endothelial cells and requires an intact cytoskeleton. *Biochemical and biophysical research communications*. 2001;280(5):1300-6.
194. Oberleithner H, Ludwig T, Riethmuller C, Hillebrand U, Albermann L, Schafer C, et al. Human endothelium: target for aldosterone. *Hypertension*. 2004;43(5):952-6.
195. Waldmann R, Champigny G, Bassilana F, Voilley N, Lazdunski M. Molecular cloning and functional expression of a novel amiloride-sensitive Na⁺ channel. *The Journal of biological chemistry*. 1995;270(46):27411-4.

Chapter 1

196. Le T, Saier MH, Jr. Phylogenetic characterization of the epithelial Na⁺ channel (ENaC) family. *Molecular membrane biology*. 1996;13(3):149-57.
197. Hirsh AJ, Sabater JR, Zamurs A, Smith RT, Paradiso AM, Hopkins S, et al. Evaluation of second generation amiloride analogs as therapy for cystic fibrosis lung disease. *The Journal of pharmacology and experimental therapeutics*. 2004;311(3):929-38.
198. Loffing J, Kaissling B. Sodium and calcium transport pathways along the mammalian distal nephron: from rabbit to human. *American journal of physiology Renal physiology*. 2003;284(4):F628-43.
199. Cheitlin MD, Byrd R, Benowitz N, Liu E, Modin G. Amiloride improves hemodynamics in patients with chronic congestive heart failure treated with chronic digoxin and diuretics. *Cardiovascular drugs and therapy / sponsored by the International Society of Cardiovascular Pharmacotherapy*. 1991;5(4):719-25.
200. App EM, King M, Helfesrieder R, Kohler D, Matthys H. Acute and long-term amiloride inhalation in cystic fibrosis lung disease. A rational approach to cystic fibrosis therapy. *The American review of respiratory disease*. 1990;141(3):605-12.
201. Knowles M, Murray G, Shallal J, Askin F, Ranga V, Gatzky J, et al. Bioelectric properties and ion flow across excised human bronchi. *Journal of applied physiology: respiratory, environmental and exercise physiology*. 1984;56(4):868-77.
202. Kohler D, App E, Schmitz-Schumann M, Wurtemberger G, Matthys H. Inhalation of amiloride improves the mucociliary and the cough clearance in patients with cystic fibroses. *European journal of respiratory diseases Supplement*. 1986;146:319-26.
203. Knowles MR, Church NL, Waltner WE, Yankaskas JR, Gilligan P, King M, et al. A pilot study of aerosolized amiloride for the treatment of lung disease in cystic fibrosis. *The New England journal of medicine*. 1990;322(17):1189-94.
204. Pons G, Marchand MC, d'Athis P, Sauvage E, Foucard C, Chaumet-Riffaud P, et al. French multicenter randomized double-blind placebo-controlled trial on nebulized amiloride in cystic fibrosis patients. The Amiloride-AFLM Collaborative Study Group. *Pediatric pulmonology*. 2000;30(1):25-31.
205. Noone PG, Regnis JA, Liu X, Brouwer KL, Robinson M, Edwards L, et al. Airway deposition and clearance and systemic pharmacokinetics of amiloride following aerosolization with an ultrasonic nebulizer to normal airways. *Chest*. 1997;112(5):1283-90.
206. Hofmann T, Stutts MJ, Ziersch A, Ruckes C, Weber WM, Knowles MR, et al. Effects of topically delivered benzamil and amiloride on nasal potential difference in cystic fibrosis. *American journal of respiratory and critical care medicine*. 1998;157(6 Pt 1):1844-9.
207. Mentz WM, Brown JB, Friedman M, Stutts MJ, Gatzky JT, Boucher RC. Deposition, clearance, and effects of aerosolized amiloride in sheep airways. *The American review of respiratory disease*. 1986;134(5):938-43.
208. Hirsh AJ. Altering airway surface liquid volume: inhalation therapy with amiloride and hyperosmotic agents. *Advanced drug delivery reviews*. 2002;54(11):1445-62.
209. Kleyman TR, Cragoe EJ, Jr. Amiloride and its analogs as tools in the study of ion transport. *The Journal of membrane biology*. 1988;105(1):1-21.

Chapter 1

210. Blank U, Ruckes C, Clauss W, Hofmann T, Lindemann H, Munker G, et al. Cystic fibrosis and non-cystic-fibrosis human nasal epithelium show analogous Na⁺ absorption and reversible block by phenamil. *Pflugers Archiv : European journal of physiology*. 1997;434(1):19-24.
211. Rodgers HC, Knox AJ. The effect of topical benzamil and amiloride on nasal potential difference in cystic fibrosis. *The European respiratory journal*. 1999;14(3):693-6.
212. Li JH, Cragoe EJ, Jr., Lindemann B. Structure-activity relationship of amiloride analogs as blockers of epithelial Na channels: I. Pyrazine-ring modifications. *The Journal of membrane biology*. 1985;83(1-2):45-56.
213. Li JH, Cragoe EJ, Jr., Lindemann B. Structure-activity relationship of amiloride analogs as blockers of epithelial Na channels: II. Side-chain modifications. *The Journal of membrane biology*. 1987;95(2):171-85.
214. L'Allemain G, Franchi A, Cragoe E, Jr., Pouyssegur J. Blockade of the Na⁺/H⁺ antiport abolishes growth factor-induced DNA synthesis in fibroblasts. Structure-activity relationships in the amiloride series. *The Journal of biological chemistry*. 1984;259(7):4313-9.
215. Cuthbert AW, Fanelli GM. Effects of some pyrazinecarboxamides on sodium transport in frog skin. *British journal of pharmacology*. 1978;63(1):139-49.
216. Carr MJ, Gover TD, Weinreich D, Udem BJ. Inhibition of mechanical activation of guinea-pig airway afferent neurons by amiloride analogues. *British journal of pharmacology*. 2001;133(8):1255-62.
217. Coote KJ, Atherton H, Young A, Sugar R, Burrows R, Smith NJ, et al. The guinea-pig tracheal potential difference as an in vivo model for the study of epithelial sodium channel function in the airways. *British journal of pharmacology*. 2008;155(7):1025-33.
218. Hirsh AJ, Molino BF, Zhang J, Astakhova N, Geiss WB, Sargent BJ, et al. Design, synthesis, and structure-activity relationships of novel 2-substituted pyrazinoylguanidine epithelial sodium channel blockers: drugs for cystic fibrosis and chronic bronchitis. *Journal of medicinal chemistry*. 2006;49(14):4098-115.
219. Hirsh AJ, Zhang J, Zamurs A, Fleegle J, Thelin WR, Caldwell RA, et al. Pharmacological properties of N-(3,5-diamino-6-chloropyrazine-2-carbonyl)-N'-4-[4-(2,3-dihydroxypropoxy)phenyl] butyl-guanidine methanesulfonate (552-02), a novel epithelial sodium channel blocker with potential clinical efficacy for cystic fibrosis lung disease. *The Journal of pharmacology and experimental therapeutics*. 2008;325(1):77-88.
220. O'Riordan TG, Donn KH, Hodsmann P, Ansede JH, Newcomb T, Lewis SA, et al. Acute hyperkalemia associated with inhalation of a potent ENaC antagonist: Phase 1 trial of GS-9411. *Journal of aerosol medicine and pulmonary drug delivery*. 2014;27(3):200-8.
221. Russ T, Ried W, Ullrich F, Mutschler E. Preparation and Diuretic Properties of Novel Amiloride Analogs. *Arch Pharm*. 1992;325(12):761-7.
222. Li JH, Shaw A, Kau ST. Stereoselective blockade of amphibian epithelial sodium channels by amiloride analogs. *The Journal of pharmacology and experimental therapeutics*. 1993;267(3):1081-4.
223. Hunt T, Atherton-Watson HC, Collingwood SP, Coote KJ, Czarnecki S, Danahay H, et al. Discovery of a novel chemotype of potent human ENaC blockers using a bioisostere approach. Part 2: alpha-Branched quaternary amines. *Bioorganic & medicinal chemistry letters*. 2012;22(8):2877-9.

Chapter 2 : Materials and Methods

This project was focussed on increased understanding of whether mucin, a heavily glycosylated protein contained in the mucus, may limit the access of ENaC molecules to their site of action. Moreover, the project aimed to increase the understanding of the relationship between ENaC blocker physico-chemical properties and mucin binding. Different sources of mucus and mucin have been used but the larger part of experiments were carried out using a commercial partially purified gastric mucin, and later in the project, porcine gut mucin has been purified and used.

An ultrafiltration binding assay has been developed, Calu-3 cells have been used for absorption studies of ENaC blockers, and a very powerful NMR technique, the Saturation Transfer Difference NMR, was applied as mechanistic method for studying mucin-drug interactions.

This chapter is intended to present general information of the source of material, sample preparation procedures and methodologies used throughout this PhD project.

2.1 Normal Human Bronchial Epithelial

Normal human bronchial epithelial (NHBE) cells were cultured at an air-liquid interface in order to produce an *in vitro* model of the respiratory epithelium for the production of human mucus and for the study of transportation assay using small drug molecules.

2.1.1 NHBE cells culture reagents and media preparation

B-ALI TM growth medium, B-ALI TM differentiation medium, Human Bronchial Epithelial cells, trypsin EDTA, bronchial epithelial cell growth medium supplemented

were purchased from Lonza (Walkerville, USA), Alexaflour-633 labelled WGA and goat anti-rabbit AlexaFluor 488 antibody were purchased from Life Technologies (Paisley, UK), anti-mucin 5AC purchased from Santa Cruz (Texas, USA from life technologies, Paisley, UK). Dulbecco's modified Eagle's medium, gentamicin was bought from Gibco (Carlsbad, California). Recombinant Human IL-13 (PetroTech, USA). DAPI, trans- retinoic acid purchased from Sigma (Poole, UK), Leica TCS-SP1 Laser scanning confocal microscope (Leica Microsystems, Wetzlar, Germany), Image-Pro Plus 7.0 software (Media Cybernetics INC., Silver Spring, MD). Olympus BX60 epifluorescent microscope (Olympus, Japan) and images captured by a ProgRes c10Plus digital camera (Janoptik, Schwenningen, Germany). Epithelial voltammeter Millicell-ERS was from Millipore (Bedford, MA, USA).

2.1.2 NHBE Cell Culture

Cells were seeded into plastic T-75 flasks and grown in bronchial epithelial cell growth medium supplemented with bovine pituitary extract (52 µg/ml), hydrocortisone (0.5 µg/ml), recombinant human EGF (0.5 ng/ml), epinephrine (0.5 µg/ml), transferrin (10 µg/ml), insulin (5 µg/ml), retinoic acid (0.1 µg/ml), triiodothyronine (6.5 ng/ml), gentamicin sulphate (50 µg/ml) and amphotericin-B (50 µg/ml). Medium was changed every 48 h until cells were ~80% confluent. Cells were then seeded at 24.3×10^4 cells/insert onto 6.5-mm-diameter polyester Corning Costar Transwell-Clear inserts with 0.4 µm pores. Cells were submerged in differentiation medium containing a 1:1 mixture of Dulbecco's modified Eagle's medium and bronchial epithelial cell growth medium (DMEM:BEEM) with the same supplements as above, except that triiodothyronine and retinoic acid were omitted, and replaced with all-

trans retinoic acid at a final concentration of 50 nM. Cells were submerged for the first 7 days in culture, after which time the apical medium was removed and cells were exposed to an air–liquid interface that was maintained for the remainder of the culture period (Figure 2.1). Medium was exchanged three times weekly: Monday, Wednesday, and Friday. The apical surface of the cells was rinsed with 100µl of warm PBS twice weekly to remove debris. Cells were maintained at 37°C in 5% CO₂ in a humidified incubator.

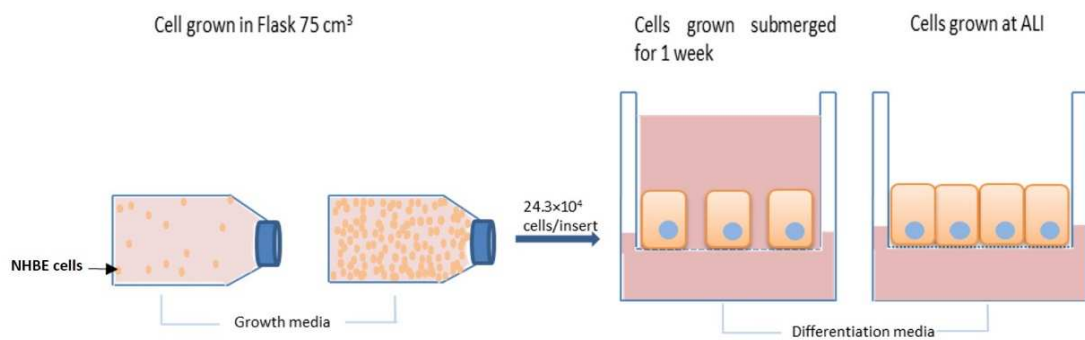


Figure 2.1 NHBE cells ALI culture. Cells grown into plastic T-75 flasks in Growth media. Once the cells are 80% confluent are transferred onto inserts (24.3×10^4 cells/insert) submerged in differentiation media for 1 week. Media is then removed from the apical side and cells grown at ALI.

2.1.3 Cell counting and viability

When passaging cells, the cell suspension was diluted 1:1 with 0.4% trypan blue solution. 10 µl of the solution was added onto the haemocytometer allowing the cell suspension to be drawn out by capillary action and visualised with a light microscope with a 10X objective. Trypan blue dye was used to calculate the cell viability. Live, unstained cells were counted in one set of 16 squares. The trypan blue dye is able to penetrate the cells in which the membrane is not intact and therefore dead cells stained are non-viable.

2.1.4 Cytokine Treatment

Lyophilized recombinant human IL-13 was prepared as 1000X stock solution in PBS +0.1% BSA then stored at -20°C. IL-13 was added to the differentiation medium to increase mucus production for all the duration of ALI cultures at a final concentration of 1ng/ml ⁽¹⁾.

2.1.5 Electrical Measurements

The Millicell-ERS (Electrical Resistance System) measures membrane potential and the Trans Epithelial Resistance (TER). An increase in TER detected with the electronic circuit electrode is an indication of cell monolayer confluency and integrity. A silver/silver chloride (Ag/AgCl) pellet (4mm wide and 1mm thick) on each electrode tip measures voltage.

Once cells were 100% confluent, the TER ($\Omega \cdot \text{cm}^2$) was measured every Monday, Wednesday and Friday before the media was refreshed. TER was measured across the cell layers using an epithelial voltohmmeter and silver chloride 'chopstick' electrodes. For ALI cultures measurements were made at 37°C after a 15 min equilibration period with 100 μl of warmed PBS (10 Na_2HPO_4 , 2 KH_2PO_4 , 2.7 KCl , 137 NaCl mmol/L) in the apical chamber and 500 μl of media in the basolateral chamber. The resistance across a cell-free culture support was subtracted from the resistance measured across each cell layer to yield the TER of the epithelial cells:

$$(\Omega \cdot \text{cm}^2)_{\text{epithelia cells}} = (\Omega \cdot \text{cm}^2)_{\text{Cell culture}} - (\Omega \cdot \text{cm}^2)_{\text{Cell-free culture}}$$

2.1.6 Immunochemistry assay for MUC5AC identification

After 15 post-seeding, NHBE cells and cells cultured with IL-13 were fixed adding onto the apical side of each inserts 100µl of ice-cold acetone and methanol (1:1) for 5 minutes. Nonspecific binding was blocked by the addition of 5% bovine serum albumin (BSA) in PBS with 0.05% Tween 20 and incubated for 30 minutes. The inserts were subsequently rinsed with PBS. Cells were then incubated for 2h with anti-MUC5AC antibody at 0.4µg/ml in 1% BSA. After rinsed with PBS cells were incubated for 1h with anti-rabbit Alexaflour-488 secondary antibody at 0.4µg/ml in PBS. The cultures were stained with Alexaflour-633 labelled WGA to visualise all glycoproteins and incubate for another hour. Cell nuclei were counterstained with 300 nM 4,6-diamidino-2-phenylindole (DAPI) for 10 min after washing twice with PBS-Tween 20 and once with PBS. After DAPI staining, cells were washed once with PBS for 5 minutes. The Transwell membranes were removed by scalpel, placed (apical side on the top) on a microscope slide with a drop of Fluoroshield for preserving fluorescence. The slides were examined using an Olympus BX-60 epifluorescent microscope and images captured by a ProgRes c10 Plus digital camera. Analysis was conducted using a Leica SP1 confocal microscope with assistance from Balazs Bajka (Institute of Food research).

2.1.7 Human mucus harvesting from NHBE cells

To detach the slimy mucus from the NHBE monolayer 100 µl were added to each insert (+/- IL13) and left into the incubator for 10 min at 37°C. The mucus was then collected and frozen at 4°C for future use.

2.1.8 Identification of mucin structure by AFM

During sample preparation for immunohistochemistry it was observed that significant amounts of mucus were removed from the apical membrane. The PBS washes containing the secreted mucus was centrifuged (5,000 g at 4°C for 30 minutes). The supernatant was aspirated and the pellet was diluted 10-fold in ultrapure water. Four microliters of the diluted sample were spotted onto freshly cleaved mica, then incubated for 1 min to allow glycoprotein adsorption to take place. The sample was blown dry using dry nitrogen gas. Patrick Gunning from the Institute of Food Research analysed the sample with an MFP-3D BIO atomic force microscope. The cantilevers were Olympus AC160TS (Olympus, Tokyo, Japan) with a nominal spring constant of ~42 N/m, oscillated at a frequency 10% below resonance (typically around 320 kHz). The damping set point for imaging was kept to the minimum value that allowed stable tracking of the sample surface to minimize any sample deformation. Images were acquired at a scan rate of 1 Hz.

2.2 *Ex vivo* system using porcine respiratory tract mucus

NHBE cell culture is expensive and it takes a long time to obtain a small amount of mucus. An *ex vivo* system using porcine respiratory mucus was investigated as a source of fresh porcine mucus.

2.2.1 Materials for porcine lung mucus extraction

Porcine lungs were donated by H G Blake, Ltd. Bull Farm Abattoir (Norwich, UK). Nitrocellulose transfer membrane 0.45um RPMI 1640, Antibiotic-antimycotic mixture (100x) was bought from Gibco (Carlsbad, California), NaCl and gentamicin solution 50mg/ml were bought from Sigma.

2.2.2 Tracheal and lung dissection and mucus harvest

Dissection was performed on fresh porcine lungs. Each trachea was removed intact by sectioning below the larynx and above the first bronchial branch (15-18cm long). Primary and secondary bronchi (60-80mm long) were dissected intact from lung tissue (Figure 2.2). Sterile saline solution (NaCl 0.150 M) was used to rinse off blood contamination. After several washes with NaCl, dissected tissue was rinsed and rolled with a tube roller (Stuart®) for 30 minutes in 5 ml of RPMI 1640 supplemented with a mix of antibiotics: penicillin (100 or 300Units/ml), streptomycin (100 or 300µg/ml), fungizone (25 or 75µg/ml) and gentamicin (5 or 15µg/ml). Tracheal and bronchial explants were then incubated at room temperature, 4°C and 37°C for 24 and 48 hours with 5ml of fresh RPMI, supplemented with antibiotics as above (Figure 2.2). After incubation, the trachea and bronchi were cut open longitudinally and porcine lung mucus (PLM) was collected by scraping gently with a cell scraper and frozen at -20°C until required. The same was followed after 48 hours of incubation.

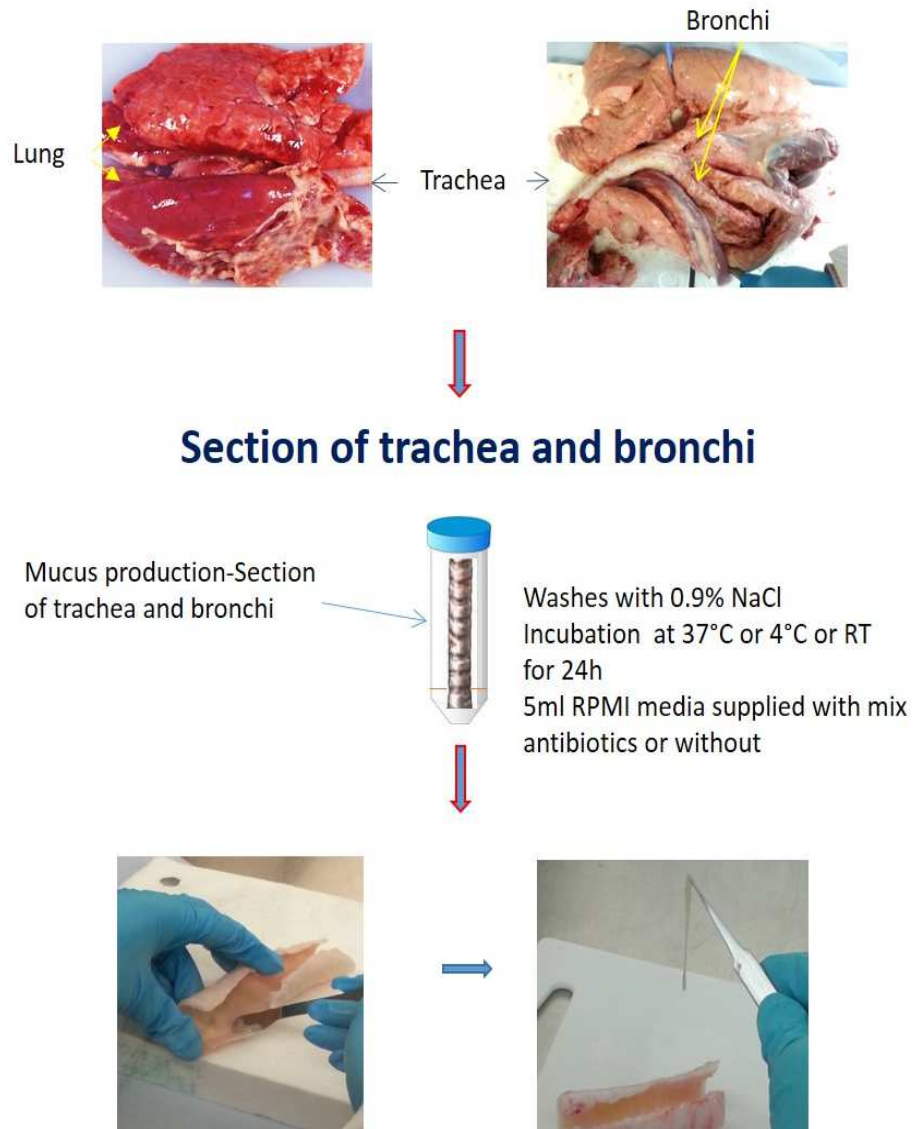


Figure 2.2 Porcine lung dissection. Trachea and bronchi were cut out from the porcine lung and washed with 0.9% NaCl before be keep at different temperature (RT, 4 and 37 C). Tissue fraction were cut and mucus was collected.

2.2.3 Alcian Blue Staining

Alcian blue (AB) is a dye containing a group of water soluble polyvalent basic dyes. The blue colour is due to the presence of copper in the molecule. When used in an aqueous solution Alcian blue can react with anionic groups (mucin, mucosubstances, and DNA). It is believed that AB forms salt linkages with the acid groups of acid mucopolysaccharides that act as the binding force.

To stain mucus with AB a piece of nitrocellulose membrane (7cm x 4cm) were washed in distilled water for 5 min. 2 μ l of mucus isolated from NHBE cell cultures (\pm IL-13), and fraction of mucus isolated from porcine lungs/ileum, were dropped onto the membrane and air-dried. As a control, 2 μ l of water were used. The membrane was stained by immersion in a solution of 1% Alcian blue (AB) stain dissolved in 3% acetic acid pH 2.5 for ~30 minutes. The membrane was rinsed three times with distilled water, soaked for 10 minutes in distilled water and left to air dry.

2.2.4 Determination percentage dry weight of sample harvest from porcine trachea and bronchi and purified gut porcine mucin

The dry weight of harvested mucus (W_{dry}) was determined by placing 4 sample aliquots of mucus (180-200 mg for respiratory mucus and porcine jejunal mucus) in pre-weighed eppendorfs tube (W_{ep}) and freeze-dried for 4 days. Every day the weight of each tube was recorded and the freeze -dry was stopped when the weights of the eppendorfs were stable (Table 2.1). The dry weight of the mucus is:

$$W_{dry} = W_{ep +dry} - W_{ep}$$

Where $W_{ep +dry}$ is the weight of the eppendorf with dry mucus after freeze-dry

The percentage of dry mucus (dry) was given by

$$\%dry = \frac{W_{dry}}{W_{wet}} \times 100 \quad \text{Where } W_{wet} \text{ (liquid weight mucus) is}$$

$$W_{wet} = W_{ep +wet} - W_{ep}$$

2.3 Solute transport assays using purified PGM

Transport assays were carried out for the establishment and validation of mucin gel model for studying the ability of probes and drug molecules to penetrate mucin gels.

2.3.1 Franz-cell chamber

The Franz cell system (Figure 2.3) consists of two chambers, the donor and receiver chamber separated by a membrane impermeable to mucus. The mucus and drug are added onto the membrane (or mucus layer) in the donor chamber and drug transport into the basal chamber determined by sampling the receiver chamber. The maximum capacity of the receptor chamber in this thesis was 5 ml and is kept under stirring throughout the experiment using a small magnetic stirrer bar.

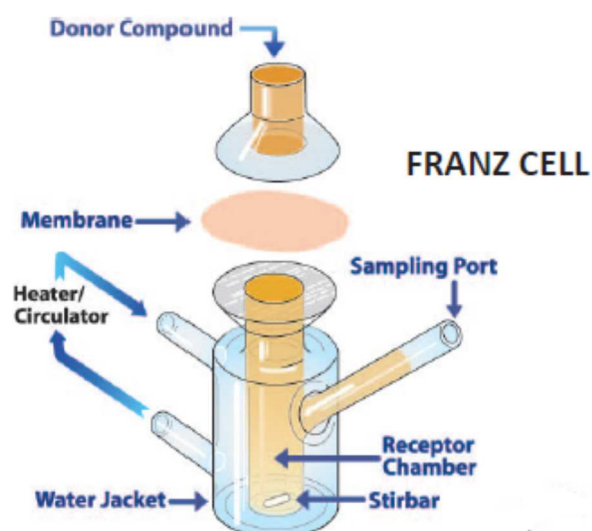


Figure 2.3 Franz-cell system

The donor and receptor chambers are separated by a membrane. The test product is applied to the membrane via the top chamber. The bottom chamber contains fluid from which samples are taken at regular intervals for analysis. *Taken from, pharma science and monitor, vol-1, Figure 1, Issue-2, 2010. Shah et al.*

2.3.2 High-performance liquid chromatography (HPLC)

HPLC is an analytical technique (Figure 2.4) used to separate and quantify one or more components in a mixture ⁽²⁾. All forms of chromatography work on the same principle. The mobile phase is forced through the stationary phase by high pressure pumps. Pressure may reach 60 MPa, or about 600 atmospheres. The separation of single component of a mixture depends on the equilibrium affinity between the *stationary phase* (solid or liquid) packed inside the column and a *mobile phase* (liquid or gas) that flows through it. Column dimensions are typically 30–250 mm length and 2.1–4.6 mm diameter. The particle size in the columns are made with sorbent particles of about 2–50 μm . The most used stationary phase is silica but some column may be packed with alumina. The silica spheres efficiency is controlled by the size of the; the smaller the particle size distribution, the more efficient and robust the packing material. Modern HPLC systems (such as Ultra High Performance Liquid Chromatography) have been improved to work at much higher pressures, up to 120 MPa, and are therefore able to use much smaller particle sizes in the columns ($<2 \mu\text{m}$) which gives a much greater surface area for interactions between the stationary phase and the analytes flowing through it leading to improved separation of all components of the mixture.

After the sample has been injected, the analyte first encounters a guard column which is responsible for removing contaminants from solvents or samples that would bind to and damage the expensive analytical column. The composition of the guard column packing should match that of the column to which it is connected, although particle size is usually larger. The time that any component takes to elute the column

and move to the detector is known as *retention time* and can be used to identify the different compound of a mixture. How fast each component of a mixture moves through a column depends from their relative affinity for the mobile phase and stationary phase; an analyte with stronger interaction with the stationary phase will take a longer time to move through the column compare to a molecule with weaker interaction with the stationary phase and stronger interaction with the mobile phase. The solvent emerging from the column and carried the separated components of the mixture pass in the detector. A wide range of detectors can be used and the most used one is a UV-Vis absorbance detector. The fluorescence detection offers greater sensitivity than a UV-VIS detector but in comparison to light absorbing compounds the number of naturally fluorescent compounds is smaller. Another detector type used in HPLC systems is mass spectrometer which offers very high sensitivity and selectivity and can be combined with UV-Vis detector (LCMS).

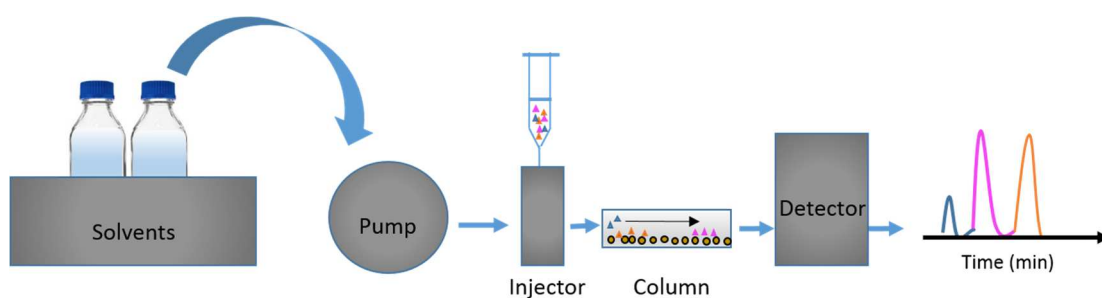


Figure 2.4 HPLC system. The pumps move the solvents and the sample injected through the column. The analyte with weaker interaction with the stationary phase will be eluted and detected first.

Depending on whether the stationary phase and mobile phase are polar or non-polar is possible to distinguish between Normal phase HPLC and Reverse phase HPLC.

Normal phase HPLC

The solvent is non-polar (hexane) and the column is filled with tiny silica particles, and uses a non-polar, non-aqueous mobile phase (e.g. chloroform).

Therefore, a polar analyte will have a stronger interaction to the polar silica than a non-polar one. The non-polar compound will have a shorter retention time as will move quickly through the column.

Reversed phase HPLC

It is the most used form of HPLC. The stationary phase is made of silica which is modified to make it non-polar by attaching hydrocarbon chains (8-18 carbon atoms) to its surface. The mobile phase used is polar with can be a mixture of water and less-polar but water miscible organic solvents e.g. alcohols. Polar compounds will stronger interact with the polar solvent and passed through the column rapidly. Non-polar compounds will therefore more retained to the hydrocarbon chain. Depending on whether the ratio of solvent used is changed during the elution, we can distinguish between two methods: isocratic system and gradient system.

An isocratic elution involves a single solvent or solvent mixture but the composition remains constant all the time. In this way the system and column are equilibrated throughout the elution. *A gradient elution* involves two or more solvent with different polarity (such as water and acetonitrile) are employed. The ratio of the solvents is varied in a programmed way after sample injection. Compared to the isocratic system separation efficiency is greatly enhanced in gradient elution.

2.3.3 Materials

Purified mucin powder from porcine stomach (type III) containing ~0.5-1.5% of bound sialic acid, partially purified powder, sodium fluorescein, fluorescein isothiocyanate-conjugated dextran probes (4, 10, 40, 70 kDa), amiloride hydrochloride hydrate and benzamil hydrochloride were purchased from Sigma Aldrich (Gillingham, UK). Cellulose Ester Dialysis membrane 100 kDa cut-off were purchased from Spectra/Por® Biotech, Corning® NBS™ 96 well plates were purchased from Fisher Scientific (Loughborough, UK). Glass screw thread vial, plastic vials target PP polyspring insert and Acetonitrile were purchased (Thermo Fisher Scientific).

2.3.4 Descriptions of samples preparations

FL-Na and FITC-dex preparation

A stock solutions of sodium fluorescein (FL-Na), and fluorescein isothiocyanate-dextran probes (FITC-dex) at different molecular weight (4, 10, 40, 70 kDa) were obtained dissolving the powder into phosphate buffer (PO₄) buffer 100mM Na₂HPO₄ and NaH₂PO₄ (NaPO₄) and 50mM NaCl with pH 6.8 (PBS pH 6.8) at a concentration of 10mg/ml. The stocks were stored at -20°C until needed. Franz cell donor solutions were obtained diluting the stock solution with the same PBS pH 6.8 to a final concentration of 200 µg/ml for FL-Na and FITC-dex 4 (FD4). A dose donor of 1mg/ml for FITC-dex 10, 40 and 70 (FD10, 40, 70) was needed to ensure that high molecular weight probes were detectable at each time point of the experiment.

Amiloride and Benzamil preparation

Stock solutions (10mg/ml) of Amiloride and Benzamil were made up using DMSO and diluted to 200 µg/ml (dose donor) using PBS pH 6.8.

Preparation of mucin gels with Porcine Gastric Mucin

PGM solutions (1, 3, & 5% w/v) were prepared using PGM dissolved PBS pH6.8. PGM solutions were rolled for 2-3 hours until mucin was completely dissolved then left overnight at 4°C to hydrate fully. PGM solutions were rolled for 1h at RT immediately before commencing Franz cell experiments. Vigorous agitation of the samples was avoided to avoid the introduction of bubbles in the mucin solution.

2.3.5 Analysis of solute transport across PGM solutions

Permeation studies using PGM solutions or buffer (PBS pH 6.8) were conducted using the Franz-cell diffusion system. The surface of the donor and receiver chambers was greased before adding a cellulose ester membrane (MWCO 100,000) which separated the two chambers. The donor (9mm diameter) and receiver chambers (5 ml) were fixed together using a clamp. Mucin solution 1, 3 & 5%v/w (189 µl to give 3 mm deep) were applied to the membrane via the donor chamber. The receptor chamber was filled with 5 ml of PBS pH 6.8 and kept at 37°C throughout the experiment by recirculating water bath (HAAKE SC100, Thermo Scientific). Continuous stirring (500rpm) was provided by a small magnetic bar in the receiver chamber. Dose donor (50 µl), 0.2mg/ml for FL-Na and FD4 and 1mg/ml FITC-dex 4, 10, 40 and 70 kDa, were placed gently on the top of PGM. At regular intervals (10, 20, 30, 60, 90, 120min) 200µl of sample was taken from the receptor chamber for

analysis and replace with 200µl fresh, pre-warmed buffer. Permeation assays were also performed using amiloride and benamil at a dose donor of 200µg/ml in a volume of 50µl. Experiments were set and carried out in same way as described for FL-Na and FITC-dex.

2.3.5.1 Quantification of FL-Na and FITC-dex probes in diffusion assay

The amounts of FL-Na and FITC-dex probes (4, 10, 40 & 70 kDa) in receiver chamber samples was quantified by comparing their fluorescence to their calibration solutions (Table 2.1). Samples were added to black 96 well plates (Corning #3686) and the fluorescence measured a FLUOstar OPTIMA microplate reader (BMG Labtech) with excitation and emission wavelengths of 492nm and 520nm, respectively

2.3.5.2 Quantification of amiloride and benamil in diffusion assay

Quantification of amiloride and benamil was performed on a Perkin Elmer fluorescence HPLC system equipped with a Perkin Elmer LC 240 fluorescence detector (UK) using Phenomenex column C18 (4.6 x 250 mm 5µm) using a Security Guard column C18 3x4mm (Phenomenex). The isocratic elution method was composed of 50% 10 mM phosphate buffer pH 4.2 and 50% acetonitrile (solvent A and B respectively) at a flow rate of 1 mL/min. Excitation and emission were set at 362 and 417 nm for amiloride and 366 and 412 nm for benamil. The range of the calibration curve and analytical method used are showed in the Table 2.1.

Table 2.1. Summary of calibration curve range and analytical method used to analyse probes and drug molecules used for the permeation assay.

<i>Probe</i>	<i>Calibration range (ng/mL)</i>	<i>Analytical method</i>
FL-Na	0.625-50	Plate reader
FD4	25-500	Plate reader
FD10	5-400	Plate reader
FD40	2.5-200	Plate reader
FD70	2.5-50	Plate reader
Drug molecules		
Amilorde	2.5-100	HPLC
Benzamil	2.5-100	HPLC

2.3.5.3 Apparent permeability coefficients

Apparent permeability coefficients (P_{app}) for mucin gels were calculated according to the following equation:

$$P_{app} = \frac{dQ}{dt} \times \frac{1}{AC_0}$$

Where $\frac{dQ}{dt}$ is the rate of appearance of probes in the receiver side (ng/s), A is the surface area of the filter (0.189 cm²), C_0 is the initial concentration of probe in the donor chamber (ng/ml).

2.4 Biochemical Analysis of PGM, *ex vivo* PLM and porcine jejunal mucin

Biochemical analysis of the harvested mucus from porcine trachea and bronchi and purified mucin from porcine gut were carried out to calculate the percentage of dry weight, determined the mucus pH, to quantify mucin and to determine the presence of DNA. Mucin and DNA determination were performed also for PGM.

Determination of mucin concentration

2-cyano-acetamide was used for the determination of mucin percentage of the fresh porcine mucus. The assay involved the liberation of O-glycosylated glycoprotein by β -elimination with alkali and the consequent derivation of the reducing end with 2-cyano-acetamide.

Determination of DNA concentration

The reaction of 3, 5-diaminobenzoic acid (DABA) with DNA was applied for the identification and measurement of DNA contamination in fresh porcine mucus using the same aliquots used for mucin determination. Acid hydrolysis of DNA in DABA leads to a formation of a fluorescent product which is used for DNA quantification.

2.4.1 Materials details

PGM (type III) containing ~0.5-1.5% of bound sialic acid, 2-cyanoacetamide (2-CNA), 3, 5-diaminobenzoic acid (DABA), calf thymus DNA, tris-(2-carboxyethyl) phosphine (TCEP) 0.5M, borate salt, borate-HCl were purchased from Sigma Aldrich (Gillingham, UK). HyClone™ 0.1 μ m sterile filtered water was purchased from life science.

2.4.2 Respiratory porcine mucus pH determination

The porcine mucus was diluted in sterile water 1:500 and 1:100 and pH was determined using a hydru300 pH meter Thermo Fisher Scientific (UK)

2.4.3 Determination of mucin concentration

A fluorometric mucin assay was carried out to determine the mucin concentration. Eight samples of PLM and porcine jejunal mucin (PJM) was used for mucin assay. Aliquots of fresh PLM and PJM were diluted as shown in Table 2.2 using dH₂O and rolled for 2h to mix. 1ml of each dilution was boiled for 1h in sealed tubes and samples were then spun at 5000 g per 5 min to remove insoluble material. The supernatant (100 µl) was added to 120 µl of alkaline 2-CNA (20% CNA 0.6 M in 150 mM NaOH). The mixture was heated at 100°C for 30 minutes then mixed with 1ml borate buffer 0.6 M, pH 8 and samples left to cool to RT. Calibration solutions of PGM spanning 10 to 1000 µg/ml were prepared as described above. Fluorescence intensity measurements were performed on a Hitachi Fluorescent FL4500 using 0.5 cm quartz cell and 2-CNA fluorescence was measured using excitation/emission at 336/383 nm respectively. Mucin determination was performed also for 1,3 and 5% PGM diluted as showed in Table 2.2.

2.4.4 Determination of DNA concentration

All eppendorfs tubes and tips used for the DNA assay were autoclaved twice to eliminate any DNA/DNase contamination. Standards, DAPA and samples were made up using sterile filtered water. Standards were obtained using calf thymus DNA in a range between 2 to 10 µg. The Table 2.2 shows all dilution used for PLM, PJM and

PGM. Each standard and sample dilution (50 μ l) were transferred into eppendorf tubes in a laminar flow hood, and left at 60° C overnight to dry the sample. The next day, 100 μ l of DAPA 100mg/ml were added to each tube and left at 60°C for 45 minutes. The fluorescence was measured in 0.5 cm quartz cell after addition of 1ml of HCl 1N in each tube and left to cool down. The spectrophotometer excitation and emission wavelengths set on the Hitachi Fluorescent FL4500 were 420 and 490 nm respectively.

Table 2.2. Summary of dilution used for Mucin and DNA assay for different mucus/mucin model: *ex-vivo* porcine respiratory mucus, PGM 1,3,5%, purified gut mucin.

<i>ex-vivo porcine respiratory mucus</i>	<i>Purified mucin from porcine gut</i>	<i>PGM 1, 3, 5%</i>
1:50	1:5	1:2
1:100	1:10	1:5
1:200	1:20	1:10
1:400	1:50	1:20
1:800	1:100	1:50

2.4.5 Investigation of the amiloride and benzamil interaction with mucin

The investigation of the Amiloride and Benzamil interaction with mucin was investigated by fluorescence and UV–Vis spectroscopy.

2.4.6 Fluorescence spectroscopy

Fluorescent spectroscopy analyses the emission of fluorescence radiation by an analyte. Molecules have various electronic energy levels. By absorbing a beam of light they can pass from a lower to a higher energy level. The molecule's electrons are excited by absorbing a photon from its low energy state to one of the various vibrational states. The excited state lasts about 10^{-5} seconds before the molecule

collides, with a consequence loss of vibrational energy and emission of light. Each fluorescent molecule has a characteristic maximum wavelength of absorption and emission and the difference between positions of the maximum wavelengths of the absorption and emission spectra is called Stokes shift. The ratio of photons absorbed to photons emitted through fluorescence is called quantum yield. Quantum yield may be affected by environment factors (viscosity, pH, solvent) and depends on structure characteristic of the fluorophore. Higher fluorescence is given from rigid, planar molecules due to energy dissipation after absorption of photons ⁽³⁾. An intensity change of fluorescence can be observed when the fluorophore is restricted in a binding site with a consequent decrement of fluorescence intensity or increment when the quantum yield is higher than free form.

2.4.7 Ultraviolet-Visible Spectrophotometer (UV-VIS)

In analytical chemistry UV/Visible spectroscopy is used for the quantitative determination of matter. The spectrophotometer operates by passing a beam of light (stream of photons) through a sample. The analyte will absorb the photon and the instrument will measure the intensity of the light reaching a detector. The Beer-Lambert law (Eq. 1) is the base for UV and visible quantitative analysis ⁽²⁾. The Beer-Lambert law states that the absorbance of a solution is directly proportional to the molecules concentration in the solution (C), to the molar absorptivity (with units of $L \text{ mol}^{-1} \text{ cm}^{-1}$), also known as the extinction coefficient (ϵ), and to the path length (l).

$$\text{Eq. 1} \quad A = \epsilon \cdot c \cdot l$$

To simplify the calculation of absorbance and molar absorptivity a path length of 1 cm is usually used. The proportion of the light absorbed will depend on how many

molecules it interacts with and a calibration curve can be used to accurately know how quickly absorbance changes with concentration.

2.4.8 Materials

Mucin from porcine stomach, type III, amiloride and benzamil were purchased from Sigma Aldrich (Gillingham, UK).

2.4.9 Sample preparation

Mucin from porcine stomach, type III

As the molecular weight of the commercial mucin is not available the molecular weight of mucin was considered to be 1MDa. Mucin solution at 10 μ M was prepared by dissolving 10 mg lyophilized powder in 1 ml of PBS pH 6.8 and left on the roller overnight. The day after the mucin was spun at 5000 rpm for 5 minutes at room temperature and diluted as appropriate with phosphate buffer.

Amiloride and Benzamil preparation

Stock solutions at a concentration of 10 mM of both model drug were diluted with PBS pH 6.8 to have stock solution to be used for the fluorescent and UV approach.

Stock solution for fluorescent approach; 0.1 mM and of 1mM

Stock solution for UV approach; 100 μ M and 2mM.

2.4.10 Fluorescence spectroscopy

A 2.5 mL solution containing 1 μ M mucin was titrated by successive additions of 0.4 μ M of amiloride or benzamil (adding 10 μ l of 0.1 mM solution) over a range of 0 – 3.2

μM . The mucin titration was continued by successive additions of $4 \mu\text{M}$ (adding $10 \mu\text{l}$ of 1mM solution) until the final concentration of drug molecule in the mucin solution was $15.2 \mu\text{M}$. Fluorescence spectra using the same concentration of drug was also performed in PO_4 buffer pH 6.8 without mucin. Fluorescence spectra were recorded on a Hitachi Fluorescence FL-4500 using 1cm Quartz cuvette at room temperature. Amiloride was detected using excitation 362 nm and Emission 417 nm . For benzamil the excitation and emission used where 366 and 415 nm respectively.

2.4.10.1 Effect of solvent polarity on amiloride and benzamil fluorescence

The fluorescence emission of 100 nM solutions of amiloride or benzamil where mixed with $0, 1, 5, 25, 50, 75$ or 100% ethanol and fluorescence spectra recorded as described in section 2.4.10.

2.4.11 UV spectroscopic approach

A 1 ml solution containing $0.5 \mu\text{M}$ mucin was titrated by successive additions of $5 \mu\text{l}$ of $100 \mu\text{M}$ amiloride/benzamil solution. Drug concentration was then increased by addition of $5, 10$ and $20 \mu\text{M}$ (adding $2.5, 5$ and $10 \mu\text{l}$ of 2mM stock) until the final concentration of drug molecule in the mucin solution was $130 \mu\text{M}$. The UV–Vis absorption spectra of the mucin solution with concentration of drug between 0 and $130 \mu\text{M}$ was measured with an Agilent technologies Cary 60 spectrophotometer in the range of $200\text{--}450 \text{ nm}$ at room temperature. The same UV–Vis absorption spectra was carried out in a pure drug solution using the same range of drug concentration used for the mucin titration.

2.5 Development of ultrafiltration binding assay

This work was mainly focused on the development of an analytical method that allows us to understand whether ENaC blockers interact with mucin. This assay has then extended to study drug-DNA interaction as well as drug-alginate interaction.

2.5.1 96-well ultrafiltration assay

96-well ultrafiltration plate (Figure 2.5) and assembly, for the determination of ligand-protein binding, includes the MultiScreen® filter assembly with Ultracel-PPB membrane, which is specifically optimized for in-vitro plasma protein binding assays, or a MultiScreen filter plate with Ultracel-10 membrane for the concentration and purification of biological solutions. The donor solution is added onto the membrane. The system operates by centrifugation for the separation of unbound from protein-bound compound and includes a receiver plate where the free ligand is collected.

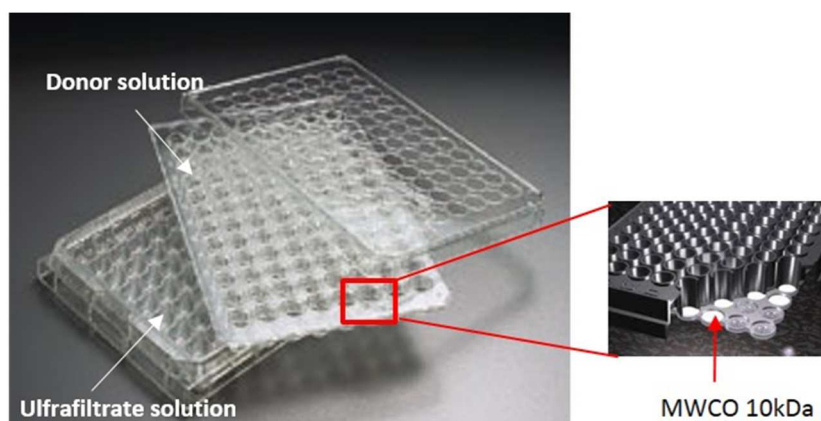


Figure 2.5 MultiScreen plate. Donor solution is added onto the membrane via the up plate. Ultrafiltration solution is taken from the bottom plate wells.

2.5.2 Materials

Amiloride, benzamil, rhodamine B, sodium alginate, DNA from fish sperm, DNase I, FL-Na and FD4 were purchased from Sigma Aldrich (Gillingham, UK). Analogues were

donated from Novartis (Basel, CH). Glass screw Thread Vial, Plastic vials target PP polyspring insert and acetonitrile were purchased from Thermo Fisher Scientific (UK), guard column C18 4x3 mm was purchase from Phenomenex (UK), MultiScreen Ultracel-10 Filter Plate 10 kDa were from Millipore (UK).

2.5.3 Sample preparation

PGM and Rhodamine B preparation

For the binding assay a concentration of 2 μ M was made up dissolving the powder into PBS pH 6.8.

Rhodamine B was dissolved in PBS pH 6.8 as appropriated and used as internal standard for FL-Na and FD4.

Stock solution and internal standard preparation for ENaC blockers

All model drugs (Figure 2.6) were dissolved in DMSO at a concentration of 20mM and stored at -20°C. When needed stock solutions were diluted, as appropriate in PBS pH 6.8. Stock solutions of internal standard were instead dissolved in DMSO to a concentration of 10mg/ml. The combination of analyte and internal standard was chosen considering their resolvability on the HPLC column (Table 2.3) and compound availability. Concentration of the internal standard was dependent of the analyte concentration into the mixture drug-mucin (or buffer solution for controls) (Table 2.4). Due to the low aqueous solubility of few compounds (amiloride, NVP-QBE170 and GD-40-QQ33) a first dilution (1 out 4) of all drug molecule was made using NaPO₄ buffer at pH 5 instead. The pH of dose donor was then verified using a hydru300 pH meter Thermo Fisher Scientific (UK).

Figure 2.6 Structure of Amiloride and its Analogues used in this project.

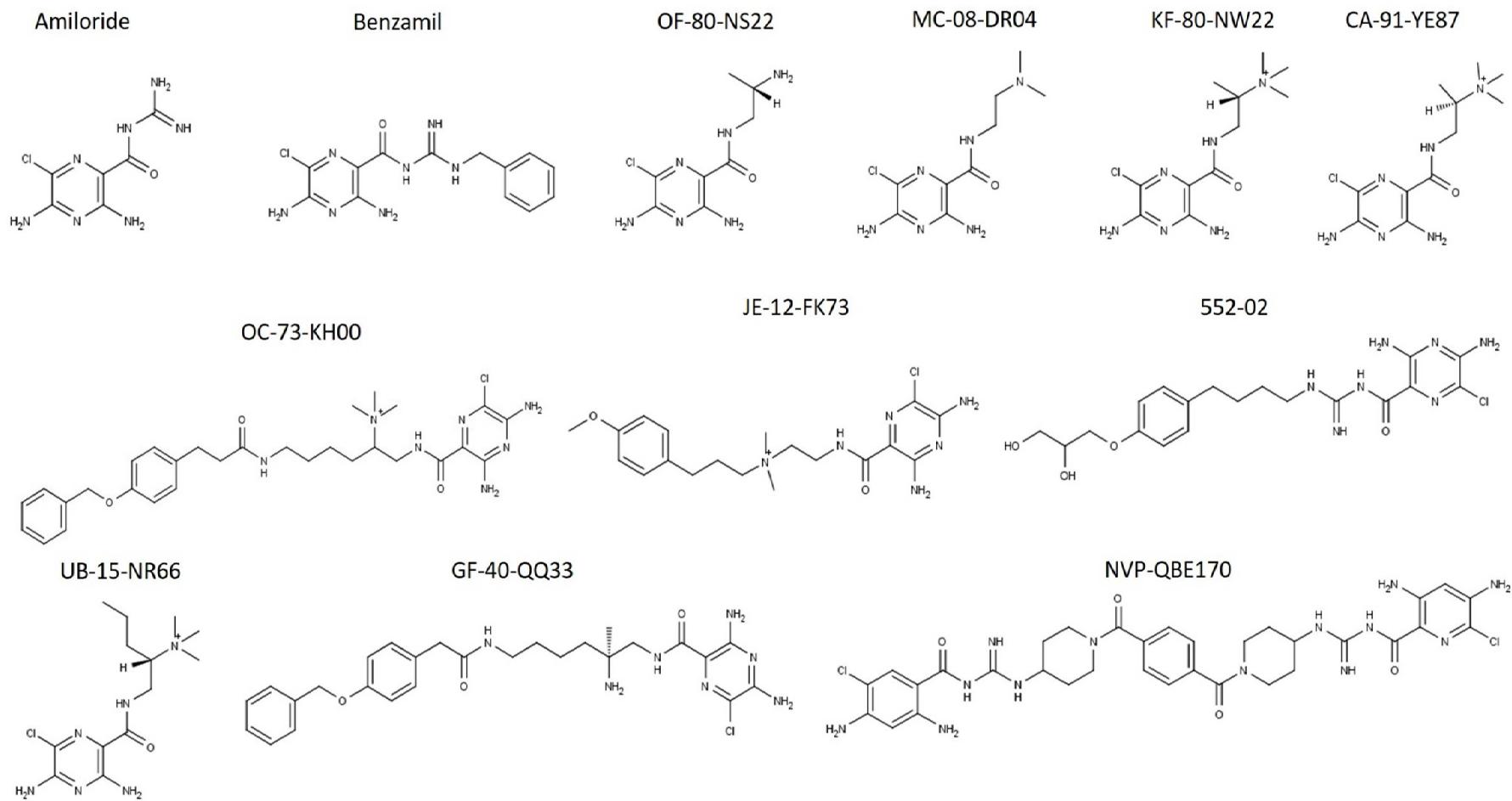


Table 2.3. Summary of Amiloride and analogues calibration range, EM/EX, Analytical method, LOD/LOQ, analyte retention time (RT) and internal standard used for the development of the multiscreen binding assay.

Analyte	Calibration range (nmol/L)	Analytical method	Excitation/Emission (nm)*	R²	LOD/LOQ (nmol/L)	Analyte RT (min)	Internal Standard
Amilorde	12.5-500	FL-HPLC	362/417	0.9996	0.324/1.81	2.88	Benzamil
Benzamil	25-600	FL-HPLC	366/415	0.9998	0.510/1.70	3.92	Amiloride
OF-80-NS22	25-500	FL-HPLC	360/416	0.9993	0.662/2.20	2.76	JE-12-FK73
MC-08-DR04	25-500	FL-HPLC	360/416	0.9996	0.543/1.81	2.93	JE-12-FK73
NVP-QBE170	50-1000	FL-HPLC	362/415	0.9998	0.275/0.92	2.33	JE-12-FK73
552-02	12.5-400	FL-HPLC	365/414	0.9997	0.478/1.59	3.15	JE-12-FK73
GF-40-QQ33	50-500	FL-HPLC	362/414	0.9984	0.265/0.88	4.87	Amilorde
UB-15-NR66	10-200	FL-HPLC	365/410	0.9995	0.101/0.31	3.4	JE-12-FK73
JE-12-FK73	10-250	FL-HPLC	360/415	0.9999	0.106/0.35	4.1	Amilorde
CA-91-YE87	12.5-400	FL-HPLC	364/416	0.9997	0.288/0.96	2.8	JE-12-FK73
KF-80-NW22	12.5-500	FL-HPLC	364/416	0.9998	0.354/1.13	2.8	JE-12-FK73
OC-73-HK00	100-1000	FL-HPLC	363/415	0.9978	2.292/7.65	4.65	Amilorde

* in 50% PO4 pH4.2 and ACN

Table 2.4. Concentration of drug molecules (analyte) used to study the interaction with mucin (1 μ M) and concentration of internal standard used for each analyte concentration.

<i>Analyte concentration</i> (μ M)	<i>Internal standard concentration</i> (mg/ml)
1	0.020
5	0.100
10	0.100
20	0.200
50	0.200
100	0.500
150	0.500
200	1.000

2.5.4 Sample preparation for ultrafiltration assay

Mucin solution (10×10^{-6} M) was prepared by dissolving 20 mg lyophilized PGM powder in 10 ml of PBS pH 6.8 and left on the roller overnight. Mucin solution (1 ml) was mixed with 1 mL of double-strength analyte solution to obtain different molar ratios; 1:1, 5:1, 10:1, 20:1, 50:1, 100:1, 200:1. Non-specific binding controls were performed by mixing 1ml of PBS buffer with 1ml of double-strength analyte solution.

Internal standard control (10 μ l), at a known concentration, were added into each well of the receiver plate to allow, after filtration, the determination of the exact filtered volume ($V_{\text{ultrafiltrate}}$). The mixture drug-mucin mixture (400 μ L) was added onto the membrane (10 kDa cut-off) of the donor plate. The plate was left to equilibrate at room temperature for 1 h and then centrifuged (Beckman centrifuge) at 2000 g for 1,5 h at 19°C. Following centrifugation, the filtrate was removed from the receiver plate and internal standard (10 μ l) was added into each donor well to be able to determine the exact retentate Volume ($V_{\text{retentate}}$). A small amount of the donor solution was processed for measurement of initial compound concentration (D_{initial}).

2.5.5 Analyses of interaction between 552-02 and benzamil with reduced mucin

Ultrafiltration binding assay was also carried out after disulphide reduction of mucin with 50 mM of Tris 2-Carboxyethyl Phosphine (TCEP) for both 552-02 and benzamil at 20 μ M.

2.5.6 Mucin precipitation

For the determination of the drug retentate concentration ($D_{\text{retentate}}$) the disruption of drug-mucin interaction was achieved by taking 50 μ l of donor solution and diluting it 1:5 with cold acetonitrile (-20°C) and spun at 10000 rpm for 5 min. Pre-cleared sample were analysed with HPLC.

2.5.7 Solute analysis

Analytes were resolved as described in section 2.3.5.2. Excitation and emission were set at 314 and 416 nm respectively for all compounds. The range of calibration curve, LOD, LOQ, Em/Ex for each molecule is show in the Table 2.3.

For FL-Na and FD4 the control used was Rhodamine B and samples were quantified by microplate reader Polar start Optima (BMG LabTech) at an excitation and emission of 495 and 510 nm For FL-Na. For rhodamine B the excitation and emission were set at 560 and 590 nm.

2.5.8 Determination of Mass Balance

The mass balance was determined according to:

$$\text{Eq.2 Mass Balance} = \left(\frac{\text{Mass}_{\text{ultrafiltrate}} + \text{Mass}_{\text{retentate}}}{\text{Mass}_{\text{initial}}} \right) \times 100\%$$

Where $\text{Mass}_{\text{ultrafiltrate}}$ is the concentration of the drug in the bottom plate after centrifugation multiplied by the ultrafiltered volume. $\text{Mass}_{\text{initial}}$ is the concentration of the dose donor added into the top plate and multiplied by the volume added. $\text{Mass}_{\text{retentate}}$ is the concentration of drug retained on the top plate after centrifugation multiplied by the unfiltered volume:

$$\text{Mass Balance} = \left(\frac{D_{\text{ultrafiltrate}} \times V_{\text{ultrafiltrate}} + D_{\text{retentate}} \times V_{\text{retentate}}}{D_{\text{initial}} \times V_{\text{initial}}} \right) \times 100\%$$

Where;

D= Drug concentration

V= Volume

$$V_{\text{retentate}} = V_{\text{initial}} - V_{\text{ultrafiltrate}}$$

The $\text{volume}_{\text{retentate}}$ and the $\text{volume}_{\text{ultrafiltrate}}$ were obtained considering the initial and final concentration of the internal standard added at the top and bottom plate using;

$$C_1 V_1 = C_2 V_2$$

C_1 = original concentration of internal standard

C_2 = final concentration of the solution

V_1 = volume added to top and bottomwell plate

V_2 = final volume

2.5.9 Determination of % binding

The percentage of model drug interacting with mucin was determined according to (4),

$$\text{Eq.3 \% Binding} = \left(1 - \frac{[Drug_{ultrafiltrate}]}{[Drug_{total}]}\right) \times 100$$

2.5.10 Determination of non-specific binding (%NSB)

The determination of the %NSB was determined using the same formula above but considering the mucin-free control of each analyte.

2.5.11 Isothermal binding curve

The isothermal binding curve for each compound was obtained plotting the free concentration ($D_{ultrafiltrate}$) of compound against the molar ratio of bound drug to mucin (mol/mol) using Graph Pad Prism 6. The free concentration of drug is the filtered drug from the mixture (drug-mucin). The molar ratio of bound drug to mucin (Eq.4) was calculated by difference between the free concentrations of drug and the molar ratio of bound drug to mucin is;

$$\text{Eq.4 Molar ratio of bound drug to mucin} \left(\frac{\text{mol}}{\text{mol}}\right) = \frac{\text{moles bound drug}}{\text{moles mucin in } V_{initial}}$$

The moles of bound compound was calculated as following;

$$\text{Molar ratio of bound drug to mucin (mol/mol)} = \frac{(D_{control\ ultrafiltrate} - D_{mixture\ ultrafiltrate}) \times V_{initial}}{\text{Mucin moles in } V_{initial}}$$

Where;

$D_{\text{control ultrafiltrate}}$ is the concentration of drug in the bottom wells plate of the control (buffer solution). $D_{\text{mixture ultrafiltrate}}$ is the concentration of drug in the bottom wells plate considering the mixture drug-mucin.

2.5.12 Ultrafiltration binding assay using DNA and Alginate

The ultrafiltration binding assay developed to study the mucin-drug interaction was also applied to study the interaction of drugs molecules with DNA and alginate. The experiment was performed as described in section 2.5.4 however only a concentration of 20 μM for all compound and FL-Na and FD4 was used. Based of viscosity the molecular weight of DNA and alginate are expected to have a molecular weight range of 12-40 kDa and 50-120 kDa respectively (Sigma-Aldrich, personal communication). An arbitrary value of 30kDa for sodium alginate and 100 kDa for DNA was chosen for this project.

2.6 Calu-3 cell culture

The Calu-3 cell line is derived from human bronchial submucosal glands ⁽⁵⁾ and is a well-differentiated under submerged culture conditions ⁽⁶⁾ and well characterized cell line. Although the mucus production is limited compared the *in vivo* phenotype, Calu-3 cells form a restrictive monolayers reflecting *in vivo* physiology ^(7, 8) and are finding increasing application in the pharmaceutical industry. For this reason, we used Calu-3 cell to study their permeation to amiloride and analogues.

2.6.1 Calu-3 cell culture reagents and media preparation

Calu-3 were purchased from ATCC. DMEM/F12 and DMEM/F12 phenol red-free (Dulbecco's Modified Eagle Medium: Nutrient Mixture F-12) and non-essential amino acids were purchased from Thermo-Fisher Scientific. Penicillin/streptomycin (10,000 U/ml and 10,000 µg/ml), 0.25% trypsin-EDTA were purchased from Invitrogen (Paisley, UK). Clear Transwell inserts (#3470) were from Corning. Amiloride and benzamil were purchased from Sigma Aldrich (Gillingham, UK) Analogues were donated from Novartis (Basel, CH). Glass screw Thread Vial, Plastic vials target PP polyspring insert and Acetonitrile were purchased (Thermo Fisher Scientific).

2.6.2 Calu-3 cell culture

The Calu-3 human bronchial epithelial cell line was grown in 75cm² cell culture flasks in a humidified 5% CO₂/95% atmospheric air incubator at 37 °C using Dulbecco's Modified Eagle Medium: Nutrient Mixture F-12 (DMEM-F12) media supplemented with 10% foetal bovine serum, 1 % v/v non-essential amino acid solution (100X), and 2 % v/v penicillin-streptomycin (full media). Medium was refreshed three times per

week until cells were ~80% confluent. Cells were then seeded onto the apical chamber of Transwell inserts (diameter 6.5 mm and a pore size of 0.4 μ m) at a density of 10×10^4 cells/insert using 100 μ l of full media. 500 μ l medium were added in the basolateral chamber. The day after the media was changed in both apical and bottom side and washed with warm PBS to remove debris. The submerged monolayer was then fed three time per week. Once cells were 100% confluent TER was tested as described in the section 2.1.5 immediately before monolayer medium was changed.

2.6.3 Sample preparation for transportation assay through Calu-3

Dose donor preparation

Due to the low solubility of amiloride, NVP-QBE170 and GD-40-QQ33 a first dilution (1:1) of all stock solutions (20 mM in DMSO) was made in DMSO. The secondary stock solution (10mM) was then diluted as appropriate with DMEM/F12 phenol free to make up a final concentration of 100 μ M (1% DMSO) which was used as donor solution for the permeation assay.

2.6.4 Transportation assay

The permeation assay through Calu-3 cells was performed when the TER was constant. All experiments were performed in quadruplicate and inserts used for each compound were carefully chosen to ensure the mean TER was comparable between groups. Before starting the assay, cells were washed twice with 100 μ l of warm PBS then replaced with 500 μ l of DMEM/F12 in the bottom side of the Transwell, and 100 μ l onto the apical side before 1h equilibration. The experiment was started by replacing the media from the top side with 100 μ l of donor dose (pre-warmed) and

200 μ l of samples were taken from the bottom side at: 0, 15, 30, 45, 60, 90, 120, 180, 240 minutes. Samples were replaced with pre-warmed DMEM/F12 phenol free.

2.6.5 Permeation assay through Calu-3 using 552-02 in mucin solution

Permeation assay were performed also dissolving 20 μ M 552-02 in 0.5 μ M purified mucin. The experiment was carried out in triplicates in the way as described in the section 2.6.4.

2.6.6 HPLC analysis

The range of calibration curve used is show in the Table 2.3 (section 2.5.3). Standards and samples were prepared using DMEM/F12 phenol free. The separation was performed on a Phenomenex column C18 (4.6 x 250mm 5 μ m) equipped with fluorescence detector (excitation 314 nm Emission 416nm) injecting 70 μ l and. Mobile phase used was a gradient of NaPO₄ buffer 10mM pH 4.2 (solvent A) and acetonitrile (solvent B) at a flow rate of 1 mL/min. The gradient method used for the separation is shown in Table 2.5.

Table 2.5. Representation of gradient method used to analyse Amiloride and Analogues after transport assay through Calu-3.

<i>Step</i>	<i>Solvent A (%)</i>	<i>Solvent B (%)</i>	<i>min</i>
1	95	5	5
2	20	80	10
3	95	5	5
4	95	5	5

2.6.7 P_{app} calculation

The apparent permeability coefficient for each compound analysed through Calu-3 and controls (without cells) was calculated as described in the section 2.3.5.3 using a surface area of 0.3318 cm².

2.7 Purification of porcine jejunal mucin

2.7.1 Materials

Porcine jejunum was sourced from the local abattoir, complete mini Tablets protease inhibitor cocktail were purchased from Roche, CsCl was purchased from Sigma Aldrich (Gillingham, UK), quick seal centrifuge tube Beckman Coulter (High Wycombe, UK), electric mix-paddle purchased from Qualtek Electronics Corporation (Fort Worth, UK), N-ethyl maleimide and Guanidine purchased from Thermo Fisher Scientific (UK), EDTA was purchased from Sigma Aldrich (Gillingham, UK), Cellulose Ester Dialysis membrane (Spectra/Por Biotech).

2.7.2 PJM collection

Porcine jejunum (Figure 2.7) was obtained from the local abattoir immediately after the sacrifice of the animal and placed in a container with ice. It was washed gently (to avoid mucus loss) with protease inhibitor buffer pH 6.5 (see Table 2.6) several times until the liquid passing through the intestine was clear. The gut was cut into sections of 20-25 cm long and open out by cutting along the line of the mesentery. It was store on tray on ice till mucus was scraped out.

The mucus was scraped out using crooked finger moved along the intestine segments and it was placed into the rehydration buffer (10ml/g mucus).



Figure 2.7. Porcine Small intestine used for mucin extraction.

2.7.3 Mucus preparation

The mixture mucus-rehydration buffer was stirred with an electric paddle at 200 rpm. After 48 h the mixture was removed from the paddle and spun for 30 minutes at 3500 rpm and temperature set at 22 °C in order to remove any insoluble material. The density of the mixture was then increased up to 1.4 g/mL with addition of CsCl mixing for 30 minutes at 200 rpm with a magnetic stirrer. The density was checked weighing 1ml of mixture and adjusted adding CsCl, to increase, or distilled water to decrease the density.

Table 2.6. Buffers needed for gut mucin preparation

<i>Rinsing buffer pH 6.5</i>	<i>Protease inhibitor buffer</i>	<i>Rehydration buffer</i>
10mM Sodium Phosphate	20 ml Rinsing buffer	300ml Rinsing buffer
	1 Protease inhibitor tablet	4M guanadinium HCl
		5mM EDTA
		5mM N-ethyl maleimide*

* Unstable in solution, necessary to add when needed

Sample preparation for 1st centrifugation step

The mixture was transferred into quick seal centrifuge tube using a syringe. Tubes were sealed using a soldering iron which was used to slightly melt the neck of the

plastic tubes. The neck of the tube was dabbed with vegetable oil and a metallic plug was put onto the neck of the tubes.

By gently pressing the soldering iron on the metallic plug the tube was sealed (Figure 2.8). The samples were then spun at 50000 rpm, 10 °C for 62 h using a Beckman Coulter centrifuge (LE80 Ultracentrifuge, Beckman, Ireland) and with fixed angle rotor type 70Ti (Beckman, Ireland).

The neck of the tubes was then cut with a scalpel and the mixture collected in 1ml aliquot. The density was recorded for each aliquot and 2µl were used for Alcian blue staining (for more details see 2.2.3).

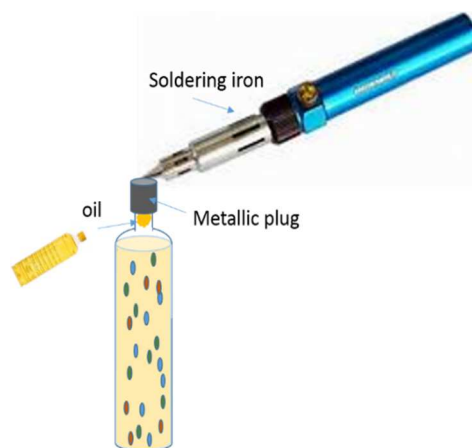


Figure 2.8 Sealing of centrifuge tube. A soldering iron is pressed on a metallic plug to seal the tubes.

Sample preparation for 2nd centrifugation step

For the second centrifugation step was necessary to decrease the concentration of guanidine from 4 to 0.5M. For this reason, aliquot that gave a blue staining were mixed together and dialyzed using membrane (cut-off 10kDa) against rinsing buffer and 0.5 M guanidine (changed 3 times per day) for 2 days. The membrane was warmed to 60 °C and left to cool three times to avoid bacterial contamination. The density was changed to 1.4 g/mL using CsCl and then centrifuged as described in the

1st centrifugation. Following ultracentrifugation the fractions were subjected to density determination, Alcian blue staining and absorbance measurement at 260 and 280 nm using a Nanodrop ND-1000 spectrophotometer (Labtech, UK) for DNA detection. Fractions that gave a blue staining and no absorbance at 260 and 280 nm were collected. Half of the volume was kept in fridge increasing GdnCl to 2 M and the other half was kept in liquid nitrogen until needed and dialysed for 24/48 h against dH₂O before further studies.

2.8 Application of STD-NMR for ligand characterization

One of the most powerful NMR techniques, the STD NMR, was applied to understand whether there is any interaction between mucin and drug molecules.

2.8.1 Nuclear magnetic resonance (NMR)

Nuclear magnetic resonance spectroscopy (NMR) is a useful analytical chemistry technique used in quality and to characterise the chemical, physical and biological properties of the matter. In order to achieve the desired results several kind of NMR techniques are available such as one and two-dimensional, solid state NMR, relaxometry NMR ⁽⁹⁾ and Saturation-Transfer Difference NMR for the study of transient receptor-ligand interaction in solution ⁽¹⁰⁾

2.8.1.1 Theoretical background

NMR can be described as a physical phenomenon that occurs when atomic nuclei aligned with an applied field and are induced to absorb energy and change their spin orientation with respect to the applied field. Whether the nuclei experience this phenomenon depends on their spin properties. Spin, like electrical charge or mass, is a fundamental property of particles. It is also called intrinsic angular momentum. The spin angular momentum (I) gives a magnetic moment on a nucleus and can be zero or comes in multiple of $\frac{1}{2}$. Yet, it can be positive or negative ⁽¹¹⁾. Only the molecules with non-zero spin are NMR active. In the absence of a magnetic field (B_0) all spin states are degenerate as orientations of the spin are random and have equal energy. When a magnetic field is applied externally, their energies are affected and nuclei

align themselves either with or against the field of the external magnet (Figure 2.9) passing from the ground state to excited state.

The difference between the ground state and excited state depends on the external magnetic field strength (ΔE). When the spin returns to its ground state level, the absorbed radiofrequency is emitted at the same frequency level. The emitted energy is directly proportional to the strength of the applied field.

$$\nu = \frac{\gamma B_0}{2\pi}$$

Where B_0 is the external magnetic field experienced and γ is the gyromagnetic ratio (the ratio between the nuclear magnetic moment and angular moment).

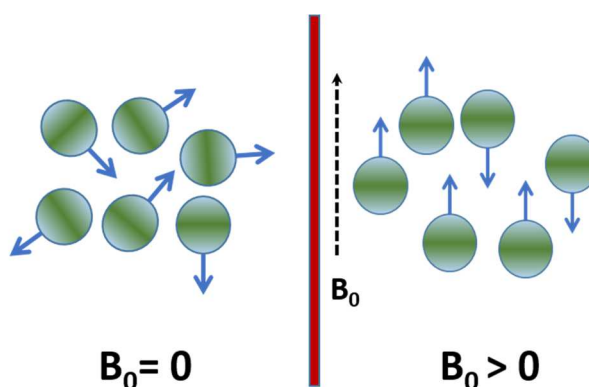


Figure 2.9. A representations of nucleus orientation. In the absence of a magnetic field, these are randomly oriented but when a field is applied they line up parallel to the applied field, either spin aligned or spin opposed.

The NMR spectrum is a plot of the intensity of NMR signals versus magnetic field (frequency). The spectrum of a molecule is diagnostic by its chemical shift. A chemical shift is defined as the difference in parts per million (ppm) between the resonance frequency of the observed proton and tetramethylsilane hydrogens (most common reference compound in NMR) which is set at δ zero ppm.

2.8.2 Saturation Transfer Difference -NMR

The STD-NMR technique is one of the most powerful NMR techniques to detect and characterize weak ligand binding ($K_d \sim \text{mM} - \mu\text{M}$), between a large molecule (receptor $>20 \text{ kDa}$) and a smaller molecule (ligand) ⁽¹²⁾ ⁽¹³⁾. It is an economical method as it does not require expensive isotope or radioisotope labelling. Moreover, for the experiment a very small concentration of receptor is required (nM-pM), although an excess of 20–1,000 times excess ligand is necessary.

The setup of experiment involves the recording of two NMR spectra. Firstly, a reference spectrum is registered under conditions of thermal equilibrium. In the 1D ^1H NMR the irradiation frequency is set at a value that is far from any ligand or protein signal (*off resonance*) with a signal intensity I_0 . In the second ^1H NMR, the irradiation condition is chosen to specifically irradiate and saturate (with cascade of Gaussian-shaped pulses) only protons of the protein (*on resonance*) (see Figure 2.10) giving a signal intensity I_{sat} . For example, it is possible to choose to irradiate the aliphatic region (from 0 to 1 ppm) or aromatic region (around 7ppm). The irradiation is applied for a period of time called *saturation time* that can be varied in the range of seconds. The intermolecular transfer of magnetization from the receptor to the bound ligand is the base of the STD-NMR. If the ligand is close in space to the site of binding, the magnetization from the receptor protons will be transferred, via spin diffusion through inter-molecular nuclear Overhauser effect (NOEs), to the ligand protons. As a result of the binding, the signal intensity of the ligand will significantly reduced. In

particular, only the chemical group involved into the transient interaction, receptor-ligand, will reduce. By subtracting both experiment (*on resonance* and *off resonance*) a positive difference signals and the STD spectrum is obtained which allows the identification and characterization of the binding ligand. The intensity of the signal of the non-binding molecules for the two spectrum will be the same and in the difference spectrum no signal will appear.

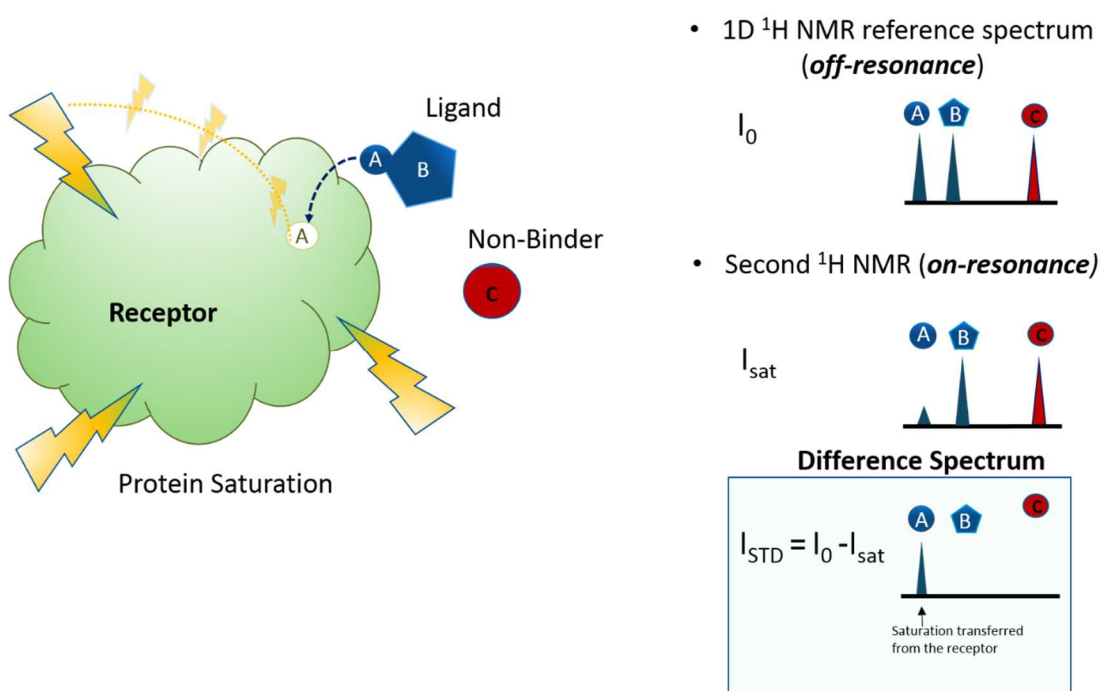


Figure 2.10 Schematic representation of STD-NMR. 1D ^1H NMR radiofrequency does not affect the molecules signal. During the Second ^1H NMR saturation is transferred from the receptor to the ligand with a reduction of the signal of the chemical group involved into the interaction. STD spectra is the difference between first ^1H NMR and second ^1H NMR.

2.8.3 Material

Tobramycin, mucin from porcine stomach, type III, Wilmad[®] NMR tube 5mm and 3.3 mm were purchased from Sigma Aldrich (Gillingham, UK), OF-80-NS22 and 552-02 were donated by Novartis (Basel, Switzerland), Salbutamol sulfate 99% was purchased from Alfa Aesar (Heysham,UK). Deuterium oxide was purchased from

Cambridge Isotope Laboratories Inc (Massachusetts, USA), and Dimethyl sulfoxide-d₆ (99.5% D) was purchased from VWR (Leuven, Belgium), vivaspin 6 10 kDa purchased from Thermo Fisher Scientific (UK) and Amicon Ultra-0.5 Centrifugal Filter 10kDa were purchased from Millipore (UK).

2.8.4 Application of STD-NMR to Salbutamol and Tobramycin using fresh PLM and PGM

Fresh mucus harvested from porcine lung and bronchi sections (see section 2.2.2) and PGM, were used for STD-NMR experiments to study its interaction with salbutamol and tobramycin.

Sample preparation for STD-NMR

The fresh porcine respiratory mucus was diluted 1 out 2 with D₂O. The diluted fresh mucus was then mixed with 10mg/ml Tobramycin to have a final concentration of 5mg/ml. In studies using PGM, tobramycin and salbutamol (stock solutions in D₂O) were added to 1.5mg/ml PGM to have a final drug concentration of 5mg/ml. Samples were left on the roller for 4/6 h before analysis by STD-NMR. Experiments were performed at 310 K on a Bruker digital Avance 800 MHz spectrometer using Wilmad[®] NMR tube 5mm diameter. The on-resonance and off resonance frequency was set at -6 and 40 ppm respectively for both compounds performed with 16 scans and 2 sec saturation time.

2.8.5 Application of STD-NMR to OF-80-NS22 and 552-02 in PGM solution and PJM

Considering the result obtained from the ultrafiltration assay, limitation of the technique and compound availability, two molecules were chosen (OF-80-NS22 and 552-02) to carry on STD-NMR experiments to study the interaction of these two compounds with PGM and PJM.

Sample preparation for STD-NMR

Before being used for STD-NMR experiment, 10 ml of purified PJM mucin were dialysed in D_2O for 48 h at room temperature. The water was changed every 2 h and the volume of the mucin was reduced to 200 μ l by filtration using vivaspin tube 10kDa. PGM, PJM, PBS pH 6.8, OF-80-NS22 and 552-02 were made up using D_2O and freeze-dried three times to exchange H_2O for D_2O . The deuterated PBS pH 6.8 was then diluted in D_2O and used to dissolve PGM, PJM and compounds. For OF-80-NS22 and 552-02 was necessary to use 25% of dimethyl sulfoxide- d_6 (DMSO- D_6) to allow the compound to be dissolved at a concentration of 10mM.

2.8.5.1 Elimination of glycerol contamination from mucin

Ultrafiltration of mucin in vivaspin tubes resulted in significant mucin contamination with glycerol. This resulted in the appearance of large peaks on the 1H NMR spectrum. Amicon Ultra-0.5 Centrifugal Filters 10kDa were used to wash the mucin and try to eliminate the glycerol. Amicon tubes were left soaked in D_2O overnight. The day after, 100 μ l of mucin were put into the Amicon tube and washed 10 times with 400 μ l of warm D_2O (40 °C) though centrifugation at 10000 rpm. The centrifuge was stopped before all sample was filtered to avoid membrane drying. At the last wash the mucin

solution was reduced at a volume of 50 μ l and volume was reconstituted to 100 μ l using D₂O

2.8.5.2 STD-NMR Analyses of OF-80-NS22 and 552-02 in PGM solution

Mucin was reconstituted in PBS pH 6.8 at a concentration of 2 μ M (using nominal Mw of 1MDa) and left to rock for 4h before being diluted as appropriate using the same buffer. The mucin and drug concentrations for the STD-NMR experiment were 600 nM and 2 mM respectively in a total volume of 500 μ l. STD NMR experiments were performed at 283K on a Bruker digital Avance 800 MHz spectrometer using Wilmad[®] NMR tube 5mm diameter. For selective protein saturation, a field strength of 115 Hz was employed. The on-resonance and off-resonance frequencies were set at -0.5 and 40 ppm, respectively. STD NMR experiments were performed with 64/256 scans, depending on saturation time.

2.8.5.3 Competition STD-NMR for the detection of high-affinity ligands

The mixture (250 μ l) mucin-OF-80-NS22 and mucin-552-02 (600nM mucin and 2mM drug) were mixed and used for a competition assay. The instrument was set as described in 2.13.4

2.8.5.4 Analyses of OF-80-NS22 and 552-02 in PJM solution

Pure lyophilised PJM was reconstituted in PO₄ pH 6.8 at a concentration of 2 μ M and left to rock for 4h. For the STD-NMR experiment, mucin and drug concentrations were 100 nM and 2.5 mM respectively (ratio 1:25000). The experiments were performed at 310K on Avance 800 MHz spectrometer in Wilmad[®] NMR tube 3.3 mm and a field

a field strength of 115 Hz (as rectangular pulse equivalence) with the total saturation time of 1 second and the on-resonance and off-resonance frequencies were set at -0.5 and 40 ppm. Depending on saturation time experiments were performed with 64/256 scans using WATERGATE for solvent suppression. Saturation curves of 552-02 were obtained by applying different saturation time (from 0.1 sec to 6 sec) to the mixture ligand-purified mucin and calculating for each saturation time point the %STD and % of magnetization transfer using Origin Pro-B programme.

2.9 References

1. Atherton HC, Jones G, Danahay H. IL-13-induced changes in the goblet cell density of human bronchial epithelial cell cultures: MAP kinase and phosphatidylinositol 3-kinase regulation. *Am J Physiol Lung Cell Mol Physiol*. 2003;285(3):L730-9.
2. Le T, Saier MH, Jr. Phylogenetic characterization of the epithelial Na⁺ channel (ENaC) family. *Molecular membrane biology*. 1996;13(3):149-57.
3. Keppler A, Gendreizig S, Gronemeyer T, Pick H, Vogel H, Johnsson K. A general method for the covalent labeling of fusion proteins with small molecules in vivo. *Nature biotechnology*. 2003;21(1):86-9.
4. Waters NJ, Jones R, Williams G, Sohal B. Validation of a rapid equilibrium dialysis approach for the measurement of plasma protein binding. *Journal of pharmaceutical sciences*. 2008;97(10):4586-95.
5. Shen BQ, Finkbeiner WE, Wine JJ, Mrsny RJ, Widdicombe JH. Calu-3: a human airway epithelial cell line that shows cAMP-dependent Cl⁻ secretion. *The American journal of physiology*. 1994;266(5 Pt 1):L493-501.
6. Fiegel J, Ehrhardt C, Schaefer UF, Lehr CM, Hanes J. Large porous particle impingement on lung epithelial cell monolayers--toward improved particle characterization in the lung. *Pharmaceutical research*. 2003;20(5):788-96.
7. Dubin RF, Robinson SK, Widdicombe JH. Secretion of lactoferrin and lysozyme by cultures of human airway epithelium. *American journal of physiology Lung cellular and molecular physiology*. 2004;286(4):L750-5.
8. Zhang Y, Reenstra WW, Chidekel A. Antibacterial activity of apical surface fluid from the human airway cell line Calu-3: pharmacologic alteration by corticosteroids and beta(2)-agonists. *American journal of respiratory cell and molecular biology*. 2001;25(2):196-202.
9. Cohen Y, Avram L, Frish L. Diffusion NMR spectroscopy in supramolecular and combinatorial chemistry: an old parameter--new insights. *Angewandte Chemie*. 2005;44(4):520-54.
10. Angulo J, Nieto PM. STD-NMR: application to transient interactions between biomolecules-a quantitative approach. *European biophysics journal : EBJ*. 2011;40(12):1357-69.
11. Evans JN, Zajicek J, Nissen MS, Munske G, Smith V, Reeves R. ¹H and ¹³C NMR assignments and molecular modelling of a minor groove DNA-binding peptide from the HMG-I protein. *International journal of peptide and protein research*. 1995;45(6):554-60.
12. Meyer B, Klein J, Mayer M, Meinecke R, Moller H, Neffe A, et al. Saturation transfer difference NMR spectroscopy for identifying ligand epitopes and binding specificities. *Ernst Schering Research Foundation workshop*. 2004(44):149-67.
13. Wang YS, Liu D, Wyss DF. Competition STD NMR for the detection of high-affinity ligands and NMR-based screening. *Magnetic resonance in chemistry : MRC*. 2004;42(6):485-9.

Chapter 3 : Identification and characterisation of mucus models for drug permeation studies

3.1 Introduction

The conducting airways of the respiratory tract are lined by viscoelastic and adhesive mucus layer. Mucus viscoelastic properties are mainly based on mucus glycoproteins monomers, called mucin, being crosslinked via disulphide bonds with other monomers^{(1) (2)} which helps to protect the underlying epithelium from environmental fine particles⁽³⁾ and pathogens⁽⁴⁾ by physical trapping and allows removal by the mucociliary escalator mechanism. Although it serves to protect, the barrier effect of mucus to both small and large molecules has been claimed in the literature^{(5) (6) (7) (8)}. However, a satisfactory answer has yet to be found to understand how the mucin glycoprotein builds a dynamic structure capable to act as barrier for drug molecules.

The interaction of deposited solutes with mucus essentially due to the viscous properties of mucus⁽⁹⁾. As described by Lieleg and Ribbeck⁽¹⁰⁾ particles moving through the mucus can interact strongly with mucus components and be trapped by two different mechanisms: size filtering and interaction filtering mechanism. In the size filtering the mucus mesh dimensions and the molecular size of the diffusive species have an effect on the mucus permeation. Dawson, Wirtz⁽¹¹⁾ support the idea of size filtering showing a decrease of neutral particle (<200nm) mobility on CF sputum mucus with increasing particle size. The nature and extent of interaction between the diffusive species and the mucus network are also determined by the charge and/or specific chemical groups present. This so-called interaction filtering has also been shown to limit the diffusion of molecules through the mucus layer. Experiments conducted on cervicovaginal mucus have reported a lower mobility of

small and negatively charged (100nm) than larger and neutral particles (200-500nm) (12, 13).

The interaction of small molecules to mucus layer has been demonstrated for several drugs such as aminoglycosides, ⁽¹⁴⁾ ⁽¹⁵⁾, salbutamol ⁽¹⁶⁾. Although there are various mucus models described in the literature ⁽¹⁷⁾, no standard protocols are available for mucus diffusion studies. Scientists have described the use of *ex vivo* ⁽¹⁸⁾, *in vivo* model ⁽¹⁹⁾ or *in vitro* system using mucus produced by specialized cells such as Calu-3 and Caco-2 ⁽²⁰⁾. Other research groups have described the use of simple purified pig gastric mucin ⁽²¹⁾ to artificial formulated using PGM, 1,2-diacyl-palmitoyl-glycerol-3-phosphocholine and BSA ⁽²²⁾, native human or animal (e.g. pig) mucus ⁽²³⁾ ⁽²⁴⁾ or pathological mucus ⁽²⁵⁾.

The most ideal model is the crude human mucus but is difficult to access and biochemical properties (mucin, DNA, lipid composition) can vary between batches. Mucus from pig tissue is more freely available than that of human origin but inter-batch variability can be a problem ⁽²⁶⁾. Mucus-producing cells secrete only small amounts of mucus and, as result, mucus has often been substituted by a commercial porcine mucin (PGM) model. Pathologic mucus, such as from CF, presents a high viscosity and the physical-chemical properties can be significant different compared to natural human mucus. The high viscosity in CF people is mainly due to an alternated electrochemical equilibrium on the epithelium because of chloride channel dysfunction.

The work described in this chapter aimed to identify and characterise a mucus model that can be used to study the small molecule binding characteristics of lung mucus. In particular, the studies considered a primary human bronchial epithelial cell model, *ex vivo* porcine mucus and a commercially available partially purified mucin model. A Franz cell diffusion apparatus was used to determine the permeability characteristics of a 3D mucin gel to a size range of hydrophilic dextran probes as well as two model small molecule probes, amiloride and benzamil.

3.2 Materials and Methods

Materials

NHBE cells, B-ALI™ growth medium, B-ALI™ differentiation medium and supplemented were bought from Lonza. AlexaFlour-633 labelled WGA, goat anti-rabbit AlexaFluor 488 were purchased from Life Technologies (Paisley, UK), anti-mucin 5AC purchased from Santa Cruz (Texas, USA from life technologies, Paisley, UK). Porcine gastric mucin (Type II) amiloride, benzamil, gentamicin solution, FL-Na and FITC-dextran probes were obtained from Sigma-Aldrich (Dorset, UK). Porcine lungs used were donated by H G Blake, Ltd. Bull Farm Abattoir (Norwich, UK). Antibiotic-antimycotic mixture (100x) was from Gibco (Carlsbad, California).

Methods

NHBE cell culture and mucin identification.

NHBE cells were cultured at an air interface on 0.33 cm² Transwell polyester cell culture supports according to Novartis methods (Chapter 2 section 2.1.1). Monolayer integrity was evaluated by transepithelial electrical resistance (TER) (Chapter 2 section 2.1.5). Glycoprotein secretions from air interface cultures were identified using Alcian Blue (Chapter 2 section 2.2.3) and immunofluorescence staining with an anti-MUC5AC antibody and confocal microscopy (Chapter 2 section 2.1.6). The microscopic structure of isolated NHBE mucus was observed by using AFM (Chapter 2 section 2.1.8).

Ex vivo system

Fresh porcine lung tissue was used to extract fresh tracheobronchial mucus as described in Chapter 2 section 2.2. Mucin and DNA content was determined using 2-CAN and DAPA respectively (Chapter 2 section 2.4). Solid dry percentage of mucus was determined using the following equation;

$$\% \text{ dry} = \left(\frac{W_{\text{dry}}}{W_{\text{wet}}} \right) \times 100\%$$

(see Chapter 2 section 2.2.4).

Permeation assay through PGM

A horizontal Franz-cell system was used to monitor the transport of FL-Na and FITC-dex probes (4, 10, 40, 70kDa), amiloride and benzamil (see Chapter 2 section 2.3.5). The apparent permeability coefficient (P_{app}) for each marker was calculated using the equation:

$$P_{\text{app}} = \frac{dQ}{dt} \cdot \frac{1}{A \cdot C_0}$$

The lag time was obtained from the x-axis intercept of extrapolated linear steady state portion of the cumulative transport curve.

FITC-dex probe, amiloride and benzamils analyses

A microplate reader Polar Star Optima (BMG LabTech) was used to quantify FL-Na FITC-dex in samples (Chapter 2 section 2.3.5.1)

Franz cell basolateral samples were analysed for amiloride and benzamil content using a Perkin Elmer fluorescence HPLC system equipped with a Perkin Elmer LC 240 fluorescence detector (UK) (Chapter 2.3.5.2).

3.3 Results

3.3.1 Growth and differentiation of NHBE monolayers on Transwell culture inserts

NHBE cells were cultured at air-interface on semi-permeable Transwell inserts for 20 days in the presence or absence of 1 ng/ml IL-13 to simulate a mucus hypersecretive phenotype and goblet cell hyperplasia. The cells were grown under submerged culture until day 7 post-seeding. From day 3-7 the TER rose from 30 ± 13 to 760 ± 110 Ω cm². After 7 days post-seeding the apical medium was removed, leaving the cell at the ALI, and treatment of IL-13 was started (Figure 3.1). This treatment decreased the TER to 281 ± 41 Ω cm² for (+) IL-13 and 450 ± 100 Ω cm² for (-) IL-13 at day 3 post-ALI.

For cells not treated (-) IL-13, TER started to increase again after few days (Figure 3.1) whereas for (+) IL-13 decreased and from day 12-20 post-seeding the TER plateaued was at 550 ± 101 Ω cm² for (-) IL-13 and 180 ± 35 for (+) IL-13 treatment. This TER value for (+) IL-13 exceeds the minimum acceptable resistance for polarised monolayers in monolayer transport studies (i.e. >500 Ω cm²). From day 18 post seeding, (+) IL-13 NHBE monolayer started to detach the membrane and TER dropped to an extent where transport studies are not recommended.

Statistical significance was performed using one-way analysis of variance (ANOVA) at 95% confidence limit. Comparing TER Ω cm² of (+) IL13 with (-) IL13 after 12 days post-seeding the $p < 0.0001$ indicates a significant difference (Figure 3.1 indicated with asterisks *).

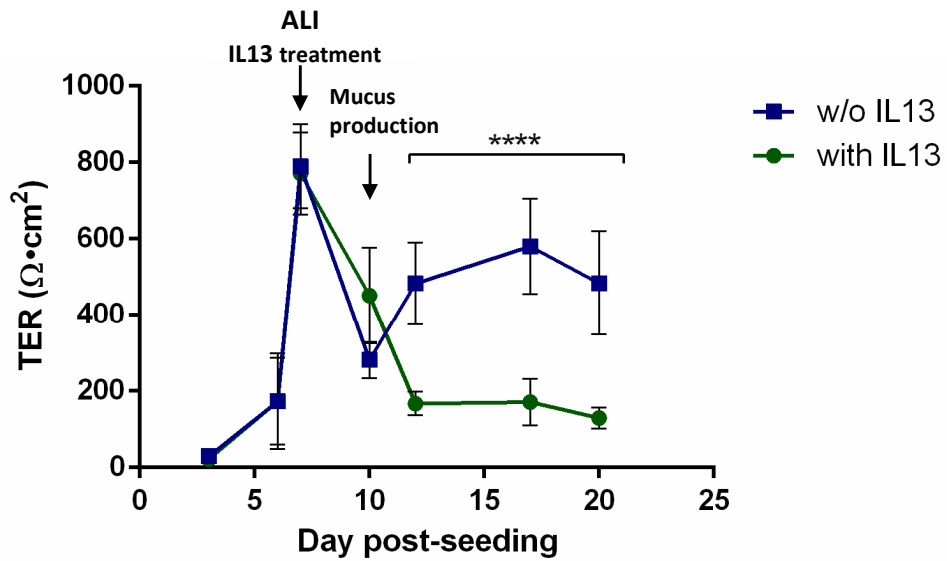


Figure 3.1. Transepithelial resistance of NHBE cells. Graphical representation of TER during cells seeding day. ALI and IL-13 treatment started at day 7 post seeding. Data shown are mean \pm SD, n=6 for each group. Significance at $p < 0.0001$ determined by paired t-test is denoted with asterisks (***)

After 10 days from the post-seeding monolayers appeared thickened and textured. The presence of mucus was visibly noticeable on both IL-13 treated and untreated NHBE cells as a slimy and reflective liquid on the cell surface. Figures 3.2 A and 1B show two different (+) IL-13 inserts at day 17 of post-seeding, with each showing a different phenotype. The monolayer in Figure 3.2 A is relatively smooth and homogenous whereas the monolayer in Figure 3.2 B is heterogeneous with four domed regions that are capped by cells that are distinct in appearance to the rest of the monolayer. This heterogeneity of cellular phenotypic is consistent with monolayer differentiation and the cells highlighted in Figure 3.2 B may be goblet cells. These features were also displayed by NHBE cell (-) IL-13 (data not shown).

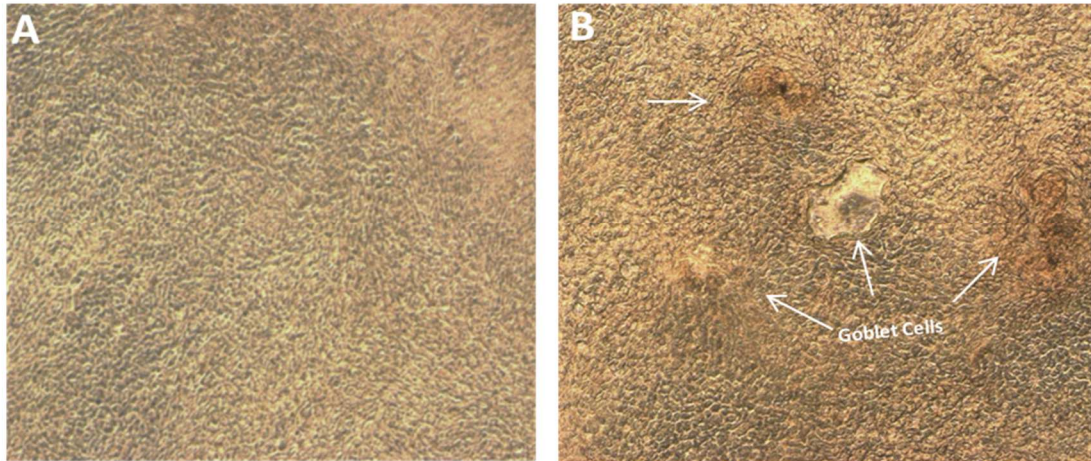


Figure 3.2 NHBE at day 3 of Air Lift (10x). (A) Morphology of NHBE cell (+IL13) on Transwell with 100% confluency without presents of goblet cells. (B) Shows the presence of four goblet cells (indicates with arrows) on the confluent monolayer. The apical surface of inserts was washed with warm PBS (37°) before imaging.

At day 10 days post-seeding, the total volume of the viscous liquid covering the NHBE monolayers was approximately 30 μ l per insert (+/- IL-13) and was firmly attached to the monolayer. This is a positive indicator of mucus production. To allow mucus harvest without damage to the monolayer PBS (100 μ l) was added into each insert. At the same day, the presence of mucin was demonstrated by Alcian blue (AB) staining of the apical washes of NHBE cells. A positive AB signal was seen for samples taken from NHBE (+) IL-13 and (-) IL-13 (Figure 3.3). The negative control (dH₂O), as expected, did not stain blue.

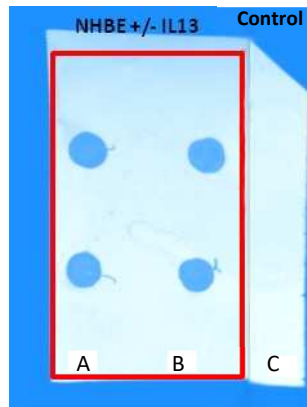


Figure 3.3. Alcian Blue Staining of NHBE cell +/- IL13 mucus. Alcian blue stained nitrocellulose membrane dried with NHBE cells mucus sample from two inserts treated (A) and not treated (B) with IL13 after 10 days post-seeding. As control (C) was used dH₂O.

NHBE cells +/- IL-13 at day 15 post-seeding were fixed and stained using an anti-MUC5AC antibody which recognises the predominant mucin secreted by NHBE cell. Unfortunately, some mucus was lost during the wash and fixation steps as evidenced by a slimy viscoelastic appearance of the PBS washes. In spite of this evident loss of mucus, MUC5AC staining (green) (Figure 3.4) demonstrated that a near continuous mucus layer had formed on NHBE IL-13 treated (Figure 3.4 A & B). Control NHBE monolayers (no IL-13 treatment) were damaged during washes and excluded from analyses.

The Figure 3.4 A reveals that the intensity of MUC5A staining is heterogeneous with areas of high signal intensity (central regions) as well as lower density regions that show intricate crosslinked strands. A zoomed image of a low density region in Figure 3.4 A is shown in Figure 3.4 B. At higher magnification it is possible to see faint staining of mucins branches in the areas in between bundles of mucin branches that stain strongly. Figure 3.4 C is a low magnification epifluorescent image that demonstrates the confluent NHBE monolayer using DAPI stain (blue) and the heterogeneous pattern of MUC5AC staining.

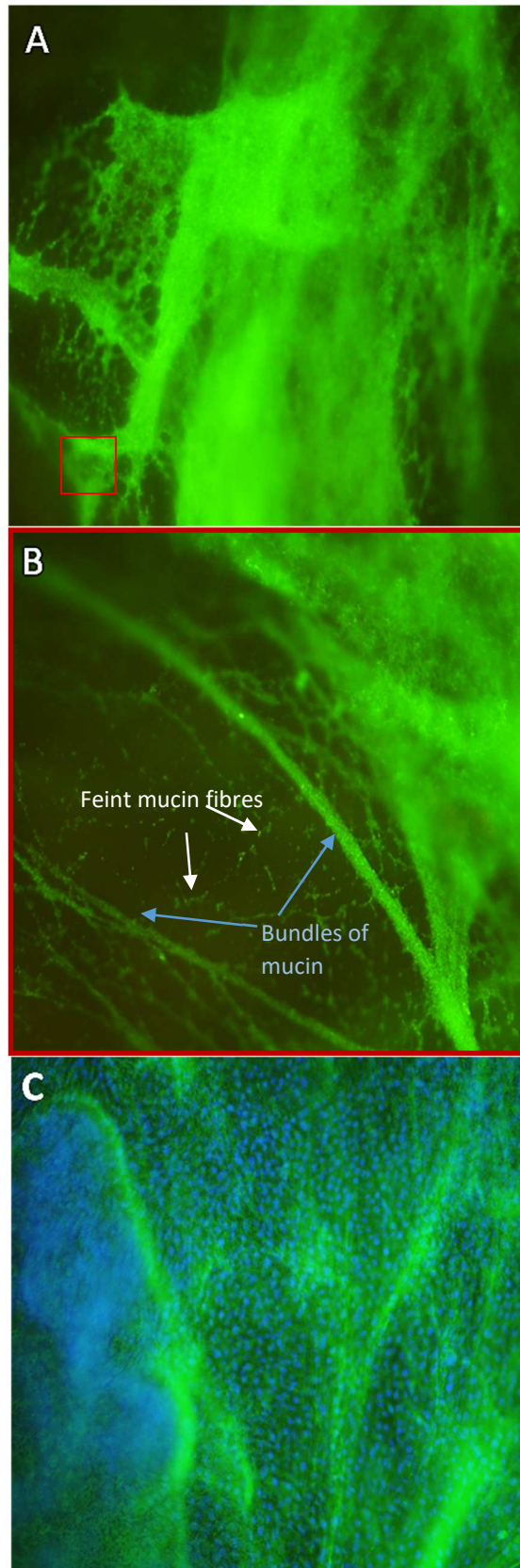


Figure 3.4 Immunofluorescence images of (+) IL-13 NHBE cells (10X). (A) & (B) show extracellular mucus layer. (B) Represent a zoomed picture of mucus mesh of picture (A) showing bundles of mucin fibres (blue arrows) and the faint fibres (white arrows). (C) Low power image to demonstrate confluent monolayer. (C) Cell stained with anti-MUC5AC (green) and nuclei with DAPI (blue).

Confocal imaging of the NHBE (+) IL-13 showed an added layer of mucin complexity (Figure 3.5). The 3D confocal reconstruction of the MUC5AC layer (Figure 3.5 A) includes continuous areas with high density staining and other with lower density. Clearly evident are mucin strands that span the Z axis of the monolayer to form an intricate network of mucin fibres. A zoomed image (Figure 3.5 B) was taken and it shows clearly bundle formation and mucus branches. The red staining in Figure 3.5 A&B results from wheat germ agglutinin (WGA) staining of sialic acid and N-acetylglucosamine groups within the mucus layer.

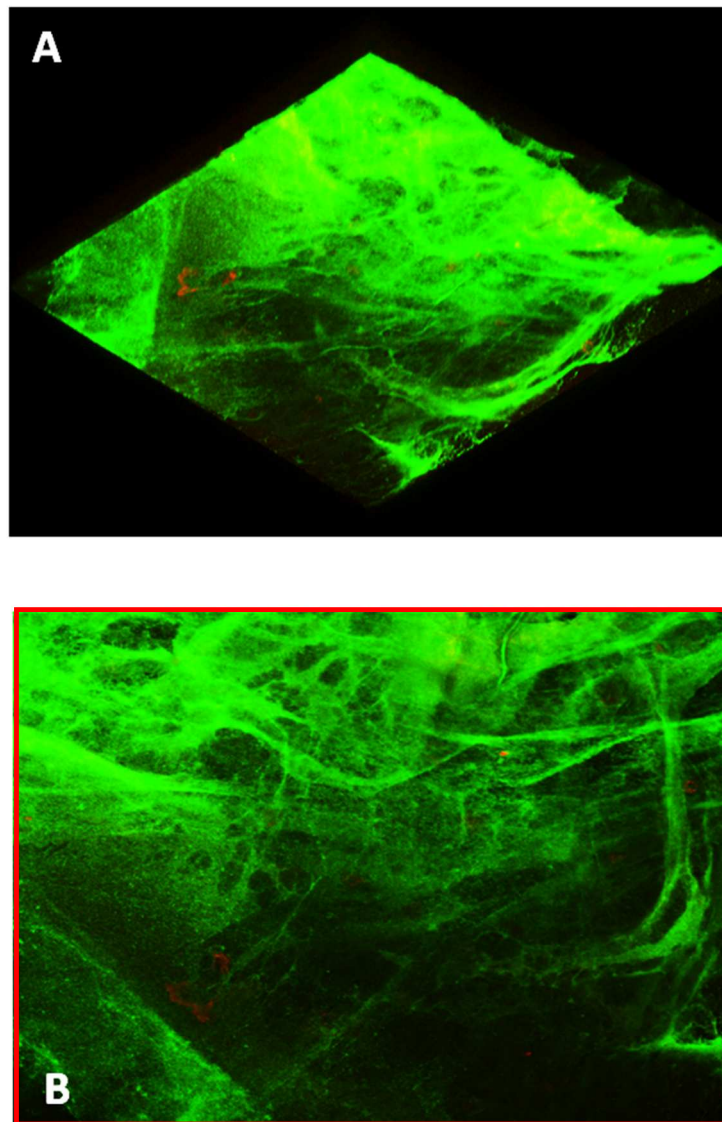


Figure 3.5. Confocal images from NHBE cell IL-13 treated. The heterogeneity of mucus is evident from the dense green regions (A) (B). (B) Represent a zoomed picture of mucus mesh of picture (A). WGA signal (red) evident in A and B.

Mucus harvested from (+) IL-13 NHBE cultures after 15 days post-seeding was concentrated by centrifugation and analysed by Atomic Force Microscopy. Figure 3.6 A includes a short single strand of approximately 1 μm . Figure 3.6 B includes strands of similar diameter intertwined with areas of inter- or intra-strand cohesion. Indeed, Figure 3.6 C & D show a more complex "knotted" structure. In particular, the sample in Figure 3.6 C starts as a single strand and this is followed by an entanglement with another mucin chain. The sample shown in Figure 3.6 D has high crosslink density along its entire length indicating a cluster of mucin monomers.

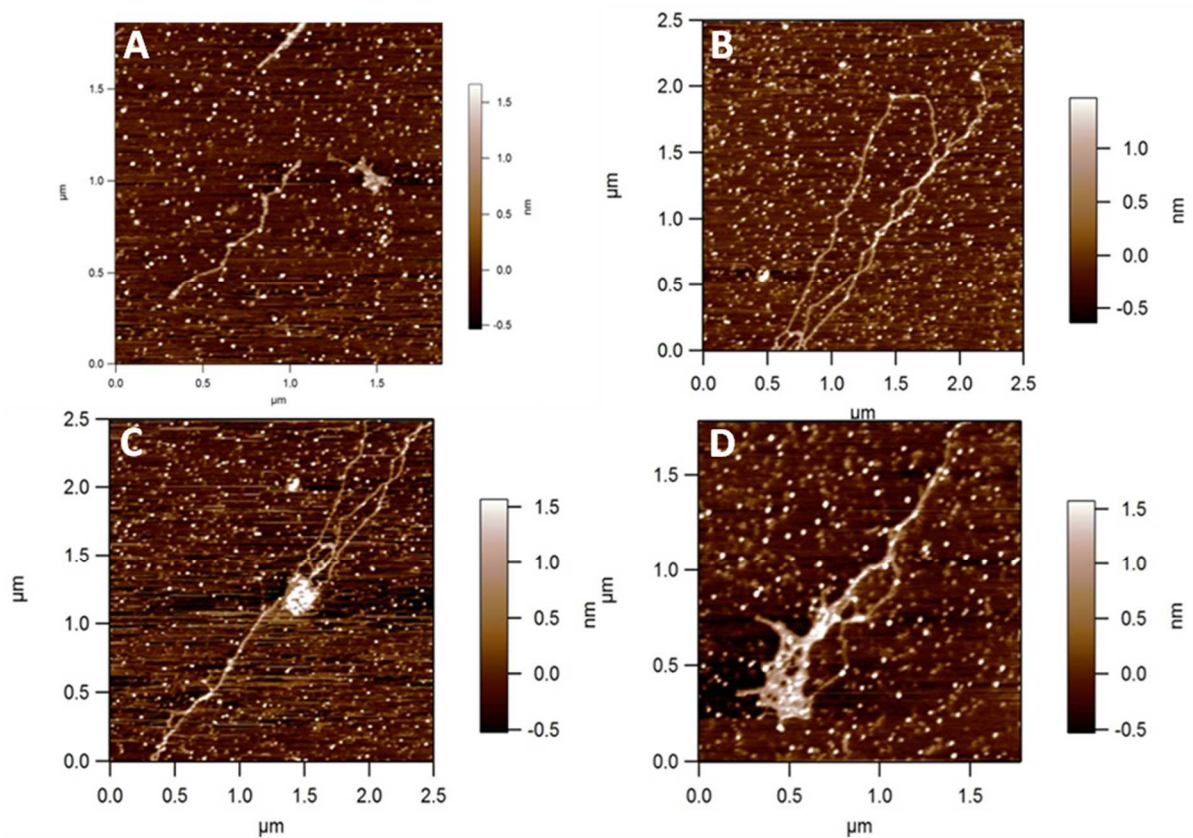


Figure 3.6. AFM images of mucus harvested from NHBE cells

The images show a single strand of mucin (A), a multi-strand (B). C&D show a more complex network among mucins. The bright puncta dispersed throughout the samples are dried salts which were not removed completely by washing before sample imaging.

3.3.2 Investigation of porcine lung tissue as a source of respiratory mucus

Intact lung tissue and individual tracheas from freshly slaughtered pigs were obtained from a local abattoir and as an alternative source of respiratory mucins. The method of animal sacrifice results in the entry of blood into the respiratory tract and mucus harvest by simple scraping of the tissue failed to give mucus without significant blood contamination. Gentle washing of the tissue with sterile NaCl solution caused a significant loss of the luminal lung mucus and a reduction in mucus yield. When the lung tissue was gently rinsed with NaCl solution and maintained in an *ex vivo* culture condition at RT, 4 or 37 °C with or without antibiotic/antimycotic mixture there were differences in the amount of harvested mucus (Table 3.1). When tissue was dissected and incubated on the open bench and maintained at 37°C in the absence of antimicrobials (Table 3.1 N° condition 7) the tissue was odorous and showed signs of necrosis (discolouration and uneven texture) and infection (Figure 3.7).

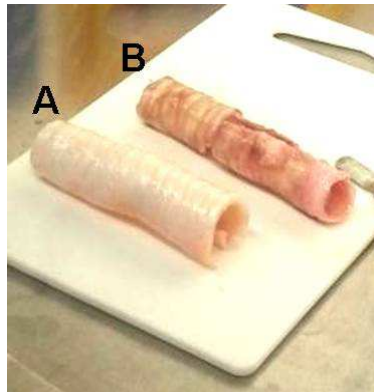


Figure 3.7. Tissue kept in aseptic (A) and non-aseptic (B) condition.

(A) Tissue washed with 0.9% NaCl, treated with antibiotics and dissection obtained using sterilized instruments. (B) Tissue not washed with 0.9% NaCl, without antibiotic treatment and dissection obtained without using sterilized instruments.

A small amount of mucus (~100 mg/lung) was obtained after incubating the samples at room temperature and 4°C with (Table 3.1 N° condition 1-4) no differences seen between tissues cultured in low or high concentrations of antimicrobial agents.

The highest yield of mucus was harvested after keeping the tissue at 37°C for 24 hours (Table 3.1 N° condition 5-6). In this condition it was possible to harvest ~600 mg of mucus per lung.

The different concentration of antibiotics did not change the amount of mucus harvested remaining at 600 mg/lung and no more mucus was obtained after scraping and incubating the tissue for a further 24 hours. Moreover, after 48 hours' incubation in the presence of a high concentration of antimicrobials the tissue became odorous and the RPMI culture media was yellowish in colour indicating infection with no increment of mucus harvested (Table 3.1 N° condition 8).

Table 3.1. Condition tested for respiratory porcine mucus production. Several condition were tested changing temperature, time of incubation, sterile condition and antibodies concentration. High and low antibodies concentration; penicillin (100 or 300 Units/ml), streptomycin (100 or 300 µg/ml), fungizone (25 or 75 µg/ml) and gentamicin (5 or 15 µg/ml).

<i>N° conditions</i>	<i>Temperature (°C)</i>	<i>Incubation Time (h)</i>	<i>Antibiotics concentration (High or Low)</i>	<i>Aseptic conditions (Yes or Not)</i>	<i>Mucus harvested (mg/lung)</i>
1	RT	24	Low	Yes	100
2	RT	24	High	Yes	100
3	4	24	Low	Yes	100
4	4	24	High	Yes	100
5	37	24	Low	Yes	600
6	37	24	High	Yes	600
7	37	24	No	No	-
8	37	48	High	Yes	600

3.3.2.1 Biochemical and physical analysis of porcine mucus

As expected, all porcine mucus samples showed a positive AB staining reaction (Figure 3.8).

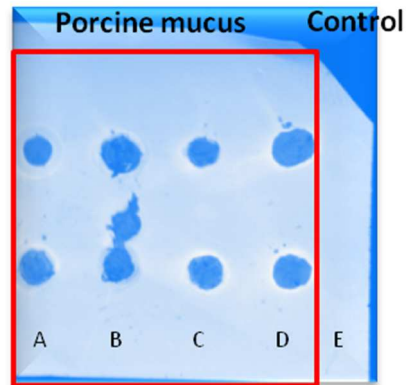


Figure 3.8. Alcian blue staining of mucus harvested from fresh porcine lung tissue. Tracheobronchial porcine mucus from tissue treated with: (A) low concentration antibiotics at 37°C for 24h, (B) low concentration antibiotics at room temperature for 24h, (C) low concentration antibiotics at 4°C for 24h, (D) high concentration antibiotics at 37°C for 24 h, (E) Control (dH₂O). Samples were spotted in duplicate.

Samples (~200mg) from four independent mucus harvests after 24h incubation at 37°C were weighed and freeze-dried until a constant weight was recorded. The mean % dry solids resulted was 12.4%±0.9 (Table 3.2).

Table 3.2 Determination of % dry solids for porcine lung mucus. Determination of the dry weight % of four mucin aliquots samples (A, B, C, D).

Mucus Samples	W_{ep+wet} (g)	W_{ep+dry} (g)	% Dry weight ($W_{dry}/W_{wet} * 100$)
A	1.110	0.967	12.80
B	1.145	0.971	12.06
C	1.132	0.961	13.20
D	1.146	0.971	11.50
			Mean 12,39%
			SD= ±0,85

Determination of mucin and DNA concentration

Quantitative biochemical assays were performed to determine the concentration of mucin and DNA in the porcine mucus samples. Table 3.3 shows the percentage of mucin and DNA corresponding to the eight lung mucus samples harvested. The mucin content varied some 4-fold between samples (0.5-2% w/v), whereas the DNA content was more consistent i.e. 0.32-0.63 %w/v. The mean DNA concentration $0.5 \pm 0.11\%$ was higher than expected and likely indicates a contamination of the sample with shed epithelial cells. The amount of DNA in PGM gels was proportional to the mucin concentration increasing from 0.03 to 0.13% as the PGM% was increased from 1% to 5%.

Table 3.3. Determination of mucin and DNA %. Determination of mucin and DNA % of eight mucus samples (A-H) from porcine respiratory mucus and PGM. Data shown are mean \pm SD (n=3).

<i>Mucus Samples</i>	<i>Average Mucin % w/v</i>	<i>Average DNA % w/v</i>
A	1.2	0.32
B	2	0.52
C	0.9	0.39
D	0.5	0.42
E	1.42	0.6
F	0.81	0.5
G	1.11	0.6
H	0.8	0.63
	Mean 1.09%	Mean 0.50%
	SD= $\pm 0.50\%$	SD= $\pm 0.11\%$
PGM 1%	-	0.03
PGM 3%	-	0.09
PGM 5%	-	0.13

The pH of the harvested mucus after 24h of incubation was measured as 6.8 ± 0.11 (n=8, mean \pm SD).

In summary, the yield of porcine lung mucus was low and contained a significant amount of contaminating DNA. For practical reasons it was decided to seek an alternative mucin model that was more abundant and less labour-intensive to harvest or manipulate in the laboratory.

3.3.3 Application of Sigma PGM model to mucin permeability studies

Initial studies were performed using a horizontal Franz-cell system to determine the permeability profile of PGM models to FL-Na and a size range of FITC-dex probes; the size range was 376 to 70000 Dalton (stokes diameter from 1 to 12 nm) (Table 3.4). This size range include the hydrodynamic radii of many biological molecules that are under investigation for pulmonary administration by Novartis and other major Pharma companies. These include scFv, Fab fragments and minibodies ⁽²⁷⁾.

Table 3.4. Nominal molecular weight and Stokes diameter of all fluorescent probes applied to PGM gels. Values of Stokes diameter supplied from manufacturer (Sigma).

<i>Probe</i>	<i>Molecular Weight (Dalton)</i>	<i>Stokes Diameter (nm)</i>
FL-Na	376	1
FD4	4000	2.8
FD10	10000	4.6
FD40	40000	9
FD70	70000	12

3.3.3.1 Validation of fluorescence-based analytical methods

Table 3.5 shows the calibration curve ranges, coefficient of determination, limit of detection and limit of quantification for each of the fluorescent probes used in the

study. From Table 5, it can be seen that all calibration curves were linear ($R^2 > 0.999$ for all probes) and the LOQ was ~ 3 fold lower than the lowest calibration standard.

Table 3.5. Linearity and sensitivity of the method.

The table includes a summary of the calibration curve range, analytical method used, coefficient of determination (R^2), limit of detection (LOD), limit of quantification (LOQ).

Probes	Calibration range (ng/mL)	Analytical method	R^2	LOD/LOQ (ng/ml)
FL-Na	0.625-50	Plate reader	0.9999	0.048/0.163
FD4	25-500	Plate reader	0.9989	0.302/1.007
FD10	5-400	Plate reader	0.9998	0.064/0.214
FD40	2.5-200	Plate reader	0.9998	0.719/2.19
FD70	2.5-50	Plate reader	0.9989	0.560/1.867
Drug molecules				
Amiloride	2.5-100	HPLC	0.9998	0.065/0.216
Benzamil	2.5-100	HPLC	0.9996	0.132/0.440

3.3.3.2 Permeability of reconstituted PGM gels to a molecular weight range of fluorescent probes

The transport of each fluorescent probe across PGM models (1,3 or 5% w/v in PBS pH 6.8 at 37°C) was monitored over 120 min using a Franz cell (Figure 3.9). The cumulative mass transport profile displayed a biphasic trend for all probes studied. Specifically, the rate of transport across the gel was low from 0 – 30 min after which the rate increased 7-fold from 30 – 120 min for FL-Na and FD4 and ~ 3 -fold for all other probes. The steady state flux of each probe was linear over the 2 hour timecourse of the experiment. The same biphasic profile was observed for 3 and 5% PGM (data not shown) although the rate of cumulative mass transported decreased with incremental increases in PGM concentration.

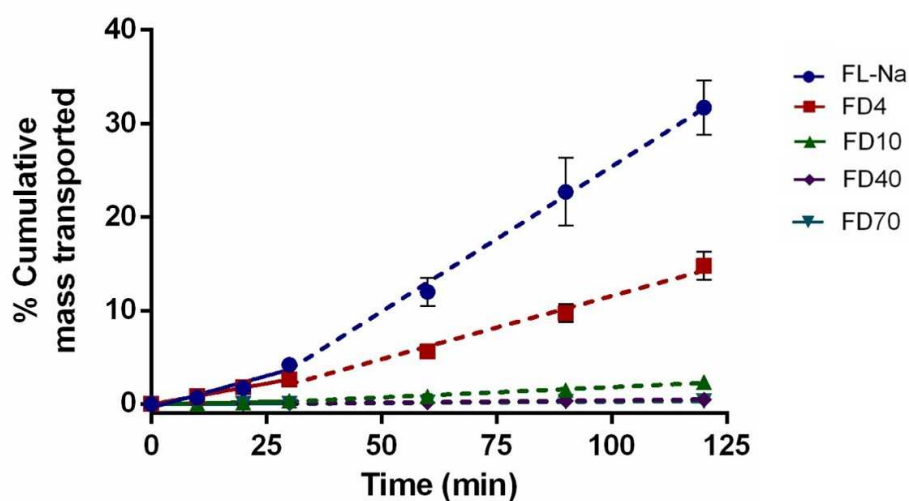


Figure 3.9. Cumulative transport of FL-Na and FITC-dextran probes across 1% PGM gels using Franz cell diffusion cells.

Concentration added to donor chamber was 0.20 mg/ml for FL-Na and FD4 and 1 mg/ml for FD10, FD40 and FD70. Solid lines correspond to linear regression fits for 0-30 min, dashed lines are for 30-120 min. Data shown are mean \pm SD, n=6 for each probe.

Table 3.6 includes the permeability profile of PGM and a control membrane alone (without PGM) to the molecular weight range of solutes. The P_{app} was calculated considering 30-120 min of transportation assay except for the control (mucin free) membranes which displayed steady state transport across the membrane from time =0 min. For blank membranes the rate of solute transport reduced after approximately 30 min consistent with the end of steady-state flux and approach to equilibrium. The application of PGM reduced the rate of solute transport into the receiver chamber as evidenced by an iterative reduction in P_{app} as probes increased in molecular size (Table 3.6).

When the P_{app} of each gel was calculated for different probes, there was a clear reduction in the permeability as the % PGM increased. This indicates that the

diffusion of each probe is incrementally restricted as the mucin concentration increases. The P_{app} values for all probes across 1% PGM was significantly lower ($p < 0.0001$) than that of the bare membranes. The permeability to both FL-Na and FD4 decreased about 7 or 8 -fold when 1% PGM was added to the bare membrane. The permeability to FD4 decreased further by ~ 10 and 13-fold at a gel concentration of 3% and 5% respectively. Intriguingly, the relative fold-decreases in P_{app} to FL-Na and FD4 was similar ($p > 0.05$) for all three concentrations of mucin used. For FD10, the P_{app} of 1% PGM was very low ($0.30 \pm 0.09 \times 10^{-6}$ cm/s). Yet, the permeation of FD10 through PGM decreased further (28 and ~ 83 -fold from the 0% control) when the concentration of mucin was increased to 3 and 5% (Table 3.6). The relative decrease in the permeability was greater when comparing 1% and 3% PGM ($p < 0.01$) than when comparing 3 to 5% ($p < 0.05$) (Table 3.6 A).

From Table 3.6 C, it is evident that the lag time calculated for penetration of the bare membrane increased steadily with incremental molecular weight. The lag times for FD 40 and FD70 were identical, indicating a restricted passage of FD70 across the membrane as described above. FL-NA and FD4 lag time is influenced by the addition of mucin gel onto the bare membrane. Specifically, it increased 26-fold ($p < 0.0001$) for FL-Na and ~ 4 -fold for FD4 ($p < 0.001$), whereas no significant increment of lag time was noticed for FD10, 40 and 70 ($p > 0.05$). Following the addition of PGM gel, the lag time was slightly increased to 22/23 min for FL-Na and, therefore, only marginally influenced by the change of PGM. The increment of lag time for higher molecular weight probes (4-70kDa) was of about 10 min increasing from an average of 18 to 28 min for both 3 and 5% PGM.

Table 3.6. Influence of PGM concentration on FL-Na and FITC probes diffusion 30-120 min.
A Apparent permeability mean ($\times 10^{-6}$ cm/s) and respective SD of FL-Na and FITC probes through 0, 1, 3, 5% PGM gel using Franz cell system (n=6). **B** Fold decreased of all probes used compared to 0% mucin gels. **C** Lag time in minute of FL-Na and FITC probes. Statistical analysis by one-way ANOVA and multiple comparison test.

A Apparent Permeability (10^{-6} cm/s) FL-NA and FITC probes (mean \pm SD)						
PGM%	FL-Na	FD4	FD10	FD40	FD70	
****	0	28.5 \pm 3.21	16.2 \pm 2.86	8.25 \pm 0.97	1.754 \pm 0.521	0.575 \pm 0.037
	1	4.2 \pm 0.52	2.1 \pm 0.33	**	0.30 \pm 0.09	0.064 \pm 0.031
	3	3.0 \pm 0.41	1.6 \pm 0.35	*	0.17 \pm 0.09	0.035 \pm 0.010
	5	2.2 \pm 0.25	1.2 \pm 0.21	*	0.10 \pm 0.01	0.029 \pm 0.013
					0.012 \pm 0.005	
B N. Fold decreased from 0 to 5% PGM using FL-NA and FITC probes						
PGM%	FL-Na	FD4	FD10	FD40	FD70	
0	-	-	-	-	-	-
1	7	8	28	27	17	
3	9	10	49	50	26	
5	13	13	83	70	48	
C Lag time FL-NA (minutes) and FITC probes (mean \pm SD)						
PGM%	FL-Na	FD4	FD10	FD40	FD70	
0	0.7 \pm 0.3	4.8 \pm 0.6	6 \pm 1.3	12 \pm 9	13 \pm 10	
****	1	***	17 \pm 3	19 \pm 4	17 \pm 7	
	3		31 \pm 1	29 \pm 4	30 \pm 2	
	5		33 \pm 1	30 \pm 7	27 \pm 9	

An inverse relationship between the molecular weight and apparent permeability of each PGM solution was recorded (Figure 3.10). PGM displayed higher P_{app} values when probes with smaller molecular weight (FL-Na and FD4) are considered as they can easily diffuse through the microenvironment of the mucin mesh. For the probes with highest molecular weight, (such as FD40 and FD70) the total mass transported was very low compared to other probes showing a low P_{app} (Figure 3.10). Moreover, PGM permeability to probes with a molecular weight of >10 kDa was much lower for all the different PGM concentrations tested (Figure 3.10).

From Figure 3.10 A, an exponential decrease in permeability is observed for the bare dialysis membrane (0% PGM). In the corresponding plot of P_{ap} versus $\frac{1}{\sqrt[3]{M_w}}$ (Figure 3.10 D) there is a linear relationship, supporting a free diffusion of through the bare membrane. Figure 3.10 B and E show the 1% PGM permeability profile. Figure 3.10 C appears similar profile to 0% PGM although there is a more restricted difference between 1% PGM permeability to FL-Na and FD4 in 0% PGM. In Figure 3.10 E, this is visible as a non-linearity that becomes more apparent in the permeability profiles of the 3% and 5% PGM samples (Figures 3.10 F). This indicates that the permeation of FD40 and FD70 is restricted by PGM and / or the membrane filter. In the case of FD10 there is a clear restricted diffusion in 3% and 5% PGM and a subtle indication of restricted permeation in 1% PGM.

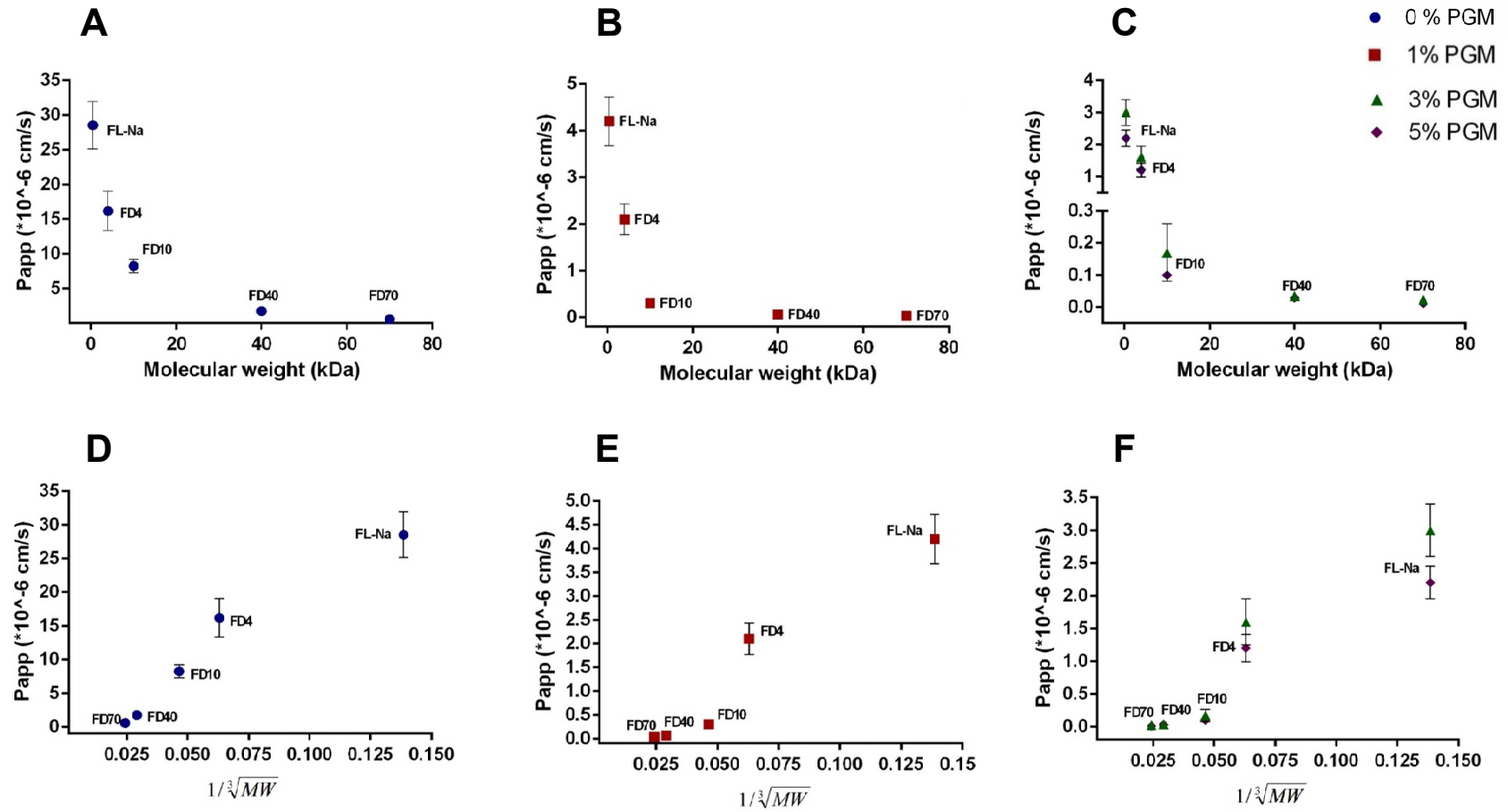


Figure 3.10. Influence of the molecular weight of probes on the P_{app} . The P_{app} decreases with increase of the molecular size of FL-Na and FITC dex without (A & D) and with of mucin concentration at 1 (B & E), 3 and 5% (C & F). Data shown are mean SD n=6.

3.2.4 Transport of amiloride and benzamil across PGM gels

Figure 3.11 shows the cumulative mass transport of amiloride/benzamil 1% PGM. The transport of amiloride across the PGM gel (Figure 3.11, red) was linear and rapid. Approximately 40% of the applied amiloride dose was transported to the receiver chamber by 120 min. The cumulative transport profile of benzamil was biphasic. The rate of transport was slower in the first 30 minutes, 8 ± 2.91 and $2.6 \pm 0.42\%$ of 200 $\mu\text{g}/\text{ml}$ dose donor, compared to a more rapid permeation from 30-120 mins, 36 ± 8.6 and $27.1 \pm 2.08\%$ for amiloride and benzamil respectively, indicating a delay before steady state transport through PGM.

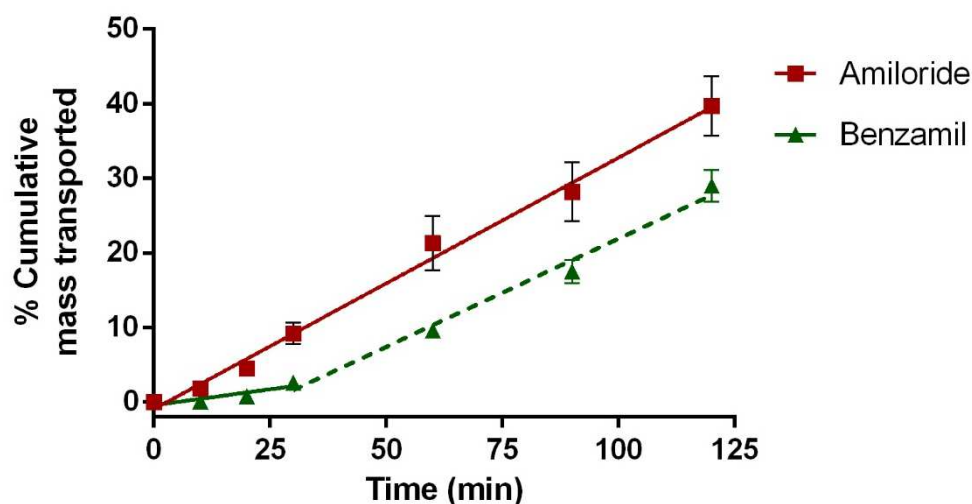


Figure 3.11. Example cumulative mass transport of amiloride and benzamil across 1% PGM. Drugs were applied to the Franz cell donor chamber at a concentration of 0.20 mg/ml. The biphasic profile of benzamil is shown with solid lines correspond to linear regression fits for 0-30 min, dashed lines for 30-120 min. Data shown are mean SD n=8. Experiments were also performed on 3% and 5% PGM for which P_{app} data are shown in table 3.7.

As shown in Table 3.7, the steady state permeability of the bare membrane decreased of about 6-fold following the addition of 1% PGM gels for FL-Na, amiloride and benzamil ($p < 0.0001$). The PGM P_{app} to FL-Na and amiloride was very similar for all mucin gel used. In contrast, the PGM P_{app} to benzamil was lower than amiloride and FL-Na in each condition. The permeability to benzamil was 1.5-fold lower with 0% PGM. Interestingly, the relative difference between P_{app} for benzamil and amiloride grew ($p < 0.05$) with incremental increases in PGM concentration i.e. the P_{app} to amiloride was 1.5-fold, 3-fold and 4-fold greater than amiloride for 1%, 3% and 5% PGM, respectively. This differential transport of amiloride and benzamil is unexpected considering their similar molecular weight (229.6 and 319.8 Da respectively).

From Table 3.7 C, the addition of 1% mucin gel onto the membrane significantly influenced the lag-time of the molecules ($p < 0.001$), whereas no significant increment of lag time was noticed for increment of mucin to 3 and 5% ($p > 0.05$). Amiloride showed a lower lag-time at 1% PGM of 8 minutes which increased to 16 and 20 minutes with the increment of mucin to 3% and 5% respectively ($p > 0.05$). Benzamil lag-time at 0% PGM was about ~10-fold higher than FL-Na and amiloride and not significant increment of lag time were noticed with increment of mucin concentration to 5% ($p > 0.05$).

Table 3.7. Influence of mucin concentration on Amiloride and Benzamil compared with FL-Na. A Apparent permeability mean ($\times 10^{-6}$ cm/s) and respective SD through 0, 1, 3, 5% PGM gel using Franz cell system (n=9). **B** Fold decreased of Amiloride, Benzamil and FL-Na compared to 0% mucin gels. **C** Lag time in minute of FL-Na amiloride and benzamil. Statistical analysis by one-way ANOVA and multiple comparison test.

A Apparent Permeability amiloride and benzamil 30-130 min (mean \pm SD)

PGM%	FL-Na	Amiloride	Benzamil
**** { 0	28.53 \pm 3.21	26.6 \pm 0.55	16.42 \pm 0.60
**** { 1	4.24 \pm 1.39	**** { 4.51 \pm 0.26	**** { 3.11 \pm 0.18
3	3.04 \pm 1.02	*** { 2.70 \pm 0.17	**** { 1.00 \pm 0.17
5	2.19 \pm 0.84	2.52 \pm 0.14	* { 0.61 \pm 0.17

B N. fold decreased from 0 to 5 % PGM amiloride and benzamil

PGM%	FL-Na	Amiloirde	Benzamil
0	-	-	-
1	7	6	5
3	9	9	16
5	13	11	28

C Lag time (minutes) amiloride and benzamil (mean \pm SD)

PGM%	FL-Na	Amiloride	Benzamil
**** { 0	0.7 \pm 0.3	0.4 \pm 0.3	5 \pm 1
**** { 1	18 \pm 4	8 \pm 5	18 \pm 2
3	22 \pm 3	16 \pm 3	23 \pm 2
5	23 \pm 5	20 \pm 3	24 \pm 1

3.4 Discussion

Specialized epithelial cells called goblet cells and submucosal exocrine glands secrete, the mucus, which serves to protect the airway. Mucin, glycosylated protein, are the main non-water component of mucus and the main responsible for mucus viscoelasticity.

Button, Cai ⁽²⁸⁾ propose a gel-on-brush model stating that different mucins are differentially expressed in different locations in the ASL. The mucus layer over the PCL is formed by secreted mucin, mainly represented by MUC5AC and MUC5B for the airway, while PCL comprises membrane-associated mucins, MUC1 and MUC4, responsible of the strong interaction of the ASL with the epithelia ⁽²⁹⁾. The complexity of the gel-on-brush model appears impossible to recreate without mucus-producing cell line or tissue sections. *In vitro* cell culture models are very attractive and the NHBE cell cultures have made important contributions to the understanding of the pathogenesis in CF and COPD ^(30, 31) thanks to their ability to reproduce a similar *in vivo* epithelial mucin and mucus production phenotype, unlike transformed or malignant cell lines.

In this study we investigated NHBE cells as a model of the bronchial epithelial source of mucus. To produce fully differentiated cell monolayers capable of mucus production cell monolayers must reach 100% confluency before starting the air lift procedure. Moreover, the use of cell culture models for drug transport studies requires the formation of tight polarized monolayers as an essential precondition. The transepithelial electrical resistance (TER) is widely used as a measure of the resistance presented by the paracellular pathway of a confluent monolayer. The cells

formed tight junctions as evidenced by the measurement of TER $\sim 800 \Omega \text{ cm}^2$. Treatment with IL-13 was associated with a decrease in TER and a change in the appearance of the cells with producing of a viscous liquid, the mucus.

Low passage number NHBE cell model has a proven capacity for mucus production^(30, 31) however, the yield of mucus is low as observed in the healthy lung. Normal NHBE cells mucus production may be increased by inflammatory stimulation. Malavia, Mih⁽³²⁾ showed that the treatment of NHBE cells with the pro-inflammatory cytokine IL-13, at a concentration of 1 up to 10 ng/ml induces increasing levels of MUC5AC demonstrated by immunofluorescence. IL-13 has also been shown to increase goblet cell density on NHBE cells by Alcian blue staining by directly interacting the airway epithelium and with involvement of ERK, p38 MAP kinase, and phosphatidylinositol 3-kinase pathways⁽³³⁾.

To avoid phenotypic drift that is associated with serial passaging of primary cells, the NHBE monolayers described here were performed using NHBE cell on passage 1, which ensure mucociliary differentiation as described by others^(30, 32). In particular, it has been shown that NHBE cilia-genesis decreases in P-3 and P-4 cell cultures as for the bioelectric properties characteristic of airway epithelium⁽³⁰⁾.

TER is a well-established method and a widely accepted in vitro culture technique of monitoring TJ integrity (tight junction), differentiation and polarisation of monolayers⁽³⁴⁾. Unexpectedly, environmental contamination of the (+) IL-13 NHBE monolayers caused cells to detach from the membrane and TER dropped before they were ready for the permeation assay.

Mucus was strongly attached to the epithelium and for collection was necessary to solubilise it with apical washes of PBS washes at 37°C⁽³⁵⁾ ⁽³⁶⁾. Considering the volume added and volume collected we may state that the total mucus yield was about 30µl/well. To the best of our knowledge, has not been reported the amount of mucus produced by NHBE. This yield of mucin is insufficient for the routine performance of mucin binding assays that required volumes in the millilitre range. However, up-scaling of these cultures onto larger diameter inserts in greater numbers is an alternative, yet costly option.

Different methods have been used to show mucin presence on NHBE cell surface such as AB stain in detection of sialylated or sulphated groups on mucin but non-mucin specific (Figure 3.3)⁽³⁷⁾ where blue staining may indicate the presence of mucin fractions and DNA⁽³⁸⁾ without apparent differences between the mucus from NHBE +/- IL13 (Figure 3.3).

Mucus secretion is supported also by immunochemistry using antibody against MUC5AC (Figure 3.4) and images taken with confocal microscope (Figure 3.5), which show a dense green area as a result of MUC5AC stain. In fact, the use of specific antibodies against the MUC5AC mucin is a useful method to study MUC5AC protein levels⁽³⁹⁾. AFM analysis of washed mucus revealed single strands and more complex mesh-like strands. A major challenge in AFM imaging is the differentiation between mucin and DNA which appears structurally similar on the AFM length scale. A quantitative DNA assay was not performed on the NHBE mucus however it is not expected to be significantly contaminated by DNA. As a source of DNA apoptotic

and/or necrotic NHBE cells were washed from the surface throughout the culture process and before harvest. This increases the likelihood that AFM images represent mucin glycoproteins rather than DNA.

The principle secreted lung mucin MUC5AC has been studied by AFM. Round et al Round, McMaster ⁽⁴⁰⁾ investigated affinity purified MUC5AC from human ocular origin. They showed that the intramolecular conformational of the mucin complex was heterogeneous; from the display of a single molecules to a complex glycoprotein aggregation. In fact, mucins are macromolecule with a complex organization and different structures due to glycosylated regions and their tendency to form different multimers with different length. It is evident that the 3D structural complexity of mucin gels cannot be studied by AFM imaging. However, AFM offers opportunities to understand the single molecule associations that contribute to the complex viscoelastic behaviour of mucins and mucus.

In contrast to the *in vitro* NHBE cell model, *ex vivo* porcine lung tissue represents an alternative source of larger amounts of intact lung mucus. In this study, freshly isolated porcine lungs were incubated in different condition to minimise microbial contamination and degradation while maximising mucus harvest. The optimal conditions involved incubation at 37°C and for 24h in the presence of antibiotics (penicillin, streptomycin, fungizone and gentamicin). These conditions produced ~600 mg of mucus per lung. Biochemical analyses demonstrated that the % dry solid and the DNA content was supraphysiological for a healthy lung mucus. In spite of this the mucin concentration (1%) was typical for a healthy sputum ⁽⁴¹⁾. The high amount

of cell that come off during the mucus harvesting may have contribute to the high solid dry %.

This high solid dry % is in agreement with Martens, Inglis⁽⁴²⁾ studies on mucus isolated from *ex vivo* porcine bronchi, cystic fibrosis human, and non-cystic fibrosis human bronchi. In porcine and “normal” human mucus, the solid percentage was ~8% increasing up to 18 % for cystic fibrosis mucus. A high percentage was also showed by Larhed, Artursson⁽⁴³⁾ were the solid component of undiluted pig intestinal mucus resulted to be between 14-17% and comparable to the dry percentage obtained from the rat native intestine mucus (16.2%)⁽⁴⁴⁾.

The large amount of other mucus components than mucin is also in agreement with previous studies and could represent the presence of lipids, proteins and salts.

DNA concentration in the PLM was about 5 mg/ml (0.5% w/v), more similar to DNA concentration found in CF sputum (0.5 mg/ml up to 9 mg/ml) than DNA found in health people sputum which is ~3µg/ml⁽⁴⁵⁾. Probably, during mucus collection cells have been damaged releasing DNA which can interfere with our analyses. In fact, as showed by⁽⁴⁶⁾ drug molecules can bind to DNA and the interaction of drugs with nucleic acid is a significant feature in pharmacology. Is necessary to consider the mucus as a heterogeneous complex containing mucin, DNA, lipids, enzymes, antibodies, and as a result of cells damage all this substance will be released in the mucus layer with a consequent variation of mucus rheology and mucus-drug interaction.

Larhed, Artursson⁽⁴³⁾ studying the influence of pig intestinal mucus components, demonstrated that mucin dry percentage was mucin only 5% (w/w %) compared to

lipids (37%) and protein (39%) and the remaining 19% comprising ~6% DNA and 13% inorganic salts and that all mucus component may reduce diffusion of drugs in native intestinal mucus.

In summary, the *ex vivo* porcine lung mucus model was low yielding, work intensive and, more importantly, lacking in physiological similarity to *in vivo* healthy lung mucus.

Transport assay using PGM

Porcine gastric mucin (type III) from Sigma Aldrich is a cost-effective mucin model that has been used by many as a mucus model for the purposes of studying nanoparticle transport and the formation⁽²²⁾ or persistence of bacterial biofilms⁽⁴⁷⁾. It is known that this crudely purified mucus model does not retain its ability to form a complex 3D gel matrix. However, PGM has the advantages of abundant supply, low cost, ease of use by rehydration and overnight swelling and a ~10-fold lower concentration of contaminating DNA (compared to harvested PLM) and was used for further transportation experiments.

PGM because of its denatured state does not form a reliable gel structures and is considered a poor gel model⁽⁴⁸⁾ but could be used to study binding interactions⁽⁴⁹⁾.

The Franz diffusion cell system is a well-established and simple method for *in vitro* permeation studies. It is one of the most important methods for researching transdermal drug administration but has been also used for studying gel, mucus permeations and formulation release studies. For instance, the side-by-side diffusion

chamber has been used by Bhat, Flanagan ⁽⁵¹⁾ to studying the diffusion of p-aminosalicylic acid, isoniazid, and pyrazinamide with a range of molecular weight of 123-430 Da, through PGM mucin gel (4% w/v). For each compound the permeability of aqueous solution compared to PGM solutions decreased of ~4 (isoniazid and p-aminosalicylic acid) and 2-folds (pyrazinamide) indicating a significant reduction in permeation due to the mucus solutions and that indicate that absorption of nebulized drugs can be reduced by drug-mucin interactions.

To understand the size-filtering effect, diffusion experiments were carried out using FL-Na (376 Da) and FITC-dex probes at different molecular weight (4-70kDa) through three mucin concentration (1, 3 and 5%). Buffer permeability studies (0% PGM) were performed to provide a baseline to compare with mucus solution permeability. The physiological thicknesses of mucus layer ranges from 1 μm in the oral cavity to 500 μm in the gastrointestinal tract ⁽⁵²⁾ ⁽⁵³⁾ ⁽⁵⁴⁾ but the mucus thickness used for our studies to produce an experimental mucus layer was around 3 mm to ensure consistent mucus barriers that could be easily and reproducibly pipetted to form a homogenous layer on the support membrane.

A reduction in effective diffusion was observed with the increase of probes molecular weight (376-70 kDa) and increment of PGM concentration (1-3%). All probes showed a significantly increased permeation lag-time, associated with decreased steady-state solutes fluxes, when buffer solution was substituted by 1% PGM. Moreover, the retardation of solutes appeared greatly enhanced for molecules with a molecular weight >10 kDa.

The diffusion coefficients for each probes used was defined by the Stokes Einstein equation. Is it possible to calculate the diffusion coefficient from the Daynes and Barrier lag time relationship (eq. 3.1) ⁽⁵⁵⁾ where “D” is the diffusion coefficient, “ τ ” the lag time and “h” is the barrier thickness but the difficulty to use this equation resulted from the complexly of the barrier used represented by two different materials; membrane support and mucin thickness.

$$\text{Eq. 3.1 } D = \frac{h^2}{6\tau}$$

Desai, Mutlu ⁽⁵⁶⁾ used a Perspex diffusion chamber to study the permeation through native porcine gastric mucus of ¹²⁵I-labelled solute in a range of 148-200000 Da (Na⁺, lysozyme, rennet, bovine serum albumin and glucose oxidase). The passage through mucin gels appeared greatly restricted for solute at molecular weights >30 kDa Daltons (5-fold decrease) and solute flux decreased of ~30-fold when comparing Na¹²⁵I (148 Da) and glucose oxidase (200 kDa). The membrane, to support the mucus solution used by Desai and co-worker, had a pore size of ~100 nm, about 10 times larger of the largest molecules used, glucose oxidase (13 nm), leading them to suppose than mucus layer may have significantly affected the molecules diffusion.

In the experiments we performed, the largest molecules used were 9, 12 nm (FD40 and FD70), while the membrane used had pore size of ~15 nm, so the diffusion of larger solutes through 3D cylindrical pores of the membrane support may have been retarded by the closeness between molecular size and membrane pore cut-off.

Most inhaled drug are small molecules used for the symptomatic relief of chronic diseases such as asthma. To date, there is very little published data that reports upon mucin binding of inhaled drug solutes ^(15,57). With the closure of the Novartis R&D site

in Horsham UK the project shifted focus to the study of small molecule interactions with mucus. In this chapter amiloride and benzamil were used as examples of inhaled experimental therapeutics for investigation of their transport through PGM.

Amiloride and benzamil have similar molecular weights (229.6 and 319.8 Da respectively) but surprising the percentage of mass transported through the experiment was lower for benzamil (~27%) than amiloride (37%) and the relative decrease in transport rate observed when increasing PGM concentration was ~2 to 3 times higher for benzamil than amiloride and FL-NA. A structural comparison of the two solutes show that the introduction of a benzyl group onto the amiloride guanidine group leads to a significant retardation in the transport rate through PGM. The increased hydrophobicity of benzamil may have enhanced the interaction with the hydrophobic pocket of mucus glycoprotein.

The mucus lining the upper respiratory tract may adversely affect the absorption and action of aerosolized drugs which may lead to a dramatic change of the drug's efficiency in vivo. Therefore, the investigation of drug binding to mucus is extremely important to understand the importance of hindered diffusion of inhaled compounds.

Diffusion of solutes through mucin is an important factor in the design of drugs which have to diffuse through the mucus layer and the identification of parameters involved into the drug-mucin interaction will help the design of new drug molecules.

Conclusion

In this chapter we have investigated different mucus models to be used for diffusion studies of solutes in a molecular range of 376-70000 Da. Following the low mucus production of mucus-producing cells and high DNA contamination of the *ex vivo* porcine mucus, diffusion experiments have been performed using a commercial mucin PGM which showed low contain of genetic material.

In transport assay, the substitution of buffer solution with 1%PGM significantly affected the diffusion of all probes although, from this study, is not clear the relationship between solutes >10 kDa molecular weight and mucus “size-filtering” due to the closeness of the size of two probes used (FD40 and FD70) to the membrane cut-off. Although the “size-filtering” appears to not significantly affect the diffusion of macromolecule 376- 4000 Da, surprising the mucin gel permeation of two small molecules <500 Da, amiloride and benzamil, appears different with benzamil showing a retarded diffusion.

The results of these studies indicate that the “interaction-filtering” may reduce permeation rates across mucus layers also of same size molecules and could play an important role in reduced inhaled drug disposition. Therefore, further studies are needed to investigate mucin-amiloride analogues interaction.

3.5 Reference

1. Thornton DJ, Sheehan JK. From mucins to mucus: toward a more coherent understanding of this essential barrier. *Proceedings of the American Thoracic Society*. 2004;1(1):54-61.
2. Carlstedt I, Sheehan JK. Structure and macromolecular properties of cervical mucus glycoproteins. *Symposia of the Society for Experimental Biology*. 1989;43:289-316.
3. Jachak A, Lai SK, Hida K, Suk JS, Markovic N, Biswal S, et al. Transport of metal oxide nanoparticles and single-walled carbon nanotubes in human mucus. *Nanotoxicology*. 2012;6(6):614-22.
4. Lai SK, Hida K, Shukair S, Wang YY, Figueiredo A, Cone R, et al. Human immunodeficiency virus type 1 is trapped by acidic but not by neutralized human cervicovaginal mucus. *Journal of virology*. 2009;83(21):11196-200.
5. Boegh M, Nielsen HM. Mucus as a barrier to drug delivery - understanding and mimicking the barrier properties. *Basic & clinical pharmacology & toxicology*. 2015;116(3):179-86.
6. Chang M, Alsaigh T, Kistler EB, Schmid-Schonbein GW. Breakdown of mucin as barrier to digestive enzymes in the ischemic rat small intestine. *PloS one*. 2012;7(6):e40087.
7. Fishman JE, Levy G, Alli V, Zheng X, Mole DJ, Deitch EA. The intestinal mucus layer is a critical component of the gut barrier that is damaged during acute pancreatitis. *Shock*. 2014;42(3):264-70.
8. Suk JS, Kim AJ, Trehan K, Schneider CS, Cebotaru L, Woodward OM, et al. Lung gene therapy with highly compacted DNA nanoparticles that overcome the mucus barrier. *Journal of controlled release : official journal of the Controlled Release Society*. 2014;178:8-17.
9. Olmsted SS, Padgett JL, Yudin AI, Whaley KJ, Moench TR, Cone RA. Diffusion of macromolecules and virus-like particles in human cervical mucus. *Biophysical journal*. 2001;81(4):1930-7.
10. Lieleg O, Ribbeck K. Biological hydrogels as selective diffusion barriers. *Trends in cell biology*. 2011;21(9):543-51.
11. Dawson M, Wirtz D, Hanes J. Enhanced viscoelasticity of human cystic fibrotic sputum correlates with increasing microheterogeneity in particle transport. *The Journal of biological chemistry*. 2003;278(50):50393-401.
12. Lai SK, O'Hanlon DE, Harrold S, Man ST, Wang YY, Cone R, et al. Rapid transport of large polymeric nanoparticles in fresh undiluted human mucus. *Proc Natl Acad Sci U S A*. 2007;104(5):1482-7.
13. Lai SK, Wang YY, Hida K, Cone R, Hanes J. Nanoparticles reveal that human cervicovaginal mucus is riddled with pores larger than viruses. *Proceedings of the National Academy of Sciences of the United States of America*. 2010;107(2):598-603.
14. Davis SD, Bruns WT. Effects of sputum from patients with cystic fibrosis on the activity in vitro of 5 antimicrobial drugs on *Pseudomonas aeruginosa*. *The American review of respiratory disease*. 1978;117(1):176-8.
15. Huang JX, Blaskovich MA, Pelington R, Ramu S, Kavanagh A, Elliott AG, et al. Mucin Binding Reduces Colistin Antimicrobial Activity. *Antimicrobial agents and chemotherapy*. 2015;59(10):5925-31.

16. Bhat PG, Flanagan DR, Donovan PD. Drug binding to gastric mucus glycoproteins. *Int J Pharm.* 1996;134(1-2):15-25.
17. Groo AC, Lagarce F. Mucus models to evaluate nanomedicines for diffusion. *Drug discovery today.* 2014;19(8):1097-108.
18. Wadell C, Bjork E, Camber O. Nasal drug delivery--evaluation of an in vitro model using porcine nasal mucosa. *European journal of pharmaceutical sciences : official journal of the European Federation for Pharmaceutical Sciences.* 1999;7(3):197-206.
19. Takatsuka S, Kitazawa T, Morita T, Horikiri Y, Yoshino H. Enhancement of intestinal absorption of poorly absorbed hydrophilic compounds by simultaneous use of mucolytic agent and non-ionic surfactant. *European journal of pharmaceuticals and biopharmaceutics : official journal of Arbeitsgemeinschaft fur Pharmazeutische Verfahrenstechnik eV.* 2006;62(1):52-8.
20. Vllasaliu D, Fowler R, Garnett M, Eaton M, Stolnik S. Barrier characteristics of epithelial cultures modelling the airway and intestinal mucosa: a comparison. *Biochemical and biophysical research communications.* 2011;415(4):579-85.
21. Grubel P, Cave DR. Factors affecting solubility and penetration of clarithromycin through gastric mucus. *Alimentary pharmacology & therapeutics.* 1998;12(6):569-76.
22. Dawson M, Krauland E, Wirtz D, Hanes J. Transport of polymeric nanoparticle gene carriers in gastric mucus. *Biotechnology progress.* 2004;20(3):851-7.
23. Schuster BS, Suk JS, Woodworth GF, Hanes J. Nanoparticle diffusion in respiratory mucus from humans without lung disease. *Biomaterials.* 2013;34(13):3439-46.
24. Shaw LR, Irwin WJ, Grattan TJ, Conway BR. The influence of excipients on the diffusion of ibuprofen and paracetamol in gastric mucus. *Int J Pharm.* 2005;290(1-2):145-54.
25. Bhat PG, Flanagan DR, Donovan MD. Drug diffusion through cystic fibrotic mucus: steady-state permeation, rheologic properties, and glycoprotein morphology. *Journal of pharmaceutical sciences.* 1996;85(6):624-30.
26. Groo AC, Saulnier P, Gimel JC, Gravier J, Ailhas C, Benoit JP, et al. Fate of paclitaxel lipid nanocapsules in intestinal mucus in view of their oral delivery. *International journal of nanomedicine.* 2013;8:4291-302.
27. Mowbray. *A Comparative Pharmacokinetic (pk) Analysis Of Systemic Vs. Inhaled Administration Of Therapeutic Biologics.* American Thoracic Society. 2016.
28. Button B, Cai LH, Ehre C, Kesimer M, Hill DB, Sheehan JK, et al. A periciliary brush promotes the lung health by separating the mucus layer from airway epithelia. *Science.* 2012;337(6097):937-41.
29. Sheehan JK, Kesimer M, Pickles R. Innate immunity and mucus structure and function. *Novartis Foundation symposium.* 2006;279:155-66; discussion 67-9, 216-9.
30. Gray TE, Guzman K, Davis CW, Abdullah LH, Nettekheim P. Mucociliary differentiation of serially passaged normal human tracheobronchial epithelial cells. *American journal of respiratory cell and molecular biology.* 1996;14(1):104-12.
31. Mall M, Kreda SM, Mengos A, Jensen TJ, Hirtz S, Seydewitz HH, et al. The DeltaF508 mutation results in loss of CFTR function and mature protein in native human colon. *Gastroenterology.* 2004;126(1):32-41.

32. Malavia NK, Mih JD, Raub CB, Dinh BT, George SC. IL-13 induces a bronchial epithelial phenotype that is profibrotic. *Resp Res.* 2008;9.
33. Atherton HC, Jones G, Danahay H. IL-13-induced changes in the goblet cell density of human bronchial epithelial cell cultures: MAP kinase and phosphatidylinositol 3-kinase regulation. *American journal of physiology Lung cellular and molecular physiology.* 2003;285(3):L730-9.
34. Cereijido M, Robbins ES, Dolan WJ, Rotunno CA, Sabatini DD. Polarized monolayers formed by epithelial cells on a permeable and translucent support. *The Journal of cell biology.* 1978;77(3):853-80.
35. Lever AR, Park H, Mulhern TJ, Jackson GR, Comolli JC, Borenstein JT, et al. Comprehensive evaluation of poly(I:C) induced inflammatory response in an airway epithelial model. *Physiological reports.* 2015;3(4).
36. Tam A, Wadsworth S, Dorscheid D, Man SF, Sin DD. Estradiol increases mucus synthesis in bronchial epithelial cells. *PloS one.* 2014;9(6):e100633.
37. Goso Y, Hotta K. Dot blot analysis of rat gastric mucin using histochemical staining methods. *Analytical biochemistry.* 1994;223(2):274-9.
38. Whiteman P. Quantitative-Determination of Glycosaminoglycans in Urine with Alcian Blue 8gx. *Biochemical Journal.* 1973;131(2):351-7.
39. Argueso P, Balaram M, Spurr-Michaud S, Keutmann HT, Dana MR, Gipson IK. Decreased levels of the goblet cell mucin MUC5AC in tears of patients with Sjogren syndrome. *Investigative ophthalmology & visual science.* 2002;43(4):1004-11.
40. Round AN, McMaster TJ, Miles MJ, Corfield AP, Berry M. The isolated MUC5AC gene product from human ocular mucin displays intramolecular conformational heterogeneity. *Glycobiology.* 2007;17(6):578-85.
41. Carlstedt I, Sheehan JK, Corfield AP, Gallagher JT. Mucous glycoproteins: a gel of a problem. *Essays in biochemistry.* 1985;20:40-76.
42. Martens CJ, Inglis SK, Valentine VG, Garrison J, Conner GE, Ballard ST. Mucous solids and liquid secretion by airways: studies with normal pig, cystic fibrosis human, and non-cystic fibrosis human bronchi. *Am J Physiol-Lung C.* 2011;301(2):L236-L46.
43. Larhed AW, Artursson P, Bjork E. The influence of intestinal mucus components on the diffusion of drugs. *Pharmaceutical research.* 1998;15(1):66-71.
44. Winne D, Verheyen W. Diffusion coefficient in native mucus gel of rat small intestine. *The Journal of pharmacy and pharmacology.* 1990;42(7):517-9.
45. Fahy JV, Steiger DJ, Liu J, Basbaum CB, Finkbeiner WE, Boushey HA. Markers of mucus secretion and DNA levels in induced sputum from asthmatic and from healthy subjects. *The American review of respiratory disease.* 1993;147(5):1132-7.
46. Sirajuddin M, Ali S, Badshah A. Drug-DNA interactions and their study by UV-Visible, fluorescence spectroscopies and cyclic voltametry. *Journal of photochemistry and photobiology B, Biology.* 2013;124:1-19.
47. Macfarlane S, Woodmansey EJ, Macfarlane GT. Colonization of mucin by human intestinal bacteria and establishment of biofilm communities in a two-stage continuous culture system. *Applied and environmental microbiology.* 2005;71(11):7483-92.

48. Kocevar-Nared J, Kristl J, Smid-Korbar J. Comparative rheological investigation of crude gastric mucin and natural gastric mucus. *Biomaterials*. 1997;18(9):677-81.
49. Chaires JB, Dattagupta N, Crothers DM. Studies on interaction of anthracycline antibiotics and deoxyribonucleic acid: equilibrium binding studies on interaction of daunomycin with deoxyribonucleic acid. *Biochemistry*. 1982;21(17):3933-40.
50. Besterman JM, Elwell LP, Blanchard SG, Cory M. Amiloride intercalates into DNA and inhibits DNA topoisomerase II. *The Journal of biological chemistry*. 1987;262(27):13352-8.
51. Bhat PG, Flanagan DR, Donovan MD. Drug diffusion through cystic fibrotic mucus: Steady-state permeation, rheologic properties, and glycoprotein morphology. *J Pharm Sci*. 1996;85(6):624-30.
52. Kersey S, Allen A, Garner A. A simple method for measuring thickness of the mucus gel layer adherent to rat, frog and human gastric mucosa: influence of feeding, prostaglandin, N-acetylcysteine and other agents. *Clin Sci (Lond)*. 1982;63(2):187-95.
53. Sims DE, Horne MM. Heterogeneity of the composition and thickness of tracheal mucus in rats. *The American journal of physiology*. 1997;273(5 Pt 1):L1036-41.
54. Atuma C, Strugala V, Allen A, Holm L. The adherent gastrointestinal mucus gel layer: thickness and physical state in vivo. *American journal of physiology Gastrointestinal and liver physiology*. 2001;280(5):G922-9.
55. Daynes. The process of diffusion through a rubber membrane. *Proceedings of the Royal Society of London Series A, Containing Papers of a Mathematical and Physical Character*. 1920;97(685):286–307.
56. Desai MA, Mutlu M, Vadgama P. A study of macromolecular diffusion through native porcine mucus. *Experientia*. 1992;48(1):22-6.
57. Sakagami M, Byron PR. Respirable microspheres for inhalation: the potential of manipulating pulmonary disposition for improved therapeutic efficacy. *Clinical pharmacokinetics*. 2005;44(3):263-77.

**Chapter 4 : Understanding of physical-chemical relationship
between mucin-ENaC blockers interactions**

4.1 Introduction

The epithelium of the respiratory tract plays a major role in maintaining the conduit for air to and from the alveoli ⁽¹⁾ and thanks to the combined function of mucus secretion and ciliated cells the airway epithelium has a critical role in the defenses of the lung against particulates and pathogens inhaled from the environment ^(2, 3). The beating cilia of the epithelium are separated from the mucus layer by the presence of a periciliary liquid layer (PCL) (~7µm) and together, these two airway surface liquid components make up the airway surface liquid (ASL) ⁽⁴⁾. The efficiency of mucus clearance depends in large part on the volume and hydration state of both layers ⁽⁵⁾ which depends by the active action of ion transport processes involving the epithelial sodium channel of the glands and superficial epithelium ^(4, 6, 7).

ENaC is a key element for the maintenance of sodium balance in a number of epithelial tissues, is thought to play a significant role in influencing mucus hydration levels ⁽⁸⁾ and it is a target for several diseases characterized by aberrant epithelial Na⁺ transport such as in CF patients. In people with CF, ENaC is abnormally hyperactive with increment of Na⁺ and H₂O absorption, attributable to the impaired function of CFTR ⁽⁹⁾ resulting in a reduced Cl⁻/HCO₃⁻ and H₂O secretion. These effects lead to mucus dehydration and failure of MC.

A ENaC blocker would be predicted to improve hydration and MC reducing the rate of sodium and water absorption from the luminal aspect ⁽¹⁰⁾. This hypothesis is supported by *in vitro* data showing the amiloride (an epithelium sodium channel blocker) effect on

ASL height using confocal scanning microscopy, and variation of ASL volume measuring changes in concentration of blue dextran dye on primary cultures⁽¹¹⁾. However, *in vivo* clinical studies failed to demonstrate a significant improvement of MC after amiloride treatment^(10, 12). The failure of amiloride reflected both its low potency (IC₅₀ 0.34 μM) for ENaC blockade and short duration of action on airway surfaces^{(13) (14)}.

To achieve a more favorable pharmacological potency, the amiloride drug structure has been modified for the development of more potent, long-acting analogues for CF pharmacotherapy⁽¹⁴⁾. Benzamil and phenamil, two second generation amiloride analogs have been considered as ENaC blocker alternatives to amiloride. Both these ENaC blocker are significantly more potent than amiloride i.e. the ENaC IC₅₀ values for phenamil and benzamil are 17- and 9-fold lower than amiloride⁽¹⁵⁾ but their lipophilic character is associated with rapid absorption across both human and ovine bronchial epithelia⁽¹⁶⁾. This predicts increased absorption into the systemic circulation and resultant hyperkalemia.

Compound 552-02 and GS9411 (undisclosed structure) have been designed for inhaled dosing and appeared more potent than amiloride⁽¹⁷⁾ and considered a lead for CF treatment. After that GS9411 was reported to induce hyperkalemia⁽¹⁸⁾ the development of these compounds was halted.

NVP-QBE170 *in vitro* assay in NHBE showed a longer duration of action compared to amiloride and 552-02 and *in vivo* assay in guinea pig airways, showed an enhancement of potency and duration of action and no hyperkaliemia problems but the clinical

development have been halted due to the irritancy response in the airways after 28-day inhalation.

Defective function and expression of CFTR in CF are associated with mucus hypersecretion and dehydration which allow bacteria to grow leading to infection and inflammation. CF mucus is characterized by an increased carbohydrate content in the mucin, because of this, it has a highly branched oligosaccharide structure with higher tendency to interact and form gel which may lead to an obstruction of drug transport *in vivo* ⁽¹⁹⁾. This may be made worse by the presence of DNA, mostly coming from host cells or released from bacteria after antibody response ⁽²⁰⁾, and from alginate, a bacterial polysaccharides that may contribute to increase mucus viscoelastic properties ⁽²¹⁾ and diffusion rate of drug molecules and their efficiency of inhalation may dramatically decrease.

The literature reports the interaction of several drug molecules to mucus. Aminoglycosides activity, class of drug used to treat pseudomonal infection in CF, have been shown to be limited by mucin ⁽²²⁾; tobramycin was shown to interact to sputum ⁽²³⁾ and porcine mucin ⁽²⁴⁾, colistin or polymyxin E, polymyxin B shown interaction to porcine mucin ⁽²⁴⁾. Braybrooks, Barry ⁽²⁵⁾ reported that tetracyclines intestinal absorption was reduced by mucin and Bhat, Flanagan ⁽²⁶⁾ showed the interaction of albuterol to porcine gastric mucin.

The mechanism of interaction between mucus and inhaled drug molecules is rarely studied and poorly understood. Better understanding of the physico-chemical properties that dictate mucin-drug interactions may lead to the development of more efficacious therapies that are not bound by mucus.

For the determination of plasma protein binding most protocols describe the use of ultracentrifugation ^(27, 28) although improved throughput have been reported with the use of a 96-well equilibrium dialysis methodologies ⁽²⁹⁾. These methods have also been applied for the studying of mucus-drug interaction ^(23, 26) but to investigate the mechanism of mucin-drug interaction is necessary to develop and introduce simple methods which may be used for quick screening a range of drug candidates *in vitro*.

The aim of this chapter was to tested the hypothesis that inhaled amiloride analogues are bound by mucin and that the extent of binding can be correlated with standard physicochemical drug properties. To do so, our studies were motivated by the need to develop an easy method for the screening of a range of ENaC blocker designed by Novartis.

Initial studies used fluorescence and ultraviolet spectroscopy explored to study the mucin interactions of two prototype ENaC blockers, amiloride and benzamil. The need for a more sensitive and higher throughput system led us to develop a 96-well ultrafiltration assay. This method afforded the screening of a panel of 12 amiloride analogues with a range of physicochemical properties against three distinct CF sputum

Chapter 4

components i.e. mucin, DNA and alginate. Finally, we used restrictive Calu-3 monolayers to determine the effect of mucin on the rate of transepithelial transport of select amiloride analogues.

4.2 Material and methods

Materials

Amiloride, benzamil, rhodamine B, alginic acid sodium salt (sodium alginate, from brown algae), DNA from fish sperm, Tris (2-carboxyethyl) phosphine hydrochloride (TCEP) 0.5 M solution, FL-Na and FD4 and PGM (type III) containing ~0.5-1.5% of bound sialic acid were purchased from Sigma, Aldrich. Amiloride analogues were donated from Novartis (Basel, CH). MultiScreen Ultracel-10 Filter Plate 10 kDa (Product # MAUF01010) were purchased from Millipore (UK).

Methods

Fluorescence spectroscopy

Fluorescence spectra were recorded after mixing PGM solution (1 μM) titrated with amiloride or benzamil at different concentration (0.4, - 15.2 μM) (Chapter 2 section 2.4.10). Effect of solvent polarity on the fluorescence emission 100 mM of amiloride or benzamil was tested as described in Chapter 2 section 2.4.11. Fluorescence spectra were recorded on Hitachi Fluorescence FL-4500 in 1cm Quartz cells (Chapter 2 section 2.4.10).

UV-Visible spectrophotometry

Mucin solution, 0.5 μM , was mixed with amiloride or benzamil at different concentration (0.0-130 μM). The absorption spectra were obtained from an Agilent technologies Cary 60 spectrophotometer in a range of 200-450 nm using a Quartz cuvette with 1 cm path length (Chapter 2 section 2.4.11).

Ultrafiltration binding assay

ENaC blockers were mixed with either PGM mucin solution (ratio from 1:1 to 200:1), alginate (ratio 20:1) or DNA (ratio 20:1) and experiments performed as described in Chapter 2 section 2.5.4 and 2.5.12.

Some experiments included TCEP-treatment of mucin to study the binding of benzamil and 552-02 (drug: mucin molar ratio 20:1) (see Chapter 2 section section 2.5.5)

Mass balance was determined as described in Chapter 2 section 2.5.8 and the extent of specific and non-specific binding was calculated as following;

$$\text{bound drug to mucin (mol/mol)} = \frac{(D_{\text{ultrafiltrate}} - D_{\text{mixture ultrafiltrate}}) \times V_{\text{initial}}}{\text{Mucin moles in } V_{\text{initial}}}$$

Calu-3 cells culture

Calu-3 cell culture reagents and media preparation are described in Chapter 2 section 2.6.1. Cells were seeded onto polyester Transwell supports using a liquid covered culture as described in Chapter 2 section 2.6.2 and Monolayer integrity was evaluated by transepithelial electrical resistance (TER) (Chapter 2 section 2.1.5).

Permeation assay

Transport studies were performed as described in Chapter 2 section 2.6.4.

Transportation studies were also performed using a mixture of purified porcine jejunal mucin (0.5 μM) and 552-02 (20 μM) (Chapter 2 section section 2.6.5).

Chapter 4

Compound analyses by High-Performance Liquid Chromatography (HPLC)

Amiloride and analogues were analyzed onto a Phenomenex Luna C18 column (250x 4.6 mm 5 μ m) attached to a Perkin Elmer HPLC system equipped with a Perkinelmer LC 240 fluorescence detector (UK). Analytes were resolved using an isocratic method for the binding assay (Chapter 2 section 2.3.5.2) and using a linear gradient for analyzing samples from permeation assay (Chapter 2 section 2.6.6).

Compound analysis microplate fluorescence spectroscopy

A microplate reader Polarstar Optima (BMG LabTech) was used for FL-NA, FD4 and rhodamine B analysis as described in section Chapter 2 section 2.5.7.

4.3 Results

4.3.1 Identification of amiloride and benzamil binding to PGM study by fluorescence and UV-Visible spectrophotometry

Amiloride and benzamil are both strongly fluorescent molecules showing an excitation and emission in aqueous solution of 362 and 417 nm and 366 and 412 nm, respectively. Mucin is a glycoprotein which has a weak intrinsic fluorescence due to a low abundance of aromatic amino acids with excitation and emission maxima of 290 nm and 350 nm respectively.

The interaction of mucin with amiloride and benzamil was evaluated firstly by exploring the fluorescence signal of the drug after titration into PGM solution (1 μM). The fluorescence spectra of the mixtures at different concentrations are shown in Figure 4.1 A and B. An incremental and proportional increase in fluorescence intensity was observed upon titration of both amiloride and benzamil. The two compounds in PBS pH 6.8) and in absence of mucin have a strong fluorescence emission at 417 nm for amiloride and 415 nm for benzamil (data not shown) but when the mixture mucin-drug was considered the emission peak of amiloride did not shift significantly staying stable at 419 nm for each concentration of drug used (Figure 4.1 Aa). In contrast, in the mixture mucin-drug, benzamil at the lower concentration, 0.8 μM , showed a maximum emission wavelength of 422 nm but following the addition of more benzamil there is a blue shift of the fluorescence emission peaks to 417 nm (Figure 4.1 Bb) which may indicate that benzamil is placed in a less polar environment and less exposed to the solvent ^(30, 31).

Figure 4.2 shows a linear relationship between drugs concentration and fluorescence intensity in a concentration range of 0-15.2 μM for both amiloride and benzamil.

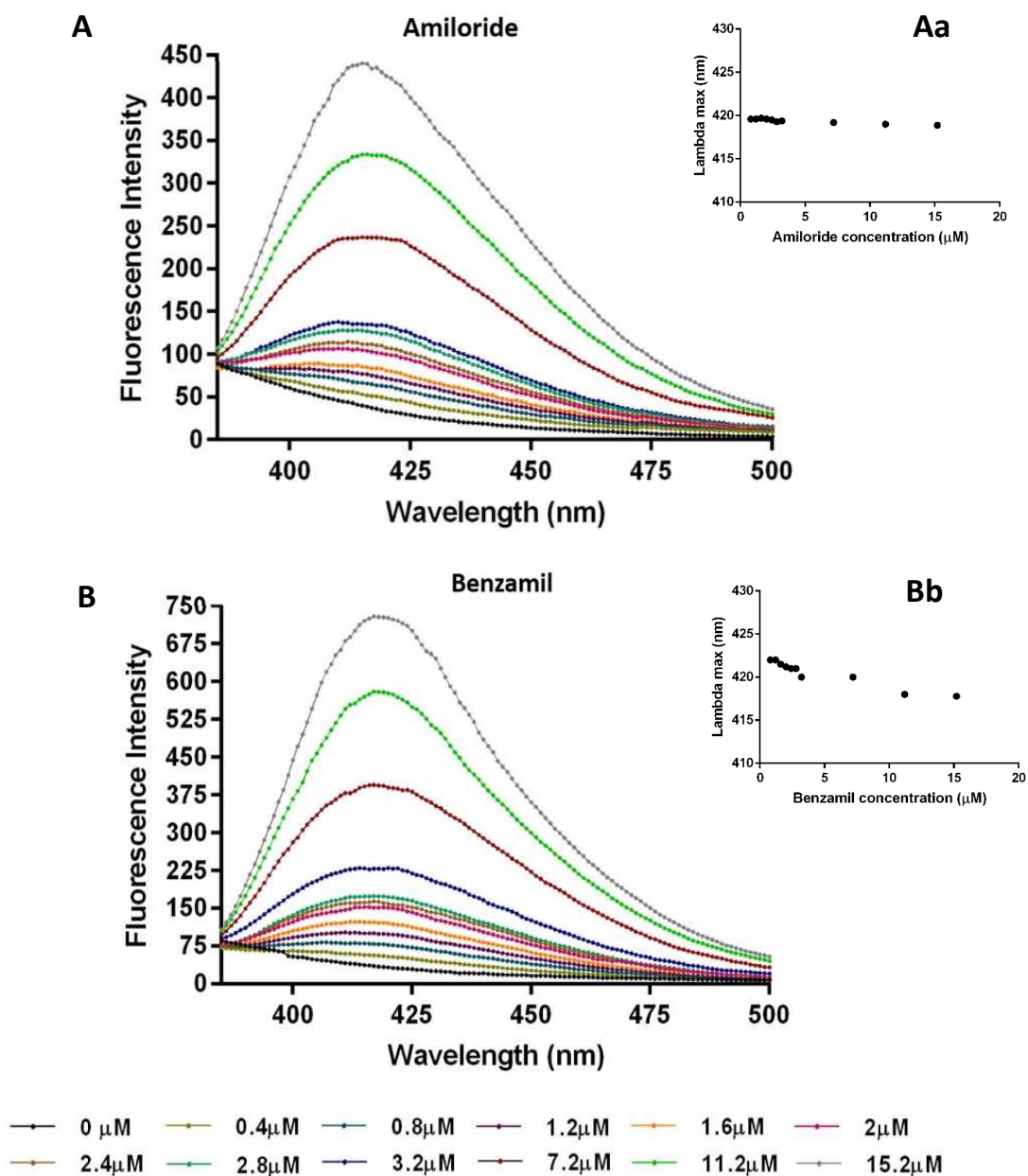


Figure 4.1. Fluorescent emission of amiloride and benzamil upon titration into mucin. Amiloride (A) and benzamil (B) was titrated with PGM (1 μM) and emission spectra recorded after excitation at 362 nm (amiloride) or 366 nm (benzamil). Amiloride lambda max was stable (Aa) whereas benzamil lambda blue shifted (Bb) as drug concentration increased.

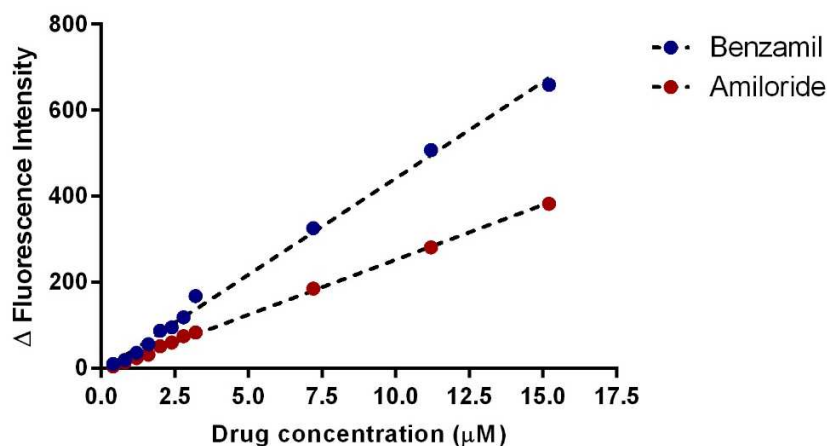


Figure 4.2. The linear relationship between Δ fluorescence intensity and drugs concentration. Δ fluorescence intensity increase proportionally to drug concentration (0.4-11.2 μM) during mucin titration (1 μM). Benzamil blue circle, amiloride red circle.

The fluorescence of 100 nM of amiloride and benzamil were than analyzed using different proportions of EtOH (from 0 to 100%). As shown in Figure 4.3 the fluorescence intensity increases as the proportion of the less polar solvent increases from 0 to 100%.

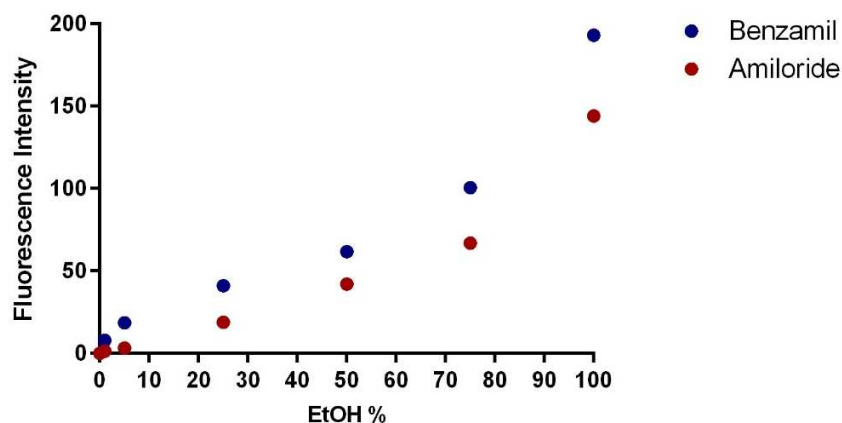


Figure 4.3. Fluorescence intensity of amiloride and benzamil in different proportions of EtOH. Fluorescent intensity of amiloride (red) and benzamil (blue) increase as EtOH % proportion increases. Data corrected for drug fluorescence at 0% EtOH.

Another simple and applicable method to investigate the formation of a complex is UV-Vis absorption measurement ⁽³²⁾. The absorption spectra of mucin in absence and

presence of amiloride or benзамил at different concentration are shown in Figure 4.4. The UV-vis spectra of mucin (0.5 μM) shows a strong peak at 260 nm while amiloride (Figure 4.4 A m) and benзамил (Figure 4.4 B n) both display strong absorbance bands at 290 and 366 nm which proportionally increases as the concentration of drug added is increases from 0.5 to 130 μM (Figure 4.4 a-l). Yet, mucin and drug compounds show a peak at 210 nm which increasing drug concentration appear to red-shift and the same was noticed increasing drug concentration in phosphate buffer solution (100mM NaH_2PO_4 50mM NaCl pH6.8) in absence of mucin (data not shown).

Figure 4.5 shows an extract of the UV absorbance data for amiloride and benзамил-mucin mixtures at three concentrations – 10 μM , (Figure 4.4 A, C), 70 μM , (Figure 4.4 B, D) and 130 μM , (Figure 4.4 C, F). For both drugs no peak shift of absorbance was noticed but comparing the spectrum of the mixture (mucin-drug) and the spectrum of a summed absorbance of mucin and drug alone is possible to notice differences between amiloride and benзамил (Figure 4.5).

In particular, during the titration of amiloride or benзамил into 0.5 μM mucin the mixture spectrum (Figure 4.5 dotted line) with amiloride at 10 μM (Figure 4.5 A) is similar to the control spectrum (Figure 4.5 A red solid line) but with increasing of drug concentration to 70 μM (Figure 4.5 B) and 130 μM (Figure 4.5 C) the peak at 260 and 290 nm decreased in the mixture spectrum.

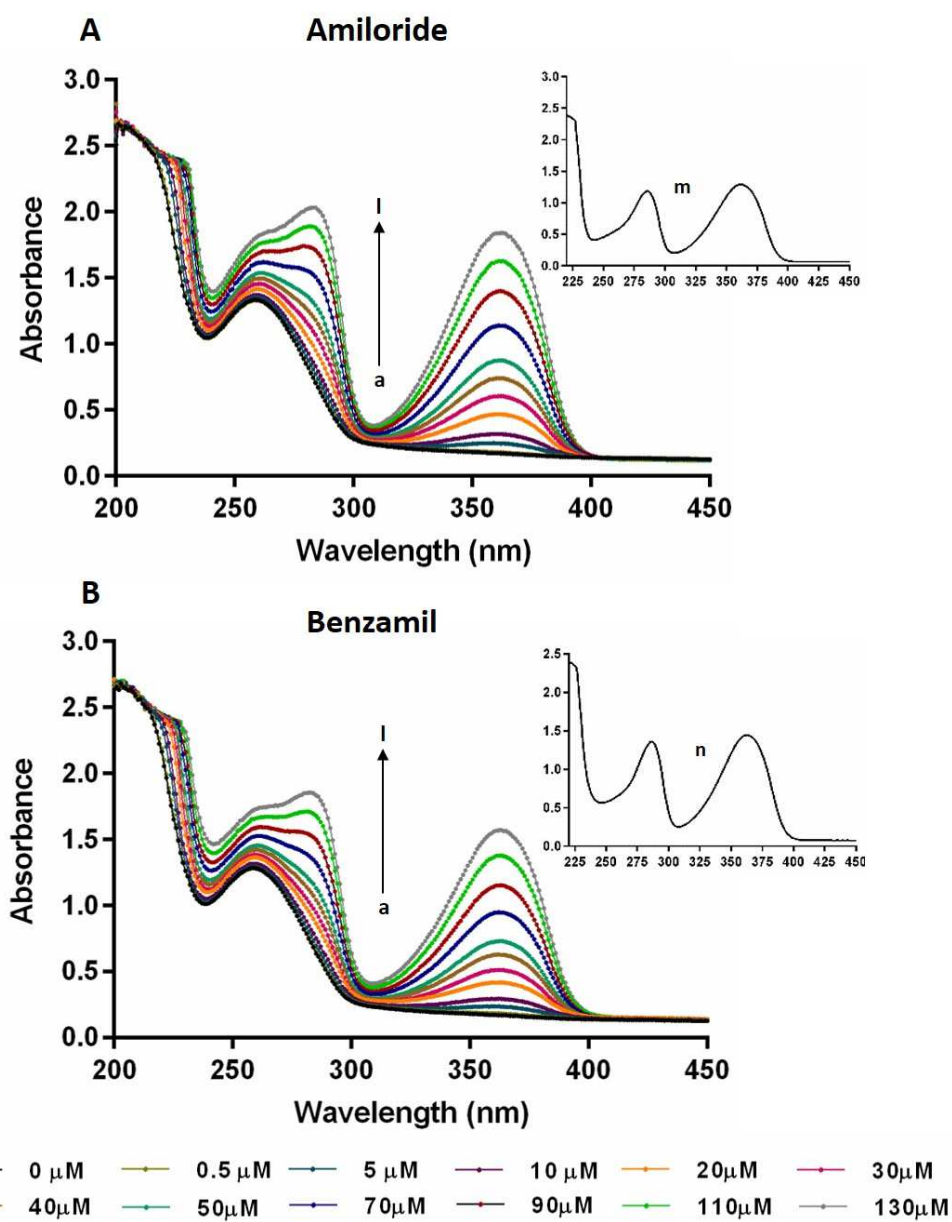


Figure 4.4. UV-Vis absorption spectra of the mixture mucin-drug in the presence of different concentration (a-l) of amiloride (A) or benzamil (B). The inserts in A and B are the spectrum of 90 μM amiloride and benzamil respectively. All spectra are buffer background corrected for PBS pH6.8.

Titration of benzamil into mucin (Figure 4.5 D, E and F) effected a larger change in absorbance, which is especially visible at the mucin 260 nm band and the 290 and 366 nm bands after titration with 70 (Figure 4.5 E) and 130 μ M benzamil (Figure 4.5 F). In fact, the absorption of the mixture appears lower compared with the summed absorbance of a pure benzamil and pure mucin solution (Figure 4.5 E and F, mixture solid blue line, control dotted line). The peak at 210 nm was noticed in the two drugs and mucin alone and for both amiloride and benzamil red-shift as drug concentration increases but not increment of absorbance was noticed. In fact, same shifting was noticed when increasing drug concentration in buffer solution without mucin (data not shown).

Although UV-Vis spectroscopy is a convenient method for studying small numbers of compounds in a detailed manner an alternative experimental method was required for screening larger numbers of compounds. Towards this end a 96-well ultrafiltration binding assay was explored as a method to screen a panel of amiloride analogues for mucin binding.

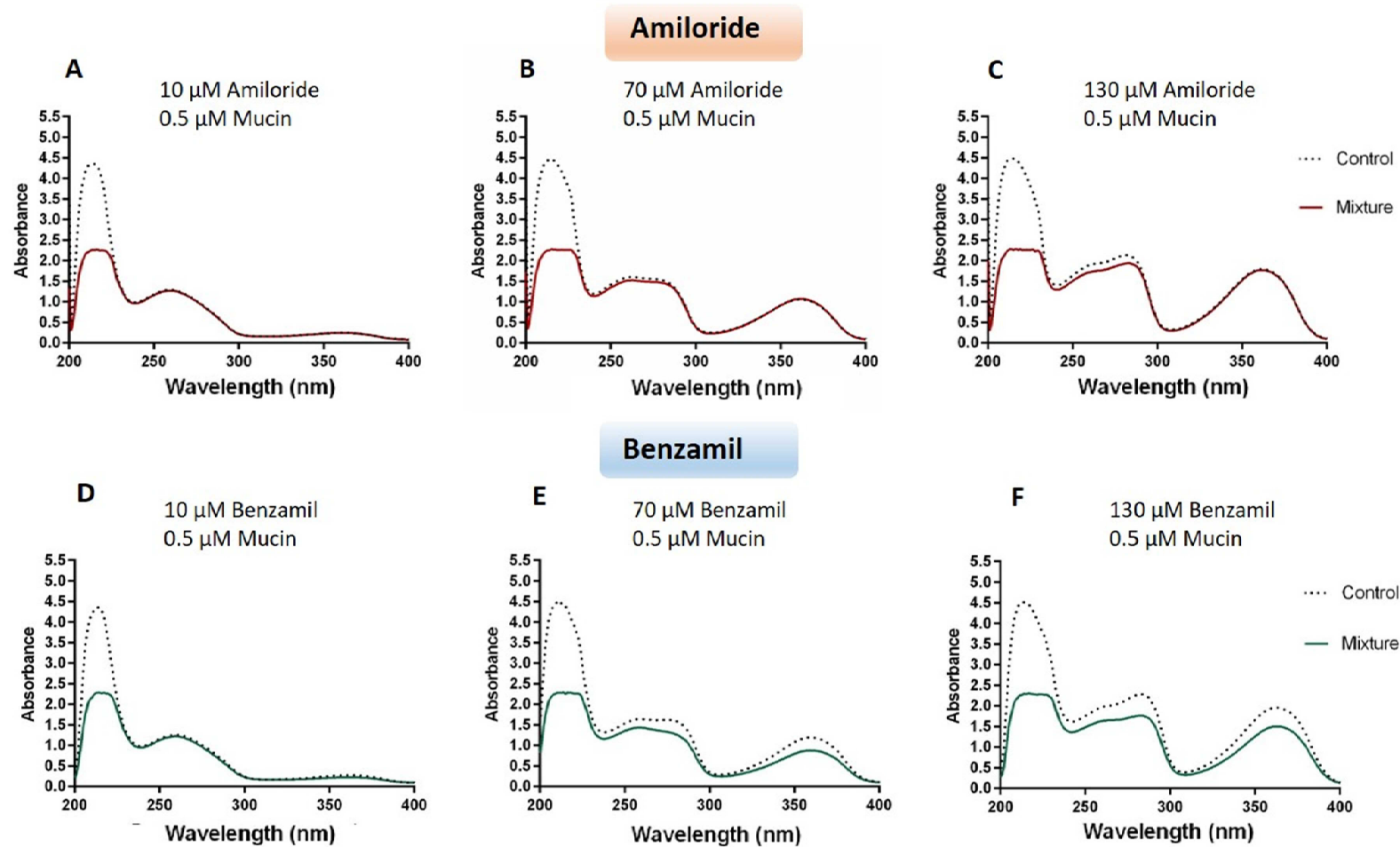


Figure 4.5. UV-Vis absorption UV-vis spectra of the mixture mucin-drug mixture (solid line) and summed absorbance of mucin and drug alone (control dotted line). A-F mixture and control spectrum of three representative concentrations (10,70,130 μM) used for mucin titration (0.5 μM) with amiloride (A-C) and benzamil (E-F). Data corrected for PO_4 buffer Abs

4.3.2 Development of fluorescence-based analytical methods for amiloride and analogues using PGM

Calibration curve ranges are shown in Table 2.3 in Chapter 2 which also includes coefficient of determination, excitation/emission wavelength, limit of detection, limit of quantification and internal standard used for each amiloride analogues for the ultrafiltration binding assay. From Table 2.3, it can be seen that all calibration curves were linear ($R^2 \geq 0.998$ for all compounds) and the LOQ was ~10 fold lower than the lowest calibration standard.

4.3.2.1 Validation of ultrafiltration binding assay using a multiscreen 96-wells plate

Ultrafiltration binding assays are widely used in pharmaceutical industry to screen candidate compounds for plasma protein binding^(33, 34). Cognizant of the non-uniformity of ultrafiltration across the MultiScreen plate experiments were performed to validate the method. These included the determination of mass balance for each well on the plate and the extent of non-specific binding to the plate.

The mass balance (recovery) was determined for each compound after ultrafiltration of the drug-mucin mixture in the ratio 1:1 to 200:1 and a mucin-free drug solution. For NVP-QE170 the highest ratio used was 20:1 (20 μ M :1 μ M) due to the solubility limit (100 μ M). The method developed involved the inclusion of a known mass of internal standard in the receiver chamber of the plate that was chromatographically resolvable from the analyte under investigation. HPLC analysis of the ultrafiltrate revealed both the analyte

and internal control concentration. The latter was used to determine the dilution factor and hence filtrate volume. The mass balance was determined for all drug-mucin ratio and resulted lower at the lower drug concentrations for all other compounds, due to NSB, but appeared to be very similar for each concentration of amiloride tested (data not shown).

Screening of 12 amiloride-based compounds for mucin binding at 20 μ M revealed a wide range of binding variability (Table 4.1). A concentration of 20 μ M was chosen as it lies in the concentration range expected in lung lining fluid following inhalation delivery of typical low molecular weight solute. This concentration was also easily detectable by HPLC and was far from the expected solubility limits of each drug tested.

Table 4.1 shows that all compounds have a recovery of over 95% with and without mucin. The only compound showing a low mass balance was GF-40-QQ33 which displayed a recovery of 66 and 72 % with and without mucin respectively and displayed also a high NSB (15%), possibly due to their highly lipophilic nature and low aqueous solubility. The NSB for all other compounds was not higher than 4.5%.

GF-40-QQ33, Benzamil and OC-73-KH00 displayed a high specific mucin interaction with 38> 33>21% respectively, followed by 552-02, JE-12-FK73 and UB-15-NR66 with 20> 18> 15%. Amiloride appears to be the compound with lowest percentage of mucin binding (0.7%) similar to FL-Na used as probe control. Other molecules that displayed a relatively low mucin interaction (lower than 15%) were MC-12-DR04, CA-91-YE87, KF-08-NW22,

OF-80-NSS22, and the dimer NVP-QBE170 with 7-12%. FD4 (MW 4 kDa) displayed a low mucin interaction (3%) but a very high NSB (~75%) probably due to the closeness to the membrane molecular weight which was 10kDa.

Table 4.1. Validation of ultrafiltration binding assay using PGM as mucin model. Compounds, FL-Na and FD4 mass balance in solution +/- mucin determinate by the use of internal standard, % NSB and % mucin binding determined after ultrafiltration assay. Data shown are mean \pm SD (n=3).

<i>Compounds</i>	<i>Mass Balance (%) - mucin</i>	<i>Mass Balance (%) + mucin</i>	<i>%NSB</i>	<i>% Mucin Binding corrected for %NSB</i>
CA-91-YE87	98.8 \pm 3.7	98.0 \pm 1.3	0.6 \pm 0.1	7.7 \pm 0.2
KF-80-NW22	114.0 \pm 3.0	103.2 \pm 7.3	0.4 \pm 0.9	9.7 \pm 0.6
UB-15-NR66	106.6 \pm 3.5	102.1 \pm 4.6	2.6 \pm 0.2	15.3 \pm 1.3
JE-12FK73	102.0 \pm 4.2	98.9 \pm 4.6	1.9 \pm 0.5	18.2 \pm 1.7
OC-73-KH00	99.6 \pm 2.5	96.6 \pm 3.8	4.5 \pm 3.7	21.2 \pm 1.7
Amiloride	99.0 \pm 2.2	101.0 \pm 1.8	0.3 \pm 0.5	0.7 \pm 0.4
OF-80-NS22	103.4 \pm 1.5	102.7 \pm 1.2	1.3 \pm 0.2	6.9 \pm 1.4
NVP-QBE170	103.3 \pm 0.3	104.1 \pm 3.1	1.1 \pm 0.9	6.7 \pm 0.7
MC-08-DR04	101.2 \pm 1.6	98.4 \pm 2.1	1.4 \pm 0.9	12.36 \pm 0.5
552-02	99.2 \pm 5.0	102.2 \pm 2.0	2.5 \pm 1.8	20.0 \pm 2.5
Benzamil	97.8 \pm 4.0	103.0 \pm 3.0	2.3 \pm 0.5	32.5 \pm 1.8
GF-40-QQ33	72.5 \pm 1.5	66.0 \pm 3.5	15.1 \pm 1.2	37.5 \pm 1.7
FL-Na	119.7 \pm 10	118.4 \pm 4.0	0.7 \pm 0.6	1.2 \pm 0.1
FD4	107.9 \pm 0.3	110.5 \pm 12.5	74.6 \pm 1.0	3.0 \pm 0.6

4.3.3 Isotherm binding and physical-chemical correlation between mucin (PGM) and amiloride analogues.

Based on the variability in the extent of mucin binding for ENaC blockers at 20 μ M, binding isotherms were constructed for each compound by plotting the free versus bound drug concentration across a range of drug: mucin ratios. The binding isotherms for 12 ENaC blockers plus two probes FL-Na and FD4 are shown in Figure 4.6 and 4.7.

For all eight compounds shown in Figure 4.6 the isotherm shows that the molar ratio of bound drug : mucin increases sharply, reaching a maximum with increasing free concentration of drug. Non-linear regression analysis demonstrated that the data were well described by the Langmuir monolayer absorption model (Eq. 4.1) where B_{max} is the maximal extent of binding, K_d is concentration of ligand necessary for half occupancy of the binding sites, X is the concentration of the ligand and Y is the specific binding.

Amiloride displayed the lowest molar ratio of bound drug to mucin (B_{max} 1.4 mol/mol) very similar to the control probe, FL-Na (Figure 4.7 E). For NVP-QBE170 at the highest ratio used (20:1) the bound drug is 1.2 mol/mol and for all other compounds in Figure 4.6 the bound drug was between 6 and 30 mol/mol. Langmuir monolayer absorption model was also followed by FL-Na and FD4 in Figure 4.7 (E-F) used as control.

For compounds shown in Figure 4.7 (A-C) the binding isotherm displayed a distinct trend to other compounds. At low concentrations the binding approached a pseudo-plateau around 100 μ M before increasing sharply at the highest tested concentration. This binding isotherm was not consistent with monolayer binding models such as the Langmuir isotherm. However, the isotherms were well described by the Guggenheim-Anderson-deBer (GAB) isotherm model (Eq. 4.2) where y is the amount of ligand bound per protein (mol/mol), q_m the amount of monolayer binding of ligand per protein (mol/mol), C_{eq} the free ligand concentration, and K_s and K_L are the monolayer and multilayer binding constant.

This model represents a multilayer liquid phase adsorption to mucin as described previously ⁽³⁵⁾. The non-linear regression model fit parameters for QQA using Langmuir isotherms gave a $R^2 < 0.250$ (data not shown). It is apparent from the model fit that the Langmuir model is inappropriate for application to these data.

$$(Eq. 4.1) \quad y = B_{max} \cdot \frac{x}{(K_d + x)}$$

$$(Eq. 4.2) \quad y = q_m \frac{K_s C_{eq}}{(1 - K_L C_{eq})(1 - K_L C_{eq} + K_s C_{eq})}$$

During our studies the Millipore MultiScreen plates were discontinued and only 4 different concentrations were used for the binding isotherm for CA-91-YE87 (Figure 4.7 D) and parameters did not converge with any equation although appears to follow the trend of its stereoisomer KF-80-NS22 (for structure see Chapter 2 section 2.6). Like for compound in Figure 4.6 also analogues in Figure 4.7 (A-D) displayed a large difference in the mucin binding with compounds KF-80-NS22 and CA-91-YE87 displaying the lowest molar ratio of bound drug to mucin of ~12 mol/mol at a ratio of 1: 200 (mucin : drug). OC-73-QQ33 (Figure 4.7 C) displayed the highest interaction to mucin with 42 mol/mol followed by JE-12-FK73 with molar ratio of bound drug to mucin of ~22 mol/mol.

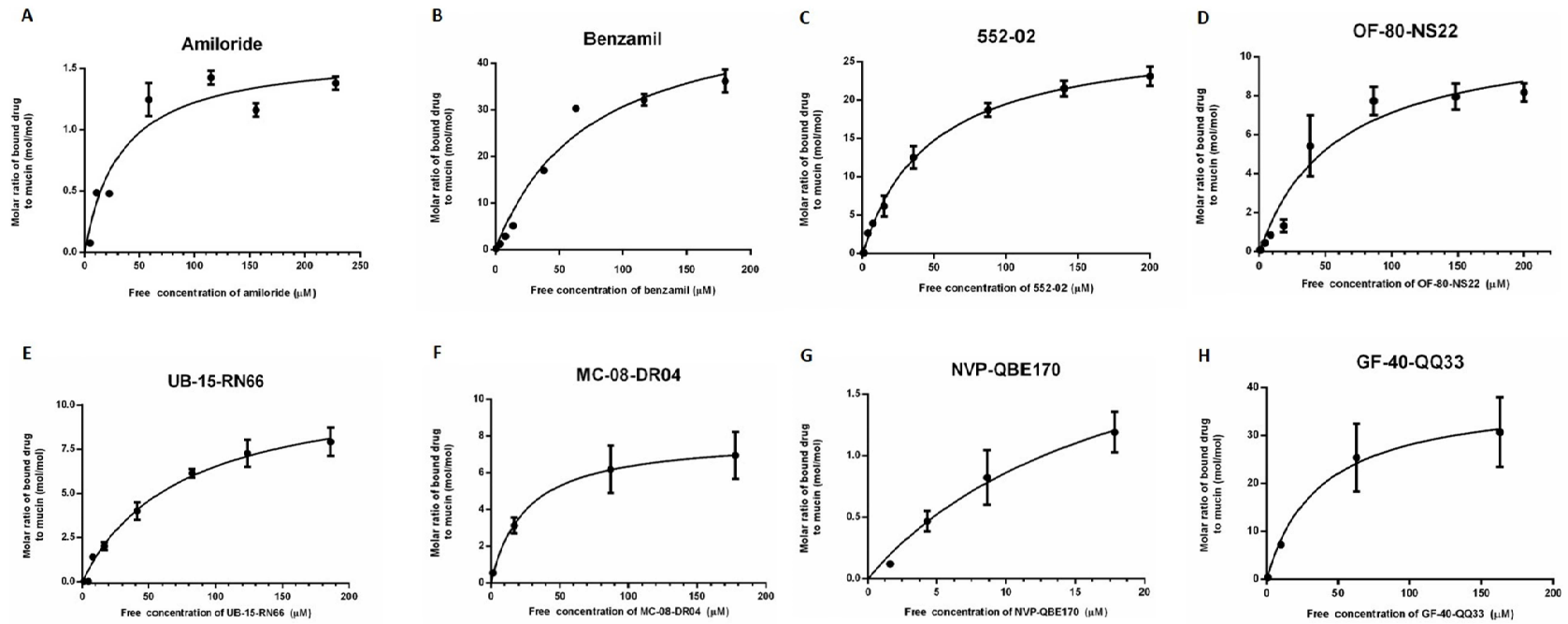


Figure 4.6. Drug-mucin binding isotherm(1). Data for each compound from the ultrafiltration binding assays were fitted by a langmuir model: $y=B_{\max} \cdot x/(K_d+x)$ using GraphPad Prism v5. Data shown are mean \pm SD, (n=3)

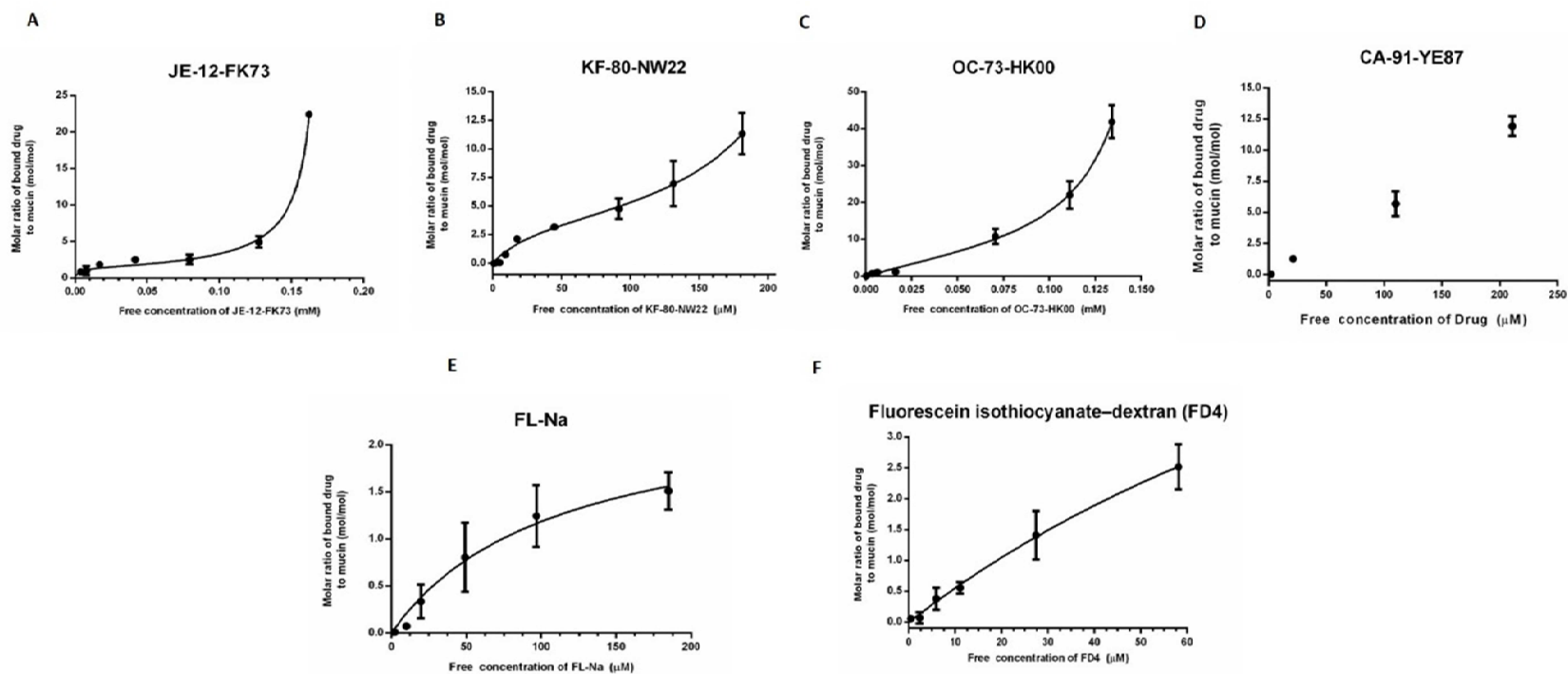


Figure 4.7. Drug-mucin binding isotherm (2). Data for compound A-D from the ultrafiltration binding assays were fitted by a GAB isotherm model: $y = q_m \cdot K_S C_{eq} / (1 - K_L C_{eq})(1 - K_L C_{eq} + K_S C_{eq})$
 Data for compound E and F were fitted by a languir model: $y = B_{max} \cdot x / (K_d + x)$ using GraphPad Prism v5. Data shown are mean \pm SD, (n=3)

Chapter 4

Seeking to correlate the extent of mucin binding with standard physicochemical properties we examined $\text{Log } P_{\text{octanol/water}}$, molecular weight, polar surface area (PSA), van der Waals Volume, polarizability, H-donor, H-acceptor, and rotatable bonds as determinant of binding (Table 4.2).

Taking together the 12 amiloride-based compounds there was a weak correlation between the extent of mucin binding and compounds physical properties. Figure 4.8 shows two examples of poor correlates of binding: $\text{Log } P_{\text{o/w}}$ ($R^2= 0.421$) and rotatable bonds ($R^2=0.360$) (Figure 4.8 A and B respectively). For the other physical-chemical properties the correlation was weaker, displaying a $R^2 < 0.200$ (data not shown).

Table 4.2. Physical properties of amiloride and analogues; Log $P_{o/w}$, PSA, MW, Van der Waals Volume, polarizability, H donor, H acceptor and rotatable bonds were calculated using Marvin Sketch 6.2 (Chemaxon)

	<i>Compounds</i>	<i>LogP_{o/w}</i>	<i>PSA (Å²)</i>	<i>MW</i>	<i>Van Der Waals Volume (Å³)</i>	<i>Polarizability</i>	<i>H Donor</i>	<i>H Acceptor</i>	<i>Rotatable bonds</i>
Quaternary Amine ↓	CA-91-YE87	-3.72	106.9	287.8	426.6	28.2	3	5	4
	KF-80-NW22	-3.72	106.9	287.8	426.6	28.2	3	5	4
	UB-15-NR66	-2.76	106.9	315.8	487.8	31.9	3	5	6
	JE-12FK73	-1.84	116.2	407.9	611.4	42.0	3	6	9
	OC-73-KH00	-0.19	145.3	583.1	902.1	62.1	4	7	15
Non-Quaternary Amine ↓	Amiloride	-0.89	156.8	229.6	250.8	19.6	5	7	1
	OF-80-NS22	-0.38	132.9	244.7	317.2	22.8	4	6	3
	NVP-QBE170	-0.3	329.2	755.6	937.8	70.5	10	16	6
	MC-08-DR04	0.02	110.2	258.7	359.8	24.6	3	6	4
	552-02	1.15	192.5	451.0	613.6	43.8	7	10	10
	Benzamil	1.45	142.8	319.8	394.5	30.8	5	7	3
	GF-40-QQ33	2.71	171.3	526.0	746.9	54.8	5	8	13
	FL-Na	-1.5	-	-	-	-	-	-	-
FD4	-2**	-	-	-	-	-	-	-	

** Log P obtained from literature

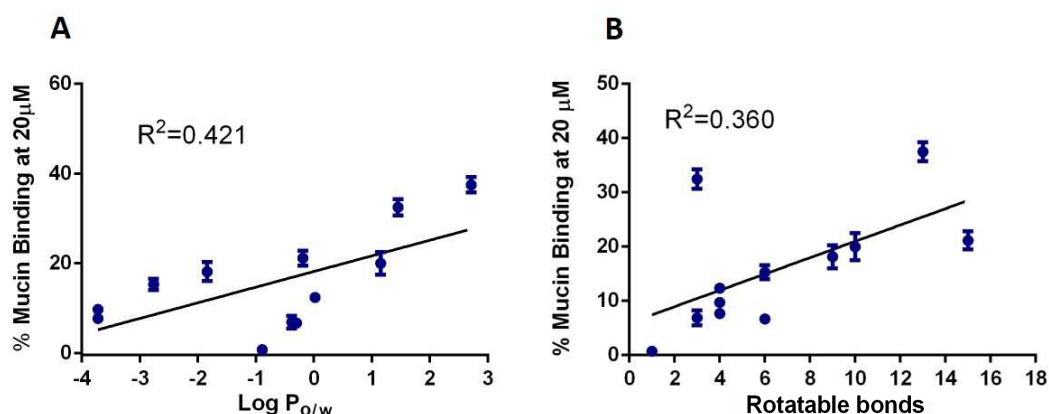


Figure 4.8. Mucin- binding at 20 μM correlated with amiloride and analogues physical parameters. A percentage of mucin binding vs Log P_{o/w}. **B** percentage of mucin binding vs rotatable bonds.

In particular, mucin binding versus Log P_{o/w} displayed clearly two trends. The percentage of mucin binding increases for compounds with a Log P_{o/w} between -3.72 to 0 and the same trend can be notice considering compounds with Log P_{o/w} in the range of ~-1 to 2.70, which is consistent with the polarity of the two groups, quaternary amine (QQA) and non-quaternary amine (NQQA) analogues (Table 4.2). Considering all physical properties shown in Table 4.2, a strong positive correlation was observed between mucin binding and Log P_{o/w} for both NQQA (R² =0.952) (Figure 4.9 A) and QQA (R² =0.899) (Figure 4.9 B). For NQQA other parameters were poor binding predictor (R² <0. 400). Opposite to this, for QQA a weaker but positive correlation with almost all physical properties was observed; van der Waals Volume (R²=0.770), rotatable bonds (R²=0.838), PSA (R² =0.613) (Figure 4.9 D, F, & H), polarizability (R² =0.767), molecular weight (R² =0.758), H acceptor (R² =0.730) (Figure 4.10 J, L & N). No correlation was possible to

observe with H donor as four of the QQA considered are characterized by the same number of H donor (Figure 4.10 P).

In the case of NQQA strong correlations were prohibited by a small sample set of four compounds. However, an inverse correlation was observable for PSA ($R^2=0.032$) and H donor ($R^2=0.023$) appear inversely correlated with the percentage of mucin binding. In Figure 4.9 C, mucin interaction appears to increase with increasing van der Waals volume for smaller molecules (amiloride, OF-80-NS22 and MC-08-DR04) but there is not clear correlation for benzamil, 552-02, GF-40-QQ33 and NVP-QBE170. For stronger correlations it would be necessary to extend the range of compound.

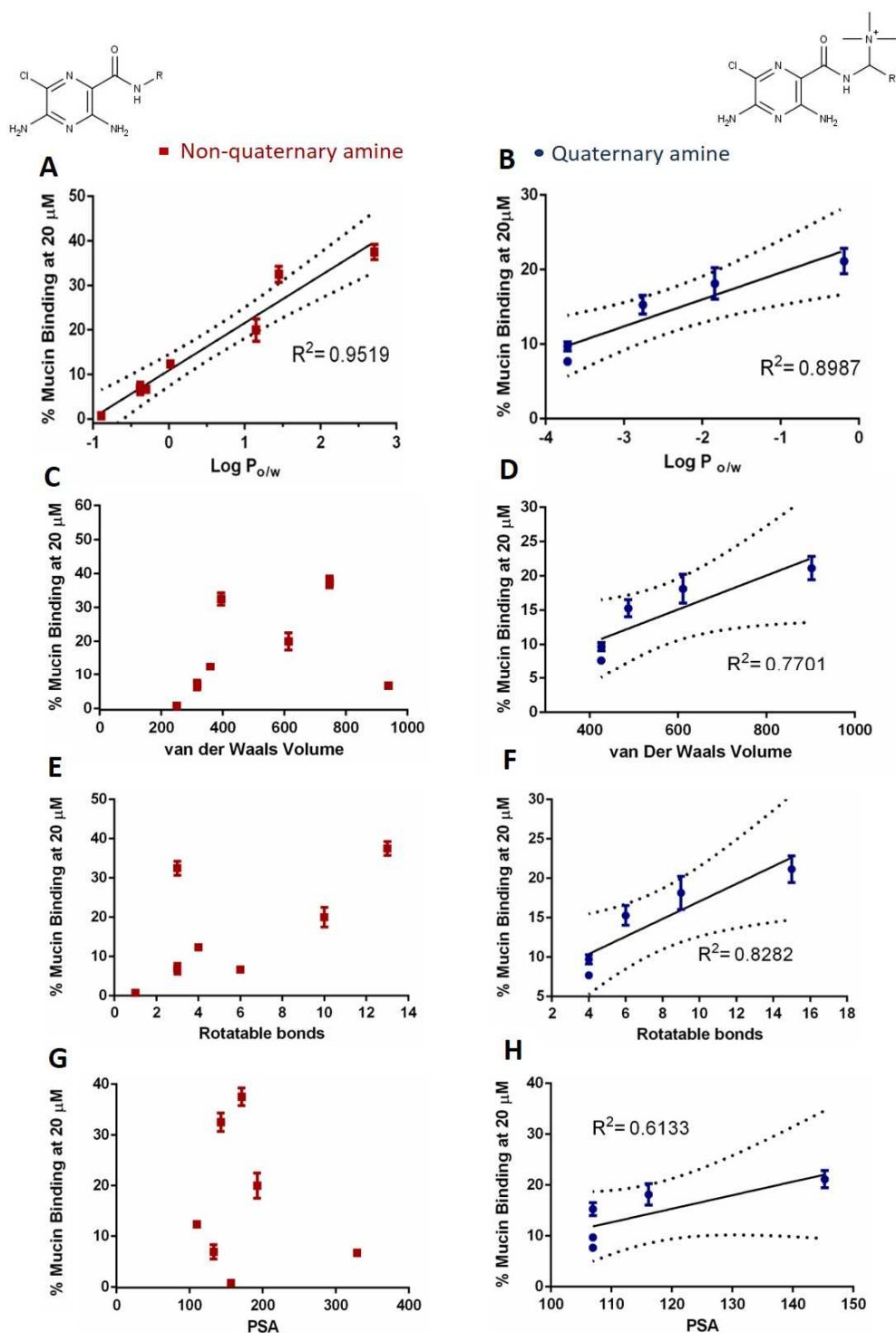


Figure 4.9. Mucin-binding at 20 μM correlated with amiloride and analogues physical parameters (1). Dashed lines indicate 95% confidence intervals. Mucin-binding of QQA (blue circle) and NQQA (red rectangles) analogues vs Log P (A-B), van der Waals Volume (C-D), rotatable bonds (E-F) and PSA (G-H). Data corrected for %NSB and shown are mean \pm SD (n=3)

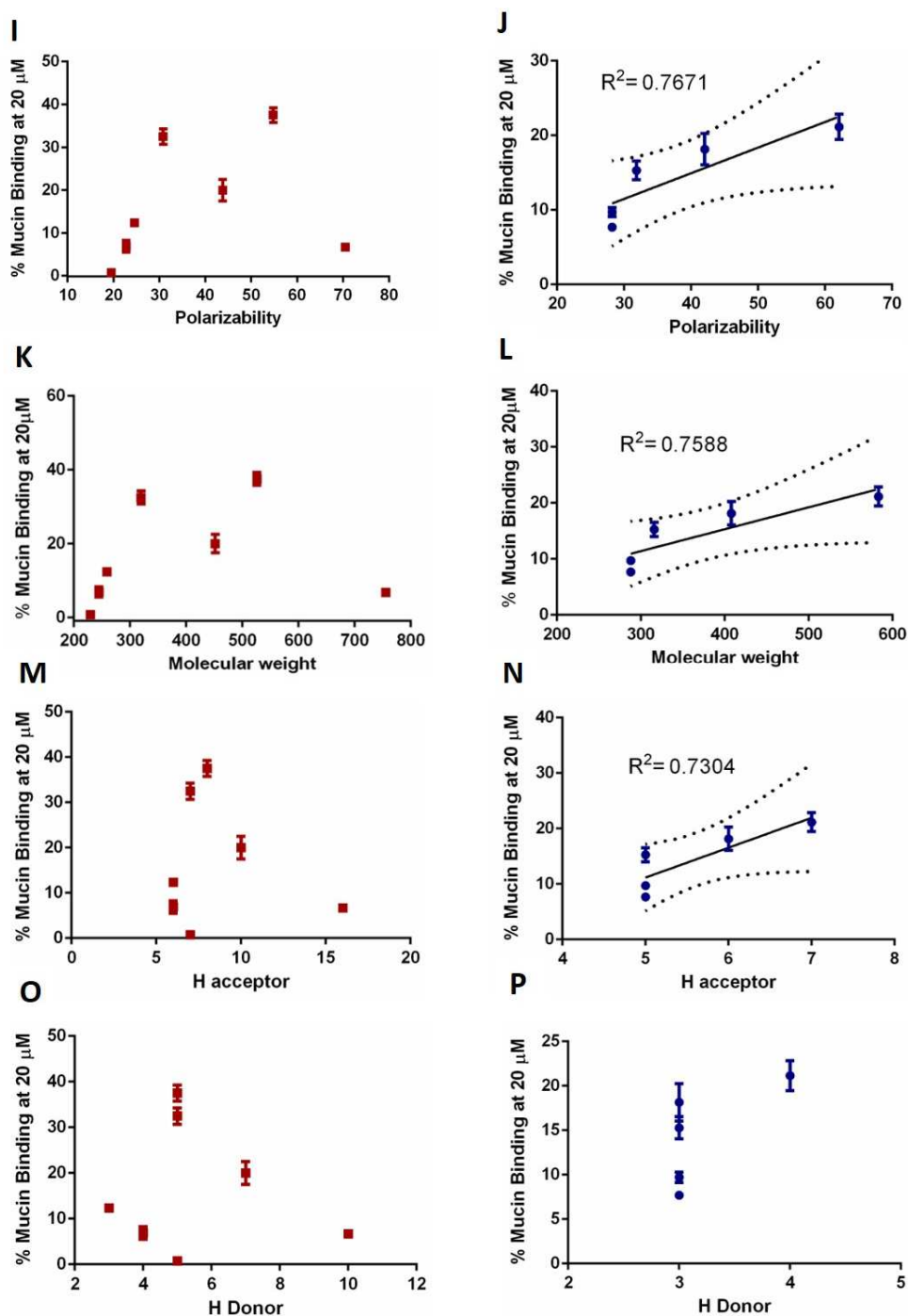


Figure 4.10. Mucin- binding at 20 μM correlated with amiloride and analogues physical parameters (2). Dashed lines indicate 95% confidence intervals. Mucin-binding of QQA (blue circle) and NQA (red rectangles) analogues vs polarizability (I-J), molecular weight (K-L), H acceptor (M-N) and H donor (O-P). Data corrected for %NSB and shown are mean \pm SD (n=3)

Moreover, the retention time of NQQA (Figure 4.11 A) and QQA (Figure 4.11 B) appeared correlated with $\text{Log } P_{o/w}$ (NQQA $R^2=0.833$, QQA $R^2=0.973$). The elution time is governed by the water solubility of the analogous and the carbon content of the molecules. In fact, for each group as the $\text{Log } P_{o/w}$ increases stronger is the interaction of the compounds with the stationary phase of the column being retained for a longer time.

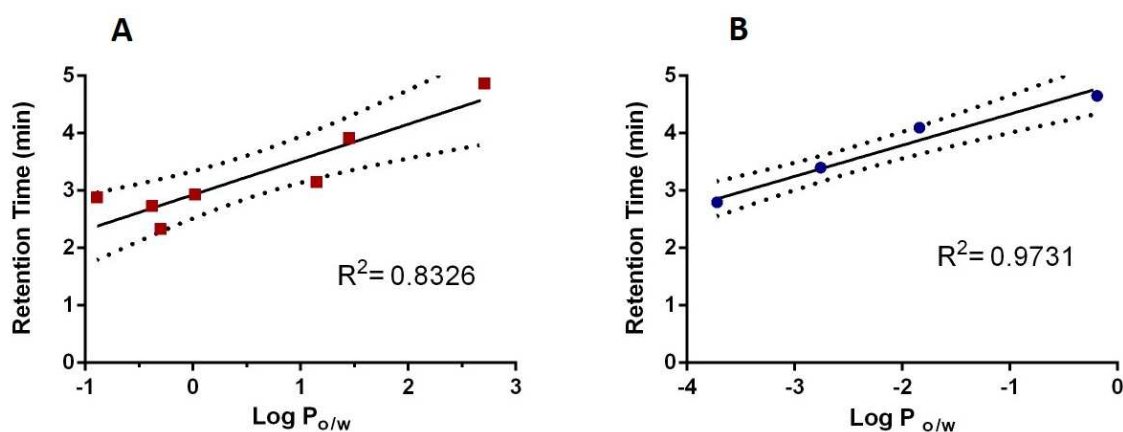


Figure 4.11. Retention time of amiloride and analogues correlated with $\text{Log } P_{o/w}$. Dashed lines indicate 95% confidence intervals. (A) NQQA, (B) QQA.

As shown in the Table 4.1, a part from GF-40-QQ33 which displayed a 15% NSB due to its high hydrophobic character, the percentage of NSB was not higher of 2.6 % all other amiloride analogues, and mucin binding (corrected for NSB) was at least 5-fold higher suggesting that the binding behavior is significantly alternated in the presence of mucin. In fact, $\text{Log } P_{o/w}$ was the physical properties with strongest correlation with percentage of mucin binding for both QQA and NQQA but resulted not correlated with percentage of NSB (Figure 4.12 A) as for van der Waals Volume (Figure 4.12 B) and other physical

properties (data not shown) indicating that the results of mucin binding were not affected by the device used.

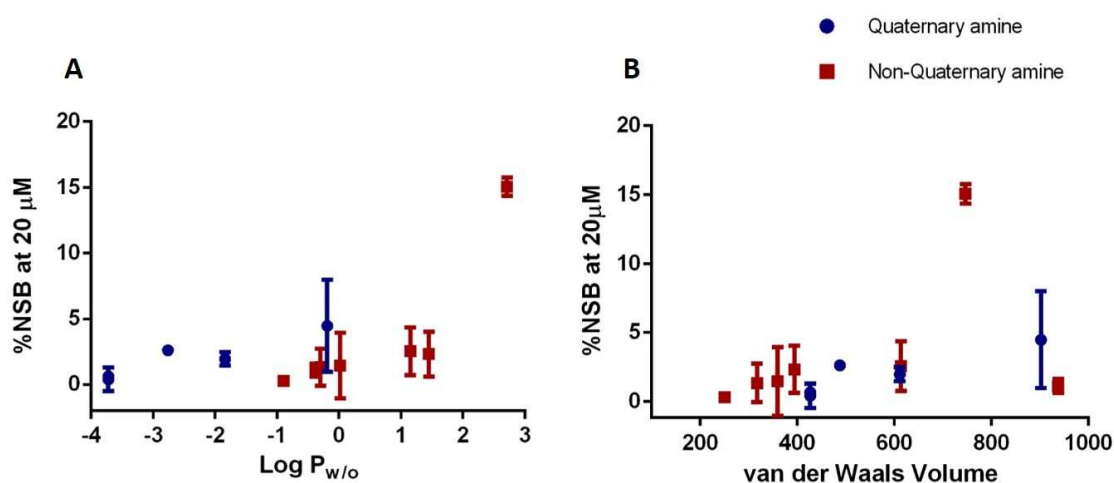


Figure 4.12. Non Specific Binding at 20 µM correlated with amiloride and analogues physical parameters. A % NSB vs Log P_{o/w}. B % NSB vs van der Waals Volume. Data shown are mean ± SD (n=3).

4.3.4 Influence of Alginate and DNA in ENaC blocker disposition.

ENaC blockers, as experimental therapeutics for CF, would encounter a complex cocktail of macromolecules in the airway lumen of a CF patients. Alginate and DNA are two macromolecule components of CF sputum that have been shown to sequester and attenuate the activity of inhaled molecules^{(36) (23)}. Moreover, amiloride is known to be a DNA binding molecule^{(37) (38)}. The ultrafiltration method was exploited to screen for binding of amiloride analogues to calf thymus DNA and brown algae alginate to understand whether also these two macromolecule may modulate the disposition of inhaled ENaC blockers.

Figure 4.13 shows the specific and non-specific binding of amiloride analogues to alginate. It is possible to see that the %NSB for NQQA non significantly changes the extend of binding in the presence of alginate staying under 5% for all range of compounds but GF-40-QQ33 displayed the highest %NSB at about 30%. The specific binding to alginate, calculated as the difference between binding in the presence and absence of alginate, was consistently less than 5% except for UB-15-NR66, JE-FK-73 and OC-73-HK00 that shown a specific interaction of 12, 15 and 18% respectively (Figure 4.13). The total and non-specific binding of the two quaternary ammonium stereoisomers, KF-08-NW22 and CA-91-YE87, were near identical ($p > 0.05$).

No strong correlations were observed between specific alginate at 20 μ M and eight commonly considered physicochemical parameters (Figure 4.14 and 4.15, red rectangle). Interestingly, a plot of alginate binding against QQA physical properties (Figure 4.14 and 4.15) displayed a similar positive correlation obtained for percentage of mucin (Figure 4.9 and 4.10). For example, Log $P_{o/w}$ ($R^2 = 0.875$) and rotatable bonds ($R^2 = 0.794$) (Figure 4.14 B & F) appear strongly correlated and weaker correlation was found for van der Waals Volume, polarizability, H acceptor and molecular weight (Figure 4.14 and 4.15) with $R^2 < 0.680$. No strong correlation was observed for PSA (Figure 4.14 H) and H donor (Figure 14.15 P) ($R^2 < 0.450$). This observation would suggest that similar binding interactions may occur between amiloride analogues and alginate as those that drive the

binding to mucin. However, it is noticeable that the extent of binding is greater for mucin than alginate.

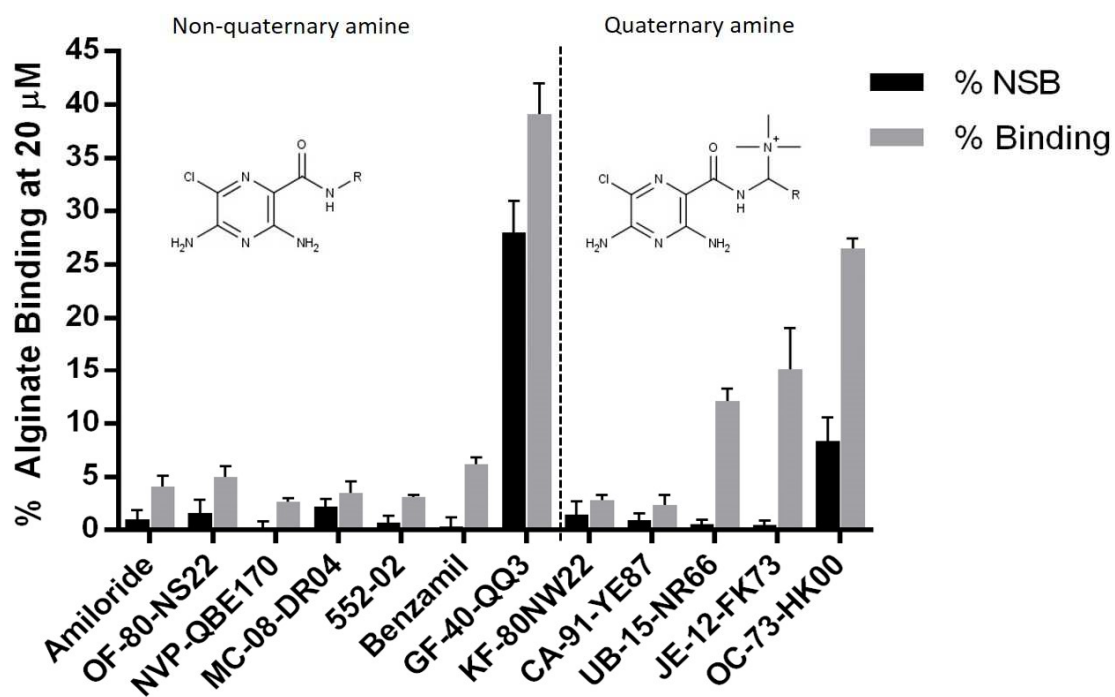


Figure 4.13. Alginate binding (gray bar) and non-specific binding (black bar) at 20 μM of NQQA and QQA after ultrafiltration assay. Data shown are mean ± SD (n=3).

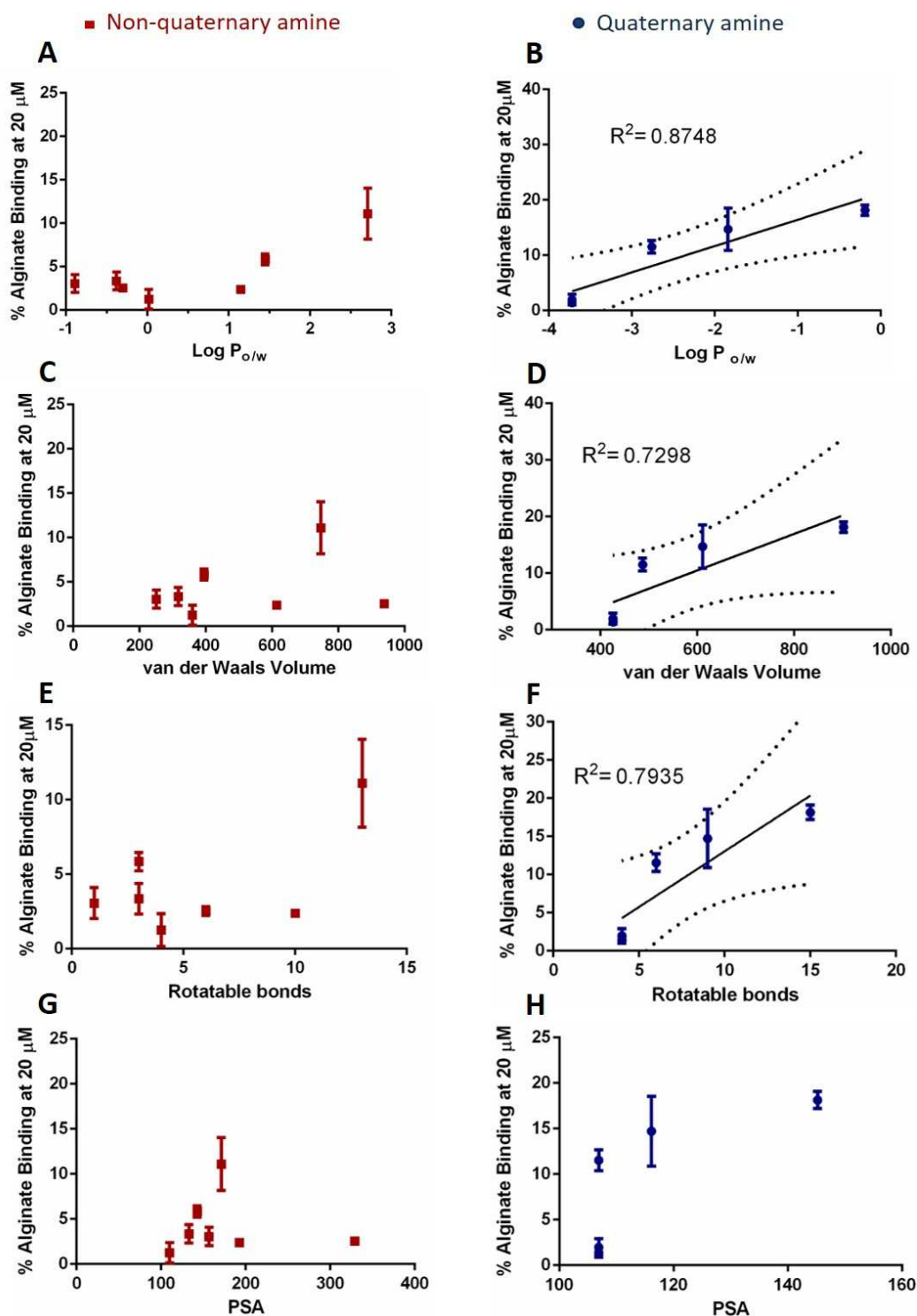


Figure 4.14. Alginate-binding at 20 μM correlated with amiloride and analogues physical parameters (1). Dashed lines indicate 95% confidence intervals. Alginate-binding of QQA (blue circle) and NQQA (red rectangles) analogues vs Log P (A-B), van der Waals Volume (C-D), rotatable bonds (E-F) and PSA (G-H). Data shown are corrected for %NSB represent the mean \pm SD ($n=3$).

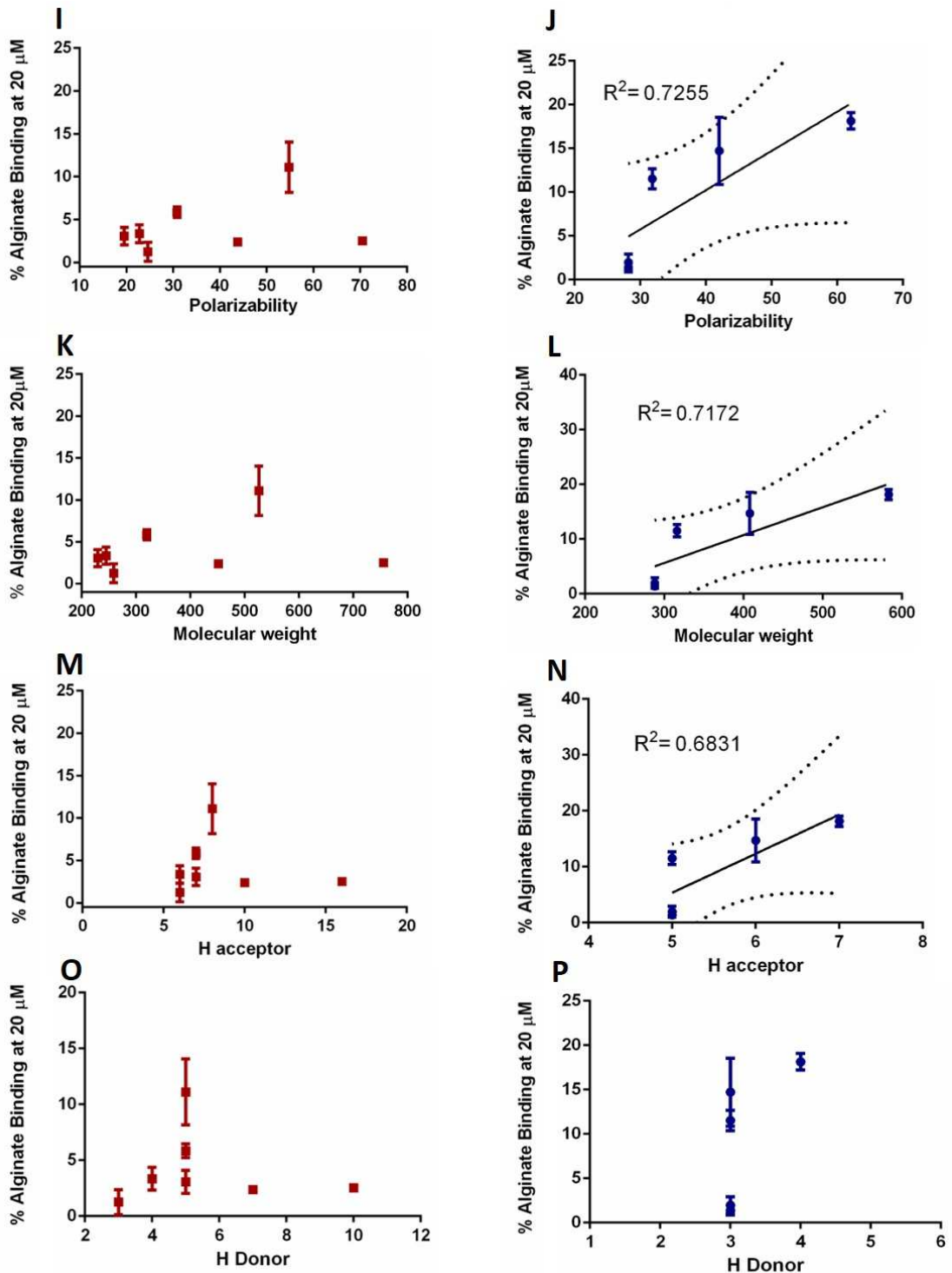


Figure 4.15. Alginate-binding at 20 μM correlated with amiloride and analogues physical parameters (2). Dashed lines indicate 95% confidence intervals. Alginate-binding of QQA (blue circle) and NQA (red rectangles) analogues vs polarizability (I-J), molecular weight (K-L), H acceptor (M-N) and H donor (O-P). Data corrected for %NSB and shown are mean \pm SD (n=3).

Amiloride analogue binding to DNA

Figure 4.16 shows the total and non-specific binding of amiloride analogues to DNA. At first glance it is possible to notice that the %NSB appears lower compared the extend of binding for amiloride analogues in the presence of DNA, staying under 6% for all range of compounds but GF-40-QQ33 which displayed the highest %NSB at about 35%. Compounds that appear to be extensively bound by DNA are Benzamil and 552-02 displaying a specific binding of ~32%, followed by JE-12-FK73 and OC-73-HK00 at ~23%. Amiloride, which showed the lowest mucin binding and not significant interaction to alginate, displayed a 16% of specific interaction to DNA. The analogues least bound by DNA were OF-80-NS22, CA-91-YE87 and KF-80-NW22 showing a specific binding of about 5%.

The plot of specific DNA binding (corrected for NSB) against physical properties (Figure 4.17 and 4.18) appear poor binding predictor for NQQA with all $R^2 < 0.305$. Regarding QQA, seeking for correlations, was noticed a strong positive correlation with most of the physical properties considered; Log $P_{o/w}$, van der Waals Volume, rotatable bonds, PSA, polarizability, molecular weight and H acceptor ($R^2 \geq 0.700$) (Figure 4.17 and 4.18). A poor correlation was found for H donor ($R^2 < 0.400$) (Figure 4.18 P).

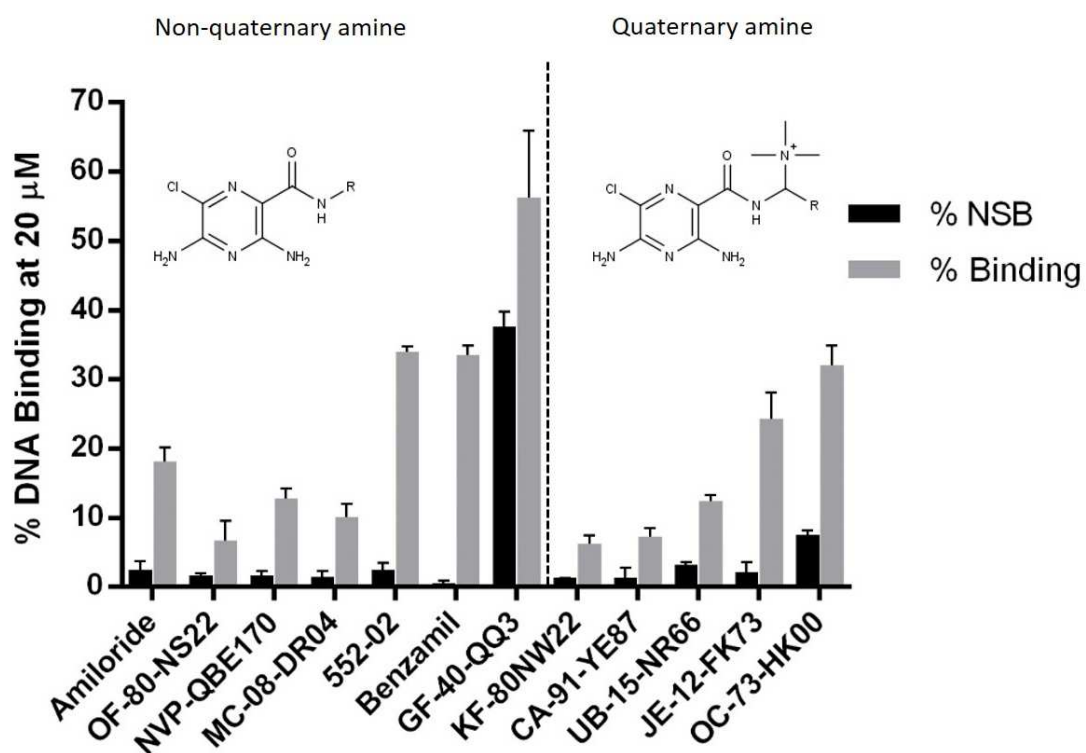


Figure 4.16. DNA binding (gray bar) and non-specific binding (black bar) at 20 μM of NQQA and QQA after ultrafiltration assay. Data shown are mean ± SD (n=3).

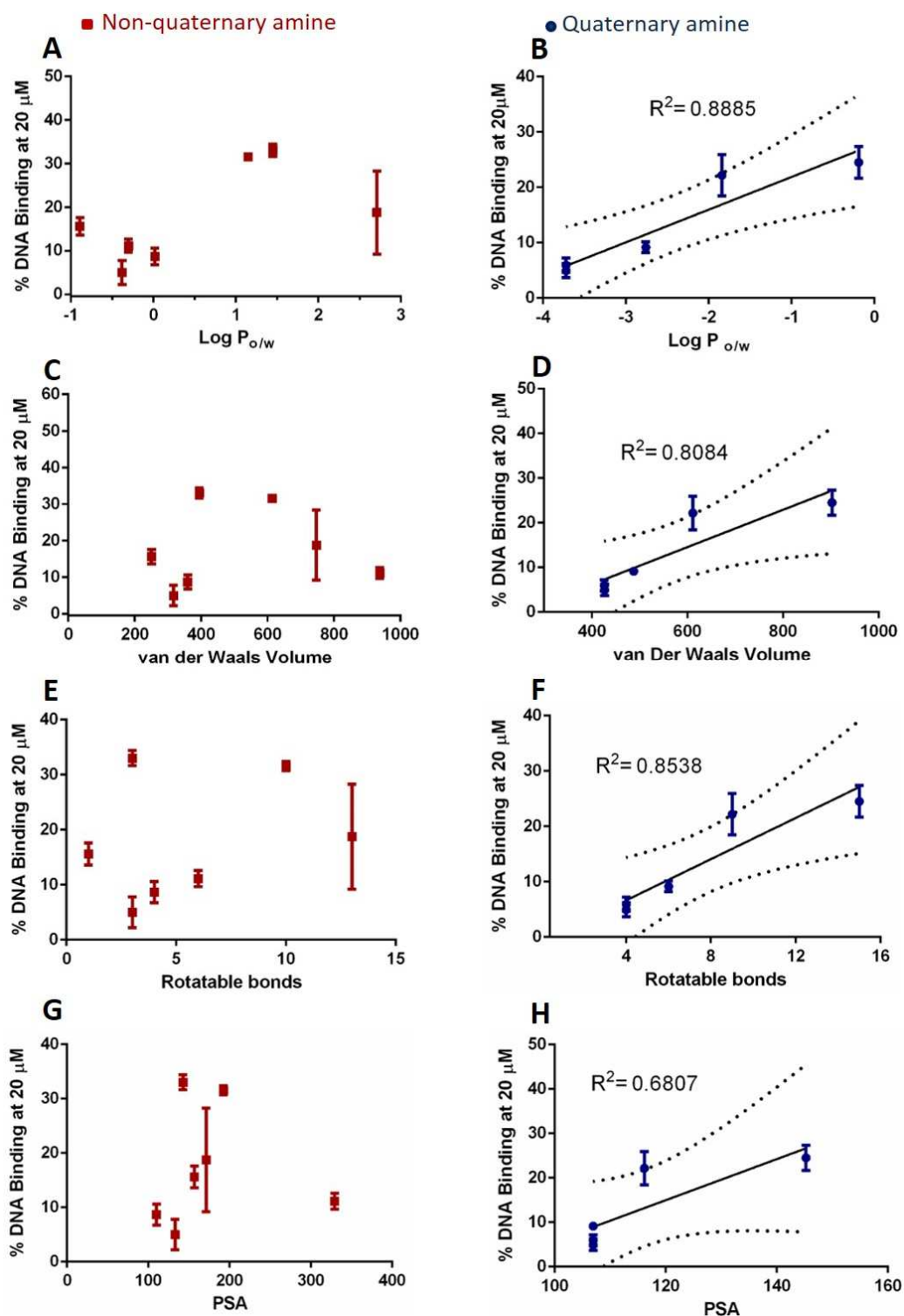


Figure 4.17. DNA- binding at 20 μM correlated with amiloride and analogues physical parameters (1). Dashed lines indicate 95% confidence intervals. DNA binding of QQA (blue circle) and NQQA (red rectangles) analogues vs Log P (A-B), van der Waals Volume (C-D), rotatable bonds (E-F) and PSA (G-H). Data corrected for %NSB and shown are mean \pm SD (n=3).

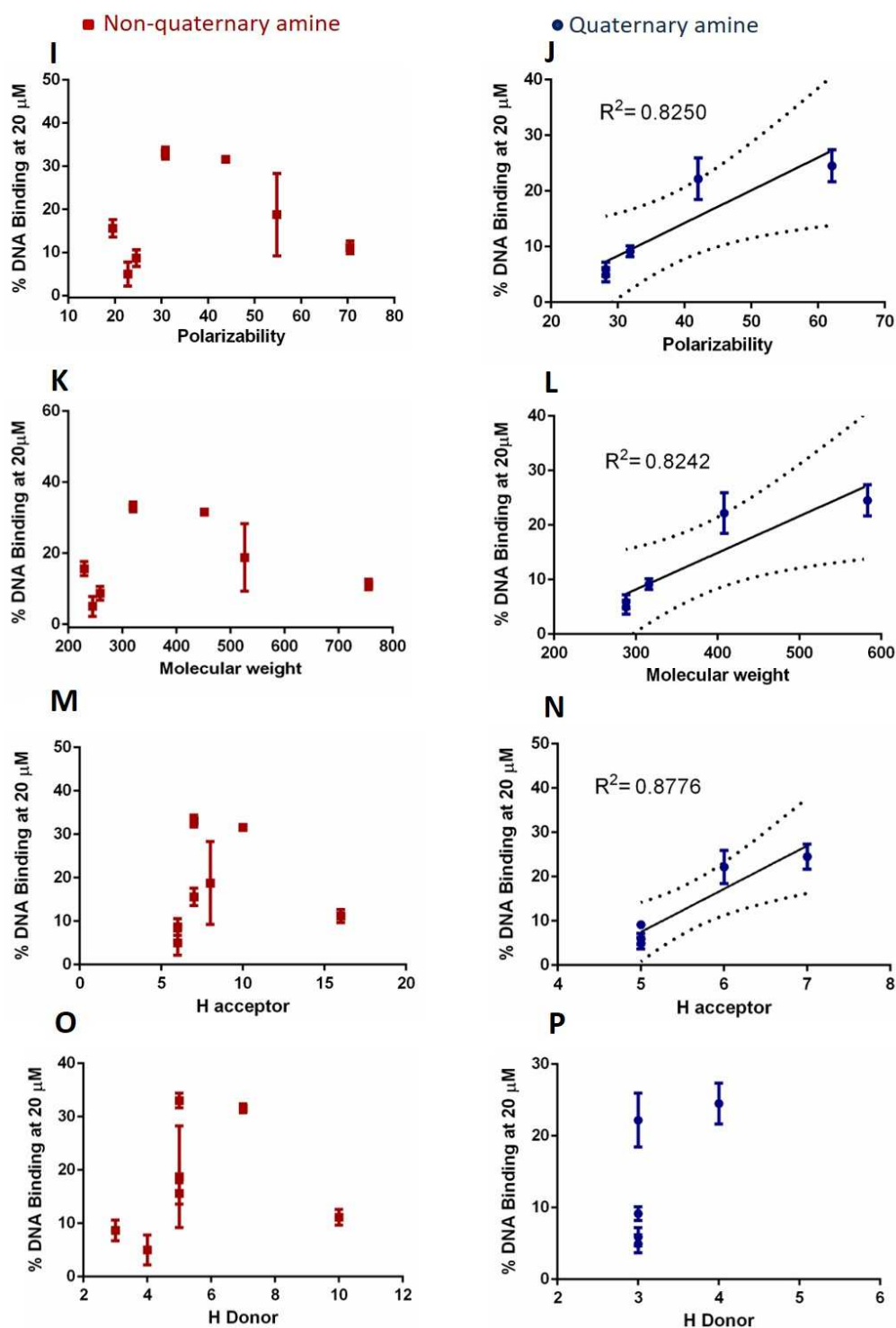


Figure 4.18. DNA- binding at 20 μM correlated with amiloride and analogues physical parameters (2). Dashed lines indicate 95% confidence intervals. DNA -binding of QQA (blue circle) and NQQA (red rectangles) analogues vs polarizability (I-J), molecular weight (K-L), H acceptor (M-N) and H donor (O-P). Data corrected for %NSB and shown are mean \pm SD (n=3).

4.3.5 Effect of TCEP on Benzamil and 552-02 mucin binding

A positive correlation between Log $P_{o/w}$ and mucin binding was consistent with a hydrophobic binding interaction. To probe this further the mucin binding of select ENaC blockers was evaluated in the presence of TCEP which is capable of reducing the mucin disulfide bonds which tether together mucin chains to form cross-linked hydrophobic pockets⁽³⁹⁾. As can be seen from the results in Figure 4.19, when TCEP is added into mucin mixtures containing benzamil or 552-02 there is a significant reduction of mucin binding for both benzamil (10-fold, $p < 0.0001$) and for 552-02 (3-fold, $p < 0.001$).

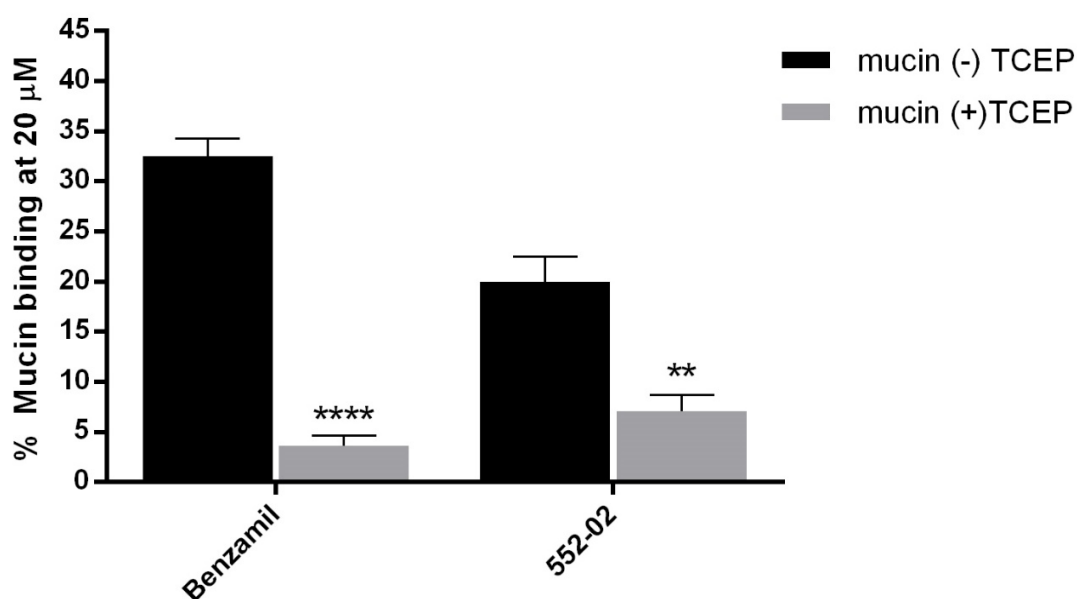


Figure 4.19. Mucin binding of benzamil and 552-02 at 20 μM with (gray bar) or without (black bar) 50mM TCPE treatment. Significance at $p < 0.0001$ denoted with asterisks (****) and $p < 0.001$ with (**) determinate by unpaired t-test. Data shown are mean \pm SD ($n=3$).

4.3.6 Permeability characteristic of calu-3 monolayer: *in-vitro* correlation to predict amiloride and analogue absorption in the lung

In this thesis the Calu-3 lung adenocarcinoma cell line was used to generate a restrictive lung epithelial barrier model suitable for studying the transport of ENaC blockers across the airways. Four days after seeding onto 6.5mm Transwell inserts the Calu-3 cell monolayers reached 100% of confluence and TER ($\Omega \cdot \text{cm}^2$) was measured post-confluence up to day 18 post-seeding (Figure 4.20 A). TER increased sharply from the first day it was measured (4-6) and between day 14 and 18 the TER reached a plateau around $1200 \Omega \text{ cm}^2$ for each plate a part for plate 4 which displayed a higher TER of $1305 \pm 45 \Omega \text{ cm}^2$, for each plate the P_{app} for F-Na was determined to judge the restrictiveness of the monolayers (Figure 4.20 B). At TER plateau monolayer permeability to FL-Na was measured. All four plates used for permeation studies displayed a P_{app} value between 0.349 and $0.495 \times 10^{-6} \text{ cm/s}$.

Apical to basolateral (A→B) transport of all amiloride and analogues, except OC-73-HK00, across polarized Calu-3 monolayers and cell-free Transwell inserts was monitored over 4 h.

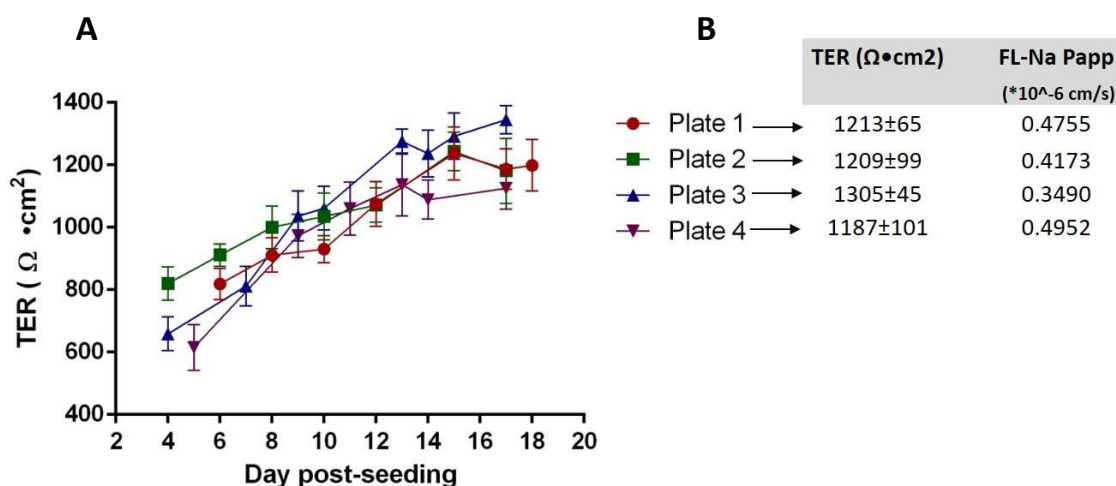


Figure 4.20. Transepithelial resistance of Calu-3 cells. (A) Graphical representation of TER during cells seeding day. (B) mean TER and summary of FL-Na P_{app} for each plate of Calu-3 monolayer used. Data shown are mean \pm SD, n=4.

The cumulative mass transport profile for both NQQA (Figure 4.21 A) and QQA (Figure 4.21 B) across Calu-3 increased linearly throughout the experiment. Table 4.3 shows the permeability coefficients for Calu-3 across the cell layer and control (cell-free insert) varied greatly across the range of amiloride and analogues which comprised NQQA and QQA. Notably, the permeability to NQQA was \sim 3-fold higher than that of QQA analogues. Compound MC-08-DR04 displayed the highest mass transported with 6.4 nmol transported in 4 h. This was \sim 3 fold higher than benzamil (1.8 nmol / 4 h) ($p < 0.0001$) and over 50-fold higher than 552-02 ($p < 0.0001$), which alongside amiloride, displayed the lowest mass transported; amiloride 0.123 nmol / 4 h, 552-02 0.103 nmol 4 h ($p > 0.05$).

The A→B transport for UB-15-NR66 and JE-12-FK73 was very similar (~ 0.16 nmol / 4 h) ($p > 0.05$) and about 4-fold lower than CA-91-YE87 and KF-80-NW22 (Figure 4.21 B) ($p < 0.0001$).

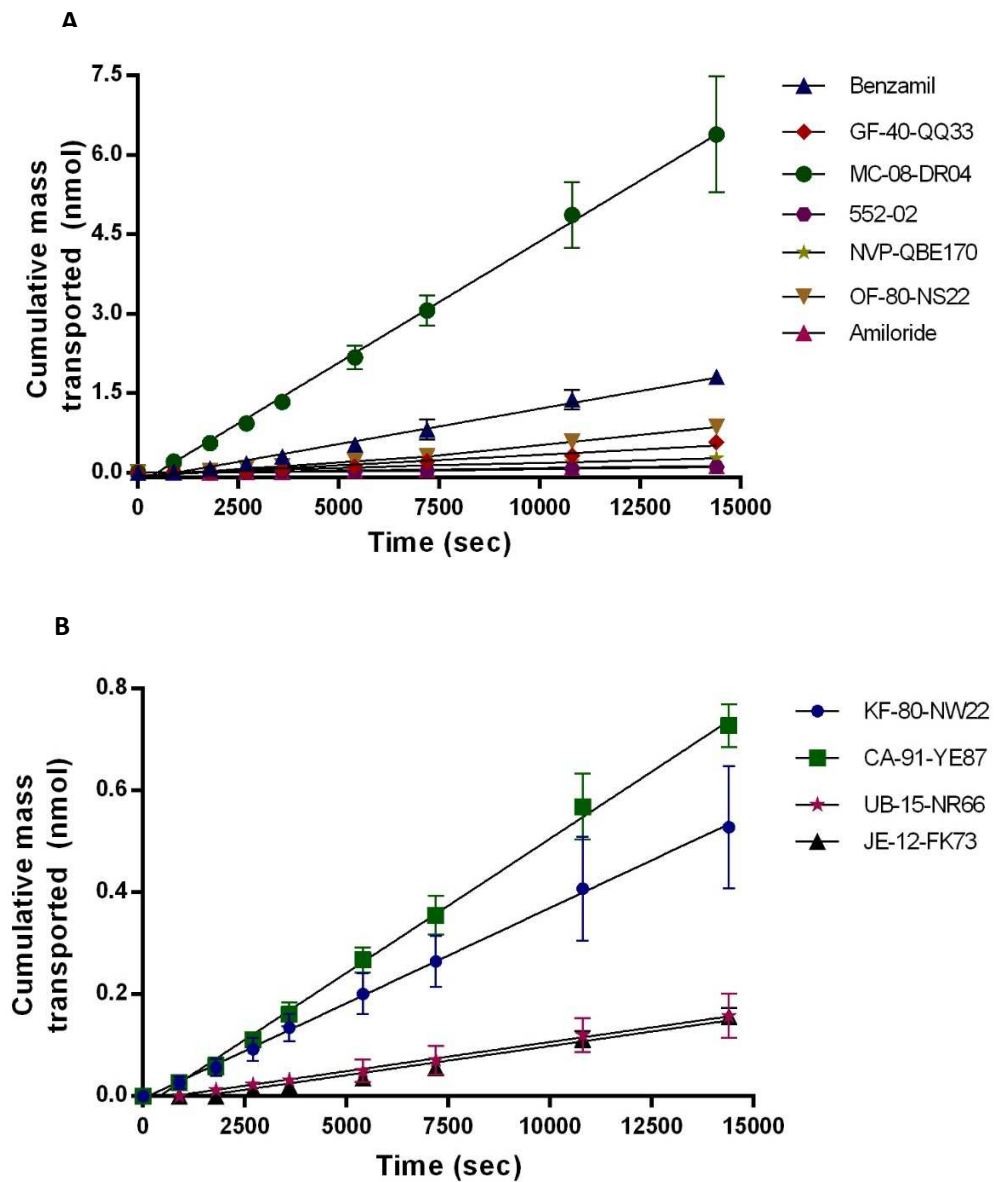


Figure 4.21. Cumulative transport of amiloride and analogues across Calu-3 monolayer. (A) NQQA and (B) QQA. Concentration added to apical chamber was 100 μ M. Data shown are mean \pm SD, n=4.

Table 4.3. Permeability of Calu-3 monolayers or bare Transwell inserts to amiloride and analogues. Data are mean \pm SD, n=3-4.

Compounds	Average P _{app} (*10 ⁻⁶ cm/s) mean (n=4)	Control P _{app} (*10 ⁻⁶ cm/s) mean (n=3)	Fold decreased (P _{app_control} /P _{app_Calu3})*
Non-Quaternary amine			
Amiloride	0.69 \pm 0.14	38.05 \pm 0.84	55.5
OF-80-NS22	1.55 \pm 0.33	40.01 \pm 4.49	25.8
MC-08-DR04	13.70 \pm 1.19	41.05 \pm 2.10	3.0
552-02	0.28 \pm 0.03	17.99 \pm 3.67	72.4
Benzamil	4.26 \pm 0.76	28.24 \pm 3.24	6.6
GF-40-QQ33	1.61 \pm 0.43	2.81 \pm 0.09	1.8
NVP-QBE170	0.53 \pm 0.09	3.86 \pm 0.16	7.3
FLNA	0.43 \pm 0.07	38.16 \pm 4.93	88.0
Quaternary amine			
KF-80-NW22	1.22 \pm 0.23	30.17 \pm 1.94	24.7
CA-91-YE87	1.66 \pm 0.14	33.97 \pm 5.32	20.5
UB-15-NR66	0.37 \pm 0.08	15.26 \pm 0.67	41.7
JE-12-FK73	0.37 \pm 0.01	24.03 \pm 0.40	64.7
OC-73-HK00	<LQ	0.007 \pm 0.0004	N/A

Compound 552-02 displayed slower transepithelial transport than amiloride i.e. 0.28 for 552-02 versus 0.69 10⁻⁶ cm/s for amiloride. The P_{app} of blank Transwells was determined because of the extensive NSB recorded for some compounds in ultrafiltration studies. The presence of Calu-3 cells on the Transwell insert resulted in a decreased P_{app} of 72-fold for 552-02 similar to FL-Na (88-folds) and 56-folds for amiloride. Surprising, although MC-08-DR04 shows a low Log P_{o/w} 0.02, appears the fastest amiloride analogue to cross the cell monolayer having a P_{app} that decreased of only 3-fold compared with the control. The most hydrophobic QQA and NQQA compounds, OC-73-HK00 and GF-40-QQ33

respectively, showed extensive binding to the Transwell insert as evidenced by a low P_{app} in the absence of cells (Table 4.3). Notably, the P_{app} measured for Calu-3 to GF-40-QQ33 was less than 2-fold lower than the cell-free Transwell: 2.81×10^{-6} cm/s versus 1.61×10^{-6} cm/s. Unfortunately, OC-73-HK00 appears to have a high NSB showing a very low P_{app} even without monolayer (0.007×10^{-6} cm/s). When applied to Calu-3 monolayers the mass transported to the receiver chamber was lower than the LOD. These data were excluded from further analysis.

Compounds were prepared as 20 mM stocks in DMSO and before dilution to 100 μ M for permeation experiment. HPLC analysis of drug dose solution, before and after experiments, excluded the possibility of precipitation for all amiloride analogues included GF-40-QQ3.

4.3.6.1 Relationship between drug physicochemical properties and transport across Calu-3 cell

When seeking correlation between drug properties and Calu-3 permeability the QQA set contained only 4 compounds, of which two were isomers (KF-80-NW22 and CA-91-YE87). Figure 4.22 A-F demonstrates that there are no strong correlates for transport across restrictive Calu-3 monolayers ($R^2 < 0.200$ for all parameters). Distinct from the trends seen for mucin binding, $\log P_{o/w}$ correlated poorly with Calu-3 transport for both groups, notwithstanding a ~ 4 -Log range of lipophilicity for both groups.

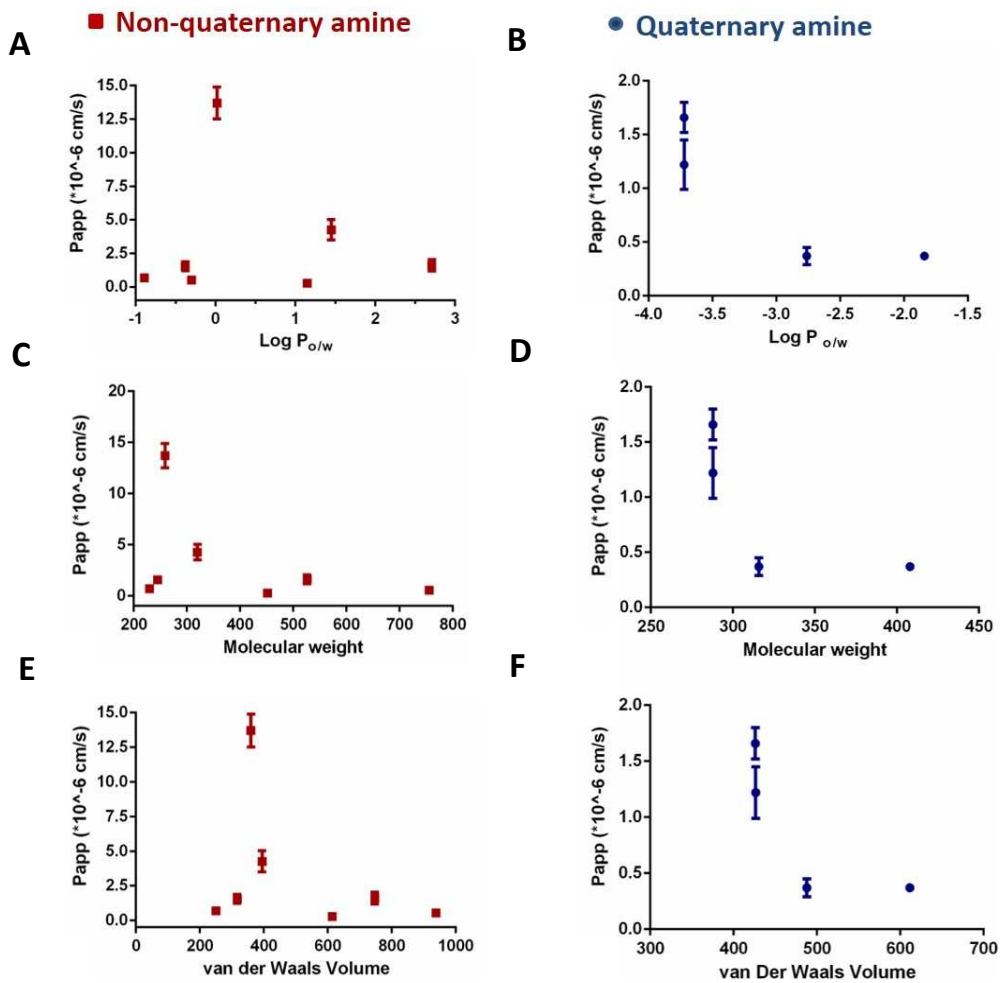


Figure 4.22. Apparent permeability of amiloride and analogues at 100 μM correlated vs physical parameters. P_{app} of QQA (blue circle) and NQQA (red rectangles) analogues vs Log P (A-B), molecular weight (C-D) and van der Waals Volume (E-F). Data shown are mean \pm SD (n=4).

Figure 4.23 shows the P_{app} of amiloride and analogues across insert cell-free and is possible to observe a negative correlation between filter permeability and amiloride analogues standard physical properties. In particular, is observed a strong correlation with van der Waals Volume for P_{app} of both NQQA ($R^2=0.9001$) and QQA ($R^2=0.7762$) (Figure 4.23 C and D respectively) and also correlation with QQA P_{app} versus Log $P_{o/w}$

($R^2=0.8001$) (Figure 4.23 B) which may indicate that the filter used to seed Calu-3 cells may have affected the P_{app} of amiloride analogues.

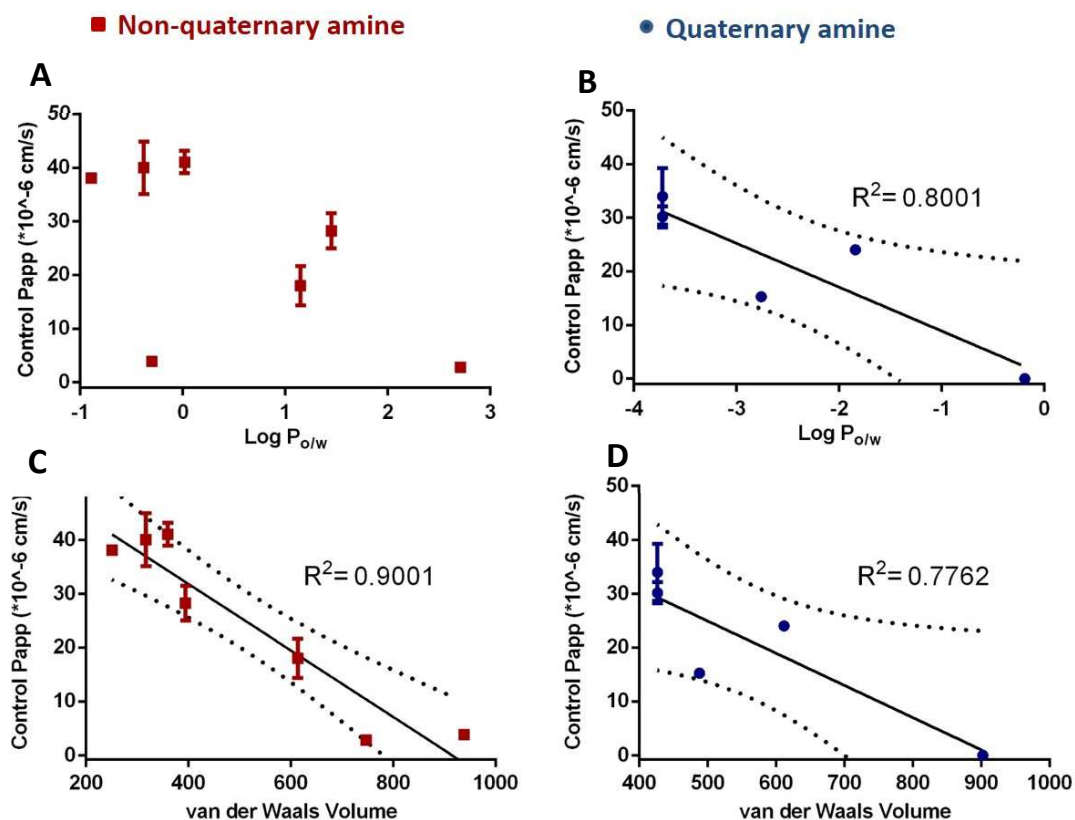


Figure 4.23. Apparent permeability of amiloride and analogues at 100 μ M across cell-free Transwell inserts correlated vs physical parameters. P_{app} of QAA (blue circle) and NQAA (red rectangles) analogues vs Log P (A -B) and van der Waals Volume (C-D). Data shown are in mean \pm SD (n=3).

4.3.6.2 Statistical analysis of mucin binding and P_{app} across Calu-3 with SPSS.

Correlations between physical parameters and P_{app} were also determined by calculating the Pearson correlation coefficient. As shown in Table 4.4 A, correlations displayed for QQA are comparable (green rectangles) to those obtained from linear regression (Figure 4.9 and 4.10) showing a strong positive correlation with all physical parameters, except H-donor number, for which it was not possible to obtain any correlation due to a low

number of compounds. For QQA transport across Calu-3 correlated negatively with Log $P_{o/w}$ and rotatable bonds ($R^2=0.873$ and $R^2=0.821$, respectively) and weaker correlation for other physical properties. In Table 4.4 A it is possible to notice that all physical parameters appear correlated to each other displaying a $R^2 > 0.749$. For example, rotatable bonds were strongly correlated with Van der Waals Volume ($R^2= 0.997$) and polarizability ($R^2=0.990$).

For NQQA (Table 4.4 B), the Pearson's correlation, displayed also a negative correlation with rotatable bonds (red rectangle) and opposite to QQA, NQQA physical properties displayed a very variable correlation to each other. For instance, Log $P_{o/w}$ resulted strongly correlated to rotatable bonds ($R^2=0.818$) but correlated poorly with PSA, molecular weight and H-acceptor ($R^2 < 0.100$).

Table 4.4. Statistical analysis of mucin binding and P_{app} across calu-3 with SPSS. % mucin binding at 20 μM and P_{app} at 100 μM correlated versus amiloride analogues parameter A QQA B NQAA s: molecular weight, Log $P_{o/w}$, PSA, van der Waals Volume, polarizability, H-donor, H-acceptor and rotatable bonds. Yet, each physical parameter correlated versus each other. Green rectangle indicates pearson correlation comparable to linear regression results.

		Correlations Quaternary amine									
		%Mucin Binding 20 μM	MW	LogP	PSA	Wdv	polarizability	H donor	H acceptor	Rotatable bonds	P_{app} average (*10 ⁻⁶ cm/s)
Pearson	%Mucin Binding 20 μM	1.000	.877	.969	.749	.919	.891		.749	.942	-.965
Correlation	MW	.877	1.000	.958	.973	.995	.999		.973	.984	-.721
	LogP	.969	.958	1.000	.865	.982	.967		.865	.993	-.873
	PSA	.749	.973	.865	1.000	.944	.965		1.000	.917	-.554
	Wdv	.919	.995	.982	.944	1.000	.998		.944	.997	-.783
	polarizability	.891	.999	.967	.965	.998	1.000		.965	.990	-.742
	H donor							1.000			
	H acceptor	.749	.973	.865	1.000	.944	.965		1.000	.917	-.554
	Rotatable bonds	.942	.984	.993	.917	.997	.990		.917	1.000	-.821
	P_{app} average	-.965	-.721	-.873	-.554	-.783	-.742		-.554	-.821	1.000
		Correlations Non-Quaternary amine									
		%Mucin Binding 20 μM	MW	LogP	PSA	Wdv	polarizability	H donor	H acceptor	Rotatable bonds	P_{app} average (*10 ⁻⁶ cm/s)
Pearson	%Mucin Binding 20 μM	1.000	.175	.954	-.18	.275	.272	-.129	-.151	.637	.029
Correlation	LogP	.954	.425	1.000	.063	.527	.519	.097	.090	.818	-.113
	PSA	-.180	.913	.063	1.000	.841	.862	.973	.990	.262	-.507
	MW	.175	1.000	.425	.913	.987	.993	.872	.922	.584	-.392
	Wdv	.275	.987	.527	.841	1.000	.997	.799	.858	.699	-.348
	polarizability	.272	.993	.519	.862	.997	1.000	.821	.872	.665	-.378
	H donor	-.129	.872	.097	.973	.799	.821	1.000	.974	.272	-.583
	H acceptor	-.151	.922	.09	.99	.858	.872	.974	1.000	.296	-.426
	Rotatable bonds	.637	.584	.818	.262	.699	.665	.272	.296	1.000	-.237
	P_{app} average	.029	-.392	-.113	-.507	-.348	-.378	-.583	-.426	-.237	1.000

Variance inflation factor (VIF) quantifies the severity of multicollinearity measuring the impact of colinearity among the variable in a regression model and a value >10 indicates the presents of multicollinearity. In our analysis VIF resulted to be 12 and 35 for QQA and 22 and 286 indicating that early analysis of multivariate regression indicates multicollinearity and insufficient population size for both groups of compounds.

4.3.7 Influence of porcine purified jejunal mucin on 552-02 apparent permeability across Calu-3 monolayer

To assess the effect of mucin-binding on the transport rate of amiloride analogues across the lung epithelium experiments were performed in which 552-02 (a high binding drug) was pre-equilibrated with purified porcine gut mucin before application to restrictive Calu-3 monolayers. Surprisingly, the rate of 552-02 transport increased 20-fold ($p < 0.0001$) compared to control monolayers (Figure 4.24). The resistance of mucin-treated monolayers was reduced by $\sim 80\%$ (from 1125 to $217 \pm 82 \Omega \text{ cm}^2$) after 4h treatment compared to a 25% (from 1201 to $899 \pm 151 \Omega \text{ cm}^2$) for mucin-free treatment ($p < 0.05$).

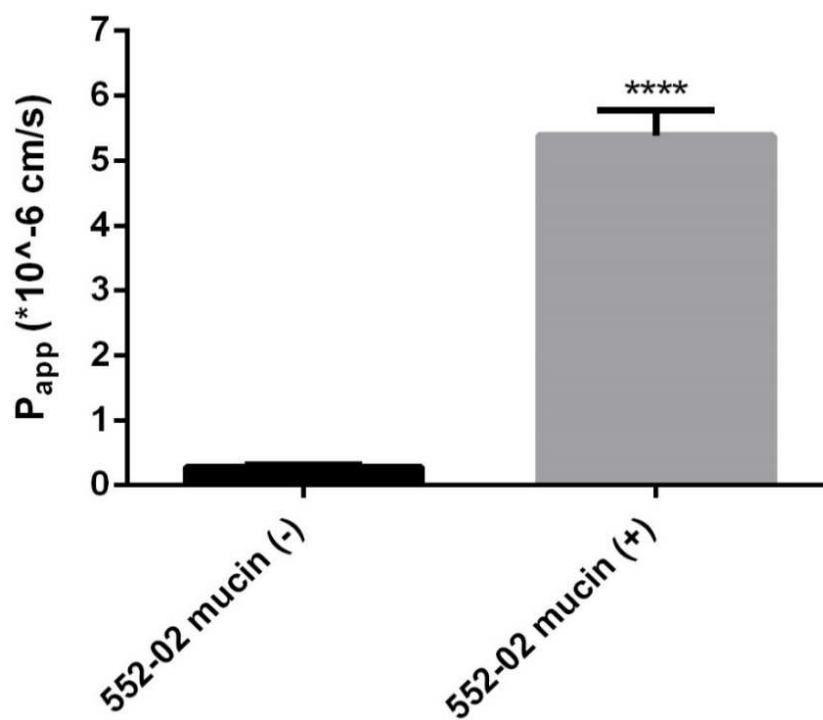


Figure 4.24. Transport of 552-02 across Calu-3 cell monolayers in the presence and absence of purified mucin. P_{app} of 552-02 dissolved in aqueous solution (black bar) and 552-02 dissolved in 0.5 μ M purified mucin (gray bar) after 4 h experiment. Significance at $p < 0.0001$ denoted with asterisks (****) as determined by unpaired t-test. Data shown are in mean \pm SD ($n=3$).

4.4 Discussion

CF is a genetic disease and the abnormal anion transport in the respiratory conducting epithelia leads to impaired MC. The use of ENaC blocker may help to reconstitute mucus hydration on the airways and improve people with CF quality of life. Developed in the early 1960s to act as ENaC blocker at the lumen of distal renal cortical collecting duct, it was several decades before nebulized amiloride was studied for its effect on the pulmonary function of CF patients. Its poor PK/PD properties led to the synthesis of more potent and durable ENaC blockers like benzamil and 552-02 but the low solubility of these compounds led to further attempts to develop improved amiloride analogues⁽⁴⁰⁾. To better design inhaled CF therapeutics it is imperative to better understand if mucus binding in the lung can negatively affect the inhaled disposition of solutes.

Work in this chapter aimed to determine if a panel of inhaled ENaC blockers⁽¹²⁾ undergo non-specific binding to secreted mucin. We supposed that mucin binding can reduce the free concentration of drug available for transport to the epithelial surface and therefore reduce the pharmacological activity of the drug.

Many methodologies exist for determine the extent of drug-DNA and drug-plasma protein binding but no standard method is available for specifically study drug-mucin interactions in industry. This chapter explored the use of fluorescent and UV-Vis spectroscopy for the study of interaction between mucin and small molecules in a similar way to that described previously^(35, 41). The fluorescent spectroscopy study aimed to

observe changing of amiloride and benzamil spectrum following titration of drugs (0.4 to 15.2 μM) into 1 μM mucin. The absence of any mucin-induced changes in the amiloride spectrum (Figure 4.1 and 4.2) indicate no measureable binding in this experimental condition. In contrast, in the fluorescence spectrum of benzamil a maximum blue shift of 5 nm was noticed after mucin titration with benzamil at highest concentration (15.2 μM).

The interaction of one molecule with another molecule can result in a bathochromic or hypsochromic shift of the fluorescence peak implying that the conformation of one molecule was changed ⁽⁴²⁾, or in a fluorescence quenching where a fluorescence intensity of a given substance is reduced as a consequence of molecular rearrangements, energy transfer, collision or complex formation ⁽⁴³⁾.

The binding of a ligand to a macromolecule may causes changes in their structure which may have an effect on the environment around the fluorophore. The recorded blue shift may be due to a reorientation of the solvent molecules around the fluorophore when excited which leads to a change in the dipole moment of the solvent in the binding site compared to free solution. Moreover, the exposition of the fluorophore to a less polar environment leads to the increment of the fluorescence intensity (quantum yield increased) as we observed when adding ethanol to a ligand solution (Figure 4.3). The interaction of the ligand to a hydrophobic region of the mucin may lead to an increment of the quantum yield. Therefore, the shift observed may be due to molecular interaction but more investigation was necessary.

The use of UV spectroscopy allowed further investigation of the formation of a drug-mucin complex. To achieve analytical sensitivity, the mucin and drug concentrations were 0.5 μM and 130 μM (maximum), respectively. Comparing the absorbance of the control (sum of mucin and ligand absorbance) and the absorbance of the mixture, a distinct reduction of absorbance in the spectrum in the UV spectra of both compounds was observed using a mucin: drug ratio of 1:140 for benzamil and 1:260 for amiloride (Figure 4.5) which is evidence that they have formed a mucin-drug complex ⁽⁴²⁾. An explanation for these changing in absorption for amiloride and benzamil may come from the formation of a drug-mucin complex. In particular, the absorbance spectra after benzamil titration into mucin displayed a greater suppression of absorbance bands than amiloride indicating that there was differential mucin binding for two structurally similar compounds. This mucin: drug ratio is higher than that used in the fluorescence spectroscopy assay and indicates that the binding interaction is of low-affinity.

A new method was sought that facilitated work towards two distinct objectives: to screen for mucin binding in a range of related compounds; and to investigate in detail drug-mucin binding events. At present, pharmaceutical companies do not screen for mucin binding, however plasma protein binding (PPB) screening is a routine step in the drug development pathway. Fung, Chen ⁽⁴⁴⁾ showed the determination of plasma protein binding using a new method. Commercially available compounds with different structure (12 in total) were mixed with plasma and unbound and bound fraction were separated by a 96-well plate filtrate assembly. The unbound percentage obtained using the

Microcon-96 assay was plotted with literature data and resulted to have a good correlation ($R^2=0.900$), although no information regarding the physical-chemical parameters and NSB of compound used are indicated.

The donor plate and receiver plate of the multiscreen 96-well plate are separated by a membrane filters at a cut-off of 10 kDa which have been used for several years to separate unbound drugs from protein-bound drugs ⁽⁴⁵⁾. The optimization of the ultrafiltration conditions used in the centrifugation process were necessary to improve the separation of the free and bound drug. For instance, spin time and temperature were chosen to avoid sample evaporation in a non-temperature controlled centrifuge. Sample evaporation was experienced in preliminary experiments and caused a sizeable reduction in the donor and filtrate volume. This made mass balance determination very challenging and could have resulted in drug precipitation in greatly reduced volumes of solvent (data not shown).

A drawback of any multiwell plate-based assay is heterogeneous activity across the plate. The manufacturers of the Multiscreen plate used here recognise this heterogeneity and state explicitly in the manual that filtrate rates are particularly variable in the peripheral wells of the plates. Although the extent of binding can be determined by comparison of drug concentrations in control (mucin free) and treatment (drug + mucin) wells it is prudent to determine the mass balance of analytes within experiments. To calculate the filtrate volume and to determine the mass balance a precise volume of internal standard at known concentration was “spiked” into each well. The volume of the filtrate which

dilutes the standard can be determined by calculating the dilution factor of the standard through simultaneous HPLC detection of analyte and standard in the retentate. The same procedure was performed for the determination of the retentate volume after centrifugation. Using this approach, the mass balance was 96-104% for 11 out of 12 amiloride analogues. The low mass balance and high NSB for GF-40-QQ33 is most likely attributable to membrane- and plastic plate-binding.

NSB has been reported to be correlated to lipophilic molecules⁽⁴⁶⁾ and is typically estimated by measuring the $\text{Log } P_{o/w}$ but this is a gross simplification of a complex phenomenon as showed by Dickson, Gee⁽⁴⁷⁾ who demonstrated, using a quantum mechanical calculations, a correlation between NSB and drugs whose interacting with lipid molecule whereas the water-octanol partition coefficient did not show good predictive power. High non-specific binding is a poorly understood phenomenon and has been reported as a particularly challenging issue for the determination of plasma protein binding⁽²⁷⁾ due to the lipophilicity of these molecules. Lee, Mower⁽⁴⁸⁾ demonstrated that pre-treating the filter membrane with 5% tween 80 or 5% benzalkonium chloride, the interactions with lipophilic drug molecules (such as vinblastine, hydrocortisone and propranolol), is reduced of over 70%. The surface-active agent did not cause significant damage of the membrane resulted by a serum protein leakage of 0.7 and 1.2% without and with treatment.

Using the 96 well ultrafiltration assay the binding isotherm was determined for 12 amiloride analogues. Midway through the studies the Millipore MultiScreen plates were

discontinued by the manufacturer. As a result, for four compounds isotherms were constructed with 4 concentrations rather than 8. From the binding assay it was found that all ENaC blockers bound to mucin, with the extent of binding at 20 μ M ranging from 0.7 to 37.5% (Table 4.1). The variability of drug binding between amiloride analogues of varying structure indicates that binding is determined by drug physicochemical properties that vary between the compounds, rather than any consistent structural features such as the pyrazinoyl group (Figure 4.6 and 4.7). Further evidence of a non-specific binding event is the observation of identical binding between the stereoisomeric pair of compounds, CA-91-YE87 and KF-80-NW22 (Table 4.1).

Mizushima, Takanaka ⁽⁴⁹⁾ investigated the metabolic kinetics of R and S-oxybutynin showing that were slightly different and that R-oxybutynin in human plasma was approximately two-fold higher than that its S-enantiomer. The stereoselectivity of chiral drug metabolism and pharmacokinetic profiles have been reported in several studies ⁽⁵⁰⁾ ⁽⁵¹⁾ ⁽⁵²⁾ and the binding of chiral drugs to plasma proteins appears to exhibit stereoselectivity.

Albani, Riva ⁽⁵³⁾ studied the binding of propranolol enantiomers to human albumin and human α -AGP by equilibrium dialysis demonstrating the preference of (S) propranolol to bound α -AGP displaying a free fraction of 30 % and 23 % for (R) propranolol.

Ofori-Adjei, Ericsson ⁽⁵⁴⁾ using equilibrium dialysis, determine the protein binding of racemic chloroquine to human albumin and α -AGP showing that (R) chloroquine strongly binds to albumin whereas, (S) chloroquine strongly binds to α -AGP.

The binding isotherm showed two different trend of absorption model. Amiloride analogue in Figure 4.7 suggested a multilayer binding to mucin rather than a simple monolayer binding as showed by compounds in Figure 4.6. The multilayer absorption may appear to be combined with QQA in amiloride analogue structure although UB-15 NR66 showed a monolayer absorption.

The binding isotherm allows the determination of binding properties between the equilibrium concentrations of bound and free ligand over a certain concentration range by fitting the Langmuir or GAB adsorption integral (Eq 4.1 and 4.2) to generate the corresponding affinity distribution. Langmuir isotherm is used to describe ligand-protein monolayer binding ⁽⁵⁵⁾ and the assumption of the model consist in; the absorbed layer should be a monolayer, there are finite number of equivalent (identical) site, each site can hold at most one molecule, there are no interactions between adsorbate molecules on neighbouring sites. Due to these assumption, Figure 4.25 A shows a theoretical Langmuir isotherm binding where increasing the ligand-protein ratio the ligand binding reaches a maximum as all site on the protein are occupied by a ligand molecule.

This is not the case of a GAB isotherm (multilayer liquid phase adsorption) (Figure 4.25 B) which is used to describe a multilayer binding equilibrium. GAB isotherm assumes a random distribution of sites that are empty or that are covered by one or more monolayers. In contrast to the monolayer model, increasing the ligand-protein ratio the ligand binding does not reach a maximum but keeps increasing.

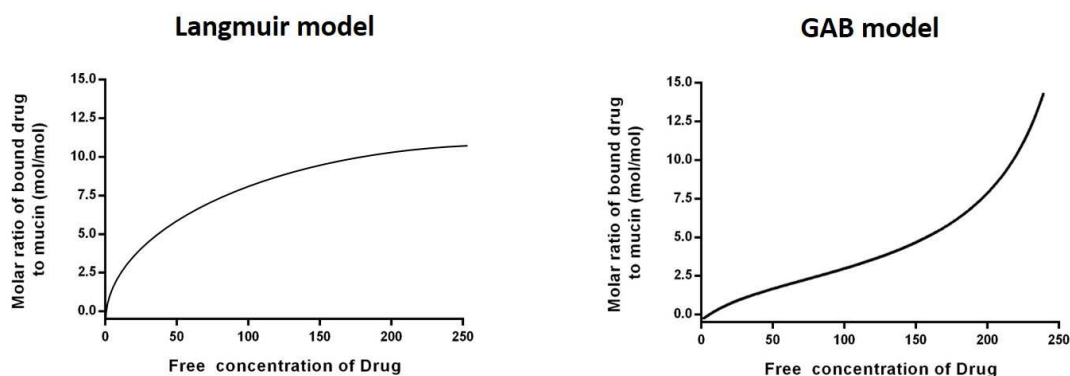


Figure 4.25. Theoretical representation of monolayer binding fitted by Langmuir model and multilayer binding fitted by GAB model.

Hydrophobicity and solubility in water are often inversely correlated⁽⁵⁶⁾. In our studies before each experiment the solubility of compounds was accurately tested to avoid precipitation issue in experimental condition. Different concentration of drug-mucin mixture and pure drug solution at same concentration were diluted as appropriate and analysed through HPLC. The maximum concentrations of drug used in ultrafiltration experiments were 5/10 fold lower than the solubility provided by Novartis or determined by HPLC (data not shown). No solid formed was noticed with indication of absence of analyte precipitation.

GAB isotherm was used by Zhao, Chen⁽³⁵⁾ to describe the multilayer binding of epigallocatechin gallate (EGCG) to purified porcine gastric mucin. EGCG-mucin interaction was studied using a combination of UV-Vis spectroscopy, transmission electron microscopy and ultrafiltration isothermal titration microcalorimetry (ITC). Using

ITC, Zhao, Chen ⁽³⁵⁾ noticed a decreasing in the binding energy while increasing temperature affirming that the multilayer binding may imply hydrogen bonding but there is no a clear picture of the drug-mucin interactions at the molecular level ⁽⁵⁷⁾ ⁽⁵⁸⁾.

To gain an insight into the intermolecular forces governing the mucin interactions of ENaC blockers we correlated standard physicochemical parameters with the extent of binding. The extent of drug binding at 20 μ M was chosen as a concentration that could be expected after delivery of a therapeutic amiloride aerosol ⁽⁵⁹⁾. The extent of mucin binding varied greatly across the range of amiloride analogues which comprised QQA and NQQA analogues. Amiloride displayed the lowest mucin specific interaction (0.7%) and GF-40-QQ30 the highest (37.5%). The data indicate that drug hydrophobicity is could be a key factor in determining whether ENaC blockers bind extracellular mucins. Values of Log P_{o/w} used in this study were generated in silico. However, HPLC analysis using a consistent eluent program confirmed the ranking of cLogP values for both groups of compounds. Yamagami, Kawase ⁽⁶⁰⁾ used a range of heteroaromatic compounds such as thiophenes, furans and (di)azines with a Log P_{o/w} in the range of -0.8-1.84, reported the use of reversed phase HPLC retention times to provide a convenient method for estimating drug hydrophobic character.

In contrast to NQQA, QQA compounds showed correlation also with other physical parameter, (such as H-acceptor, van der Wall Volume). The NQQA group compounds were characterized by a wide heterogeneous structure, presenting a wide range of

molecular weight (230-756 g/mol) and van der Waals Volume (251-938 Å³). Since our analysis is based on a small dataset, the drawn of correlation between percentage of mucin binding and ENaC blocker physical-chemical properties may require the extension of the range of model drug analyzed.

Komiya, Park ⁽⁶¹⁾ studied mucus binding of 7 steroids (testosterone, progesterone, androst-4-ene-3,17-dione, deoxycorticosterone, corticosterone, hydrocortisone and dexamethasone) in a range of 1.53-3.99 in Log P_{o/w} demonstrating that following rat intestinal perfusion, steroids binding to mucus may be due hydrophobic regions of the glycoprotein.

Bhat, Flanagan ⁽⁶²⁾ used a diafiltration system, which combines characteristics of equilibrium dialysis and ultrafiltration in a continuous system, to study the extent of binding to porcine gastric mucus fractions (400 kDa) and BSA of six compounds (albuterol, rifampicin, p-amino-salicylic acid, isoniazid, pyrazinamide and pentamidine). This compound set includes a molecular weight range of 123-822 g/mol, and a clogP from -1.23 to 2.85. The model compounds used were structurally diverse and selected on the basis of their potential therapeutic application for pulmonary route rather than on their physico-chemical parameters. Despite the structural variability within the group the association constants, as determined by Scatchard analysis, were within one order of magnitude, suggesting that the binding events were non-specific and that similar binding forces may be involved. In comparison to drug binding to BSA the association constants for mucin were lower (for 3 of the 5 reported drugs). The authors proposed that

hydrophobic binding to mucin polypeptide cores could explain the binding phenomenon, although there was no clear trend between cLogP and the K_a of binding to mucin.

Kearney and Marriott⁽⁶³⁾ studied the tetracycline interaction nature to mucin using equilibrium dialysis in different pH condition (1 to 11). The percentage of drug bound increased from 15 to 60% when pH was increased from 1 to 3. Around pH 3 the mucin and tetracycline have opposite charge and an electrostatic interaction may occur. At higher pH tetracycline are neutral due to the ionization of the acid group and the drug bound gradually decreases back to 15% which may be due to hydrophobic interaction of drug molecule with the globular protein region of mucin. Following this observation, they attributed the binding of compounds to gastric mucin to a combination of electrostatic forces and hydrophobic interactions.

Several studies demonstrated that positively-charged, low-molecular weight drugs bind electrostatically to the negatively charged components in mucus. In particular, Niibuchi, Aramaki⁽⁶⁴⁾ using equilibrium dialysis studied the interaction of 13 β -lactam and 3 aminoglycoside antibiotics to rat intestinal mucin demonstrating a strong interaction of gentamicin to the mucin sugar moiety resulted from a significant decrease of the bound drug after treating the mucin with glycosidase.

Mucin forms a complex gel network that presents both un-glycosylated non-polar domains that may serve as drug binding pockets and polar glycosylated domains with oligosaccharide chains that confer negative charge to the mucins through carboxyl and sulfate groups, therefore, the interaction of NQQA and QQA may fall within different

drug with the disulfide reducing agent, TCEP. Due to the limited availability of 96-well plate, the treatment with TCEP was used only with benzamil and 552-02. As can be seen from Figure 4.19, there is an increase of free drug concentration when TCEP was used to reduce mucin for both benzamil (10-folds) and 552-02 (3-folds). These observations support the assumption that disulfide bridges could potentially increase the ability of mucin to interact with ENaC blockers. The difference between the similar binding but big difference in effects of TCEP on benzamil and 552-02 may be due to a different binding modes. Different Log $P_{o/w}$ values mean different baseline affinities for mucin.

Influence of other sputum components on ENaC blocker disposition

The inhalation of amiloride analogues into the CF lung will lead to drug exposure to wide range of complex anionic macromolecules that may sequester drug extracellularly. Alginate is bacterially-derived anionic polymer with carboxyl end groups that forms highly viscous aqueous solutions that contribute to obstruction of small airways and respiratory congestion in patients with CF and chronic pulmonary infection. The most widely studied alginate secreting bacterium is the opportunistic pathogen, *P. aeruginosa* and the concentration in CF sputum has been reported to range from 4 to ~100 $\mu\text{g}/\text{ml}$ when measured by enzyme-linked immunosorbent assay ⁽⁶⁵⁾.

Bacterial polymer differ from the algal alginates in that mannuronate residues may be modified with *O*-acetyl groups ⁽⁶⁶⁾. *Pseudomonas aeruginosa* activates the *algD* operon in response to environmental conditions such as high osmolarity, nutritional deprivation and the presence of ethanol,⁽⁶⁷⁾ ⁽⁶⁸⁾ ^(69, 70) leading to the biosynthesis and secretion of

alginate as a self-defense mechanism against host immune clearance and also enhances adhesion to solid surfaces.

Like mucin, alginate is an anionic carbohydrate polymer with mucoadhesive properties, but unlike mucin, lacks a protein hydrophobic core. Similarly, extracellular DNA is an abundant extracellular macromolecular component of sputum. The concentration of DNA found in lung sputum from healthy people is $\sim 3\mu\text{g/ml}$ ⁽⁷¹⁾ but is often present at high levels in CF sputum (0.5 mg/ml up to 9 mg/ml) ^{(71) (72)}.

As showed in Figure 4.13 and 4.16, QQA showed similar correlation obtained with mucin for both alginate and DNA, while for NQQA the extent of binding to alginate was lower than observed for mucin and equivalent concentrations but resulted higher for DNA binding. The similarity of correlation between mucin and alginate may lead us to think that are due to interaction of model drug to the polysaccharide chain of mucin and alginate.

Evans and Linker ⁽⁶⁶⁾ found that *P. aeruginosa* polysaccharide differ from the algal alginates for the presence of *O*-acetyl instead of mannuronate residues. Although this difference Gordon, Hodges ⁽³⁶⁾ studied, with equilibrium dialysis, the binding of aminoglycosides antibiotic to alginate (β -lactams, gentamicin and tobramycin) to two alginate model; commercial alginate and that extracted from a cystic fibrosis-derivate mucoid strain of *P. aeruginosa*. The similar results obtained with these two alginate model support the use of commercial alginate as a model for *P. aeruginosa* polysaccharide.

Moreover, all amiloride analogues appear to bind DNA with 552-02 and benzamil showing the highest binding (~35 %), and OF-8-NS22 and the two stereoisomer (KF-80-NW22 and CA-91-YE87) showing the lowest binding (~5%). NQQA compounds are characterized by a strong correlation between percentage of mucin binding with $\text{Log}P_{o/w}$, but there is no correlation between percentage of DNA binding and $\text{Log} P_{o/w}$ for NQQA (Figure 4.17). As show in Chapter 3, PGM used as mucin model for our studies contains DNA (Chapter 3 Table 3.3). The application of the 96-wells plate binding assay was also used to understand whether the DNA contamination has affected the results of percentage of mucin binding. The absence of correlation with $\text{Log} P_{o/w}$ may be an indication that percentage of mucin binding was not affected by DNA.

In 1987, the interaction of amiloride to DNA was demonstrated by Besterman, Elwell⁽⁷³⁾. They studied the relationship for 12 amiloride analogs to DNA demonstrating that amiloride can intercalate into DNA and inhibit the catalytic activity of DNA topoisomerase II. In 1993 Bailly, Cuthbert⁽⁷⁴⁾, using the technique of foot-printing, demonstrated that the interaction of amiloride with DNA involves a sequence-specific recognition process. In particular, amiloride was shown to bind selectively to sites rich in A-T residues using three DNA restriction fragments of defined sequence. The intercalation of amiloride into ds-DNA was then confirmed by Mirmomtaz, Ensafi⁽³⁸⁾ who developed a sensitive DNA biosensor for the determination of amiloride in vitro using a pencil graphite electrode.

High-sensitivity calorimetric techniques have allowed the thermodynamics studies of drug–DNA interactions demonstrating that this complex is stabilized by a number of noncovalent interactions such as van der Waals interactions, hydrogen bonds and hydrophobic forces. Drugs that exhibit a binding preference for A-T base pairs appear favorable to hydrophobic contacts between the adenine C2 hydrogen atoms and the aromatic rings in the drug. Moreover, the hydrogen bond acceptors on the A-T base pairs (C2 carbonyl oxygen of thymine or N3 nitrogen of adenine) appeared to interact with any hydrogen bond donors on the drug (such as amide groups) ⁽⁷⁵⁾.

Permeability characteristic of calu-3 monolayer: *in vitro* correlation to predict amiloride and analogues absorption in lung.

The pulmonary epithelium is considered the most significant barrier to the absorption of compounds delivered into the lungs ⁽⁷⁶⁾. Calu-3 cell line forms tight monolayers ^(77, 78) and is considered a good cell culture model that mimics the transport and metabolic properties of human bronchial epithelium. In spite of its good barrier properties the Calu-3 line does not form fully pseudo-stratified differentiated, mucus secreting monolayers as found in NHBE cells. However, their cost, reproducibility and high proliferative capacity allows for easy application in academic laboratories.

In our studies, the Calu-3 model showed TER and FL-Na paracellular permeability of $\sim 1200 \Omega \text{ cm}^2$ and $\sim 0.400 \times 10^{-6} \text{ cm/s}$, respectively. This is comparable to other published works that employed the submerged Calu-3 culture ^{(79) (80)}.

Our results show a higher cell monolayer permeability to amiloride compared to 552-02, which is in agreement with Hirsh, Zhang ⁽¹⁷⁾. However, contrast the idea where more hydrophobic molecules are predicted to be absorbed more rapidly ⁽¹⁴⁾. For the QQA compounds, Calu-3 P_{app} decreased with increment of Log $P_{o/w}$. However, the range of compounds is very limited (Figure 4.22) and three of the four quaternary compounds are 1-3 Log units more hydrophilic than the most hydrophilic NQQA. The hydrophilic character of QQAs is likely to limit the transport pathway into / across the epithelia to the passive paracellular or active/facilitated transport pathways.

Mathia, Timoszyk ⁽⁸⁰⁾ evaluated the potential of Calu-3 cells as a permeability screen to predict in vivo absorption of hydrophobic (such as propranolol, antipyrine) and hydrophilic solute (such as caffeine, mannitol and theophylline) showing that Calu-3 cell line has low permeability to hydrophilic drugs and that hydrophilic drugs transport across the cell line via paracellular or active uptake. Saha, Kim ⁽⁸¹⁾ used primary cultured rat alveolar epithelial cell monolayers to investigate the influence of lipophilicity on the penetration of β -blockers. A combination of hydrophilic β -blockers (sotalol and atenolol) and lipophilic probes (propranolol, metoprolol, timolol, betaxolol) were used to demonstrate that lipophilic compounds were translocated primarily via the transcellular route whereas hydrophilic β -blockers traverse the alveolar epithelium via paracellular route.

As a corollary of this the permanently cationic character of QAA compounds should decrease epithelial permeability which is a major limitation for the airway efficacy of amiloride (Log P -0.89) and benzamil (Log P 1.45). Contrary to expectations, in our studies compound MC-08-DR04 which is a NQAA with cLog $P_{o/w}$ 0.02 was the most permeant ENaC inhibitor.

Unexpectedly, as showed in Figure 4.23, although the filter used in Transwell insert had a diameter of 0.4 μm appears to affect the permeation of molecules. This is obviously not size-restricted diffusion but instead binding to plasticware.

Correlation of percentage of mucin binding and P_{app} versus physical parameter of drug model were analyzed also using SPSS which did not show significant correlation between P_{app} and physical properties was found. SPSS was used to calculate the VIF which describes the extent of multicollinearity (or correlation between predictors) that exists in a regression analysis. The presence of high correlation between predictors can increase the variance of the regression coefficients, making them unstable and difficult to interpret. Our results indicate that both group of compounds, quaternary and NQQA, have a high multicollinearity indicating the need to extend significantly the range of compounds analyzed.

Sakamoto, Matsumaru ⁽⁸²⁾ reported the protein expression of 7 membrane transporters on human trachea bronchial Cell lines (Calu-3); OCT1, OCT3, OCTN1 and OCTN2 for the solute carrier transport family (SLC), and for ABC transporter family multidrug resistance

associated protein (MRP) 1, 2 and breast cancer resistance protein (BCRP). As shown by Horvath, Schmid⁽⁸³⁾ OCTNs transporters appear to be involved in the uptake of inhaled drugs, such as albuterol have a high interaction with charged compounds. Furthermore, Biermann⁽⁸⁴⁾ using fluorescence microscopy, provided supporting evidence for the role of OCT2-facilitated uptake of amiloride into cells using an OCT2-overexpressing HEK293 cell model. Future investigations should investigate further the role of OCT(N) transporters in the uptake and transport of ENaC blockers across lung epithelial cells such as Calu-3 monolayers. The use of intact, *ex vivo* or *in vivo* lung models⁽⁸⁵⁾ would provide an optimal model for studying drug disposition in a complex multicellular architecture.

Influence of porcine purified mucin on 552-02 apparent permeability across Calu-3 monolayer.

The guanidine-containing analogue 552-02 showed extensive mucin-binding (20% at 20 μ M) and was available in good amounts from our collaborators. Moreover, preliminary NMR experiments (described in Chapter 5) had shown promising results. For these reasons 552-02 was chosen to investigate the effect of mucin-binding on Calu-3 permeability. The hypothesis of this work was that extensive mucin binding would reduce the free concentration of 552-02 available for transepithelial transport which would be observed as a reduction in the P_{app} of Calu-3 monolayers. Unexpectedly, the addition of highly purified and extensively dialyzed mucin (see Chapter 5) severely disrupted Calu-3 monolayer and increased transport some 20-fold. Although this effect was unexpected, others⁽⁸⁶⁾ have reported an increased Caco-2 intestinal epithelial

permeability after exposure to biosimilar mucus. This mucus model was composed of polyacrylic acid, mucin (5% w/v), lipid mixture with linoleic acid content ranged 0.06-2.46% (w/v), cholesterol, phosphatidylcholine and polysorbate 80. The permeability enhancing effects of the biosimilar model was attributed to the high concentration of linoleic acid which has been demonstrated to be highly cytotoxic on human umbilical vein endothelial cells ^(87, 88). When the linoleic acid content was restricted to 0.06-0.11% w/v resulted fully compatible with the Caco-2 cells following MTS assay. Only at concentration above 2.4 % Caco-2 cell viability was reduced.

In the CsCl density gradient centrifugation lipids are expected to display a buoyant density of 1.00-1.200 g/ml ⁽⁸⁹⁾ and distinct from the fraction at ~1.4 g/ml from where mucin was harvested. The persistence of guanidine in purified mucin is a more likely cause of decreased monolayer viability. In spite of a 24 hours dialysis regime it is feasible that the concentration of guanidine did not reduce sufficiently from 4M guanidine to avoid a toxic effect of Calu-3 monolayer. Cytotoxicity effect of polyhexamethylene guanidine hydrochloride on human alveolar A549 cells was demonstrated by ⁽⁹⁰⁾ who showed that cell death after treatment with polyhexamethylene guanidine hydrochloride was associated with formation of intracellular reactive oxygen species and apoptosis at even 2 µg/mL concentration.

Alternatively, fatty acid contamination could have imparted a cytotoxic effect. For example, Hansson and coworkers Hansson, Sheehan ⁽⁹¹⁾ reported that the fatty acid content of human airway, human cervix and pig stomach mucin after CsCl purification ranged from 0.4 to 0.9 µg of fatty acid/mg of glycoprotein.

Conclusion

In conclusion, we developed and applied a sensitive and quantitative ultrafiltration mucin binding assay with opportunity for automated screening of drug-mucus binding.

We have shown that mucin-binding may affect the lung disposition of inhaled ENaC blockers in the CF lung. Hydrophobicity is generally considered to be a key determinant of drug absorption from the airways. Taken alongside the observed effect of hydrophobic character is determining mucin-binding it is feasible to conclude that the lung transepithelial transport of hydrophobic solutes could be retarded by mucin-binding.

Moreover, DNA and alginate binding appeared extensive for QQA but NQAA drug physical properties appear not correlated to DNA and alginate binding. The extension of the range of drug model may elucidate the involvement of other physical properties into the interaction as for better understand the correlation between P_{app} and drugs physical parameters.

4.5 Reference

1. Bartlett JA, Fischer AJ, McCray PB, Jr. Innate immune functions of the airway epithelium. *Contributions to microbiology*. 2008;15:147-63.
2. Knight DA, Holgate ST. The airway epithelium: structural and functional properties in health and disease. *Respirology*. 2003;8(4):432-46.
3. Puchelle E, Zahm JM, Tournier JM, Coraux C. Airway epithelial repair, regeneration, and remodeling after injury in chronic obstructive pulmonary disease. *Proceedings of the American Thoracic Society*. 2006;3(8):726-33.
4. Boucher RC. Regulation of airway surface liquid volume by human airway epithelia. *Pflügers Archiv : European journal of physiology*. 2003;445(4):495-8.
5. Tarran R, Button B, Boucher RC. Regulation of normal and cystic fibrosis airway surface liquid volume by phasic shear stress. *Annual review of physiology*. 2006;68:543-61.
6. Ballard ST, Spadafora D. Fluid secretion by submucosal glands of the tracheobronchial airways. *Respiratory physiology & neurobiology*. 2007;159(3):271-7.
7. Worthington EN, Tarran R. Methods for ASL measurements and mucus transport rates in cell cultures. *Methods in molecular biology*. 2011;742:77-92.
8. Worlitzsch D, Tarran R, Ulrich M, Schwab U, Cekici A, Meyer KC, et al. Effects of reduced mucus oxygen concentration in airway *Pseudomonas* infections of cystic fibrosis patients. *The Journal of clinical investigation*. 2002;109(3):317-25.
9. Hobbs CA, Da Tan C, Tarran R. Does epithelial sodium channel hyperactivity contribute to cystic fibrosis lung disease? *The Journal of physiology*. 2013;591(18):4377-87.
10. Hirsh AJ. Altering airway surface liquid volume: inhalation therapy with amiloride and hyperosmotic agents. *Advanced drug delivery reviews*. 2002;54(11):1445-62.
11. Tarran R, Grubb BR, Parsons D, Picher M, Hirsh AJ, Davis CW, et al. The CF salt controversy: in vivo observations and therapeutic approaches. *Molecular cell*. 2001;8(1):149-58.
12. Pons G, Marchand MC, d'Athis P, Sauvage E, Foucard C, Chaumet-Riffaud P, et al. French multicenter randomized double-blind placebo-controlled trial on nebulized amiloride in cystic fibrosis patients. The Amiloride-AFLM Collaborative Study Group. *Pediatric pulmonology*. 2000;30(1):25-31.
13. Noone PG, Regnis JA, Liu X, Brouwer KL, Robinson M, Edwards L, et al. Airway deposition and clearance and systemic pharmacokinetics of amiloride following aerosolization with an ultrasonic nebulizer to normal airways. *Chest*. 1997;112(5):1283-90.
14. Hofmann T, Stutts MJ, Ziersch A, Ruckes C, Weber WM, Knowles MR, et al. Effects of topically delivered benzamil and amiloride on nasal potential difference in cystic fibrosis. *American journal of respiratory and critical care medicine*. 1998;157(6 Pt 1):1844-9.
15. Kleyman TR, Cragoe EJ, Jr. Amiloride and its analogs as tools in the study of ion transport. *The Journal of membrane biology*. 1988;105(1):1-21.
16. Hirsh AJ, Sabater JR, Zamurs A, Smith RT, Paradiso AM, Hopkins S, et al. Evaluation of second generation amiloride analogs as therapy for cystic fibrosis lung disease. *The Journal of pharmacology and experimental therapeutics*. 2004;311(3):929-38.

17. Hirsh AJ, Zhang J, Zamurs A, Fleegle J, Thelin WR, Caldwell RA, et al. Pharmacological properties of N-(3,5-diamino-6-chloropyrazine-2-carbonyl)- butyl-guanidine methanesulfonate (552-02), a novel epithelial sodium channel blocker with potential clinical efficacy for cystic fibrosis lung disease. *The Journal of pharmacology and experimental therapeutics*. 2008;325(1):77-88.
18. O'Riordan TG, Donn KH, Hodsmann P, Ansedde JH, Newcomb T, Lewis SA, et al. Acute hyperkalemia associated with inhalation of a potent ENaC antagonist: Phase 1 trial of GS-9411. *Journal of aerosol medicine and pulmonary drug delivery*. 2014;27(3):200-8.
19. Wesley AW, Qureshi AR, Forstner GG, Forstner JF. Differences in mucus glycoproteins of small intestine from subjects with and without cystic fibrosis. *Advances in experimental medicine and biology*. 1982;144:145-6.
20. Burns MW, May JR. Bacterial precipitins in serum of patients with cystic fibrosis. *Lancet*. 1968;1(7537):270-2.
21. Krieg DP, Helmke RJ, German VF, Mangos JA. Resistance of Mucoicid *Pseudomonas-Aeruginosa* to Nonopsonic Phagocytosis by Alveolar Macrophages In vitro. *Infection and immunity*. 1988;56(12):3173-9.
22. Davis SD, Bruns WT. Effects of sputum from patients with cystic fibrosis on the activity in vitro of 5 antimicrobial drugs on *Pseudomonas aeruginosa*. *The American review of respiratory disease*. 1978;117(1):176-8.
23. Ramphal R, Lhermitte M, Filliat M, Roussel P. The binding of anti-pseudomonal antibiotics to macromolecules from cystic fibrosis sputum. *The Journal of antimicrobial chemotherapy*. 1988;22(4):483-90.
24. Huang JX, Blaskovich MA, Pelington R, Ramu S, Kavanagh A, Elliott AG, et al. Mucin Binding Reduces Colistin Antimicrobial Activity. *Antimicrobial agents and chemotherapy*. 2015;59(10):5925-31.
25. Braybrooks MP, Barry BW, Abbs ET. The effect of mucin on the bioavailability of tetracycline from the gastrointestinal tract; in vivo, in vitro correlations. *The Journal of pharmacy and pharmacology*. 1975;27(7):508-15.
26. Bhat PG, Flanagan DR, Donovan PD. Drug binding to gastric mucus glycoproteins. *Int J Pharm*. 1996;134(1-2):15-25.
27. Taylor S, Harker A. Modification of the ultrafiltration technique to overcome solubility and non-specific binding challenges associated with the measurement of plasma protein binding of corticosteroids. *Journal of pharmaceutical and biomedical analysis*. 2006;41(1):299-303.
28. Tasker RA, Nakatsu K. Factors affecting ultrafiltration-assessed values for drug binding. *Clinical chemistry*. 1982;28(5):1244-6.
29. Banker MJ, Clark TH, Williams JA. Development and validation of a 96-well equilibrium dialysis apparatus for measuring plasma protein binding. *Journal of pharmaceutical sciences*. 2003;92(5):967-74.
30. Vaughan WM, Weber G. Oxygen quenching of pyrenebutyric acid fluorescence in water. A dynamic probe of the microenvironment. *Biochemistry*. 1970;9(3):464-73.
31. Zhang HX, Huang X, Zhang M. Thermodynamic studies on the interaction of dioxopromethazine to beta-cyclodextrin and bovine serum albumin. *Journal of fluorescence*. 2008;18(3-4):753-60.

32. Ma HM, Chen X, Zhang N, Han YY, Wu D, Du B, et al. Spectroscopic studies on the interaction of a water-soluble cationic porphyrin with proteins. *Spectrochimica acta Part A, Molecular and biomolecular spectroscopy*. 2009;72(3):465-9.
33. Barre J, Chamouard JM, Houin G, Tillement JP. Equilibrium dialysis, ultrafiltration, and ultracentrifugation compared for determining the plasma-protein-binding characteristics of valproic acid. *Clinical chemistry*. 1985;31(1):60-4.
34. Bekersky I, Fielding RM, Dressler DE, Lee JW, Buell DN, Walsh TJ. Plasma protein binding of amphotericin B and pharmacokinetics of bound versus unbound amphotericin B after administration of intravenous liposomal amphotericin B (AmBisome) and amphotericin B deoxycholate. *Antimicrobial agents and chemotherapy*. 2002;46(3):834-40.
35. Zhao Y, Chen L, Yakubov G, Aminiafshar T, Han L, Lian G. Experimental and theoretical studies on the binding of epigallocatechin gallate to purified porcine gastric mucin. *The journal of physical chemistry B*. 2012;116(43):13010-6.
36. Gordon CA, Hodges NA, Marriott C. Antibiotic interaction and diffusion through alginate and exopolysaccharide of cystic fibrosis-derived *Pseudomonas aeruginosa*. *The Journal of antimicrobial chemotherapy*. 1988;22(5):667-74.
37. Besterman JM, Elwell LP, Cragoe EJ, Jr., Andrews CW, Cory M. DNA intercalation and inhibition of topoisomerase II. Structure-activity relationships for a series of amiloride analogs. *The Journal of biological chemistry*. 1989;264(4):2324-30.
38. Mirmomtaz E, Ensafi AA, Soleimani-Zad S. Determination of amiloride using a ds-DNA-modified pencil graphite electrode based on guanine and adenine signals. *Electrochim Acta*. 2009;54(3):1141-6.
39. Plunkett KN, Berkowski KL, Moore JS. Chymotrypsin responsive hydrogel: application of a disulfide exchange protocol for the preparation of methacrylamide containing peptides. *Biomacromolecules*. 2005;6(2):632-7.
40. Hunt T, Atherton-Watson HC, Collingwood SP, Coote KJ, Czarnecki S, Danahay H, et al. Discovery of a novel chemotype of potent human ENaC blockers using a bioisostere approach. Part 2: alpha-Branched quaternary amines. *Bioorganic & medicinal chemistry letters*. 2012;22(8):2877-9.
41. Yu X, Liu H, Yang Y, Lu S, Yao Q, Yi P. The investigation of the interaction between Oxymetazoline hydrochloride and mucin by spectroscopic approaches. *Spectrochimica acta Part A, Molecular and biomolecular spectroscopy*. 2013;103:125-9.
42. Zhang HX, Mei P, Yang XX. Optical, structural and thermodynamic properties of the interaction between tradimefon and serum albumin. *Spectrochimica acta Part A, Molecular and biomolecular spectroscopy*. 2009;72(3):621-6.
43. Yu JH, Li B, Dai P, Ge SG. Molecular simulation of the interaction between novel type rhodanine derivative probe and bovine serum albumin. *Spectrochim Acta A*. 2009;74(1):277-81.
44. Fung EN, Chen YH, Lau YY. Semi-automatic high-throughput determination of plasma protein binding using a 96-well plate filtrate assembly and fast liquid chromatography-tandem mass spectrometry. *Journal of chromatography B, Analytical technologies in the biomedical and life sciences*. 2003;795(2):187-94.

45. Godolphin W, Trepanier J, Farrell K. Serum and plasma for total and free anticonvulsant drug analyses: effects on EMIT assays and ultrafiltration devices. *Therapeutic drug monitoring*. 1983;5(3):319-23.
46. Wang Y, Mathis CA, Huang GF, Debnath ML, Holt DP, Shao L, et al. Effects of lipophilicity on the affinity and nonspecific binding of iodinated benzothiazole derivatives. *Journal of molecular neuroscience : MN*. 2003;20(3):255-60.
47. Dickson CJ, Gee AD, Bennacef I, Gould IR, Rosso L. Further evaluation of quantum chemical methods for the prediction of non-specific binding of positron emission tomography tracers. *Physical chemistry chemical physics : PCCP*. 2011;13(48):21552-7.
48. Lee KJ, Mower R, Hollenbeck T, Castelo J, Johnson N, Gordon P, et al. Modulation of nonspecific binding in ultrafiltration protein binding studies. *Pharmaceutical research*. 2003;20(7):1015-21.
49. Mizushima H, Takanaka K, Abe K, Fukazawa I, Ishizuka H. Stereoselective pharmacokinetics of oxybutynin and N-desethyloxybutynin in vitro and in vivo. *Xenobiotica; the fate of foreign compounds in biological systems*. 2007;37(1):59-73.
50. Campo VL, Bernardes LS, Carvalho I. Stereoselectivity in drug metabolism: molecular mechanisms and analytical methods. *Current drug metabolism*. 2009;10(2):188-205.
51. Shen Q, Wang L, Zhou H, Jiang HD, Yu LS, Zeng S. Stereoselective binding of chiral drugs to plasma proteins. *Acta pharmacologica Sinica*. 2013;34(8):998-1006.
52. Sun SY, Wang YQ, Li LP, Wang L, Zeng S, Zhou H, et al. Stereoselective interaction between tetrahydropalmatine enantiomers and CYP enzymes in human liver microsomes. *Chirality*. 2013;25(1):43-7.
53. Albani F, Riva R, Contin M, Baruzzi A. Stereoselective binding of propranolol enantiomers to human alpha 1-acid glycoprotein and human plasma. *British journal of clinical pharmacology*. 1984;18(2):244-6.
54. Ofori-Adjei D, Ericsson O, Lindstrom B, Sjoqvist F. Protein binding of chloroquine enantiomers and desethylchloroquine. *British journal of clinical pharmacology*. 1986;22(3):356-8.
55. Chitpan M, Wang X, Ho CT, Huang Q. Monitoring the binding processes of black tea thearubigin to the bovine serum albumin surface using quartz crystal microbalance with dissipation monitoring. *Journal of agricultural and food chemistry*. 2007;55(25):10110-6.
56. Aluko RE, Yada RY. Relationship of Hydrophobicity and Solubility with Some Functional-Properties of Cowpea (*Vigna-Unguiculata*) Protein Isolate. *J Sci Food Agr*. 1993;62(4):331-5.
57. Sigurdsson HH, Kirch J, Lehr CM. Mucus as a barrier to lipophilic drugs. *Int J Pharm*. 2013;453(1):56-64.
58. Caron G, Visentin S, Pontremoli C, Ermondi G. Profile of the intermolecular forces governing the interaction of drugs with mucin. *Int J Pharm*. 2015;488(1-2):67-9.
59. Knowles MR, Church NL, Waltner WE, Yankaskas JR, Gilligan P, King M, et al. A pilot study of aerosolized amiloride for the treatment of lung disease in cystic fibrosis. *The New England journal of medicine*. 1990;322(17):1189-94.
60. Yamagami C, Kawase K, Iwaki K. Hydrophobicity parameters determined by reversed-phase liquid chromatograph. XV: Optimal conditions for prediction of log P-oct by using RP-HPLC procedures. *Chem Pharm Bull*. 2002;50(12):1578-83.

Chapter 4

61. Komiya I, Park JY, Kamani A, Ho NFH, Higuchi WI. Quantitative Mechanistic Studies in Simultaneous Fluid-Flow and Intestinal-Absorption Using Steroids as Model Solutes. *Int J Pharm.* 1980;4(3):249-62.
62. Bhat PG, Flanagan DR, Donovan MD. The limiting role of mucus in drug absorption: Drug permeation through mucus solution. *Int J Pharm.* 1995;126(1-2):179-87.
63. Kearney P, Marriott C. The Effects of Mucus Glycoproteins on the Bioavailability of Tetracycline .3. Everted Gut Studies. *Int J Pharm.* 1987;38(1-3):211-20.
64. Niibuchi JJ, Aramaki Y, Tsuchiya S. Binding of Antibiotics to Rat Intestinal Mucin. *Int J Pharm.* 1986;30(2-3):181-7.
65. Pedersen SS, Hoiby N, Espersen F, Koch C. Role of alginate in infection with mucoid *Pseudomonas aeruginosa* in cystic fibrosis. *Thorax.* 1992;47(1):6-13.
66. Evans LR, Linker A. Production and characterization of the slime polysaccharide of *Pseudomonas aeruginosa*. *Journal of bacteriology.* 1973;116(2):915-24.
67. Berry A, Devault JD, Chakrabarty AM. High Osmolarity Is a Signal for Enhanced Algd Transcription in Mucooid and Nonmucooid *Pseudomonas-Aeruginosa* Strains. *Journal of bacteriology.* 1989;171(5):2312-7.
68. Devault JD, Kimbara K, Chakrabarty AM. Pulmonary Dehydration and Infection in Cystic-Fibrosis - Evidence That Ethanol Activates Alginate Gene-Expression and Induction of Mucoidity in *Pseudomonas-Aeruginosa*. *Mol Microbiol.* 1990;4(5):737-45.
69. Deretic V, Schurr MJ, Boucher JC, Martin DW. Conversion of *Pseudomonas aeruginosa* to mucoidy in cystic fibrosis: environmental stress and regulation of bacterial virulence by alternative sigma factors. *Journal of bacteriology.* 1994;176(10):2773-80.
70. Devault JD, Berry A, Misra TK, Darzins A, Chakrabarty AM. Environmental Sensory Signals and Microbial Pathogenesis - *Pseudomonas-Aeruginosa* Infection in Cystic-Fibrosis. *Bio-Technol.* 1989;7(4):352-7.
71. Fahy JV, Steiger DJ, Liu J, Basbaum CB, Finkbeiner WE, Boushey HA. Markers of mucus secretion and DNA levels in induced sputum from asthmatic and from healthy subjects. *The American review of respiratory disease.* 1993;147(5):1132-7.
72. Brandt T, Breitenstein S, von der Hardt H, Tummler B. DNA concentration and length in sputum of patients with cystic fibrosis during inhalation with recombinant human DNase. *Thorax.* 1995;50(8):880-2.
73. Besterman JM, Elwell LP, Blanchard SG, Cory M. Amiloride intercalates into DNA and inhibits DNA topoisomerase II. *The Journal of biological chemistry.* 1987;262(27):13352-8.
74. Bailly C, Cuthbert AW, Gentle D, Knowles MR, Waring MJ. Sequence-selective binding of amiloride to DNA. *Biochemistry.* 1993;32(10):2514-24.
75. Haq I. Thermodynamics of drug-DNA interactions. *Archives of biochemistry and biophysics.* 2002;403(1):1-15.
76. Patton. Mechanisms of macromolecule absorption by the lungs. *Advanced drug delivery reviews.* 1996;19(1):3-36.

77. Finkbeiner WE, Carrier SD, Teresi CE. Reverse transcription-polymerase chain reaction (RT-PCR) phenotypic analysis of cell cultures of human tracheal epithelium, tracheobronchial glands, and lung carcinomas. *American journal of respiratory cell and molecular biology*. 1993;9(5):547-56.
78. Lee MC, Penland CM, Widdicombe JH, Wine JJ. Evidence that Calu-3 human airway cells secrete bicarbonate. *The American journal of physiology*. 1998;274(3 Pt 1):L450-3.
79. Grainger CI, Greenwell LL, Lockley DJ, Martin GP, Forbes B. Culture of Calu-3 cells at the air interface provides a representative model of the airway epithelial barrier. *Pharmaceutical research*. 2006;23(7):1482-90.
80. Mathia NR, Timoszyk J, Stetsko PI, Megill JR, Smith RL, Wall DA. Permeability characteristics of calu-3 human bronchial epithelial cells: in vitro-in vivo correlation to predict lung absorption in rats. *Journal of drug targeting*. 2002;10(1):31-40.
81. Saha P, Kim KJ, Yamahara H, Crandall ED. Influence of Lipophilicity on Beta-Blocker Permeation across Rat Alveolar Epithelial-Cell Monolayers. *J Control Release*. 1994;32(2):191-200.
82. Sakamoto A, Matsumaru T, Yamamura N, Suzuki S, Uchida Y, Tachikawa M, et al. Drug Transporter Protein Quantification of Immortalized Human Lung Cell Lines Derived from Tracheobronchial Epithelial Cells (Calu-3 and BEAS2-B), Bronchiolar-Alveolar Cells (NCI-H292 and NCI-H441), and Alveolar Type II-like Cells (A549) by Liquid Chromatography-Tandem Mass Spectrometry. *Journal of pharmaceutical sciences*. 2015;104(9):3029-38.
83. Horvath G, Schmid N, Fragoso MA, Schmid A, Conner GE, Salathe M, et al. Epithelial organic cation transporters ensure pH-dependent drug absorption in the airway. *American journal of respiratory cell and molecular biology*. 2007;36(1):53-60.
84. Biermann J. Characterization of regulatory mechanisms and states of human organic cation transporter 2. *American Journal of Physiology - Cell Physiology*. 2006;290.
85. Sakagami M. In vivo, in vitro and ex vivo models to assess pulmonary absorption and disposition of inhaled therapeutics for systemic delivery. *Advanced drug delivery reviews*. 2006;58(9-10):1030-60.
86. Boegh M, Baldursdottir SG, Mullertz A, Nielsen HM. Property profiling of biosimilar mucus in a novel mucus-containing in vitro model for assessment of intestinal drug absorption. *official journal of Arbeitsgemeinschaft fur Pharmazeutische Verfahrenstechnik eV*. 2014;87(2):227-35.
87. Qin X, Dong W, Sharpe SM, Sheth SU, Palange DC, Rider T, et al. Role of lipase-generated free fatty acids in converting mesenteric lymph from a noncytotoxic to a cytotoxic fluid. *American journal of physiology Gastrointestinal and liver physiology*. 2012;303(8):G969-78.
88. Larhed AW, Artursson P, Bjork E. The influence of intestinal mucus components on the diffusion of drugs. *Pharmaceutical research*. 1998;15(1):66-71.
89. Cheung MC, Albers JJ. Distribution of high density lipoprotein particles with different apoprotein composition: particles with A-I and A-II and particles with A-I but no A-II. *Journal of lipid research*. 1982;23(5):747-53.
90. Jung HN, Zerlin T, Podder B, Song HY, Kim YS. Cytotoxicity and gene expression profiling of polyhexamethylene guanidine hydrochloride in human alveolar A549 cells. *Toxicology in vitro : an international journal published in association with BIBRA*. 2014;28(4):684-92.
91. Hansson GC, Sheehan JK, Carlstedt I. Only Trace Amounts of Fatty-Acids Are Found in Pure Mucus Glycoproteins. *Archives of biochemistry and biophysics*. 1988;266(1):197-200.

Chapter 5 : Investigation of drug-mucin interaction by STD-NMR

5.1 Introduction

Mucociliary clearance (MC) is a coordinated system of epithelial mucus secretion, cilia action, and cough, used to preserve the healthy environment in the lung ⁽¹⁾. MC is impaired in respiratory disease such as in COPD ⁽²⁾ CF ⁽³⁾ bronchiolitis ⁽⁴⁾ and asthma ⁽⁵⁾ leading airway inflammation and obstruction due to mucus hypersecretion and dehydration.

Therapy to maintain ASL hydration is important during not only in CF patients but in all chronic airway diseases ^(3, 6). It has been shown that MC in people with COPD and bronchiolitis is enhanced with administration of aerosolized salbutamol, ^(7, 8) a bronchodilator agent that significantly increases ciliary beat frequency of human nasal and bronchial epithelial cells after stimulation of adenylyl cyclase and the subsequent rises of cAMP ⁽⁹⁾. Although the disposition of salbutamol appears to be unchanged in asthma and COPD ⁽¹⁰⁾ it appears improved in CF patients showing a faster increment of concentration peak in serum ⁽¹¹⁾.

For CF it is thought that inhalation of ENaC blockers may enhance MC due to a reduction in water reabsorption which, in turn, re-establishes appropriate airway hydration ^(12, 13).

The prime cause of patient morbidity in CF is associated with chronic lung infection with pathogens such as *Pseudomonas aeruginosa* ⁽¹⁴⁾. Aggressive antibiotic treatment can only temporarily reduce *P. aeruginosa* ⁽¹⁵⁾ and it is inevitable that chronic re-infection will occur. Tobramycin is an aminoglycoside antibiotic used to treat various types of bacterial infections, particularly Gram-negative infections and the nebulised formulation

Chapter 5

is indicated in the treatment of chronic infection with *P. aeruginosa* in patients with cystic fibrosis ^(15, 16).

The efficacy of aerosol therapy in CF may be limited by the interaction of drugs with mucus components. For example, early studies of Saggars and Lawson ⁽¹⁷⁾ showed that mucus affect the activity of antibiotics. Several techniques have been used as tool to characterize the nature of drug–mucin interactions such as mucus diffusion assays ⁽¹⁸⁾, dialysis and ultrafiltration assays ^{(19) (20)}, UV-vis absorption and fluorescent spectrophotometry technique ⁽²¹⁾. Bhat, Flanagan ⁽²²⁾ using an *in vitro* diafiltration technique (combination of dialysis and ultrafiltration) showed the presence of interactions between salbutamol and commercial porcine gastric mucin, and Ramphal, Lhermitte ⁽²³⁾ demonstrated the interaction of tobramycin with whole CF mucus sputum using ultrafiltration technique. Chapter 4 detailed the development and application of a 96-ultrafiltration assay which showed the presence of interaction between ENaC blockers and commercial partially purified mucin, PGM. These techniques afford the detection of binding kinetics and stoichiometries, however It is necessary to employ complementary high resolution structural techniques to better understand the nature of mucin-drug interactions the at the molecular level.

NMR spectroscopy has been used to obtain structural insights and binding properties of the ligand-protein complexes ⁽²⁴⁾ using a variety of methods such as transfer NOEs to asses conformational analysis of the bound ligand ⁽²⁵⁾ and pulsed-gradient spin-echo

Chapter 5

NMR (PGSE-NMR) to examine the diffusion of polymers through mucus solutions ⁽²⁶⁾ ⁽²⁷⁾ ⁽²⁸⁾. STD-NMR ⁽²⁹⁾ is a relatively new technique that has been used to provide ligand structural information when bound to its target ⁽³⁰⁾ ⁽³¹⁾. Initially used to study transient protein-carbohydrate interactions, the STD-NMR applications for detection and characterization of transient ligand-macromolecule interaction has steadily increased and was rapidly used to characterize interactions between nucleic acid and ligands ⁽³²⁾, proteins and peptides ⁽³³⁾ and also used by Mari, Serrano-Gomez ⁽³⁴⁾ to study the interactions between ligands and extracellular membrane proteins using living cells. STD-NMR can be also used to have confirmation of drug-mucin binding and allow the identification of the “binding epitope” or the hydrogen atoms of the ligand involved in the interaction with its cognate receptor ⁽³⁵⁾, and may lead to the design of more powerful molecules and the improvement of inhalation therapies.

In the mucin research field STD-NMR has been applied to determine the target epitope of short MUC1-derived tumour-associated glycopeptides when bound to the breast cancer-selective monoclonal antibody SM3 ⁽³⁶⁾ and to identify the binding properties of MUC1 interactions with human macrophage galactose type lectin ⁽³⁷⁾.

The aim of this chapter was to apply, for the first time, the use of STD-NMR technique to study mucin-ENaC blocker interactions. Pilot studies included studies on the binding of tobramycin to fresh, unpurified PLM. Significant DNA contamination in PLM supported the use of PGM as a more refined mucin model to examine mucin binding interactions for salbutamol, tobramycin and two amiloride analogues; OF-80-NS22 and 552-02. The

Chapter 5

structural features of these drugs allowed for the mapping of drug structural domains as “interacting” and “non-interacting”. Studies on these ENaC blockers were extended to include the use of highly purified porcine jejunal mucin (PJM).

5.2 Material and methods

Materials

Porcine lungs and jejunum tissue were sourced freshly after slaughter from H G Blake, Ltd. (Norwich, UK). Mucin powder from porcine stomach (type III), tobramycin, EDTA, CsCl and Wilmad® NMR tube 5mm and 3.3 mm were purchased from Sigma Aldrich (Gillingham, UK), Salbutamol sulfate 99% was purchased from Alfa Aesar (Heysham, UK), deuterium oxide was purchased from Cambridge Isotope Laboratories Inc (Massachusetts, USA). Dimethyl sulfoxide-d6 (99.5% D) was purchased from VWR (Leuven, Belgium), Vivaspin 6 (10 kDa), N-ethyl maleimide and guanidine were purchased from Thermo Fisher Scientific (UK) and Amicon Ultra-0.5 Centrifugal Filter 10 kDa were purchased from Millipore (UK). Quick seal centrifuge tube Beckman Coulter (High Wycombe, UK), Cellulose ester dialysis membrane MWCO 10 kDa (Spectra/Por Biotech). Compounds OF-08-NS22 and 552-02 were donated by Novartis (CH).

Methods

Harvest of fresh porcine respiratory mucus

Respiratory porcine mucus was collected as described in Chapter 2 section 2.2.2.

Isolation and purification of jejunal porcine mucus

Jejunal porcine mucus was collected and purified purification as described in Chapter 2 section 2.7.2.

Chapter 5

Determination of biochemical properties

Mucin and DNA content were determined using 2-CAN and DAPA respectively (Chapter 2 section 2.4). Mucus solid %dry was determined using the following equation;

$$\% \text{ dry} = \left(\frac{W_{\text{dry}}}{W_{\text{wet}}} \right) \times 100\%$$

Pilot STD-NMR studies of tobramycin and salbutamol binding to fresh porcine respiratory mucus and PGM

Mucin and drug preparation for STD-NMR studies are described in Chapter 2 section 2.8.4.

STD-NMR studies of OF-80-NS22 and 552-02 binding to PGM and purified PJM

Mucin and drug preparation for STD-NMR studies are described in Chapter 2 section 2.8.5.4.

Glycerol contamination was eliminated as described in chapter 2 section 2.8.5.1.

5.3 Results

5.3.1 Tobramycin binding to PLM and PGM studies by STD-NMR

Initial STD-NMR studies involved the study of the aminoglycoside antibiotic, tobramycin binding to fresh PLM. The use of 800MHz NMR instrument afforded a well resolved ^1H spectrum of tobramycin. Although a full structural assignment was not performed the spectrum was consistent with low field NMR structural data⁽³⁸⁾. The reference spectrum (I₀) for the tobramycin and mucus are shown in Figure 5.1 A and B respectively. Tobramycin-mixture reference spectrum- (Figure 5.1 C) showed evidence of several overlapping peaks. Notably, two well-resolved and non-overlapping tobramycin peaks at ~5.5 and 5.6 ppm shifted upfield by 0.2 ppm. In the STD-NMR spectrum, very weak STD signals were observable (indicated by dashed lines in the Figure 5.1 D) which is an indicator of mucin-tobramycin interaction. The shifting of tobramycin peaks upon mixing with mucin in addition to the complex and broad peaks of mucin precluded the assignment of the tobramycin binding motif.

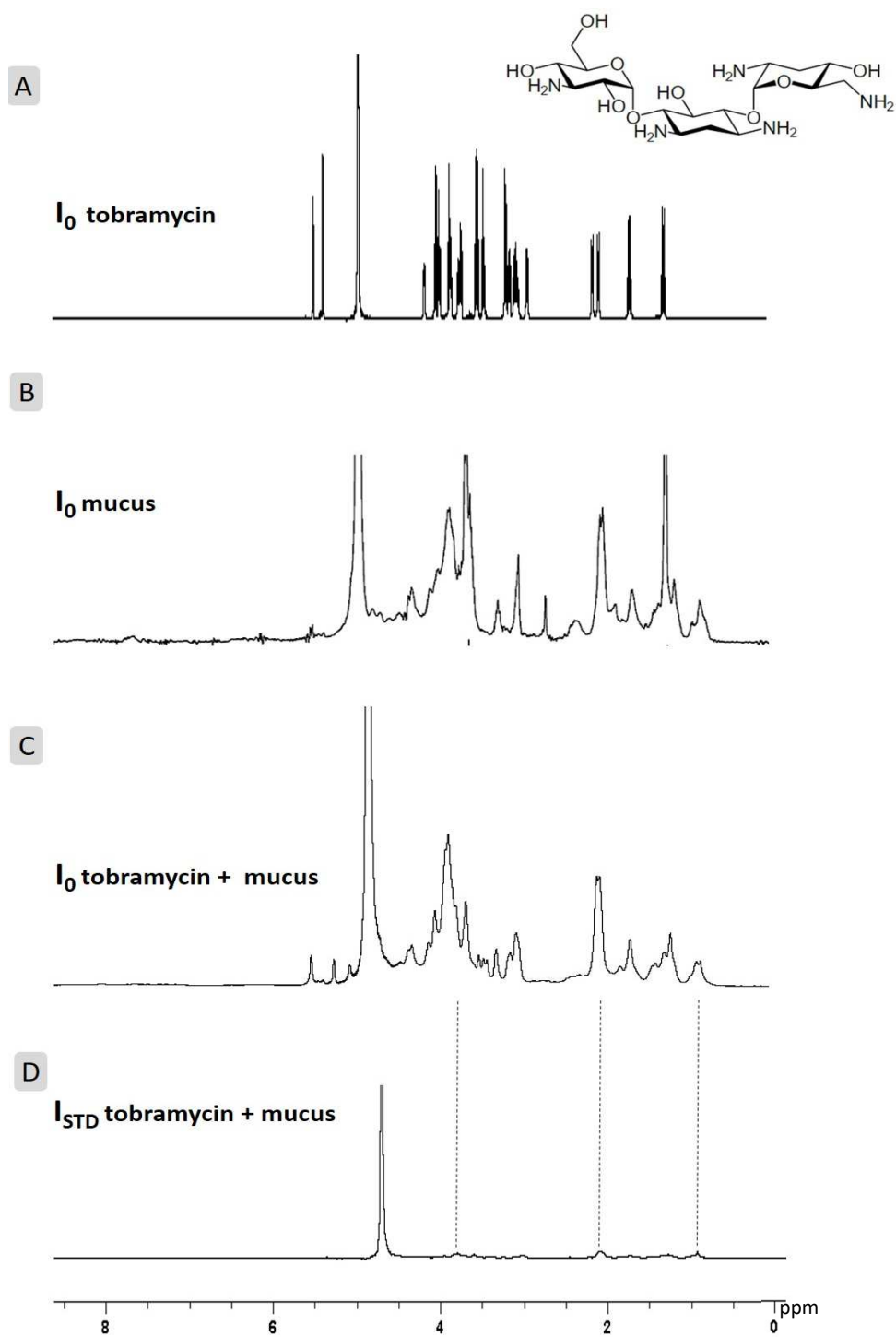


Figure 5.1. STD-NMR spectroscopy for the study of tobramycin-porcine respiratory mucus binding. **A:** reference ^1H NMR of 5mg/ml tobramycin solution in D_2O ; **B** reference ^1H NMR of mucus. **C:** 1D ^1H reference spectrum of mixture tobramycin-mucus; **D:** ^1H NMR (on-resonance) transfer of saturation from protein to ligand. Solvent (D_2O) peak at chemical shift of 4.7 ppm.

Chapter 5

Figure 5.2 shows the reference spectra and STD spectra of PGM and tobramycin-PGM mixtures. Figure 5.2C includes some non-overlapping peaks (0.88 and 2.36 ppm) that are attributable to mucin in spite of a vast molar excess of ligand (10 mM versus 1.5 μ M mucin assuming mucin MW of 1 MDa). Integration of the STD spectrum peak (Figure 5.2D) illustrates that tobramycin protons receive saturation from the glycoprotein but are very weak STD signal with intensities of 1.1%.

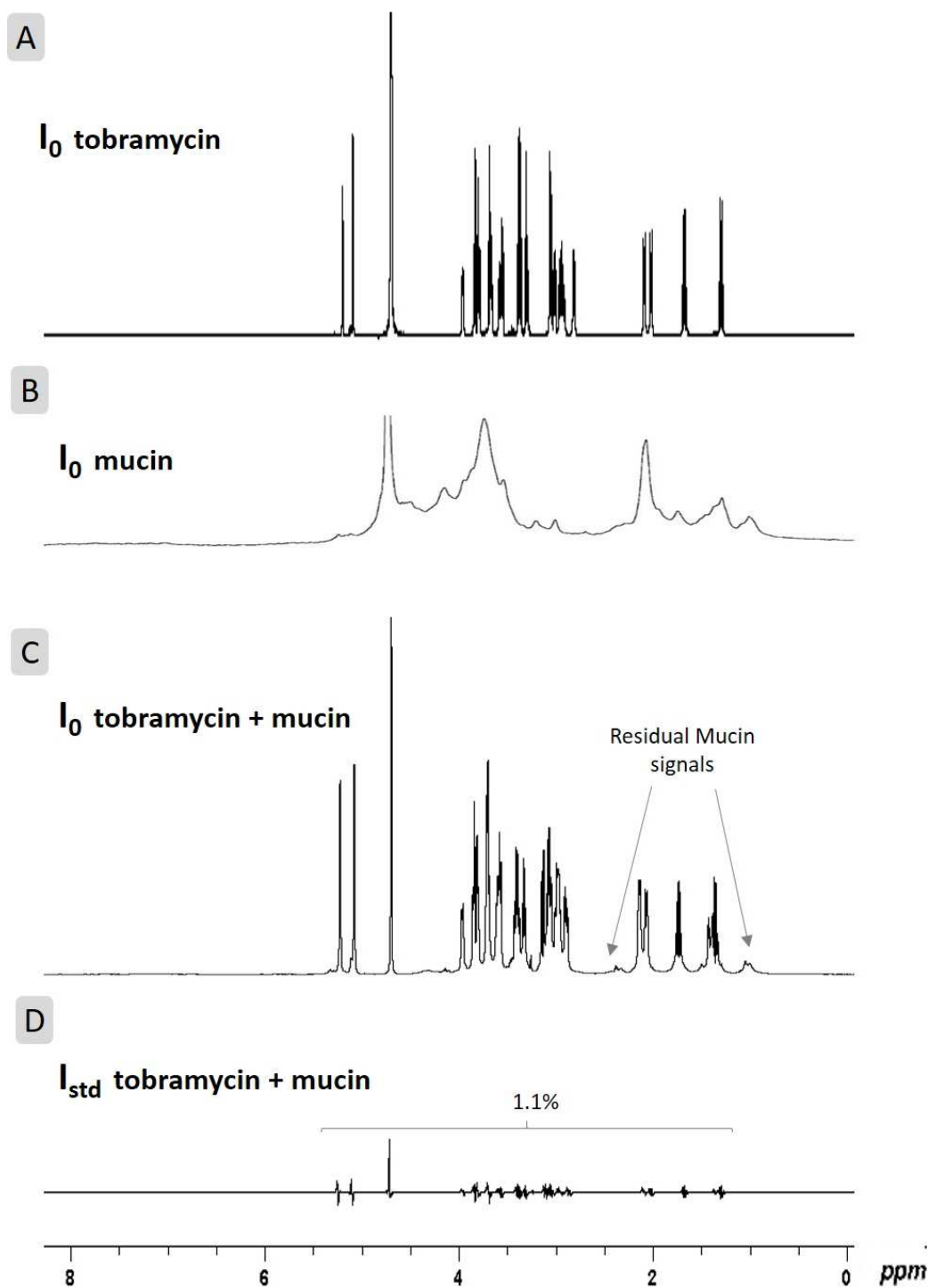


Figure 5.2. STD-NMR spectroscopy for the study of tobramycin-PGM mucin binding. **A:** reference ^1H NMR of 5mg/ml tobramycin solution in D_2O **B:** reference ^1H NMR of mucin 1.5 mg/ml (w/v) in D_2O ; **C:** 1D ^1H reference spectrum of mixture tobramycin-mucin, arrows indicates residual mucin signal; **D:** ^1H NMR (on-resonance) transfer of saturation from protein to ligand.

The mucin spectrum did not include any measurable downfield resonances from aromatic amino acids but instead included resonance peaks restricted to the region between 0.8-5 ppm. A large residual water peak remained in the mucin spectrum as expected from a highly glycosylated and hygroscopic glycoprotein

5.3.2 Salbutamol binding to PGM mucin study by STD-NMR

STD-NMR analysis of salbutamol-mucin mixtures offered a less complex and highly resolved NMR spectrum. In Figure 5.3, a standard ^1H NMR spectrum is shown for salbutamol (top spectrum) and the mixture (middle spectrum). The 1D ^1H NMR spectrum of salbutamol indicated that the two protons on the benzyl alcohol group were missing from the structure. This was confirmed by COSY and TOCSY NMR spectra (performed by Dr C. McDonald, data not shown). The commercially sourced salbutamol sample was used regardless for the purposes of validating the STD-NMR approach. The STD appears lower for protons at 1.4 and 2.4 ppm (~1.9%) and aromatic protons at 7.0 and 7.5 ppm appear to have a stronger interaction as for proton at 5.0 ppm. This identifies a binding event with PGM. Moreover, the differential STD values for individual resonances indicate preferential binding of the phenolic ring to the PGM “receptor”.

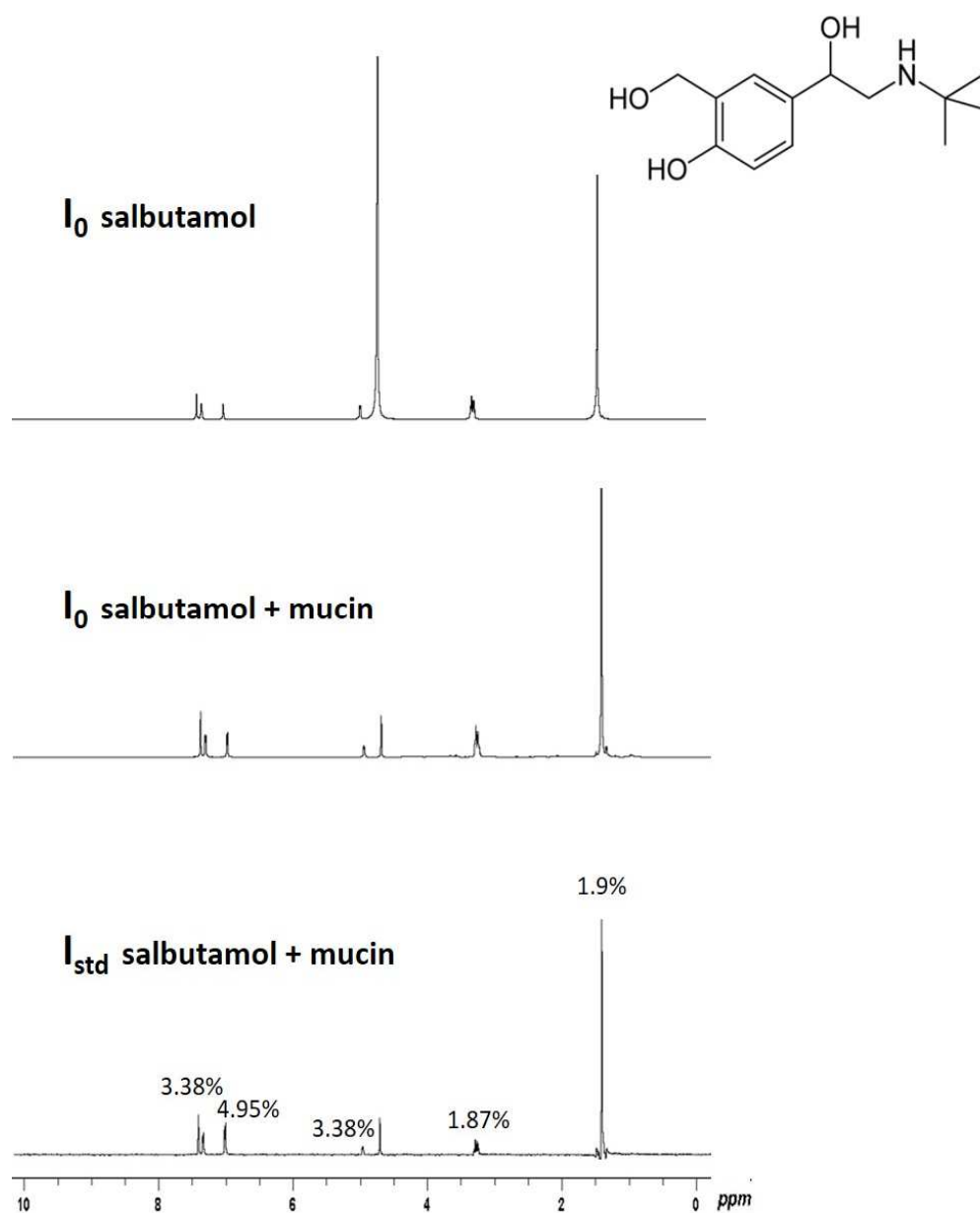


Figure 5.3. STD-NMR spectroscopy for the study of salbutamol-PGM mucin binding. Top: reference ¹H NMR of 5mg/ml salbutamol solution in D₂O; Middle: 1D ¹H reference spectrum of mixture salbutamol-mucin; Bottom: ¹H NMR (on-resonance) transfer of saturation from protein to ligand.

5.3.3 Analysis of OF-80-NS22 and 552-02 binding to PGM mucin by STD-NMR

STD-NMR studies were performed with OF-80-NS22 (Figure 5.4 A) and 552-02 (Figure 5.4 B) which displayed low and high mucin binding in the ultrafiltration studies described in Chapter 4. The top spectrum of Figure 5.4 A and B shows the reference spectrum of ligands, showing all the non-exchangeable protons of their structure highlighted by red circle for OF-80-NS22 and blue triangles, rhombus and hexagon for 552-02 whereas the pyrazinoyl protons appeared exchangeable and invisible.

The ^1H NMR reference spectrum of the model drug and mixture ligand-mucin (ratio 3300:1) are the top and middle spectrum respectively. Drug-binding is seen as resolved peaks in the STD spectrum of ligand-mucin mixtures (bottom panel Figure 5.4 A and B). The STD spectrum for OF-80-NS22 (Figure 5.4 A) indicates that the interaction with mucus glycoprotein involves all four of the aliphatic non-exchangeable protons which are detectable by NMR. This is corroborated by noticeable broadening of the signals at 1.15 and 3.3 ppm (Figure 5.4 A, red circle bottom spectrum).

Greater peak broadening was observed in the STD spectrum of the mixture 552-02– PGM mixture. Three distinct regions of 552-02 were identified on the STD spectrum (Figure 4B bottom spectrum); benzene ring moiety represented by two resonance peaks at 7.0 and 6.7 ppm (blue triangles), glycerol-like side chain at 3.5 ppm (blue rhombus) and the central butyl group (blue hexagon) at 2.4 and 1.5 ppm. Significant differences were identified in the extent of STD for the two molecules. In both experiments there was a residual mucin signal in the STD spectrum at 1.8 ppm (dashed line, Figure 5.4A and B).

Chapter 5

The extent of saturation transfer for each of the OF-80-NS22 resonances was 2%. This extent was 5-fold higher for all resonances in 552-02. This result is consistent with the difference in mucin-binding of these compounds in the ultrafiltration assay (Chapter 4).

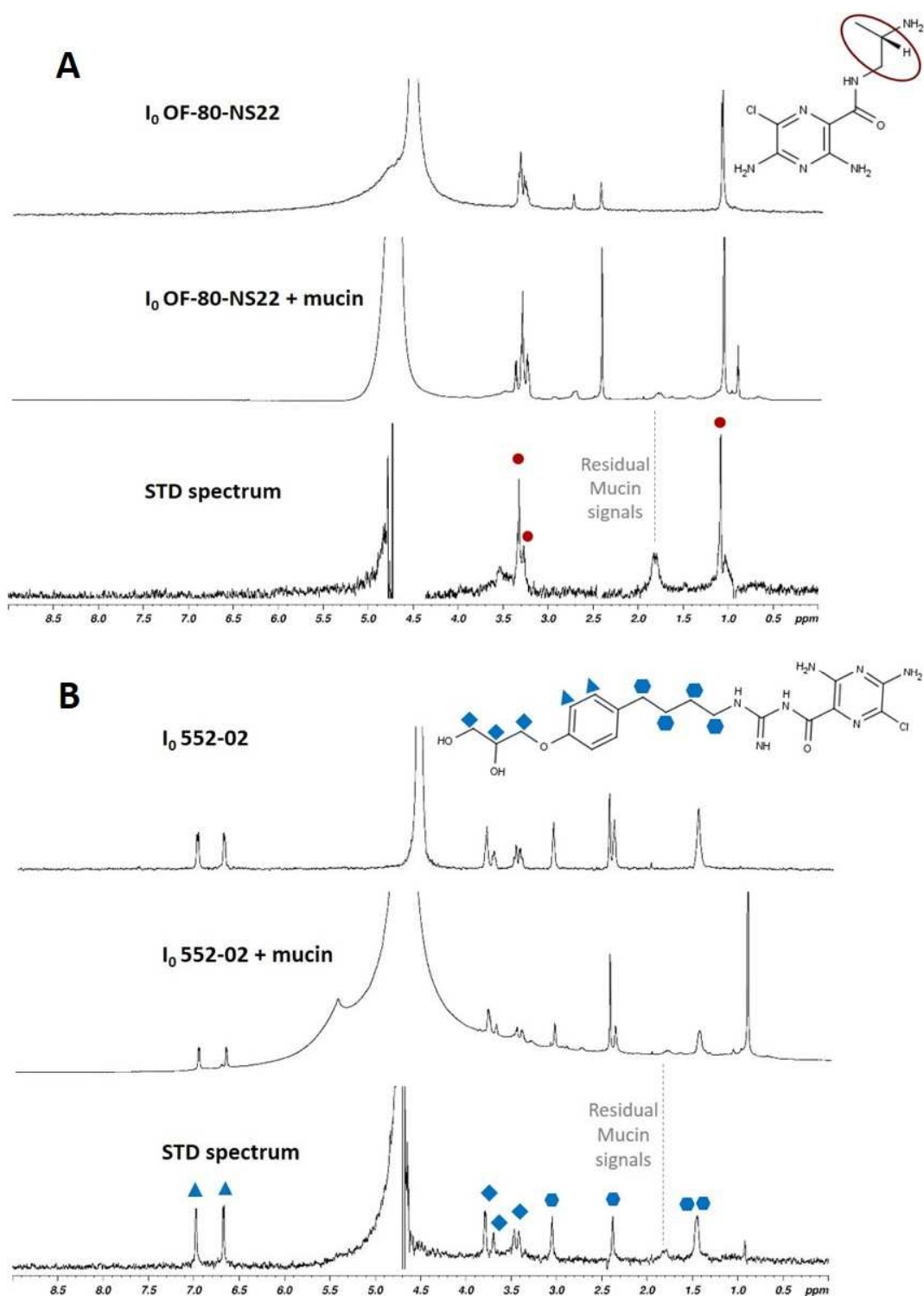


Figure 5.4. STD-NMR spectroscopy for the study of drug-mucin binding. A and B mucin binding of OF-80-NS22 and 552-02 respectively. Top: reference ^1H NMR of ligand solution in D_2O ; Middle: 1D ^1H reference spectrum (off resonance) of mixture ligand-mucin (ratio 3300:1); Bottom: ^1H NMR (on-resonance) transfer of saturation from protein to ligand.

STD-NMR competition studies were performed to understand whether OF-80-NS22 and 552-02 bind to the same site on the mucin molecule. Towards this aim, 2 mM of OF-80-NS22 and 2 mM 552-02 were mixed in 600 nM mucin and subjected to STD analysis. Figure 5 A shows reference spectrum of mixture ligands-mucin while Figure 5D shows the STD spectrum for the mixture ligands-mucin. It is possible to see in Figure 5.5, that the STD spectrum of the mixed ligands (panel D) is very similar to the composite STD spectra for the individual ligands i.e. OF-80-NS22 (spectrum B), 552-02 (spectrum C) suggesting that the two ligands do not compete for the same site of binding of the mucus glycoprotein.

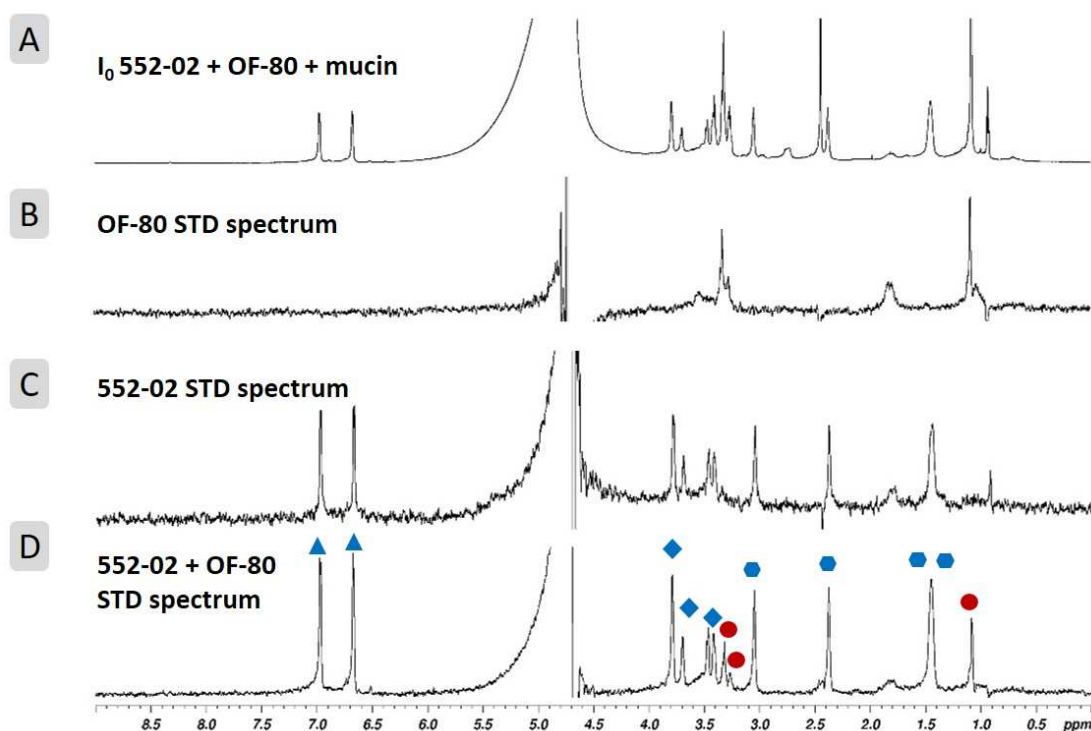


Figure 5.5. STD-NMR spectroscopy for the competitive study of ligands-mucin binding. **A** ^1H NMR reference spectrum (off resonance) of mixture ligands-mucin. **B** ^1H NMR (on-resonance) transfer of saturation from mucin to OF-80-NS22. **C** ^1H NMR (on-resonance) transfer of saturation from mucin to 552-02. **D** ^1H NMR (on-resonance) transfer of saturation from mucin both ligands, OF-80-NS22 (red) and 552-02 (blue).

5.3.4 PJM purification and biochemical analysis

Mucin was purified from porcine jejunal tissue was denatured and purified by density-gradient centrifugation in CsCl/4M GdnCl. The sample showed a thick layer of insoluble material (pellicle) at the top of the tube which was separated from lower layers and was not possible to distinguish the mucin layer from the DNA layer (Figure 5.6).

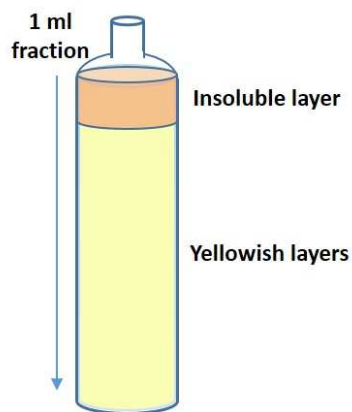


Figure 5.6. 1° Schematic of the mucin product from CsCl gradient centrifugation. Two layers are distinguishable; insoluble material and yellowish layer. Fractions were collected in a volume of 1ml from the top to the bottom.

Chapter 5

Samples of forty CsCl fractions were stained with AB (Figure 5.7A). The intensity of AB staining increased from fraction 16 to 40. In contrast the buoyant density of the fractions increased progressively from the top to bottom fractions (Figure 5.7B). AB positive fractions 16-27, displaying densities of 1.35 - 1.48 g/ml were collected in accordance with to published density of mucin.

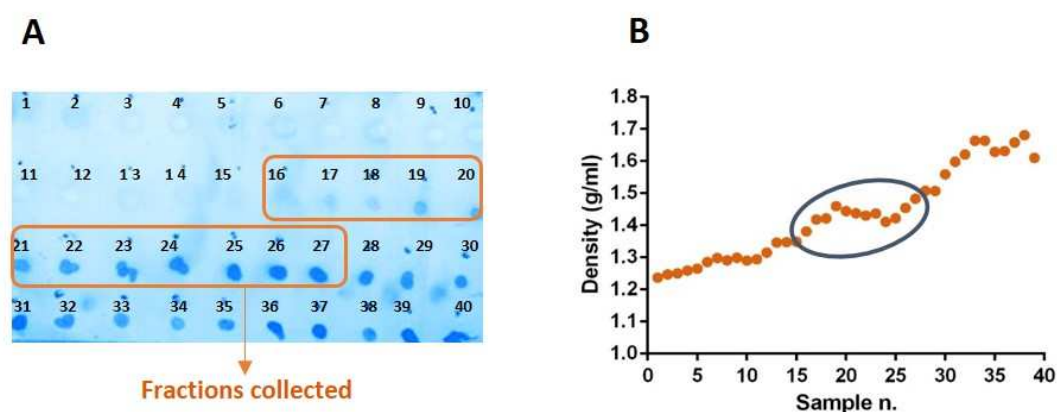


Figure 5.7. 1° CsCl gradient centrifugation. (A) Alcian blue staining of ultra-centrifuge fractions. (B) Density of fractions. Blue stained fractions with density between 1.35-1.48 g/ml were collected.

Mucin-containing fractions were subjected to a second density-gradient centrifugation step in CsCl/0.5 M GdnCl. After ultracentrifugation at least three layers were visible. A darker layer at the top of the tube corresponding to insoluble material, yellowish layer corresponding to the one containing mucin and a clearer layer, with high density at the bottom of the tube (Figure 5.8).

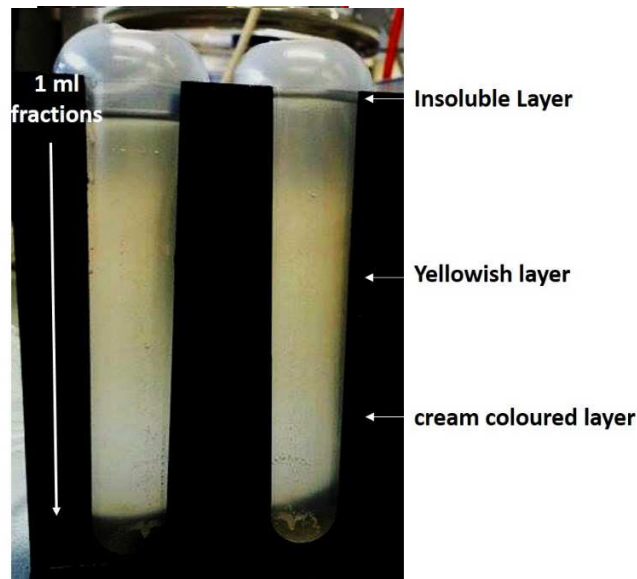


Figure 5.8. 2nd CsCl density-gradient ultracentrifugation. Three layers are distinguishable; Top: insoluble materials. Middle: Mucin. Bottom: DNA. Fractions were collected in a volume of 1ml from the top to the bottom.

Fractions from the second centrifugation step were analysed for absorbance at 260 and 280 nm (Figure 5.9 A), stained with AB (Figure 5.9 B) and measured for density (Figure 5.9 C). The A₂₆₀/A₂₈₀ for fractions 1-25 were consistently recorded as 0.2-0.3 AU but increased sharply to > 1.0 AU from fractions 26-30 and above 2.0 AU in the remaining fractions. AB staining revealed strong staining for fractions 21-39 and weak staining for fractions 18-20. The measured density for the fractions increased linearly from 1 to 40 as expected from a CsCl gradient. Taken together these three methods allowed the identification of fractions 19-25 as the mucin-positive fractions. The buoyant density of these fractions was between 1.37-1.49 g/ml and the total volume collected was 25 ml.

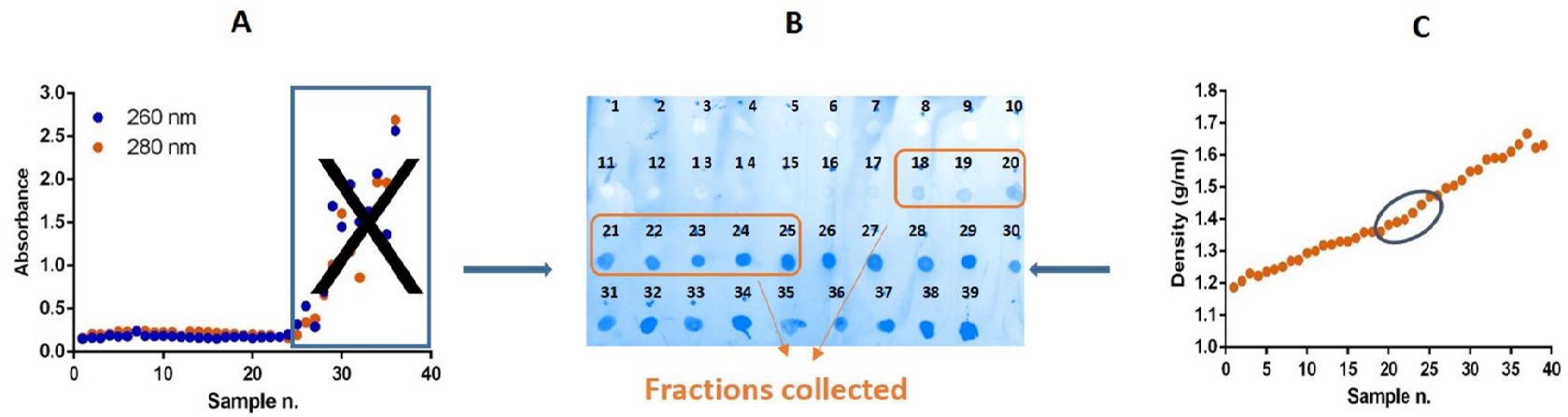


Figure 5.9. 2nd CsCl density-gradient ultracentrifugation. **A** Fractions absorbance at 260 and 280 nm. **B** Fractions alcian blue staining. **C** fractions density (g/ml).

Chapter 5

Purified PJM was dialysed for 48 h against water to remove CsCl and the chaotropic guanidine salt. The fractions yielded four aliquots of PJM of (~180mg) and freeze-dried until a constant weight was recorded. The mean % dry solids resulted was 0.51%±0.09 (Table 5.1).

Table 5.1. Determination of % dry solids. Determination of the dry weight % of four mucin aliquots samples (A, B, C, D).

<i>Mucus Aliquots</i>	<i>W_{ep+wet} (mg)</i>	<i>W_{ep+dry} (mg)</i>	%Dry weight (W_{dry}/W_{wet} *100)
A	1124.05	939.51	0.60
B	1132.20	948.65	0.39
C	1140.11	944.61	0.50
D	1125.01	934.72	0.53
			Mean 0.51 ± 0.09

The mucin concentration of the purified PJM samples after dialysis was 380 ± 45.1 µg/ml and DNA was undetectable (LOD was 2 µg/ml). The molecular weight of the PJM was approximately 4.6 x 10⁶ g/mol, as determined by analytical ultracentrifugation (data supplied by Dr Balazs Bajka from the Institute of Food Research).

5.3.5 STD-NMR studies of OF-80-NS22 and 552-02 binding to PJM

Before use in STD-NMR experiments the PJM was dialysed against water for 48 h then subjected concentration in vivaspin tubes, exchange into deuterated buffer and concentration in Amicon tube to have a final volume of 100 µL at a concentration of ~2.5µM. ¹H NMR analysis of the mucin solution (Figure 5.10) showed a small but

Chapter 5

significant NMR signal for glycerol which is used to extend the shelf-life of the filtration membrane devices. The glycerol NMR signals spanned the range 3.5 to 4.5 ppm - the region in which some OF-80 and 552-02 resonances are found. The contaminated mucin was washed with D₂O using Amicon tube and glycerol was successfully eliminated from mucin (data not shown).

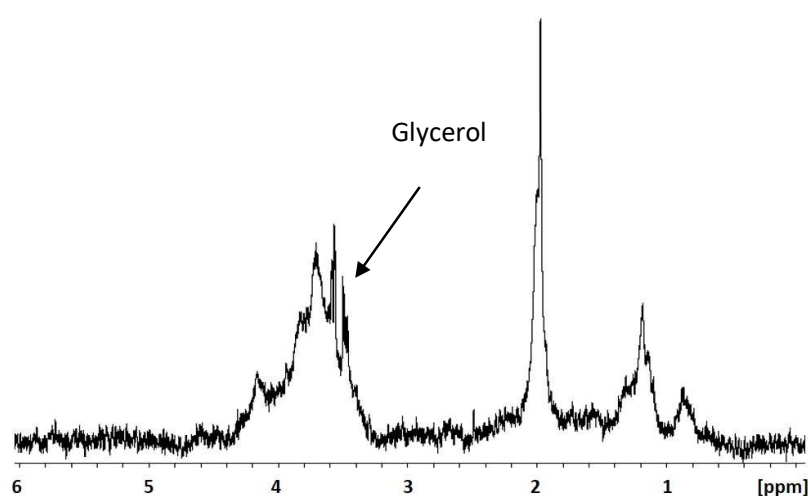


Figure 5.10. Glycerol contamination of PJM. 2.5 mM porcine mucin after washing using vivaspin tubes resulted contaminated with glycerol (arrow).

Off and on-resonance spectrum NMR of OF-80-NS22 mixed with purified PJM is shown in top and bottom spectra of Figure 5.11 A, respectively. Due to the different temperature condition used for STD-NMR experiment for PGM (283 K) and PJM (310 K), STD spectrum of OF-80-NS22 in Figure 5.11 shows peaks at 3.5 and 1.25 ppm with chemical shift slightly down moved of 0.15 ppm compared to the same drug model mixed with PGM in (Figure 4 A, bottom spectrum). Inspection of the 1D NMR spectrum reveals evidence of an interaction between OF-80-NS22 and mucin. Subtraction of the on-

resonance spectrum in which the protein was selectively saturated from the off-resonance spectrum produces the difference spectrum (^1H STD-NMR spectrum, Figure 5.11). The percentage of STD and magnetization transfer at 1 s saturation time (Figure 5.11B) was identical for all protons except B; %STD for B was 1.60 *cf.* 2.02 for others. This was matched by a reduction in magnetization transfer of 20% compared to other signals (Figure 5.11 B).

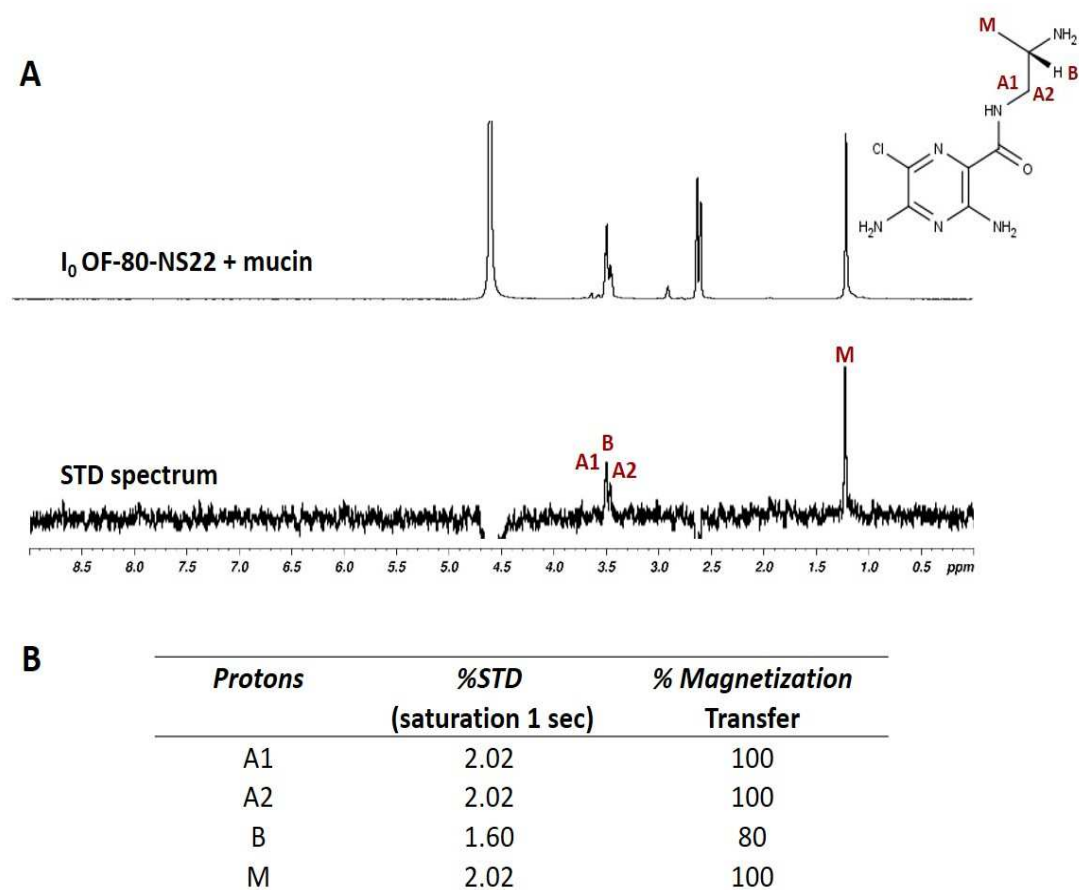


Figure 5.11. STD-NMR spectroscopy for the study OF-80-NS22 and purified mucin binding. **A** Top: reference ^1H NMR of mixture drug-mucin; Bottom: ^1H NMR (on-resonance) transfer of saturation from mucin to OF-80-NS22. Methyl group (M) at chemical shift 1.25 ppm, aliphatic group (A1 and A2) chemical shift at 3.5 ppm, proton (B) at chemical shift 3.5 ppm. Solvent suppression applied. **B** percentage of STD and magnetization transfer for each proton involved into the interaction with mucin. STD NMR experiments were performed using WATERGATE for solvent suppression.

Chapter 5

^1H STD NMR spectra of PJM mixed with 552-02 is shown in the top spectrum and the STD spectrum is shown in the bottom spectrum of Figure 5.12. The extent of STD observed with purified mucin is comparable to the data recorded for PGM (compare Figure 5.12 with Figure 4 B). Also in this case three chemical regions were identified to be involved into the interaction with the mucin: A1, A2, G1-3, L1-4 (Figure 5.12 bottom spectrum). The peak corresponding to G1 and G3 protons, appear to be split in up and down signal and opposite to this, proton L2 and L3 were identified as a unique peak. Studies with PJM were performed at 310 K whereas PGM studies were conducted at 283 K. As a consequence, some resonances shifted. For example, benzyl (A1-2) and butyl group (L1-4) showed down and up shift respectively. In particular, with the increment of temperature at 310 K, the benzyl ring down shifted at 7.4 (A2) and 7.1 (A1) and butyl group up shifted to 2.9 (L4), 2.3 (L1) and 1.1 ppm (L2 and L3), whereas the glycerol group (G1-3) did not change showing a chemical shift at 3.4 and 3.7 ppm. In general, greater peak broadening was observed for 552-02 and the extent of STD was about 15% at a saturation time of 1 second (Figure 5.12 B).

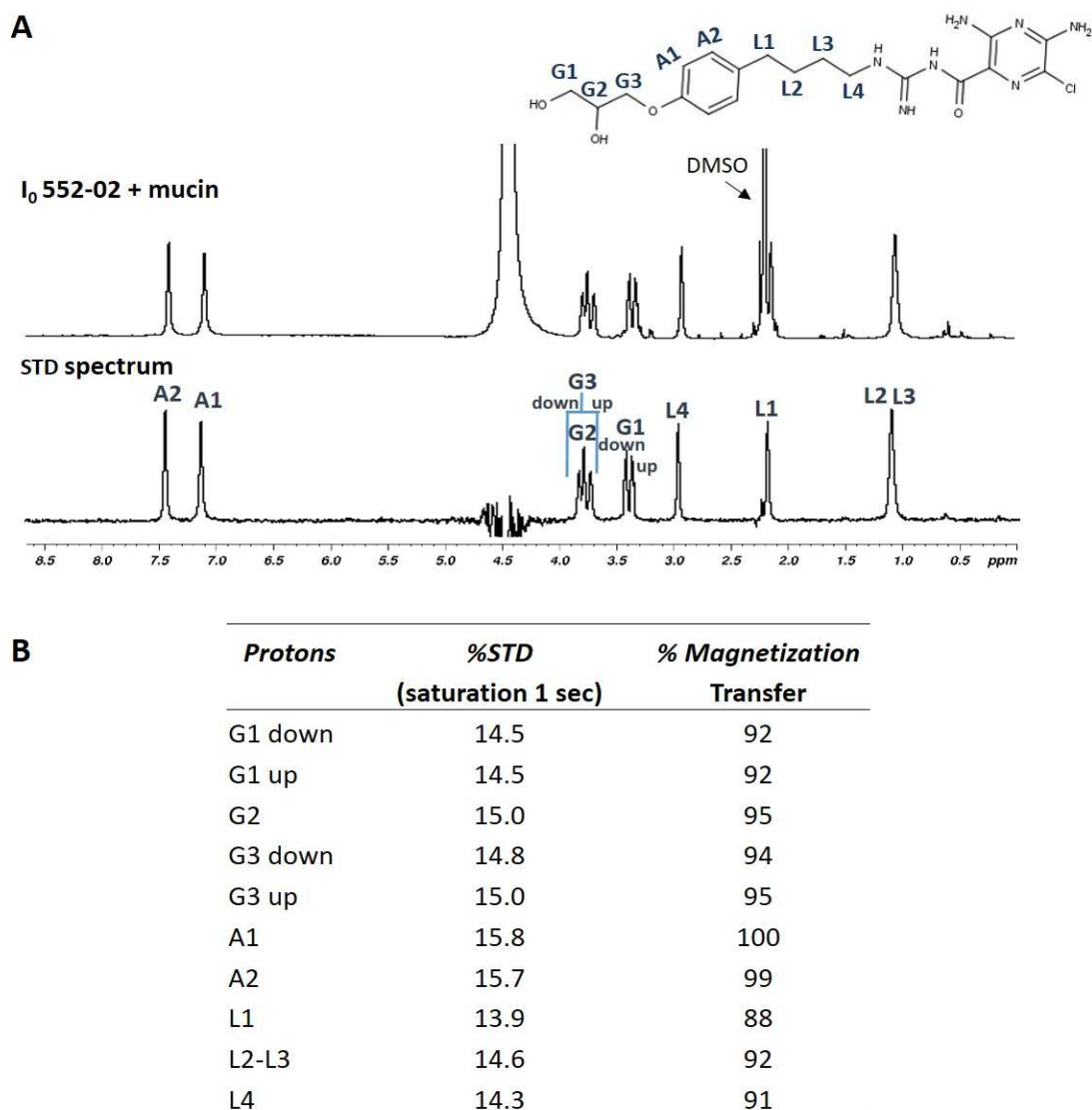


Figure 5.12. STD-NMR spectroscopy for the study 552-02 and purified mucin binding. (A) Top: reference ^1H NMR of mixture drug-mucin; Bottom: ^1H NMR (on-resonance) transfer of saturation from mucin to 552-02. Solvent suppression applied (B) percentage of STD and magnetization transfer for each proton involved into the interaction with mucin. STD NMR experiments were performed using WATERGATE for solvent suppression.

To probe for differential mucin-binding activities across the 552-02 structure a variable saturation time experiment was performed ranging from 0.1 seconds to 6 seconds. The

Chapter 5

saturation curve in Figure 5.13 shows that all protons appear to reach the saturation at same STD percentage at about 2 seconds. The initial slope of the saturation curve was consistent among all assignable protons bind equally to mucin.

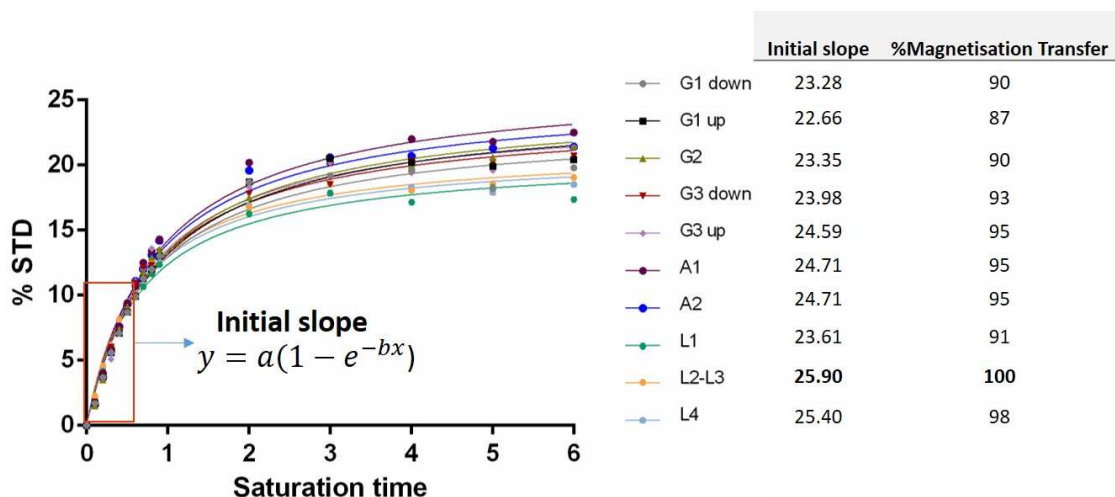


Figure 5.13. Saturation curve of 552-02 and percentage of magnetisation transfer.

STD intensities build-up curves for 552-02 in the presence of 100 nM purified mucin. Saturation applied from 0.1 to 6 sec. Initial slope calculated using Origin Pro-B Program Percentage of magnetisation transfer resulted similar for each proton.

5.4 Discussion

Towards a better understanding of whether mucin may limit the access of inhaled drugs to the lung mucosal epithelium we used NMR spectroscopy to gain a molecular level insight into mucin-binding events. Several studies report the interaction of inhaled drugs molecules to mucus such as aminoglycosides, ^{(39) (23) (40)}, colistin ⁽⁴⁰⁾, salbutamol ⁽²²⁾ and steroid ⁽⁴¹⁾ but still little is known about the chemical interaction between drugs and mucus components. NMR spectroscopy is a widely used technique to study molecular recognition of a small molecule by a macromolecule, be it a receptor, enzyme or membrane protein ⁽⁴²⁾. The STD-NMR methodology has emerged over the last 10 years to offer new insights and structural information on the binding of a ligand to its receptor without the need to perform complex and time-consuming structural deconvolution of the entire ligand-receptor complex ⁽⁴³⁾. However, no published studies exist to support the use of this technique in studying drug-mucin binding interactions.

In this work, STD-NMR was initially used for studying the transient interaction of mucin to tobramycin, drug used for the treatment of Gram negative bacterial infection in CF. In preliminary studies whole PLM was used for the investigation of tobramycin-mucin interaction but the drug showed negligible STD signal attributable to the drug. Tobramycin was chosen as a probe in initial NMR studies because of published evidence that indicates that mucin antagonises its antibiotic activity ^{(23) (40)}. These unexpected results could be explained in a number of ways. Firstly, the absence of STD could be due to a high affinity interaction, in the sub micromolar K_d range, which would prevent

Chapter 5

efficient saturation transfer from mucin to ligand and therefore be recorded as no STD⁽⁴³⁾. Alternatively, tobramycin may serve as a poor ligand for the mucin component of the intact porcine lung mucus (PLM). Mucin quantification assays in PLM revealed an amount of mucin of 1% (Chapter 3), for STD-NMR experiments is necessary have a large molar excess of ligand (1:10 to 1:1000 or more). To probe again whether tobramycin interacts with mucin future experiments would involve working with a purified lung mucin preparation or whole mucus with a defined mucin concentration that afford calculation of optimal ligand:protein ratios. Moreover, a confounding issue in these experiments is the impure nature of the lung mucus. The porcine lung mucus used here was a heterogeneous solution with significant DNA contamination by DNA (0.5% of dry weight as per Chapter 3). Commercially available PGM was trialled in subsequent NMR studies due to the 10-fold lower DNA contamination and greater product availability but notwithstanding the different biological origin and partially purified nature of the product.

Mucus is an heterogeneous material containing not only mucins but also DNA, proteins, lipid, and cellular debris⁽⁴⁴⁾. The amount of DNA in PLM resulted to be 0.5 % (Chapter 3). Scraping of the tissue could have caused significant epithelial shedding and DNA release. The interaction of tobramycin to mucin and other mucus component, DNA, has been shown by Hunt, Weber⁽⁴⁵⁾. They analysed, after dialysis of the drug-mucus mixture, the kinetics of tobramycin efflux mixed with sputum from CF patient and “mock sputum” which consisted of porcine gastric mucin and +/- calf thymus DNA. Treatment of these

Chapter 5

models with recombinant human DNase (rhDNase) indicated that rhDNase increases but not significantly the tobramycin bioactivity. Moreover, the free tobramycin in the dialysates resulted dependent on the concentration of gastric mucin suggesting that mucin may play a role in tobramycin binding.

Tobramycin inhibits the translation of mRNA into protein preventing formation of the 70S complex by binding to a site on the bacterial 30S and 50S ribosome. The interaction of tobramycin to the genetic material was also showed by Wang and Rando⁽⁴⁶⁾ who used a tobramycin affinity column to select from a RNA library sequences capable to bind to tobramycin demonstrating the specific interaction of the antibiotic tobramycin to RNA molecules.

The interaction of tobramycin with mucus macromolecules was also demonstrated by Ramphal, Lhermitte⁽²³⁾ who used sputum from cystic fibrosis patients and separating the sputum macromolecules with Sepharose CL 4B column chromatography. Mucus macromolecules were mixed with tobramycin +/- treated with DNase and pronase. Following equilibrium dialysis, the drug concentration was marginally above the LOD even when 100 µg/ml were mixed with 10 mg/ml of the mucus macromolecules indicating a strong interaction.

To reduce the potential impact of DNA binding STD-NMR experiments were repeated using PGM, which displayed a lower DNA concentration compared to the whole porcine mucus (Chapter 3). In Figure 5.2 B the mucin spectrum did not include any downfield

Chapter 5

chemical shift over 5 ppm, consistent with a low abundance of Phe, Tyr and Trp residues and a highly glycosylated structure⁽⁴⁷⁾. Under these conditions the STD spectrum (Figure 5.2 D) displayed this time a weak signal of ~1% STD for all protons which, is consistent with weak binding interactions. This is in contrast to the significant tobramycin binding to mucin showed by Ramphal, Lhermitte⁽²³⁾ although in our experiment drug concentration was 50-fold higher (5mg/ml versus 0.1 mg/ml) and a mucin concentration ~7-fold lower (1.5mg/ml versus 10 mg/ml).

Mucin glycoproteins are large polyanions and so their negative charge may form an electrostatic interaction with aminoglycosides which are cations as demonstrated for gentamicin by Saggars and Lawson⁽⁴⁸⁾. This glycoprotein in CF is characterized by an increased carbohydrate content⁽⁴⁹⁾ with higher content of fucose, N-acetyl-glucosylated and galactose but no changes in sialic acid. The increase of highly branched oligosaccharide structure may lead to the formation of a stronger interaction with tobramycin as shown by Ramphal, Lhermitte⁽²³⁾ without excluding the presence in CF sputum of another anionic polymer, alginate.

In contrast to tobramycin, STD-NMR experiments with salbutamol-mucin mixtures revealed clear interactions with PGM (Figure 5.3 bottom spectrum) as shown by STD signals of 1.9 to 4.95 %. The chemical diversity of the probe ligand allowed for rapid identification of specific regions of salbutamol which display higher binding than others. The phenolic protons and the adjacent methylene protons displayed a stronger

Chapter 5

interaction with mucus (STD 4.9 %) compared to the tert-butyl and “side-chain” portion of the molecule (STD 1.9 %). These data support well the published data from Bhat, Flanagan ⁽²²⁾ who investigated mucus binding of salbutamol (under the US name, albuterol) with other 5 compounds (rifampicin, p-amino-salicylic acid, isoniazid, pyrazinamide, and pentamidine). Specifically, gastric mucus was used to test the development of a purified model mucus system for its application in drug binding studies by diafiltration. Salbutamol and the others compounds were shown to display low binding with gastric mucin with 80-95% of the applied drug detectable in the reservoir. The low salbutamol binding (~10%) finds agreement with our results (STD ~2-5%). To date, no other published studies have reported data pertaining to salbutamol-mucin binding interactions.

Vaisman, Koren ⁽¹¹⁾ studied the disposition of inhaled salbutamol in both CF people and healthy adults showing that the peak of serum concentration of drug after inhalation was reached faster, 15-30 min, and was higher (4 ng/ml) in CF than health people for who a peak of salbutamol (2ng/ml) was reached at 30 min ($p < 0.05$). The reason for the higher system concentration of salbutamol in CF people may be that diseased tracheobronchial tree in CF patience reduces the mucociliary clearance rate with consequent higher permeation of salbutamol. In contrast, it has been shown that the inhalational PK of salbutamol is similar in both asthmatic and COPD patients ^{(10) (50)}.

Results from Chapter 4 highlighted a significant variability in the extent of mucin binding across a range of experimental ENaC blockers. Our studies moved then onto the

Chapter 5

investigation of the physical-chemical interaction of mucin and ENaC blockers and we sought to gain information on the receptor-ligand binding as well as detailed information about the binding epitope of the ligand and the extent of binding. Two ENaC blockers were chosen for investigation in these NMR studies. Factors influencing the choice of probe molecule included the following factors:

- 1) The extent of mucin binding from ultrafiltration studies. The drug-mucin binding varied greatly across the range of compound. To allow the detection of differences was decided to study molecules that showed low and high binder. The low-throughput nature of the technique and project time-limitation limited us to study two molecules.
- 2) The chemical diversity of the molecules. The range was structurally diverse and drug molecules were chosen considering STD-NMR limitations which require the use of compounds with nonexchangeable protons.
- 3) The solubility and availability of probes. Experiments with STD-NMR require the use of compounds with high solubility without the need for high concentrations of co-solvents such as DMSO which may denature mucin or interfere with binding pockets.

Taking into consideration these points, amiloride, as a low-binding drug, could not be used due to absence of visible protons, so OF-80-NS22 was chosen for STD-NMR experiments. GF-40-QQ33 and benzamil, which showed the highest binding, were discarded due to their high low aqueous solubility and limited availability of compound.

Chapter 5

552-02 was easily soluble in the mucin solution when added at concentration up to 4 mM from a DMSO stock (~6% DMSO final concentration). It was not possible to determine quantitatively the dissolved concentration of 552-02 in the mucin solution but there was no evidence of drug solubility issues e.g. precipitation in the sample tube. The solubility of OF-80-NS22 in aqueous buffer was highly favourable but to avoid DMSO-induced changes in mucin behaviour the co-solvent was added at a concentration equivalent to that used for 552-02.

Consistent with the ultrafiltration binding data from Chapter 4, 552-02 gave a 5-fold more intense STD signal than OF-80-NS22 at equivalent conditions and drug : mucin molar ratios (3300:1). That STD-NMR is based upon the Nuclear Overhauser Effect (NOE) which unequivocally supports the close contact ($< 5 \text{ \AA}$) of the ligand with mucin. The observation of comparable STD intensities for each proton resonance in both ENaC blocker molecules it is appropriate to conclude that the binding interaction is non-specific in nature. Furthermore, a competitive assay was carried out to infer whether these two ENaC blockers bind to the same site. If the two ligands compete for the same site of binding, no STD signals of the “weaker” ligand (OF-80-NS22) should be observable, since it would have no opportunity to make close contact with the receptor (mucin). Alternatively, if the two compounds bind at different sites, the STD-NMR intensity of the “weaker” compound will not be affected. In our results (Figure 5.5 spectrum D) the ligands interaction to mucin appears non-competitive as signal of both ligands are

Chapter 5

observable. This observation serves as further confirmation of a non-specific binding event that involves interactions across the ligand structure.

Amiloride has been shown to intercalate into DNA ⁽⁵¹⁾ ⁽⁵²⁾. For example, Bailly et al used DNA foot-printing to demonstrate sequence-specific DNA-amiloride interactions, specifically in AT-rich sites. The chemical interaction amiloride-DNA appears to involve the amino group at position 5 of the drug molecule ⁽⁵³⁾. The proposed binding portion, in the pyrazinoyl group, is conserved across all analogues so DNA binding would be expected to be seen for all amiloride analogues.

Within the probe molecule structures there are a number of exchangeable protons including amino and guanidine protons in addition to, and most notably, the pyrazinoyl group. These protons are invisible in the ¹H STD-NMR experiment because of a lack of magnetization transfer onto them therefore we are not able to determine their involvement into the interaction with mucin. The pyrazinoyl guanidine group of amiloride and analogues was thought to be a privileged structure for ENaC blockers ⁽⁵⁴⁾ but the replacement of the guanidine group with amino group ⁽⁵⁵⁾ or quaternary amine ⁽⁵⁶⁾ has also been shown to be capable to inhibit ENaC blocker. OF-80-NS22 is an example guanidine group substitute with an amine but also resulted invisible to STD-NMR experiment.

Chapter 5

To better deconvolute the drug-mucin binding processes and to eliminate interference from DNA, lipids and other protein a multi-step mucin purification procedure was performed. As highlighted in Chapter 3, the yield of crude mucus isolated from porcine respiratory tract was only ~ 600 µl/lung with approximately 1 % mucin. Therefore, PJM was used instead of a plentiful supply of lung mucus. Mucin purification was performed using a standard method^{(57) (58) (59)} which involves the dispersion and denaturation of the mucus in a solution of 4-6 M of GdnHCl. The combination of Alcian Blue staining, UV absorbance and buoyant density determination allowed for the identification and resolution of mucin- and DNA-rich fractions. For example, AB staining is not mucin-specific. AB-positive DNA fractions were excluded by UV spectroscopy analysis. Mucin fractions were separated from DNA, absorbing at 260 nm, and material with a high absorbance at 280 nm. Although mucin has a protein core, aromatic amino acid constitute less than 5% of the protein which represents 25% of the total molecular weight of this high glycosylated mucin^{(47) (58)}. Greater resolution of DNA and mucin fractions is also facilitated through use of a lower GdnCl concentration because of a greater difference in the buoyant density of mucins and DNA⁽⁵⁸⁾. The purified mucin showed a isopycnic point between 1.38-1.49 g/ml and in agreement with previous observations for MUC5AC mucin purification from human trachea⁽⁶⁰⁾, MUC5AC and MUC5B sputum from individual chronic bronchitic patients⁽⁶¹⁾, porcine jejunal mucin⁽⁶²⁾ and cervical mucin⁽⁵⁸⁾. Biochemical analyses were applied on the purified PJM for the determination of the dry solid %, mucin concentration and DNA contamination. The

Chapter 5

purified mucin was devoid of nucleic acids, as judged by the non-detectable DNA with fluorimetric assay using DABA.

The major secretory mucin synthesized and secreted by goblet cells in the small and large intestine is MUC2 ⁽⁶³⁾. The molecular weight of PJM was 4.6×10^6 g/mol obtained by sedimentation velocity in an analytical centrifuge. This results concurs with that obtained by Herrmann, Davies (64) i.e. $\sim 4.0 \times 10^6$ g/mol using analytical ultracentrifugation and laser light scattering. However, earlier work by Mantle and Allen ⁽⁶⁵⁾ described sedimentation coefficients of PJM equating to a molecular weight of 1.72×10^6 g/mol.

Purified PJM was used to perform STD-NMR experiments using OF-80-NS22 and 552-02. These studies also showed a shorter inter-proton distance between 552-02 protons and mucin in bound state compared to OF-80-NS22 protons. The extent of STD for 552-02 was 7-fold stronger than that of OF-80 which is comparable to the results of ultrafiltration binding studies where the percentage of binding of OF-80-NS22 and 552-02 was 6.9 and 32.5% respectively. These data validated the STD-NMR results with PGM and prove that the observed binding is attributable, to some degree, to mucin and not the DNA component of PGM. Mucus is a complex heterogenic solution also containing lipid (glycolipids, phospholipids, fatty acid, etc), plasma proteins (such as serum albumin) and secreted antibodies (IgA) ⁽⁶⁶⁾ that enhance protection against specific pathogens ⁽⁶⁷⁾. All these component have been shown to be significant important for the rheology properties of mucus capable to dramatically influence the viscosity of the mucus

Chapter 5

glycoprotein ⁽⁶⁸⁾ ⁽⁶⁹⁾. Reid and Bhaskar ⁽⁷⁰⁾ suggested that both physical and chemical properties of bronchial epithelial mucus depend on its special mix of macromolecules and lipid constituents which can be variable between normal airway and disease ⁽⁷¹⁾. Therefore, the *in vivo* mucus barrier is a complex, heterogeneous anisotropic system and neither PGM nor PJM are appropriate for studying mechanistic details of drug binding.

We next sought to confirm the non-specific nature of ENaC blocker- mucin binding using 552-02. A saturation curve was constructed over different saturation time scales from 0.1 to 6 seconds. The resultant saturation curve indicated that each assignable proton increased at similar rates and indeed plateaued at similar point (Figure 5.13). The STD signal depends on the duration of the radiofrequency irradiation of the receptor and the saturation received from the ligand protons increases with this time (saturation time) ⁽²⁹⁾. Gradually increasing the irradiation time, protons with a tight interaction to mucin are expected to reach higher saturation transfer % compared to protons with weaker interaction. Increasing the saturation time all 552-02 protons produced very similar saturation transfer which leads to the conclusion that all protons bind equally to mucin. In the case of 552-02, if one particular region of the molecule had displayed specific binding to a defined region of the mucin glycoprotein it would be detectable as an increase in maximal STD for the corresponding peaks. For instance, the hypothetical scheme in Figure 5.14 reflects a situation in which protons in the red chemical region undergo a stronger interaction with mucin, resulting in a higher saturation transfer %, compared to others in the green or pink chemical region. Moreover, it is possible to

Chapter 5

identify the specific protons that has a tight interaction to mucin. For instance, Figure 5.14 B shows a theoretical strong interaction of proton “a” in the butyl chemical region displaying the highest STD% compared to others protons of the same chemical region. STD-NMR was applied by Moller et al ⁽³⁶⁾ to determine the binding epitope of the SM3 monoclonal antibody to partially deglycosylated MUC1 glycoprotein which is highly enriched on breast cancer cells but there is no information on the literature regarding the application of STD-NMR ligand binding to intact mucin.

Conclusion

This chapter includes data supporting the use of STD-NMR to study the binding of small molecular probes to three different mucus / mucin models to the best of our knowledge, there has not yet been any literature reporting the chemical detection of the interaction between amiloride and mucin using STD-NMR technique. This afford to perform a detailed epitope mapping of the ligand bound to mucin and identification of the chemical group which contribute to the sequestration of drug in the airway luminal mucus and negatively impact on lung disposition. Amiloride and analogues are all characterised by a pyrazinoyl group which protons are exchangeable and invisible in SDT-NMR but ¹³C NMR could be used to check the extent of binding.

The understanding of chemical group limiting the access of the drug to its receptor will give a very important contribute to the development of drug in the future.

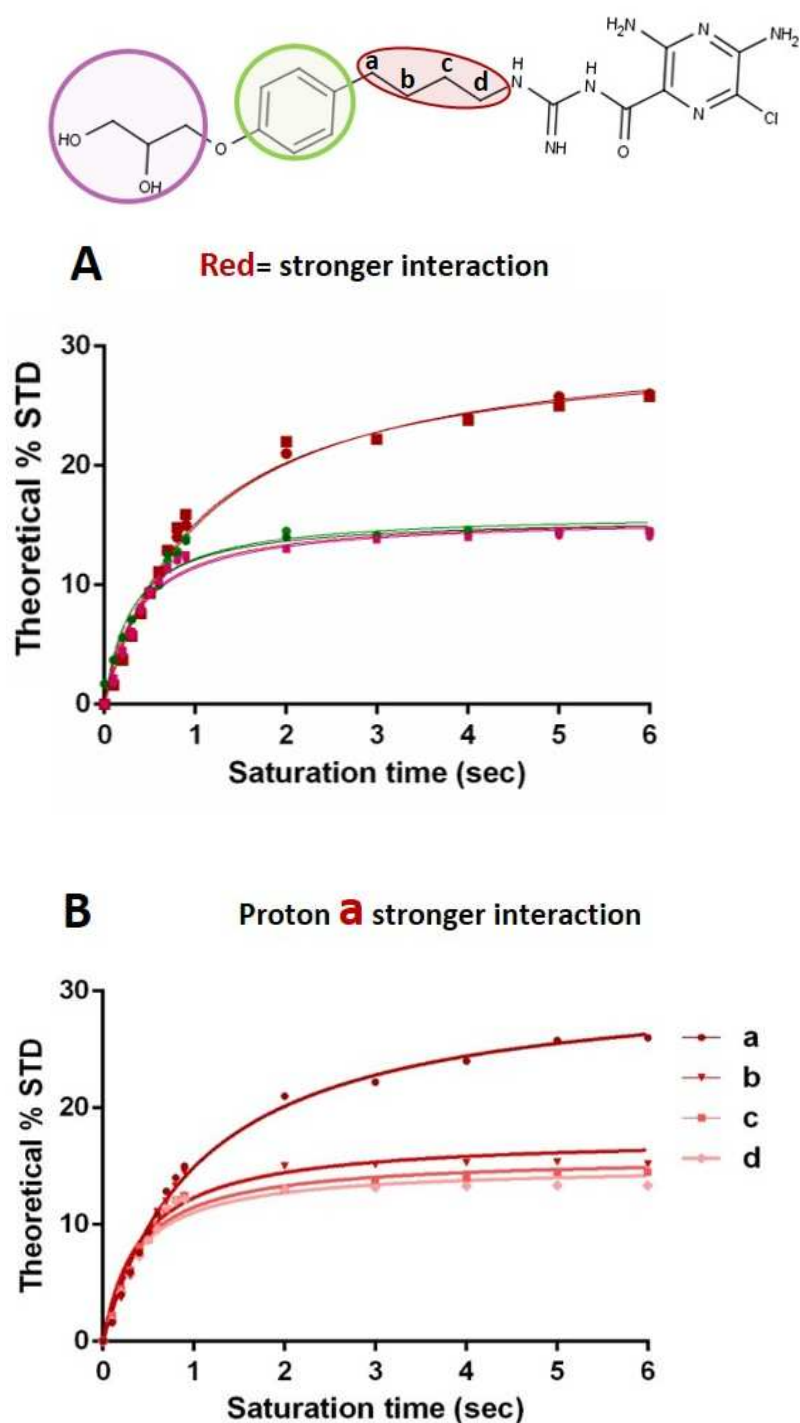


Figure 5.14. Theoretical saturation curve of 552-02.

Theoretical interaction of 552-02 butyl (red) benzyl (green) and glycerol group (pink) to mucin. (A) stronger interaction (red) of 552-02 protons of the butyl group where proton "a" displays a stronger STD% (B).

5.5 Reference

1. Knowles MR, Boucher RC. Mucus clearance as a primary innate defense mechanism for mammalian airways. *The Journal of clinical investigation*. 2002;109(5):571-7.
2. Pavia D, Sutton PP, Agnew JE, Lopez-Vidriero MT, Newman SP, Clarke SW. Measurement of bronchial mucociliary clearance. *European journal of respiratory diseases Supplement*. 1983;127:41-56.
3. Randell SH, Boucher RC, University of North Carolina Virtual Lung G. Effective mucus clearance is essential for respiratory health. *American journal of respiratory cell and molecular biology*. 2006;35(1):20-8.
4. Kellett F, Redfern J, Niven RM. Evaluation of nebulised hypertonic saline (7%) as an adjunct to physiotherapy in patients with stable bronchiectasis. *Respiratory medicine*. 2005;99(1):27-31.
5. Messina MS, O'Riordan TG, Smaldone GC. Changes in mucociliary clearance during acute exacerbations of asthma. *The American review of respiratory disease*. 1991;143(5 Pt 1):993-7.
6. Daviskas E, Anderson SD. Hyperosmolar agents and clearance of mucus in the diseased airway. *Journal of aerosol medicine : the official journal of the International Society for Aerosols in Medicine*. 2006;19(1):100-9.
7. Fazio F, Lafortuna C. Effect of inhaled salbutamol on mucociliary clearance in patients with chronic bronchitis. *Chest*. 1981;80(6 Suppl):827-30.
8. Lafortuna CL, Fazio F. Acute effect of inhaled salbutamol on mucociliary clearance in health and chronic bronchitis. *Respiration; international review of thoracic diseases*. 1984;45(2):111-23.
9. Devalia JL, Sapsford RJ, Rusznak C, Toumbis MJ, Davies RJ. The effects of salmeterol and salbutamol on ciliary beat frequency of cultured human bronchial epithelial cells, in vitro. *Pulmonary pharmacology*. 1992;5(4):257-63.
10. Taburet AM, Tollier C, Richard C. The effect of respiratory disorders on clinical pharmacokinetic variables. *Clinical pharmacokinetics*. 1990;19(6):462-90.
11. Vaisman N, Koren G, Goldstein D, Canny GJ, Tan YK, Soldin S, et al. Pharmacokinetics of inhaled salbutamol in patients with cystic fibrosis versus healthy young adults. *The Journal of pediatrics*. 1987;111(6 Pt 1):914-7.
12. Hirsh AJ. Altering airway surface liquid volume: inhalation therapy with amiloride and hyperosmotic agents. *Advanced drug delivery reviews*. 2002;54(11):1445-62.
13. Pons G, Marchand MC, d'Athis P, Sauvage E, Foucard C, Chaumet-Riffaud P, et al. French multicenter randomized double-blind placebo-controlled trial on nebulized amiloride in cystic fibrosis patients. The Amiloride-AFLM Collaborative Study Group. *Pediatric pulmonology*. 2000;30(1):25-31.
14. FitzSimmons SC. The changing epidemiology of cystic fibrosis. *The Journal of pediatrics*. 1993;122(1):1-9.
15. Steinkamp G, Tummler B, Gappa M, Albus A, Potel J, Doring G, et al. Long-term tobramycin aerosol therapy in cystic fibrosis. *Pediatric pulmonology*. 1989;6(2):91-8.
16. Ramsey BW, Dorkin HL, Eisenberg JD, Gibson RL, Harwood IR, Kravitz RM, et al. Efficacy of aerosolized tobramycin in patients with cystic fibrosis. *The New England journal of medicine*. 1993;328(24):1740-6.

Chapter 5

17. Saggars BA, Lawson D. Some observations on the penetration of antibiotics through mucus in vitro. *Journal of clinical pathology*. 1966;19(4):313-7.
18. Bhat PG, Flanagan DR, Donovan MD. Drug diffusion through cystic fibrotic mucus: steady-state permeation, rheologic properties, and glycoprotein morphology. *Journal of pharmaceutical sciences*. 1996;85(6):624-30.
19. Kwong TC. Free drug measurements: methodology and clinical significance. *Clinica chimica acta; international journal of clinical chemistry*. 1985;151(3):193-216.
20. Barre J. Problems in therapeutic drug monitoring: free drug level monitoring. *Therapeutic drug monitoring*. 1988;10(2):133-43.
21. Yu X, Liu H, Yang Y, Lu S, Yao Q, Yi P. The investigation of the interaction between Oxymetazoline hydrochloride and mucin by spectroscopic approaches. *Spectrochimica acta Part A, Molecular and biomolecular spectroscopy*. 2013;103:125-9.
22. Bhat PG, Flanagan DR, Donovan PD. Drug binding to gastric mucus glycoproteins. *Int J Pharm*. 1996;134(1-2):15-25.
23. Ramphal R, Lhermitte M, Filliat M, Roussel P. The binding of anti-pseudomonal antibiotics to macromolecules from cystic fibrosis sputum. *The Journal of antimicrobial chemotherapy*. 1988;22(4):483-90.
24. Marcelo F. The Interaction of Saccharides with Antibodies. A 3D View by Using NMR. *Anticarbhydrate Antibodies*. 2012:385-402.
25. Ni F. Recent Developments in Transferred Noe Methods. *Prog Nucl Mag Res Sp*. 1994;26:517-606.
26. Kimmich R, Fatkullin N. Polymer chain dynamics and NMR. *Adv Polym Sci*. 2004;170:1-113.
27. Griffiths P, Stilbs P. NMR self-diffusion studies of polymeric surfactants. *Curr Opin Colloid In*. 2002;7(3-4):249-52.
28. Occhipinti P, Griffiths PC. Quantifying diffusion in mucosal systems by pulsed-gradient spin-echo NMR. *Advanced drug delivery reviews*. 2008;60(15):1570-82.
29. Mayer M, Meyer B. Group epitope mapping by saturation transfer difference NMR to identify segments of a ligand in direct contact with a protein receptor. *Journal of the American Chemical Society*. 2001;123(25):6108-17.
30. Maaheimo H, Kosma P, Brade L, Brade H, Peters T. Mapping the binding of synthetic disaccharides representing epitopes of chlamydial lipopolysaccharide to antibodies with NMR. *Biochemistry*. 2000;39(42):12778-88.
31. Bernardi A, Arosio D, Potenza D, Sanchez-Medina I, Mari S, Canada FJ, et al. Intramolecular carbohydrate-aromatic interactions and intermolecular van der Waals interactions enhance the molecular recognition ability of GM1 glycomimetics for cholera toxin. *Chemistry*. 2004;10(18):4395.
32. Mayer M, James TL. Detecting ligand binding to a small RNA target via saturation transfer difference NMR experiments in D(2)O and H(2)O. *Journal of the American Chemical Society*. 2002;124(45):13376-7.

Chapter 5

33. Wagstaff JL, Vallath S, Marshall JF, Williamson RA, Howard MJ. Two-dimensional heteronuclear saturation transfer difference NMR reveals detailed integrin α v β 6 protein-peptide interactions. *Chemical communications*. 2010;46(40):7533-5.
34. Mari S, Serrano-Gomez D, Canada FJ, Corbi AL, Jimenez-Barbero J. 1D saturation transfer difference NMR experiments on living cells: the DC-SIGN/oligomannose interaction. *Angewandte Chemie*. 2004;44(2):296-8.
35. Meyer B, Peters T. NMR spectroscopy techniques for screening and identifying ligand binding to protein receptors. *Angewandte Chemie*. 2003;42(8):864-90.
36. Moller H, Serttas N, Paulsen H, Burchell JM, Taylor-Papadimitriou J, Bernd M. NMR-based determination of the binding epitope and conformational analysis of MUC-1 glycopeptides and peptides bound to the breast cancer-selective monoclonal antibody SM3. *European journal of biochemistry / FEBS*. 2002;269(5):1444-55.
37. Marcelo F, Garcia-Martin F, Matsushita T, Sardinha J, Coelho H, Oude-Vrielink A, et al. Delineating binding modes of Gal/GalNAc and structural elements of the molecular recognition of tumor-associated mucin glycopeptides by the human macrophage galactose-type lectin. *Chemistry*. 2014;20(49):16147-55.
38. Szilagyi L. Assignments of the ^1H - and ^{13}C -n.m.r. spectra of tobramycin at low and high pH. *Carbohydrate research*. 1987;170(1):1-17.
39. Davis SD, Bruns WT. Effects of sputum from patients with cystic fibrosis on the activity in vitro of 5 antimicrobial drugs on *Pseudomonas aeruginosa*. *The American review of respiratory disease*. 1978;117(1):176-8.
40. Huang JX, Blaskovich MA, Pelington R, Ramu S, Kavanagh A, Elliott AG, et al. Mucin Binding Reduces Colistin Antimicrobial Activity. *Antimicrobial agents and chemotherapy*. 2015;59(10):5925-31.
41. Vestbo J, Sorensen T, Lange P, Brix A, Torre P, Viskum K. Long-term effect of inhaled budesonide in mild and moderate chronic obstructive pulmonary disease: a randomised controlled trial. *Lancet*. 1999;353(9167):1819-23.
42. Lepre CA, Moore JM, Peng JW. Theory and applications of NMR-based screening in pharmaceutical research. *Chemical reviews*. 2004;104(8):3641-76.
43. Angulo J, Nieto PM. STD-NMR: application to transient interactions between biomolecules-a quantitative approach. *European biophysics journal : EBJ*. 2011;40(12):1357-69.
44. Roussel P, Degand P, Lamblin G, Laine A, Lafitte JJ. Biochemical definition of human tracheobronchial mucus. *Lung*. 1978;154(4):241-60.
45. Hunt BE, Weber A, Berger A, Ramsey B, Smith AL. Macromolecular mechanisms of sputum inhibition of tobramycin activity. *Antimicrobial agents and chemotherapy*. 1995;39(1):34-9.
46. Wang Y, Rando RR. Specific binding of aminoglycoside antibiotics to RNA. *Chemistry & biology*. 1995;2(5):281-90.
47. Hill HD, Jr., Reynolds JA, Hill RL. Purification, composition, molecular weight, and subunit structure of ovine submaxillary mucin. *The Journal of biological chemistry*. 1977;252(11):3791-8.

Chapter 5

48. Saggars BA, Lawson D. The differential attachment of antibiotics to glycoprotein and blood lymphocytes. *Journal of clinical pathology*. 1970;23(3):266-8.
49. Wesley AW, Qureshi AR, Forstner GG, Forstner JF. Differences in mucus glycoproteins of small intestine from subjects with and without cystic fibrosis. *Advances in experimental medicine and biology*. 1982;144:145-6.
50. Morgan DJ. Clinical pharmacokinetics of beta-agonists. *Clinical pharmacokinetics*. 1990;18(4):270-94.
51. Besterman JM, Elwell LP, Blanchard SG, Cory M. Amiloride intercalates into DNA and inhibits DNA topoisomerase II. *The Journal of biological chemistry*. 1987;262(27):13352-8.
52. Mirmomtaz E, Ensafi AA, Soleimanian-Zad S. Determination of amiloride using a ds-DNA-modified pencil graphite electrode based on guanine and adenine signals. *Electrochim Acta*. 2009;54(3):1141-6.
53. Bailly C, Cuthbert AW, Gentle D, Knowles MR, Waring MJ. Sequence-selective binding of amiloride to DNA. *Biochemistry*. 1993;32(10):2514-24.
54. Li JH, Cragoe EJ, Jr., Lindemann B. Structure-activity relationship of amiloride analogs as blockers of epithelial Na channels: I. Pyrazine-ring modifications. *The Journal of membrane biology*. 1985;83(1-2):45-56.
55. Li JH, Shaw A, Kau ST. Stereoselective blockade of amphibian epithelial sodium channels by amiloride analogs. *The Journal of pharmacology and experimental therapeutics*. 1993;267(3):1081-4.
56. Hunt T, Atherton-Watson HC, Axford J, Collingwood SP, Coote KJ, Cox B, et al. Discovery of a novel chemotype of potent human ENaC blockers using a bioisostere approach. Part 1: quaternary amines. *Bioorganic & medicinal chemistry letters*. 2012;22(2):929-32.
57. Bromberg LE, Barr DP. Self-association of mucin. *Biomacromolecules*. 2000;1(3):325-34.
58. Carlstedt I, Lindgren H, Sheehan JK, Ulmsten U, Wingerup L. Isolation and characterization of human cervical-mucus glycoproteins. *The Biochemical journal*. 1983;211(1):13-22.
59. Thornton DJ, Khan N, Mehrotra R, Howard M, Veerman E, Packer NH, et al. Salivary mucin MG1 is comprised almost entirely of different glycosylated forms of the MUC5B gene product. *Glycobiology*. 1999;9(3):293-302.
60. Hovenberg HW, Davies JR, Carlstedt I. Different mucins are produced by the surface epithelium and the submucosa in human trachea: identification of MUC5AC as a major mucin from the goblet cells. *The Biochemical journal*. 1996;318 (Pt 1):319-24.
61. Davies JR, Hovenberg HW, Linden CJ, Howard R, Richardson PS, Sheehan JK, et al. Mucins in airway secretions from healthy and chronic bronchitic subjects. *The Biochemical journal*. 1996;313 (Pt 2):431-9.
62. Gong DH, Turner B, Bhaskar KR, Lamont JT. Lipid binding to gastric mucin: protective effect against oxygen radicals. *The American journal of physiology*. 1990;259(4 Pt 1):G681-6.
63. Hollingsworth MA, Swanson BJ. Mucins in cancer: protection and control of the cell surface. *Nature reviews Cancer*. 2004;4(1):45-60.
64. Herrmann A, Davies JR, Lindell G, Martensson S, Packer NH, Swallow DM, et al. Studies on the "insoluble" glycoprotein complex from human colon. Identification of reduction-insensitive

Chapter 5

- MUC2 oligomers and C-terminal cleavage. *The Journal of biological chemistry*. 1999;274(22):15828-36.
65. Mantle M, Allen A. Isolation and characterization of the native glycoprotein from pig small-intestinal mucus. *The Biochemical journal*. 1981;195(1):267-75.
 66. Clamp JR, Cooper B, Creeth JM, Ene D, Barrett J, Gough M. The presence of polysaccharide in normal human gastric mucus. *The Biochemical journal*. 1983;215(2):421-3.
 67. Biesbrock AR, Reddy MS, Levine MJ. Interaction of a salivary mucin-secretory immunoglobulin A complex with mucosal pathogens. *Infection and immunity*. 1991;59(10):3492-7.
 68. Murty VL, Sarosiek J, Slomiany A, Slomiany BL. Effect of lipids and proteins on the viscosity of gastric mucus glycoprotein. *Biochemical and biophysical research communications*. 1984;121(2):521-9.
 69. List SJ, Findlay BP, Forstner GG, Forstner JF. Enhancement of the viscosity of mucin by serum albumin. *The Biochemical journal*. 1978;175(2):565-71.
 70. Reid LM, Bhaskar KR. Macromolecular and lipid constituents of bronchial epithelial mucus. *Symposia of the Society for Experimental Biology*. 1989;43:201-19.
 71. Hincman HO, Bhaskar KR, O'Sullivan DD, Brown R, Reid L. Lipids in airway mucus of acute quadriplegic patients. *Experimental lung research*. 1990;16(4):369-85.

Chapter 6 : General Discussion, Conclusions and Future Work

Pulmonary delivery of therapeutics is a growing market and offers a variety of opportunities in drug delivery for systemic and local delivery for the treatment of lung disease. In 2012 the Business Communications Company market research reviewed the global markets for drug delivery technologies highlighting a pulmonary drug delivery technologies market in wide increment with a valuation of \$20 billion in 2010 with a forecasts trends to about \$40 billion in 2016.

In spite of an expanding of literature on the absorption of inhaled therapeutics, there is still a lack of knowledge about the detailed processes that occur after drug deposition in the airways. This is principally due to the scant availability of tools to visualise and quantify these processes post-inhalation. For the treatment of patients with airflow obstruction the inhaled route is considered an optimal way of administration of drugs such as corticosteroids, β -agonists and aerosol administration of antibiotics against *P. aeruginosa* is commonly used in CF.

The delivery of molecules by aerosol must overcome the MC mechanism so the molecules must rapidly diffuse through the mucus layer lying the epithelium. Alternatively, inhaled antibiotics must penetrate the mucus barrier sufficiently to bind the target bacterial colonies within the sputum.

From the late 80s and early 90s, the retention of lipophilic polycyclic aromatic hydrocarbons (PAHs) within the mucus layer on the respiratory tract of dogs has been studied by Gerde, Muggenburg^{(1) (2)}. The studies consisted of installation on the airway

of benzo[a]pyrene (BaP) or phenanthrene and consequent determination of their tissues concentration. Results showed that the highly lipophilic toxicant BaP was higher retained by the mucus layer with about 35% of BaP retained after 1 min of exposure whereas only 3% of phenanthrene was retained at the same time. The authors speculated that the retention of PAHs is due to lipid content of mucus but no proof of this hypothesis was shown. The influence of the mucus and MC system on PAH retention would be expected to serve a protective role by avoiding prolonged retention of these lipophilic toxicants at the epithelium surface and reduced absorption across the airways. It should be noted that this mechanism would serve principally to protect the lung mucosa but would not prohibit exposure of the gastric/intestinal mucosae to mucus-bound BaP that is cleared from the lung and swallowed.

The consideration of drug-mucus interactions in the lung has received very little attention. In the oral drug delivery field a series of studies have indicated that drug-mucus interaction may limit the bioavailability of therapeutics via any mucosal surface reducing the efficiency with which drugs can access their target receptor which may be critical determinant of a drug's efficacy *in vivo* ^{(3) (4) (5)}.

For example, Karlsson, Wikman ⁽⁶⁾ used the mucus-producing human goblet cell model HT29-H to investigate steroid transport across polarised cell monolayers. Notably, the transport rate of the lipophilic steroid, testosterone, increased ~50% following removal of mucus from the apical side of the monolayer.

Chapter 3 of this thesis was mainly focused on the identification of an appropriate mucus model for the investigation of inhaled molecule-mucus interactions. Firstly, NHBE cells were cultured with the aim to harvest human mucus and to ensure mucociliary differentiation were chosen NHBE cell passage 1^(7,8). Mucus production was confirmed by AB staining for the detection of sialylated or sulphated groups on mucin⁽⁹⁾⁽¹⁰⁾ and also using immunocytochemistry staining of MUC5AC⁽¹¹⁾. Harvested mucins from NHBE cell were also analysed by AFM to confirm the mucin polymer morphology.

The harvest of mucin from *in vitro* lung models offers the advantages of homology to the *in vivo* mucus barrier, the expression of appropriate MUC isoforms and facile availability of the model without the need for ethical approval for human tissue harvest. Furthermore, NHBE cells mimic the *in vivo* bronchial epithelium through mucociliary differentiation⁽¹²⁾ and the formation of two discreet layers of ASL (PCL and mucus layer)⁽¹³⁾. Recent development of the gel-on-brush model of airway mucus and penetration of drugs through these epithelial barriers will rely on this model in coming decades. However, the model's high cost and the low mucus yield significantly confound these advantages and led us to explore an *ex vivo* porcine mucus model as an alternative. Biochemical analysis of PLM harvested revealed a high DNA contamination which could have influence the viscosity of the mucus glycoprotein⁽¹⁴⁾ affecting mucus rheology. Therefore, diffusion assays were performed using a commercially available mucin, PGM.

Diffusion assays were performed using a Franz-cell system, for probes spanning a 376-70 kDa molecular weight range through three mucin gels (1, 3 and 5%) with the aim of identifying size-filtering phenomena within the model. The substitution of aqueous solution with mucin significantly reduced solutes directional transport. As also showed by Desai, Mutlu ⁽¹⁵⁾ using porcine gastric mucus, the diffusion of FL-NA and FITC dex probes resulted significantly retarded in presence of mucin and appeared inversely correlated with increment of solutes molecular weight. We noticed a reduction of solutes diffusion with increased mucin concentration mostly for probes >10kDa. Desai et al noticed a significant reduction of diffusion rate for molecules >30kDa, however the disparity on the results could be explained by the ~7-fold larger pore diameter in the support membranes used in Desai's studies ⁽¹⁵⁾. For example, our data indicates that FD40 (size 9 nm) displayed restricted diffusion across the bare dialysis membrane which bore a ~15nm pore diameter. FL-Na, FD4 and amiloride did not show significant difference in mucus diffusion but benzamil, which structure differs from amiloride only by the addition of benzyl group, showed a significantly retarded diffusion through mucin solution. This observation led us to speculate about the involvement of hydrophobic forces between benzamil and mucus glycoprotein.

In Chapter 4 we showed the application of fluorescence and UV-vis spectroscopy techniques to further investigate amiloride and benzamil interaction to mucin. Consistent with Franz cell transport data benzamil demonstrated greater evidence of mucin binding than the less lipophilic amiloride. Technical limitations, including the use

of large concentration ranges of drug and mucin as well as the time-consuming nature of titration experiments, prohibited further UV/fluorescence spectroscopy investigation. Spectroscopy techniques have been used to study small molecules' interactions with mucin ^(16, 17) but such techniques are not routinely used for screening compound binding to protein / glycoprotein targets. Chapter 4 also describes the development and validation of a 96-well ultrafiltration assay as a method to study the extent of binding of a wider range of solutes. This approach benefits from a wider range of sample numbers per experiment and the ease of transfer to robotic system that are widely used in pharmaceutical industry. Mass balance calculations using an internal standard approach afforded the precise detection of mucin binding and non-specific binding to the ultrafiltration plates. Consistent with the published literature there was an increased extent of non-specific binding to the plasticware yet binding to mucin could be determined after subtraction of NSB from each experimental condition.

Binding isotherms constructed for amiloride and analogues showed most frequently a monolayer binding model, but a multilayer binding was also noticed for three QQA. This self-promoted binding site may have a significantly effect on drug disposition leading to a significant increment of drug molecules retained on the airways. To better understand the pre-determining factors for multilayer binding future work will involve the study of further analogues and unrelated compounds. Solubility of drug candidates in aqueous solvent is one of the critical physicochemical properties for the successful development of oral drugs ⁽¹⁸⁾, although solubility of compounds was accurately tested to avoid

precipitation issue it could be further probed by looking for the solid form of the precipitant in the sample by studying under polarised light microscope.

We next sought to identify physical parameters that correlated with the extent of mucin-binding at a 20 mM concentration, which is appropriate considering the deposition of therapeutic ENaC dose into the human lung. Both NQQA and QQA showed a strong correlation with $\text{Log } P_{o/w}$ and QQA also displayed correlation with PSA, rotatable bonds, van Der Waal volume, polarizability and H-acceptor number. A series of publications by Matthes, Nimmerfall ⁽¹⁹⁾ ⁽²⁰⁾ analysed binding of a series of polar and non-polar drugs to pig intestinal mucus showing that more lipophilic drugs displayed slower diffusion through mucus and higher affinity for mucus compared to more hydrophilic ones, the authors concluded that hydrophobicity may be an important factor for drug-mucin interaction. Other authors, including Kearney and Marriott ⁽²¹⁾ performed equilibrium dialysis of the tetracycline-mucin mixtures in different pH condition (1 to 11) and attributed the tetracycline interaction to mucin to a combination of electrostatic forces and hydrophobic interactions. In particular, the binding process was considered to be non-specific through a hydrophobic process at neutral pH, whereas at acidic pH was proposed a more specific electrostatic interaction between the negatively charged sialic acid residues on mucin and the positively charged tetracycline due to the net charge of dimethyl-amino group. Gordon, Hodges ⁽²²⁾ using an equilibrium dialysis, demonstrated the binding bacterial alginate to positively charged aminoglycosides antibiotic (β -lactams, gentamicin and tobramycin).

This 96-well ultrafiltration approach for screening drug-mucin presented here was methodologically similar to those used by Fung, Chen ⁽²³⁾ and Wang ⁽²⁴⁾ for the determination of PPB and data presented in Chapter 4 reinforce the benefits of ultrafiltration for the determination of drug-macromolecules interaction.

Further work should be focused on the deeper elucidation of ENaC-mucin interaction. Such as, the 96-well ultrafiltration assay may be performed pre-treating the mixture with DNase to exclude DNA influence of the results obtained using PGM as mucin source. Furthermore, the binding characteristics of the mixture in different pH condition may help in understanding the involvement of hydrophobic or electrostatic interaction interactions. For example, if the binding is governed by positive charge of ENaC blocker and negative charge of sialic acid residues of mucin at low pH we should see a more specific interaction. The increment of the pH up to 7 should causes the fall in the binding level in coincident with the reduction in the amount of the neutral species.

Pronase digestion of mucin may be used to further study hydrophobic interaction. If binding sites are on the non-glycosylated, the digestion of the mucin protein core will lead to a reduced extend of drug-mucin interaction.

Hydrophobic interaction may be further explored by studying the effect of different NaCl concentration on drug-mucin interaction. The increment of NaCl concentration will lead mucin unfolding with a higher number of hydrophobic sites exposed which may be observed with changing in fluorescence intensity.

Hydrophobic molecules have been shown to be absorbed more rapidly through epithelium⁽²⁵⁾ ⁽²⁶⁾. Tronde et al.,⁽²⁶⁾ studied the diffusion to nine drugs with range cLog P of -0.4- 3.5 to Caco-2 cell monolayers and the drug absorption in the isolated and perfused rat lung demonstrating a good correlation of both *in vitro* and *in vivo* model to drug lipophilicity. In our studies, the hydrophilic character of QQAs appeared to limit the transport of ENaC blockers and no clear *in vitro* correlation was found for NQQA probably due to the different transport pathway involved.

Hydrophilic drugs have been shown, in some cell types, to traverse the epithelium via a paracellular route whereas hydrophobic molecule appear translocated via the transcellular route⁽²⁷⁾ ⁽²⁸⁾ and there are evidence of a cation transporters for amiloride⁽²⁹⁾.

With evidence of mucin binding in hand it was desirable to determine whether the presence of mucin at the apical membrane side of lung epithelia would reduce the rate of solute transport across the lung. The influence of purified PJM on 552-02 apparent permeability across Calu-3 monolayer was measured showing a 20-fold increase of monolayer permeability with increased transport of 20-fold. This effect was also reported by Boegh, Baldursdottir⁽³⁰⁾ after exposure of Caco-2 cells to biosimilar mucus composed of purified gastric mucin, lipids and protein and was associated to the presence of high concentration of linoleic acid. And so, further work is required to further delineate the transport pathway into / across the epithelia or passive paracellular or active/facilitated transport pathways used from amiloride and analogues. Taken together with published reports these observations indicate that the application of

exogenous mucin/mucus to intact monolayer systems is very challenging. In spite of cost and labour intensiveness the primary NHBE model presents an intact, endogenous mucus layer, albeit one that is significantly less voluminous than that found in the diseased lung.

In Chapter 5 a relatively new NMR technique, STD-NMR, was used to probe mucin binding. STD-NMR analysis of 552-02 and OF-80-NS22 demonstrated a noticeably stronger interaction of 552-02 to mucin compared to OF-80-NS22. These data closely matched the ultrafiltration binding assay. Published evidence of amiloride-DNA binding prompted us to repeat STD-NMR studies on CsCl-purified jejunal mucin. Intriguingly, the results were consistent with those of PGM which indicates that DNA binding was not responsible for the binding observed in PGM studies. This allowed the mapping of 552-02 and OF-80-NS22 protons as “interacting” and “not-interacting” (Figure 6.1) and gave further confirmation of the stronger interaction of 552-02. The invisibility of the pyrazine protons in all amiloride analogues is a key deficiency of the ^1H STD-NMR technique. A number of alternative NMR protocols could be employed to better understand their binding. These include ^{15}N or ^{13}C based pulse sequences. Drawbacks include lower sensitivity and the need for isotopic enrichment.

New formulations, for more controlled drug delivery, are necessary to promote particles dissolution in the airway. Drugs disposition may be limited by mucin and other mucus

component (DNA, lipid and alginate) and more studies are needed to better understand transport pathways across the pulmonary epithelium.

In conclusion, the results obtained from this thesis have provided an insight into the physical-chemical properties between drug-mucin interaction.

The development of a new drug is a complex process and the estimation of the extent of inhaled drug interaction to mucin is a step of great value in drug candidates selection.

The sensitive and quantitative 96-well ultrafiltration binding assay developed may find industrial application for screening of a number of drug model with opportunity of automation for the screening and detailed investigation of drug binding to mucin and other macromolecules.

We also report the use of STD-NMR to probe mucin-drug interaction and results confirmed that ENaC blocker access to epithelial targets may be negatively affected by non-specific mucin binding.

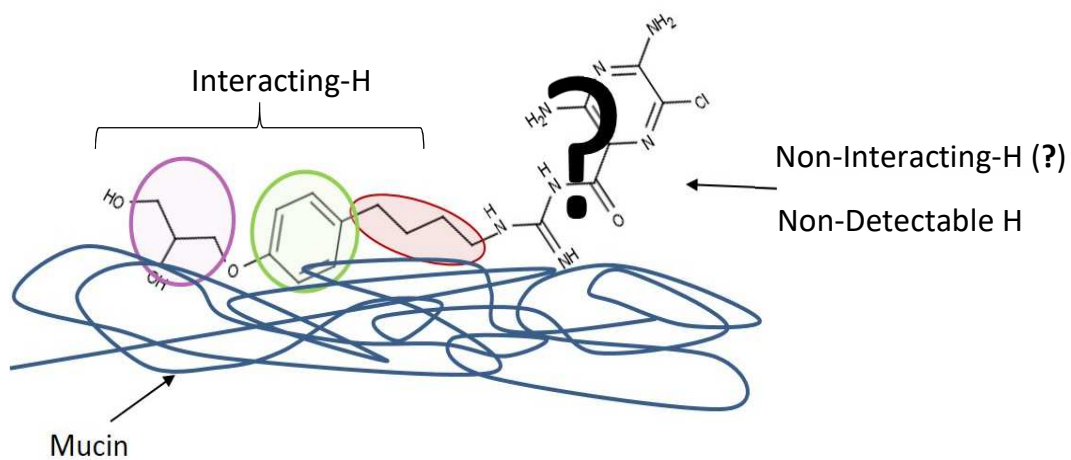


Figure 6.1. 552-02 “Interacting” and “non-interacting” protons.

STD-NMR of mucin-552-02 mixture showed Interacting-H to mucin and Non-interacting-H/Non-detectable-H.

Reference

1. Gerde P, Muggenburg BA, Sabourin PJ, Harkema JR, Hotckiss JA, Hoover MD, et al. Disposition of polycyclic aromatic hydrocarbons in the respiratory tract of the beagle dog. II. The conducting airways. *Toxicology and applied pharmacology*. 1993;121(2):319-27.
2. Gerde P, Scholander P. A mathematical model of the penetration of polycyclic aromatic hydrocarbons through the bronchial lining layer. *Environmental research*. 1987;44(2):321-34.
3. Bhat PG, Flanagan DR, Donovan MD. The limiting role of mucus in drug absorption: Drug permeation through mucus solution. *Int J Pharm*. 1995;126(1-2):179-87.
4. Barry BW, Braybrooks MP. Proceedings: Effect of mucin on the bioavailability of tetracycline from the gastro-intestinal tract: in vivo, in vitro correlations. *The Journal of pharmacy and pharmacology*. 1974;26 Suppl:64P-5P.
5. Kearney P, Marriott C. The Effects of Mucus Glycoproteins on the Bioavailability of Tetracycline .1. Dissolution Rate. *Int J Pharm*. 1986;28(1):33-40.
6. Karlsson J, Wikman A, Artursson P. The Mucus Layer as a Barrier to Drug Absorption in Monolayers of Human Intestinal Epithelial Ht29-H Goblet Cells. *Int J Pharm*. 1993;99(2-3):209-18.
7. Gray TE, Guzman K, Davis CW, Abdullah LH, Nettesheim P. Mucociliary differentiation of serially passaged normal human tracheobronchial epithelial cells. *American journal of respiratory cell and molecular biology*. 1996;14(1):104-12.
8. Malavia NK, Mih JD, Raub CB, Dinh BT, George SC. IL-13 induces a bronchial epithelial phenotype that is profibrotic. *Resp Res*. 2008;9.
9. Goso Y, Hotta K. Dot-Blot Analysis of Rat Gastric Mucin Using Histochemical Staining Methods. *Anal Biochem*. 1994;223(2):274-9.
10. Corfield AP, Carrington SD, Hicks SJ, Berry M, Ellingham R. Ocular mucins: Purification, metabolism and functions. *Prog Retin Eye Res*. 1997;16(4):627-56.
11. Groneberg DA, Eynott PR, Oates T, Lim S, Wu R, Carlstedt I, et al. Expression of MUC5AC and MUC5B mucins in normal and cystic fibrosis lung. *Resp Med*. 2002;96(2):81-6.
12. Holmen JM, Karlsson NG, Abdullah LH, Randell SH, Sheehan JK, Hansson GC, et al. Mucins and their O-Glycans from human bronchial epithelial cell cultures. *Am J Physiol-Lung C*. 2004;287(4):L824-L34.
13. Button B, Cai LH, Ehre C, Kesimer M, Hill DB, Sheehan JK, et al. A Periciliary Brush Promotes the Lung Health by Separating the Mucus Layer from Airway Epithelia. *Science*. 2012;337(6097):937-41.
14. Murty VL, Sarosiek J, Slomiany A, Slomiany BL. Effect of lipids and proteins on the viscosity of gastric mucus glycoprotein. *Biochemical and biophysical research communications*. 1984;121(2):521-9.
15. Desai MA, Mutlu M, Vadgama P. A study of macromolecular diffusion through native porcine mucus. *Experientia*. 1992;48(1):22-6.

16. Zhao Y, Chen L, Yakubov G, Aminiafshar T, Han L, Lian G. Experimental and theoretical studies on the binding of epigallocatechin gallate to purified porcine gastric mucin. *The journal of physical chemistry B*. 2012;116(43):13010-6.
17. Yu X, Liu H, Yang Y, Lu S, Yao Q, Yi P. The investigation of the interaction between Oxymetazoline hydrochloride and mucin by spectroscopic approaches. *Spectrochimica acta Part A, Molecular and biomolecular spectroscopy*. 2013;103:125-9.
18. Amidon GL, Lennernas H, Shah VP, Crison JR. A theoretical basis for a biopharmaceutic drug classification: the correlation of in vitro drug product dissolution and in vivo bioavailability. *Pharmaceutical research*. 1995;12(3):413-20.
19. Matthes I, Nimmerfall F, Sucker H. Mucus Models for Investigation of Intestinal-Absorption .2. Mechanisms of Drug-Interaction with Intestinal Mucus. *Pharmazie*. 1992;47(8):609-13.
20. Matthes I, Nimmerfall F, Sucker H. Mucus Models for Investigation of Intestinal-Absorption .1. Validation and Optimization. *Pharmazie*. 1992b;47(7):505-15.
21. Kearney P, Marriott C. The Effects of Mucus Glycoproteins on the Bioavailability of Tetracycline .3. Everted Gut Studies. *Int J Pharm*. 1987;38(1-3):211-20.
22. Gordon CA, Hodges NA, Marriott C. Antibiotic Interaction and Diffusion through Alginate and Exopolysaccharide of Cystic Fibrosis-Derived *Pseudomonas-Aeruginosa*. *J Antimicrob Chemoth*. 1988;22(5):667-74.
23. Fung EN, Chen YH, Lau YY. Semi-automatic high-throughput determination of plasma protein binding using a 96-well plate filtrate assembly and fast liquid chromatography-tandem mass spectrometry. *Journal of chromatography B, Analytical technologies in the biomedical and life sciences*. 2003;795(2):187-94.
24. Wang C. A mass balance approach for calculation of recovery and binding enables the use of ultrafiltration as a rapid method for measurement of plasma protein binding for even highly lipophilic compounds. *Journal of pharmaceutical and biomedical analysis*. 2013;75:112-7.
25. Hofmann T, Stutts MJ, Ziersch A, Ruckes C, Weber WM, Knowles MR, et al. Effects of topically delivered benzamil and amiloride on nasal potential difference in cystic fibrosis. *American journal of respiratory and critical care medicine*. 1998;157(6 Pt 1):1844-9.
26. Tronde A, Norden B, Jeppsson AB, Brunmark P, Nilsson E, Lennernas H, et al. Drug absorption from the isolated perfused rat lung--correlations with drug physicochemical properties and epithelial permeability. *Journal of drug targeting*. 2003;11(1):61-74.
27. Saha P, Kim KJ, Yamahara H, Crandall ED, Lee VHL. Influence of Lipophilicity on Beta-Blocker Permeation across Rat Alveolar Epithelial-Cell Monolayers. *J Control Release*. 1994;32(2):191-200.
28. Mathia NR, Timoszyk J, Stetsko PI, Megill JR, Smith RL, Wall DA. Permeability characteristics of calu-3 human bronchial epithelial cells: in vitro-in vivo correlation to predict lung absorption in rats. *Journal of drug targeting*. 2002;10(1):31-40.
29. Biermann J. Characterization of regulatory mechanisms and states of human organic cation transporter 2. *American Journal of Physiology - Cell Physiology*. 2006;290.
30. Boegh M, Baldursdottir SG, Mullertz A, Nielsen HM. Property profiling of biosimilar mucus in a novel mucus-containing in vitro model for assessment of intestinal drug absorption. *European*

Chapter 6

journal of pharmaceutics and biopharmaceutics : official journal of Arbeitsgemeinschaft fur Pharmazeutische Verfahrenstechnik eV. 2014;87(2):227-35.